UNIVERSITY OF BELGRADE

FACULTY OF TECHNOLOGY AND METALLURGY

Abdunnaser Hamza Fadel

AUSTENITE DECOMPOSITION IN MEDIUM CARBON
MICROALLOYED STEELS: MECHANISM,
STRUCTURE AND PROPERTIES

PhD Thesis

Belgrade 2013

УНИВЕРЗИТЕТ У БЕОГРАДУ

ТЕХНОЛОШКО-МЕТАЛУРШКИ ФАКУЛТЕТ

Abdunnaser Hamza Fadel

РАЗЛАГАЊЕ АУСТЕНИТА У СРЕДЊЕУГЉЕНИЧНИМ МИКРОЛЕГИРАНИМ ЧЕЛИЦИМА: МЕХАНИЗАМ, СТРУКТУРА И СВОЈСТВА

Докторска дисертација

Београд 2013

Supervisor:

_____
dr Nenad Radović, Associate Professor
Faculty of Technology and Metallurgy, University of Belgrade

Comittee members:

_____
dr Zorica Cvijović, Full Professor
Faculty of Technology and Metallurgy, University of Belgrade

_____
dr Branka Jordović, Full Professor
Faculty of Technical Sciences Čačak, University of Kragujevac

Candidate:

_____
Abdunnaser Hamza Fadel

Date of the defence of PhD Thesis: _____

ACKNOWLEDGMENT

AUSTENITE DECOMPOSITION IN MEDIUM CARBON MICROALLOYED STEELS: MECHANISM, STRUCTURE AND PROPERTIES

The aim of this work was to determine TTT diagrams of two mediumcarbon V microalloyed steels V-N (0.256%C, 0.0235%N, 0%Ti) and Ti-V-N (0.309%C, 0.221%N, 0.011%Ti). The isothermal treatment was carried out at 350, 400, 450, 500, 550 and 600°C. These treatments were interrupted at different times in order to analyze the evolution of the microstructure. Isothermal decomposition of medium carbon vanadium microalloyed austenite was evaluated by optical and SEM metallography.

In the first step, austenite grain size is establish in temperature range 850-1150 °C. Ti bearing steel exibits lower grain size at high temperatures. This effect is attributed to pinning effect of TiN particless. Nevertheless, temperature of 1100°C provided grain size very simillar to 60μm, value suggested as optimal for intragranular nucleation and formation of acicular ferrite.

Isothermal treatment enabled plotting the TTT diagrams. In both diagrams, equal transformations are observed. Influence of Ti addition is not very clear; it is assumed that increased level on carbon has covered expected influence on intragranular nucleation. Four curves are found to be relevant for austenite decomposition in medium carbon V-microalloyed steels:

(1) Grain boundary ferrite is the first phase to be generated at all temepratures. In the lower temperature range the widmanstetten ferrite is formed, while on higher temperatures grain boundary allotriomorphs are produced. This difference is attributed to displacive nature of transformation at lower and diffusional transformation at higher temperatures.

(2) Second curve is related to nucleation of Intragranular ferrite (IGF). In the lower temperature range (350–400°C) acicular ferrite plates are grouped in sheaves; at intermediate temperatures (450–500°C), a more interlocked microstructure of acicular ferrite was clearly observed, while microstructure generated at high temperatures (550–600°C) is characterized by polygonal idiomorphic ferrite.

(3) Third curve is related to onset of pearlite. It occurs at temperatures $\geq$ 500°C, followed by an incomplete reaction phenomenon.

(4) The transition between an acicular ferrite sheaf morphology and interlocked microstructure is observed to take place at 400/450°C. However the bainitic sheaves are frequently observed when the isothermal transformation time is increased at 400°C and temperature diminishes to 350°C.

Finish of transformation was clearly observed at temperatures below 500°C. However at 550 and 600°C, incomplete reaction phenomenon occurs. This behaviour is attributed to carbon enrichment in austenite and decrease of driving force for austenite decomposition.

Martensite start temperature is established to be 320°C and 330°C for Ti-V-N and V-N steels respectively. Slightly lower Ms temperature of Ti-V-N steel is attributed to higher content of carbon and Ti, elements that increase hardenability.

The lower yield stress for Ti-free steel (V-N) compared with titanium –containig steels (Ti-V-N) is attributed to lower carbon content compared with titanium-containing steel. Yield stress decreases from the maximum values for temperatures 350°C – 400°C for both steels investigated. It is assumed that it reflects dislocation strengthening associated with the presence of hard phases such as bainite, since the dislocation density of the ferrite increases with decreasing transformation temperature. at higher temperatures, At temperatures higher than 450°C, in both steel yield strength increases. This behaviour is more pronounced in Ti bearing steel and it is attributed to more effective stabilization of austenite in steel with higher carbon, as well as higher presence of pearlite.

Разлагање аустенита у средњеугљеничним микролегираним челицима: механизам, структура и својства

У раду су испитана два средњеугљенична челика микролегирана ванадијумом, који се међусобно разликују по садржају титана, азота и угљеника, V-N (0.256%C, 0.0235%N, 0%Ti) и Ti-V-N (0.309%C, 0.221%N, 0.011%Ti) челици. Челици су испоручени као топловаљане шипке са кованим крајевима.

У првој фази је урађена серија узорака у циљу одређивања величине полазног аустенитног зрна, у опсегу 950-1250°C. У циљу добијања дијаграма изотермалног разлагања урађена је серија узорака који су изотермално третирани на температурама између 350 и 600°C. Сви узорци су прво прогревани на 1100°C. Након изотермалног третмана, узорци су каљени у води, а затим сечени на половине, брушени, полирани и нагрижени по стандардној процедури. Након детаљног посматрања на оптичком микроскопу, изабрани узорци су посматрани на скенинг електронском микроскопу. Узорци који су коришћени за металографска испитивања су искоришћени за мерење тврдоће (једна половина) и за израду узорака за одређивање границе течења тестом притискивањем на уређају за испитивање једноосним затезањем. Утврђено је да је оптимална температура прогревања 1100°C, као и да се након каљења са 1100°C добија потпуно мартензитна структура. Нагли пораст величине зрна у челику без титана је последица одсуства честица TiN који блокирају границе зрна. Зато је за температуру прогревања одабрана 1100°C јер обезбеђује величину зрна од око 50µm која промовише ацикуларни ферит. Такође, у оквиру прелиминарних резултата, одређена је температура почетка мартензитне трансформације на 330 и 320°C, за челик са ванадијумом, односно челик са додатком титана.

Различите морфологије добијене у току изотермалног разлагања су приказане на микрофотографијама. Резултати добијени у овој дисертацији указују да у целом температурном подручју 350-600°C разлагање аустенита започиње издвајањем ферита по границама полазних аустенитних зрна. У високотемпературном подручју гранични ферити у потпуности декоришу границе зрна, док се у нискотемпературном подручју

поред граничних ферита јављају и беинитни снопови нуклеирани на границама зрна. Гранични ферити у високотемпературном настају дифузионим механизмом, пошто су температуре на којима се јављају довољно високе да омогуће дифузију. Њихова је карактеристика да расту дуж граница аустенитног зрна. Са друге стране, гранични ферити нискотемпературном подручју су идентификовани као Видманштетенов ферит, кога услед ниских температура на којима је отежана дифузија карактерише смицајни механизам и карактеристичани облик (облик плочице, иглице или труогласти облик) и које расту са границе ка унутрашњости зрна) и могу се нуклеирати и са већ претходно насталог феритног зрна.

Са продужењем времена изотермалног разлагања, ови процеси се завршавају и почиње издвајање интрагрануларно нуклеираног ферита. У питању је ацикуларни ферит чија се морфологија разликује у зависности од тога у ком температурном подручју се јавља: на вишим температурама феритна зрна су игличаста и потпуно произвољно оријентисана, док су у нискотемпературном подручју иглице паралелне и чине снопове. Завршетком издвајања ацикуларног ферита, почиње издвајање перлита у оба челика. Количина перлита је веома мала, па је после 20 минута разлагање аустенита завршено и формиране су финалне микроструктуре. На нижим температурама структура се састојала из Видманштетеновог ферита, беинитних снопова и ацикуларног ферита у облику снопова, док су на вишим температурама присутни гранични алотриоморфи, игличасти ацикуларни ферит и перлит, уз присуство заосталог аустенита. Овако познавање промена на свакој од температура је омогућило конструисање дијаграма изотермалног разлагања.

На оба ТТТ (ИР) дијаграма се запажају идентичне области, уз напомену да су криве на дијаграму челика са титаном померене ка дужим временима и на нешто више температуре. Нос криве за челик без титана је на испод 2 секунде на температури између 400 и 450°C, односно на 2 секунде на 450°C у челику са титаном. Резултати мерења тврдоће, границе течења су дати у табелама и приказани на дијаграмима.

Испитивање тврдоће свих узорака и границе течења узорака са финалном структуром указује да су највеће тврдоће измерене за тестове са најкраћим временима, док се граница течења снижава од максималне вредности до минималне, а затим поново расте. Овакво понашање је доведено у везу са смањењем количине присустних беинитних

снопова и видманштетеновог ферита. Са друге стране, на вишим температурама, пошто је присутан феномен недовршене (некомплетне) трансформације, услед каљења стабилисаног аустенита, тврдоћа поново расте.

Граница течења показује веома слично понашање. У целом температурном подручју испитивања, челик са титаном има већи границу течења. Овакво понашање је доведено у везу

У области од 350 до 450 °C граница течења опада. Добијене високе вредности указују на присуство фаза са великом густином дислокација, која је карактеристична за беинитне структуре. На температурама изнад 450°C у оба челика, долази до пораста границе течења. Ова појава је израженија у челику са титаном, што је доведено у везу са снажнијом стабилизацијом аустенита у челику са већим садржајем легирајућих елемената и повећаним садржајем перлита у структури.

КЉУЧНЕ РЕЧИ   Микролегирани челици, Фазне трансформације, ТТТ дијаграм изотермалног разлагања, Ацикуларни ферит, Беинитни снопови, Ферит по границама зрна, Видманштетенов ферит, Полигонални ферит, Перлит, Светлосна и скенирајућа електронска микроскопија

Научна област: Техничке науке
Ужа научна област: металургија
удк број: 669.017

CONTENT

1. INTRODUCTION

The relationship of structure, properties and processing control (SPPC technology) plays a vital role in controlling the properties of hot rolled products which indicate that the modeling of phase transformation behavior as one of most important parts, which is required for safe performance application. Many essential properties of iron alloys depend on the mechanism of phase change and the choice of any material is based upon fitness for purpose. The main characteristics in selecting a steel grade are; the yield strength, the tensile strength, (uniform) elongation, low temperature impact-toughness, work-hardening, hole-expansion ratio, fatigue performance and weld-ability. The ideal steel to be used in forging must have the following characteristics: (1) must be able to generate the final properties without post-forging heat treatment, (2) must be capable of being forged and cooled in a simple manner, (3) must be able to generate high strengths and toughness in large section sizes, (4) must be amenable to surface enhancement techniques such as induction hardening or nitriding. Therefore for safe MA forging application it required development program search for processing parameters & structure to improve the fracture toughness. The control of austenite grain size and precipitation strengthening are important factors in the development of the final mechanical properties of the product i.e understanding the precipitation behavior that found at different points in the thermo-mechanical processing of the steel. The size, morphology, chemical composition, crystal structure for precipitate .The precipitation strengthening due to particle present in the steel are important factors in the development of the final mechanical properties of the product. The type of particles can be classified into three groups. The first group includes the larger sized inclusions, encompassing MnS and TiN particles of sizes greater than approximately, 2 μm, which can easily be observed by optical microscopy. These types of particles have been observed to be ineffective as acicular ferrite nucleation sites. The second group are the inclusions whose size is between, approximately, 0.5 and 2 μm, which have been observed to be seen the most effective in promoting the nucleation of ferrite plates. The larger sizes belonging to this group can be seen by optical microscopy, but the majority of this group are only visible using electron microscopy and the composition of these particles has been analyzed using energy-dispersive spectrometry (EDS),examined by transmission

electron microscopy TEM. Finally, the third group includes all the inclusions smaller than 200 to 300 nm, whose effect on the austenite transformation but seems to be ineffective as acicular ferrite nucleation sites.The demand use of MA steels in the international markets such as pipelines, construction, automotative component, pressure-vessels, offshore oil and gas industries, some of them are required for service in hostile environments. So it require increased strength (combined strength and impact toughness) and reduce weight and cost level. Becouse the microalloyed steel properties are uniform throughout a cross section, whereas those of quenched-and-tempered steel, are heterogeneous with the difference between the quenched hardened layer and non-quenched core area. The difference becomes greater as the diameter of the steel rod increases. Therefore, as the diameter increases, the benefit of the micro-alloyed steel increases. Also the high strength forging steels have traditonally developed their strength and toughness by quenching and tempering following hot forging.This multi-stage process extends production time and can cause distortion in complex shaped components, so its increases in production cost. In order to overcome the previous problem the microalloyed forging steels have been developed, which achieve their strength during air cooling after forging thus removing the need for secondary heat treatment. By contrast the air cooled structure is generally composed of coarse ferrite and pearlite and this can limit impact toughness. So its needs to be accompanied by refinement of microstruture. These the reason why small addition of alloying elements such as vanadium, niobium and /or titanium typically on the order of 0.1 to 0.2 mass pct or less is necessary to be used or added. In regard to microalloyed forging steels several studies have concentrated on determining the microstructural features that control toughness. Bainite represents one of the most fertile areas of steel research and development: transformation-assisted steels for automotive applications, inoculated acicular ferrite steels for the construction of oil platforms, high-strength alloys for the defence and aerospace industries, ultra-low carbon bainitic steels for the construction industries etc. The acicular ferrite has also been developed in a medium carbon forging steels or a low carbon steel and good combination of mechanical properties of medium carbon microalloyed steels are attributed to the dominant presence of fine ferrite-pearlite and a cicular ferrite microstructure, while the presence of bainitic sheaves leads to decrase in toughness. Acicular ferrite and bainite are usually considered to be formed by the same transformation mechanism. The acicular ferrite formation is a mechanism competitive with bainite formation. Acicular ferrite, as bainite, is formed by a shear-diffusional

mechanism. The main difference between acicular ferrite and bainite is related to the nucleation sites. The acicular ferrite is in fact intragranularly nucleate bainite. Both microstructures develop in the same range of temperature: below the high temperatures where ferrite and pearlite form, but above the martensite start temperature. The bainite initiates at the austenite grain boundaries, forming sheaves of parallel plates with the same crystallographic orientation, where acicular ferrite is nucleated intragranulary at nonmetallic inclusions.. There are several mechanisms proposed to explain why non-metallic inclusions favour the nucleation of ferrite : (i) the existence of local variations of the chemistry of the matrix; (ii) generation of strain-stress field around the inclusions due to the different thermal expansion coefficient of austenite and inclusion; (iii) improvement in the global energetic balance of the transformation by the reduction of the austenite-inclusion surface; (iv) the creation of low-energy surfaces between ferrite and inclusion with the existence of a good lattice matching between them.

The microstructure of acicular ferrite is less organized when compared with the ordinary bainite, the acicular ferrite have chaotic arrangement of interlocked plates. This microstructure is better suited to deflect propagation cleavage cracks and therefore more desirable from toughness point of view in comparison to bainite sheaves. In some recent studies, an improved toughness, observed in medium-carbon steels is associated with AF. The purpose of the present study is to clarify experimentally the TTT diagram of V-N and V/Ti Steel. Moreover the influence of isothermal transformation temperature and time on the nucleation of intra-granular ferrite and indirectly, on the development of the intra-granular acicular ferrite in micro-alloyed steel have been investigated.

2. PREVIOUS WORK

2.1 MICROALLOYED (MA) STEELS

The microalloyed steels (MA) or High Strength Low Alloy (HSLA) steels are steels in which small addition of alloying elements lead to intensive grain refinement and ∕ or precipitation hardening due to precipitation of stable carbides, nitrides or carbonitrides [1, 2] As in the previous investigation [2, 3, 7]. Precipitation hardening by fine carbonitride particles has long been recognized as an important mechanism for the strengthening of microalloyed steels. The use of microalloying in steels is based on the addition of small amounts of vanadium, niobium and/or titanium, [4] typically on the order of 0.1 to 0.2 mass pct or less. Precipitates (TiN, TiC, NbCN, NbC, NbN, VN and VC), will be form and its stability depend on the composition [5]. Other elements, such as aluminium for grain size refinement and boron for hardenability, and elements residual from steelmaking, may be also present in steels in small amounts, but such elements and their effects are generally considered to be outside of microalloying technology.Compared with carbon steels , MA steels offer not only a higher yield strength , which in most cases permits savings in weight or prolonged service life of components and structures,but also favourable working properties,such as improved formability and weldability ,and optimized service properties , such as resistance to brittle fracture ,to lamellar tearing,and hydrogen−induced or stress corrosion cracking [6].The main motives for developing MA steels were:significant increase in strength, leading to either lowering the construction weight or increase in carrying capacity, and a demand on world market for steels with good weldability for pipelines[1]. Several studies have shown that HAZ grain size can be

controlled by Ti addition because the titanium nitride is stable at the high temperatures attained in the fusion boundary region of the HAZ and can prevent grain growth of austenite in this region [8-12].

The choice of any material is based upon fitness for purpose. The main characteristics in select on a steel grade are; the yield strength, the tensile strength, (uniform) elongation, low temperature impact-toughness, work-hardening, hole-expansion ratio, fatigue performance and weldability. The microalloyed steel properties are uniform throughout a cross section, whereas those of quenched-and-tempered steel,are heterogeneous with the difference between the quenched hardened layer and non-quenched core area.The difference becomes greater as the diameter of the steel rod increases. Therefore, as the diameter increases, the benefit of the micro-alloyed steel increases.The medium carbon V-microalloyed (MA) steels are increasingly used instead of traditional Q&T steels in many applications, Table 2.1. However, as have been reported at several international conferences devoted on MA forging steels its used also in the construction, automobile, pressure-vessels, offshore oil and gas industries, and are designed to be in a corrosive environment [13-17]. Figure 2.1, show some of examples of hot strip steel applied in the automotive and construction industry. In respect to automotive applications it is importance of fatigue resistance is obvious for a steel to be used in automobile components that are routinely subjected to cyclic loading [18]. However the main driving force to apply steel with higher strength than mild steel is the possibility of weight savings, based on the results in Fig. 2.2 , which not only results in reduced fabrication costs, but in case of automotive application also improves fuel economy [9,13,16,19-24].

Table 2.1. Application for microalloyed forging steels [24].

Crankshafts	Pistonshafts
Connecting Rods	Axle Shafts
U-Bolts for Leaf Springs	Suspension Arms
Steering Knuckle Supports	Transmission Shafts
Antisway Bars	Wheel Hubs
Induction Hardened Gears	Steering Arms
Drive Couplings	Axle Beams
Fasteners	Pipe Fittings
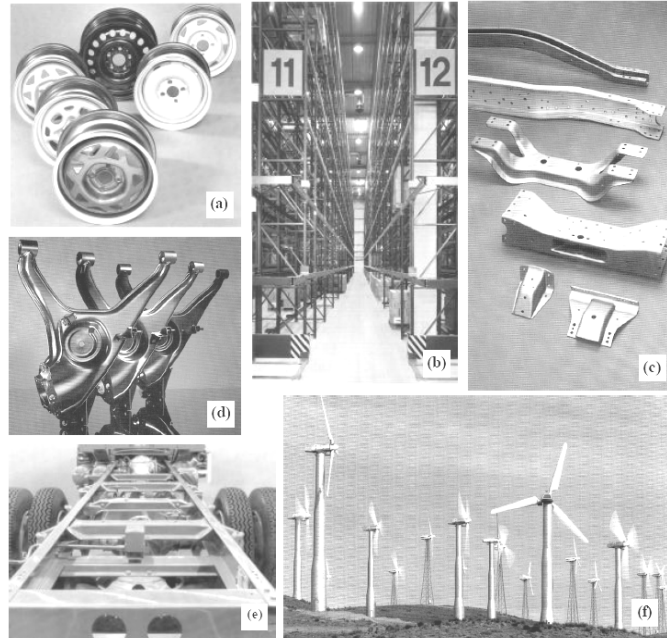
Figure 2.1: Examples of hot rolled HSLA strip steels for automotive and construction applications: (a) Passenger car wheels; (b) High level racking system; (c) Various profiles for automobiles; (d) Semi-trailing arm; (e) Truck frame; and (f) Masts for wind powered generators [25].
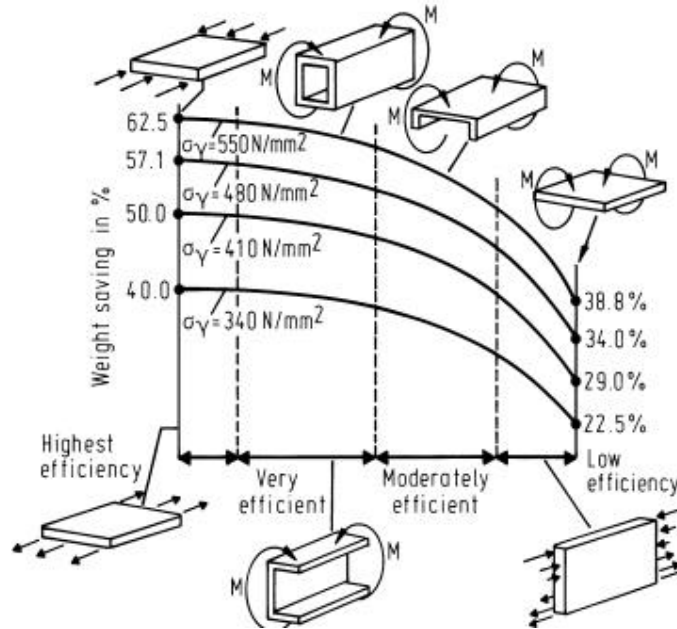
Figure 2.2: Potential weight savings when substituting a 200MPa yield strength Steel [26].

The difference in proceesing route between conventional quenched-tempered steels and microalloyed steels is shown in Fig. 2.3(a,b). The a major benefit, therefore, of MA is the

fact that save energy by eliminating the heat treatment from the production sequence as shown in Fig. 2.3 (b) i.e reduce manufacturing cost [23,24]. So there is large market for steels with strengths less than 1000 MPa, and where the total alloy concentration rarely exceeds 2 wt%. Bainitic steels are well suited for applications within these constraints. The most modern bainitic steels are designed with much reduced carbon and other alloying element concentrations. They are then processed using accelerated cooling in order to obtain the necessary bainitic microstructure. Advances in rolling technology have led to the ability to cool the steel plate rapidly during the rolling process, without causing undue distortion. This has led to the development of 'accelerated cooled steels' which have a bainitic microstructure, can be highly formable and compete with conventional control-rolled steels.The reduced alloy concentration not only gives better weldability, but also a larger strength due to the refined bainitic microstructure. The ultra-highstrength steels consist of mixtures of bainite ferrite, martensite and retained austenite. They have an enhanced hardenability due to manganese, chromium and nickel additions, and usually also contain silicon in order to prevent the formation of cementite [27-30].

High-strength steels are made with very low impurity and inclusion in concentrations, so that the steel then becomes susceptible to the formation of cementite particles, which therefore have to be avoided or refined.

Medium-strength steels with the same microstructure but somewhat reduced alloy content have found applications in the automobile industry as crash reinforcement bars to protect against sidewise impact. Another major advance in the automobile industry has been in the application of bainitic forging alloys to the manufacture of components such as cam shafts. These were previously made of martensitic steels by forging, hardening, tempering, straightening and finally stress-relieving. All of these operations are now replaced by controlled cooling from the die forging temperature, to generate the bainitic microstructure, with cost savings which on occasions have made the difference between profit and loss for the entire unit as illustrated in Figure 2.3.
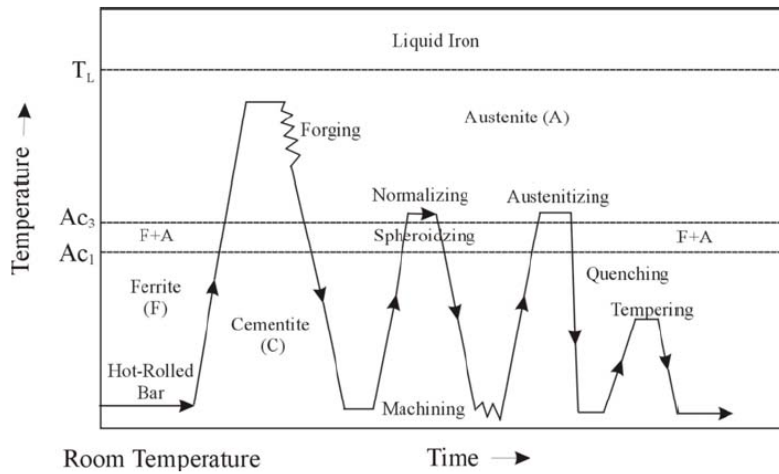
(a)
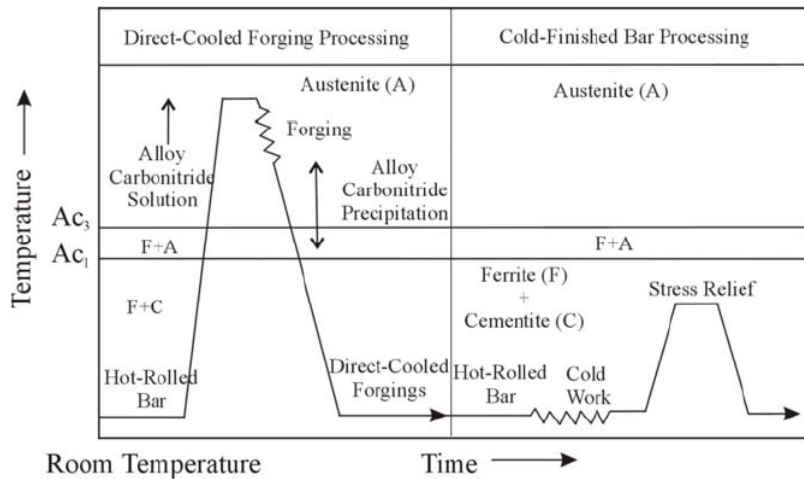
(b)

Fig.2.3. Temperature-time processing schedules for producing (a) quench and tempered forging steels (b) micro-alloyed forging steels [24].

Creep-resistant bainitic steels have been used successfully in the power generation industry since the early 1940s. Their hardenability has to be such that components as large as 1m in diameter can be cooled continuously to generate a bainitic microstructure throughout the section.The alloys contain chromium and molybdenum, which serve to enhance hardenability but also, during subsequent heat-treatment, cause the precipitation of alloy carbides which greatly improve the creep resistance [19].By contrast the inoculating molten steel with controlled additions of non-metallic particles, bainite can be induced to nucleate intragranularly on the inclusions, rather than from the austenite grain surfaces. This

intragranularly nucleated bainite is called 'acicular ferrite' [19]. It is a much more disorganized microstructure with a larger ability to deflect cracks. Inoculated steels are now available commercially and are being used in demanding structural applications such as the fabrication of oil rigs for hostile environments. The relationship of structure and properties and processing control (SPPC technology) plays a vital role in controlling the properties of hot rolled products which indicate that the modeling of phase transformation behavior as one of most important parts, which is required for safe performance application [31,32].For safe MA forging application it required development program search for processing parameters & structure to improve the fracture toughness [13].The control of austenite grain size and precipitation strengthening are important factors in the development of the final mechanical properties of the product i.e understanding the precipitation behavior that found at different points in the thermomechanical processing of the steel (the size, morphology, chemical composition, and crystal structure of precipitates) i.e by steel design. As reported by [33-35], the design of novel high strength bainitic steels for defence applications for example with a bainitic matrix which necessitated a Charpy energy of about 40 J at - 40 $^{\circ}$C, a fracture toughness (K_{IC}) of 125 MPa m$^{1/2}$, yield strength of1000 MPa, ultimate tensile strength of 1100 MPa and a minimum elongation of 12%. Regarding to precipitation strengthening due to particle present in the steel. The type of particles can be classified into three groups. The first group includes the larger sized inclusions, encompassing MnS and TiN particles of sizes greater than approximately, 2 μm, which can easily be observed by optical microscopy. These types of particles have been observed to be ineffective as acicular ferrite nucleation sites. In the second group are the inclusions whose size is between, approximately, 0.5 and 2 μm, which have been observed to be seen the most effective in promoting the nucleation of ferrite plates. The larger sizes belonging to this group can be seen by optical microscopy, but the majority of this group are only visible using electron microscopy and the composition of these particles has been analyzed using energy-dispersive spectrometry (EDS),examined by transmission electron microscopy TEM. Finally, the third group includes all the inclusions smaller than 200 to 300 nm, whose effect on the austenite transformation but seems to be ineffective as acicular ferrite nucleation sites [36].However the steels with a mixed microstructure of allotriomorphic ferrite, bainitic ferrite, retained austenite and martensite have potentially good combinations of high strength and formability [37,38].Components made of microalloyed forging steels have always suffered from lower toughness value

compared to their quenched and tempered counter parts. This has limited their application particularly for safety compnents where both high strength and toughness properties are required.

Because the first generation of microalloyed steels was (C-Mn-V steels) had ferrite-pearlite microstructure and low toughness values were associated to the inherent cleavage fracture made of pearlite. Therefore researches have been focused on eliminating or minimizing the amount of pearlite that formed during post forge cooling [13].   .

In recent years the trend has been to modify the ferrite-pearlite microstructure with high impact touhness microstructure such as acicular ferrite through a judicious control of thermomecanical processing parameters. The primary goal of a modern thermo-mechanical treatment is to refine the grain structure in order to obtain a good combination of mechanical properties. The ultimate objective is the production of high strength-high toughness parts suitable for application in automobile safety partes.

The microalloying elements are added to high strength low alloy (HSLA) steels for two purposes: (i) produce grain refinement and/or (ii) precipitation strengthening.

In both cases the desired effects are achieved by intelligent use of precipitation reaction of microalloy carbo-nitrides both in austenite prior to transformation and in ferrite, during and after transformation [39-41].In the new approach to grain refinement microalloyin elements are directly used to promote nucleation of intragranular polygonal ferrite or acicular ferrite AF inside the austenite grains [39,40].Good combination of strength, fracture toughness and weldability of V-microalloyed HSLA steels in the as hot rolled condition can be obtained by careful choice of thermo-mechanical controlled processes (TMCP) [41, 42].

2.2   TIME-TEMPERATURE-TRANSFORMATION (TTT) DIAGRAMS

TTT diagram measure the rate of transformation at a constant temperature. In other words a sample is austenitised and then cooled rapidly to a lower temperature and held at that temperature whilst the rate of transformation is measured, for example by dilatometry. Obviously a large number of experiments is required to build up a complete TTT diagram.

There are two main types of transformation diagram that are helpful in selecting the optimum steel and processing route to achieve a given set of properties. These are time-temperature transformation (TTT) and continuous cooling transformation (CCT) diagrams. CCT diagrams are generally more appropriate for engineering applications as components are cooled (air cooled, furnace cooled, quenched etc.) from a processing temperature as this is more economic than transferring to a separate furnace for an isothermal treatment.As shown in figure 2.4. The TTT diagram composed of two overlapping 'C' curves and for low-alloy steel TTT curves separated by existence of bays region and the experiments indicate that in low-alloy steels containing relatively large quantites of alloying elements, the bay is replaced by a break in the TTT diagram, so that the overlall appearance becomes that of two C curves separated by a stasis region where no transformation occurs despite prolonged heat treatment.One of which represents diffusional transformations (equiaxed or poloygonal ferrite and pearlite) and the other, three common displacive transformations in steel includeWidmanstatten ferrite, bainite and martensite [15,43]. By contrast not all three displacive reactions found in every steel and it is depends on quantities of austenite stabilizing elements [15].(driving force for transformation decrease as the alloy content increase). Sharma and Purdy [44] indicated that the incubation periods normally associated with TTT diagram (i.e. the time period before the onset of a detectable amount of isothermal transformation). Examination of a time–temperature–transformation (TTT) diagram for carbon steel (Fig. 2.4), bearing in mind the fact that the bainite forms by the decomposition of austenite at a temperature which is above Ms, but below that at which fine pearlite form (All bainite forms below the T_0 temperature) [45].
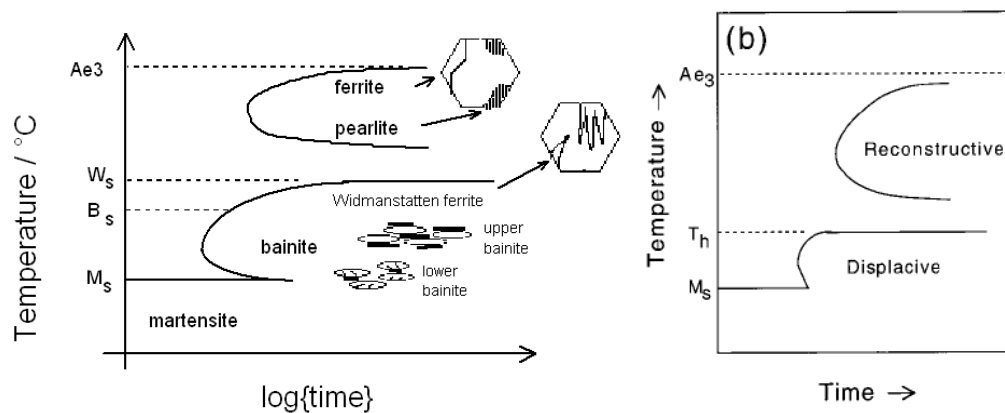

Fig. 2.4 TTT diagram showing the different domains of transformation [19].

The transformation of acicular ferrite is similar to that of bainite as shown in fig.2.4, it is form below the transformation temperature of pro-eutectoid ferrite and pearlite and above the martensite start temperature but the nucleation sites are different [15, 46-50]. Bainite is a non-lameller   aggregate of carbides and plate shaped ferrite as shown in fig.2.4, while the transformation to pearlite reaction is essentially occur   at high temperature.The nature of bainite changes as the transformation temperature is lowered. Two main forms can be identified: upper and lower bainite. As shown in figure 2.5.
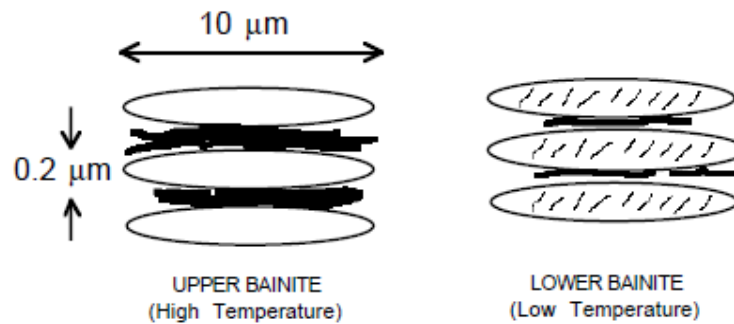
Fig. 2.5. Schematic illustration of the microstructure of upper and lower bainite [51].
.

2.2.1 TRANSFORMATION-START-TEMPERATURE

It is a common observation that the Widmanstatten ferrite-start (W_S) and bainite-start (B_S) temperatures are more sensitive to the steel composition than is the A_{e3} temperatur.The TTT diagram Fig. 2.4, which consist essentially of two C-curves.The lower C-curve has a characteristic flat top at temperature T_h, which is the highest temperature at which ferrite can form by displacive transformation.The transformation product at T_h can be Widmanstatten ferrite or bainite, but it is found no need to distinguish between these phases for the purpose of nucleation. The same nucleus can develop into either phase depending on the prevailing thermodynamic conditions. As we know the carbon must partition during the nucleation stage in order to obtain a reduction in free energy. By contrast diffusioless nucleation would in some cases lead to an increase in the free energy. According to Bhadeshia [52], the T_h can be estimated for any sreel and the free energy change ΔG_m can be caculated from readily available thermodynamic data. A full description of this calculation is given in 2.3.3.1 Thermodynamics of Bainite Formation. As we mentioned before the nucleus is identical for Widmanstatten ferrite and bainite, but it is possible to distinguish them by growth process. If

diffusionless growth cannot be sustained at T_h then the nucleus develops into Widmanstatten ferrite.

So that Th is identified with WS. A large undercooling is necessary before bainite can be stimulated. However if the driving force at Th is sufficient to account for diffusionless growt, then Th = BS and Widmanstatten ferrite does not form at all. However, theWidmanstatten ferrite and bainite is suppressed to temperature below MS in which case they do not form at all [15]. A ccording to the data fitted in Fig. 2.42, the bainite is expected to form below the To when:

$$\Delta G^{\gamma \rightarrow \alpha} < -G_{SB}$$

$$\Delta G_m < G_N$$

Where, $\Delta G\gamma \rightarrow \alpha$ is the free-energy change for the transformation, and GSB is the stored energy of bainite (about 400 J /mol).However the solubility data are available in some equations for example VN and VC [19, 53-56]. However a full description of this behaviour for Nb – C, Nb – N and Nb–C–N system is given in Ref. [46, 57-69].

$$\text{Log } [V][N] = -7840/TVN + 3.02 \qquad (2.1)$$

$$\text{Log } [V][C] = -9500/TVC + 6.72 \qquad (2.2)$$

Where [Nb] , [C] , and [N] are the concentrations in weight percent, and T is the absolute temperature.

2.2.2. QUANTITATIVE ESTIMATION OF TRANSFORMATION TEMPERATURE

The upper and lower bainite is expected to exist during isothermal transformation and it depend on the time required to decaburise a plate of ferrite (t_d) and time interval necessary to obtain a detectable amount of cementite precipitation in the ferrite (t_θ). i.e (rate of decarburization and precipitation) Therefore and according to Fig. 2.6, if the $t_d < t_\theta$ then no lower bainite exist and upper bainite is obtained, and vice vers.
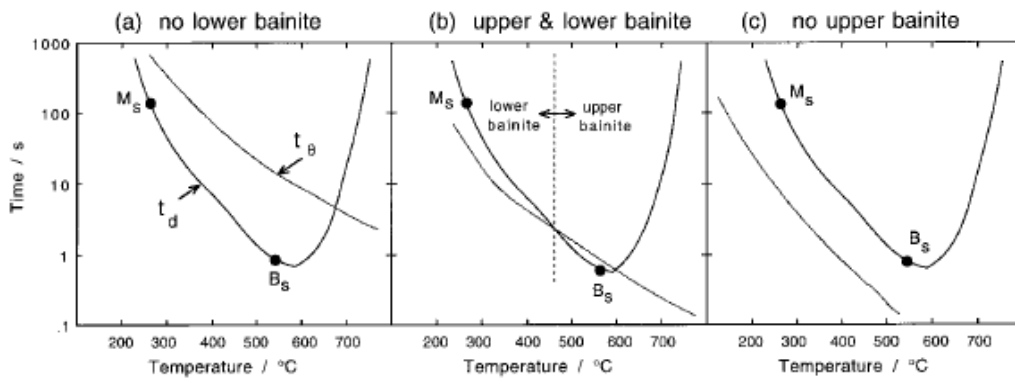
Fig. 2.6 Show how the variation of t_d and t_θ can lead to (a) Steel incapable of transforming to lower bainite (b) Steel able to transform to upper or lower bainite (c) Steel able to transform to lower bainite (no upper bainite) [15].

Some caculated data [51] on the plain carbon steels are presented in Fig. 2.7. Indicate that the lower bainite should not be observed in plain carbon steels with carbon concentrations less than 0.32 wt%. Furthermore, only lower bainite (no upper bainite) is expected in steels with carbon concentrations exceedinig 0.4 wt%. However steels containing between 0.32 and 0.4 wt% of carbon should exhibit both upper and lower bainite, depending on the reaction temperatures. As indicated in Fig. 2.7. Lower bainite can be observed in plain carbon steel with more than 0.32 wt% carbon. But as the transformation proceeds, the austenite becomes enriched in carbon. This lead to the possibility of upper bainite being followed by lower bainite during isothermal transformation.That reason why mixed microstructures can be obtained in plain carbon steel containing less than 0.32 wt% carbon, especially if the rate of carbide precipitation from the austenite is slow enough to allow the austenite to become enriched. By contrast , the mixtures of upper and lower bainite can be obtained by transformation at temperatures just above LB_S (Lower Bainite Start Temperature).
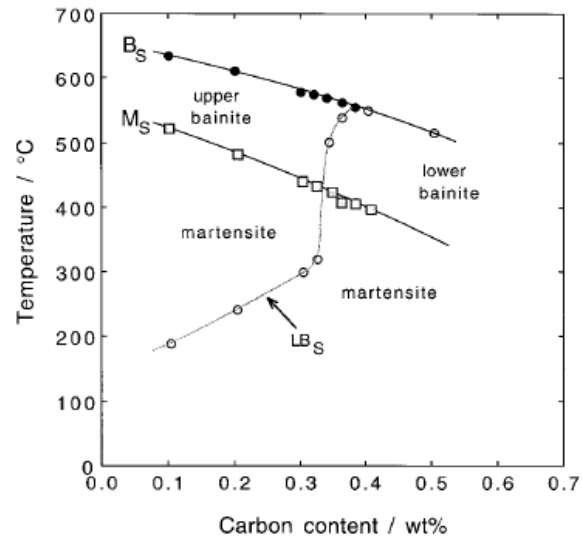
Fig. 2.7 Calculated LB$_S$ (Lower Bainite Transformation Start Temperature), B$_S$ and M$_S$ temperatures as function of transformation temperature [51].

2.2.2.1.   Isothermal Transformation Kinetics

The progress of an isothermal phase transformation can be conveniently represented by Avrami equation :

$$ X = 1 - \exp\left(k \cdot t^n \right) $$

(2.3)

where:

X – fraction of transformed structure

t – time for X

n - Avrami exponent

k – constant

Increase of transformed fraction (*f*) with time elapsing, t, during isothermal transformation of temperature T, can be illustrated on TTT diagram. One example of TTT diagram is shown on figure 2.8 [70]. In the case of transformation γ→α, *f* is the volume fraction of β phase in any moment. Therefore values of are limited to range between 0 and 1.

Factors affecting realtion $f(t,T)$ are: nucleation rate, growth rate and distribution of preferential places for nucleation, overlaping of neighbouring diffusion fields of new grains, impeachment of new grains etc.

Regarding austenite decomposition, type of transformation γ→α, transformation is finished at the moment when complete fraction of α phase is transformed. During transformation, growth rate of new grains can be treated as constant, implying that transformation will be finished not because of the decrease in grain growth rate, but because of impeachment of new grains.

During γ→α transformation, nuclei of α are formed continuously during transformation, with constant rate N. Assuming that newly formed nuclei grow in sphere shape manner, with radii r, with growth rate v, the volume of all nucleii formed in starting time (boundary condition when t=0), can be described with following equation:
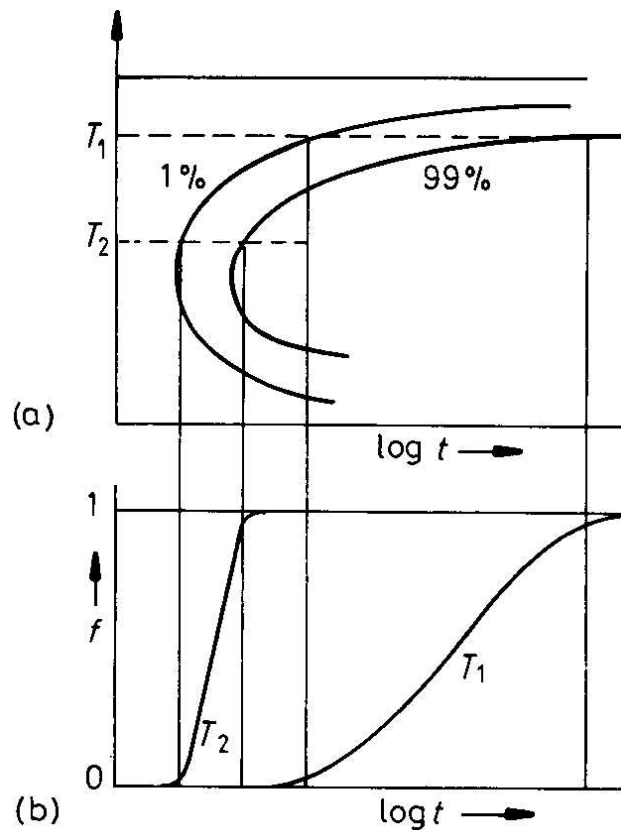

Fig.2.8. Diagram of isothermal decomposition [70]

$$V = \frac{4}{3}\pi r^3 = \frac{4}{3}\pi(vt)^3$$

(2.4)

Total volume of all nucleii formed up to time τ can be described with next equation:

$$V = \frac{4}{3}\pi v(t-\tau)^3$$

(2.5)

Number of nuclei formed during increment of time $d\tau$ is equal to $Nd\tau$, per unit volume of strating (non-transformed) phase γ. Assuming that grains will not get in contact up to the end of transformation, for unit volume, fraction transformed f, can be calculated as:

$$f = \Sigma V' = \frac{4}{3}\pi N v^3 \int_0^t (t-\tau)^3 \, d\tau$$

(2.6)

i.e.

$$f = \frac{4}{3}\pi N v^3 t^4$$

(2.7)

This equation is valid only in the case when f«1. With time elapsing the probability for contact between new α grains increases, leading to decrease in transformation rate. Taking into account random distribution of nucleation sites, both for short and long times, transformation kinetics can be described with following equation:

$$f = 1 - \exp\left(-\frac{4}{3}\pi N v^3 t^4\right)$$

(2.8)

For short times, this equation is equal to equation (2.7) because 1-exp(-z)≈z. Also, in the case of long time, (t→∞); f→ 1.

Using replacement,

$$k = \left(\frac{4}{3}\pi N v^3\right)$$

(2.9)

Equation (2.9) is equal to (2.3). Equation (2.3) is known as JMAK (**J**ohnson-**M**ehl-**A**vrami-**K**olmogorov), or more often *Avrami equation*.

After double ln of eqation (2.3):

$$\ln\ln\frac{1}{1-f} = \ln k + n \cdot \ln t \qquad (2.10)$$

Avrami exponent n, is derived as slope from equation (2.10). Theoretically, values of n are in the range 1 to 4. In the case when there is no change of transformation mechanism value of n is constant and shows no temperature dependence.

Driving force for transformation is lower energy of α than γ phase; therefore there was a need or quantification of transformation kinetics that takes into account the influence of material and processing parameters. Therefore, equation (2.3) can be rewritten::

$$X = 1 - \exp\left[-B\left(\frac{t}{t_F}\right)^n\right] \qquad (2.11)$$

where:

X - fraction of transformed structure

t – time

t_F – time for transformation of fraction

n - Avrami exponent

B – constant calculated from equation (2.12):

$$B = -\ln(1-F) \qquad (2.12)$$

Usually, this is time for 50% of transformed fraction (F=0.5), and equation (2.11) can be rewritten:

$$X = 1 - \exp\left[-0.693\left(\frac{t}{t_{0.5}}\right)^n\right] \qquad (2.13)$$

where

$t_{0.5}$ – time for 50% of transformation,s

Time for 50% transformation is calculated from eq(2.14) [71-81].

$$t_{0.5} = A\exp(\frac{Q}{RT})$$

(2.14)

where

A – constant

T – absolute temperature

R – universal gas constant

Q – activation energy for transformation

2.3. DECOMPOSITION OF AUSTENITE AND MECHANISMS OF TRANSFORMATION

The rate at which austenite decomposes to form ferrite, pearlite and bainite is dependent on the composition of the steel, as well as on other factors such as the austenite grain size, and the degree of homogeneity in the distribution of the alloying elements [19]. One of the reasons why there is a great variety of microstructures in steels is because the same allotropic transition can occur with a variety of ways in which the atoms can move to achieve the change in crystal structure. The austenite can transform to ferrite either by breaking all the bonds and rearranging the atoms into an alternative pattern (reconstructive transformation), or by homogeneously deforming the original pattern into a new crystal structure (displacive or shear transformation) without diffusion. All the phase transformations in steels can be discussed in the context of these two mechanisms as illustrated in Figure 2.9 [19] The pearlite is the good example of a reconstructive transformation. All experimentall data show that the pearlite grows with the diffusion of substitutional solute atoms [82,83].The substitutional solutes do not diffuse at all during displacive transformation. For this reason, the observed effect of solutes, on the rate of transformation, is larger for reconstructive than for displacive transformation (Fig.2.10)

Dubé [19], proposed a classification of morphologies of ferrite which occur as the γ/α transformation temperature is lowered. Dubé recognized four well-defined morphologies based on optical microscopy:

RECONSTRUCTIVE

Diffusion of all atoms during nucleation and growth. Sluggish below about 850 K.

DISPLACIVE

Invariant plane strain shape deformation with large shear component.
No iron or substitutional solute diffusion.
Thin plate shape.

ALLOTRIOMORPHIC FERRITE

IDIOMORPHIC FERRITE

WIDMANSTÄTTEN FERRITE

Carbon diffusion during paraequilibrium nucleation & growth.

MASSIVE FERRITE

No change in bulk composition.

BAINITE & ACICULAR FERRITE

Carbon diffusion during paraequilibrium nucleation. No diffusion during growth.

PEARLITE

Cooperative growth of ferrite & cementite.

MARTENSITE

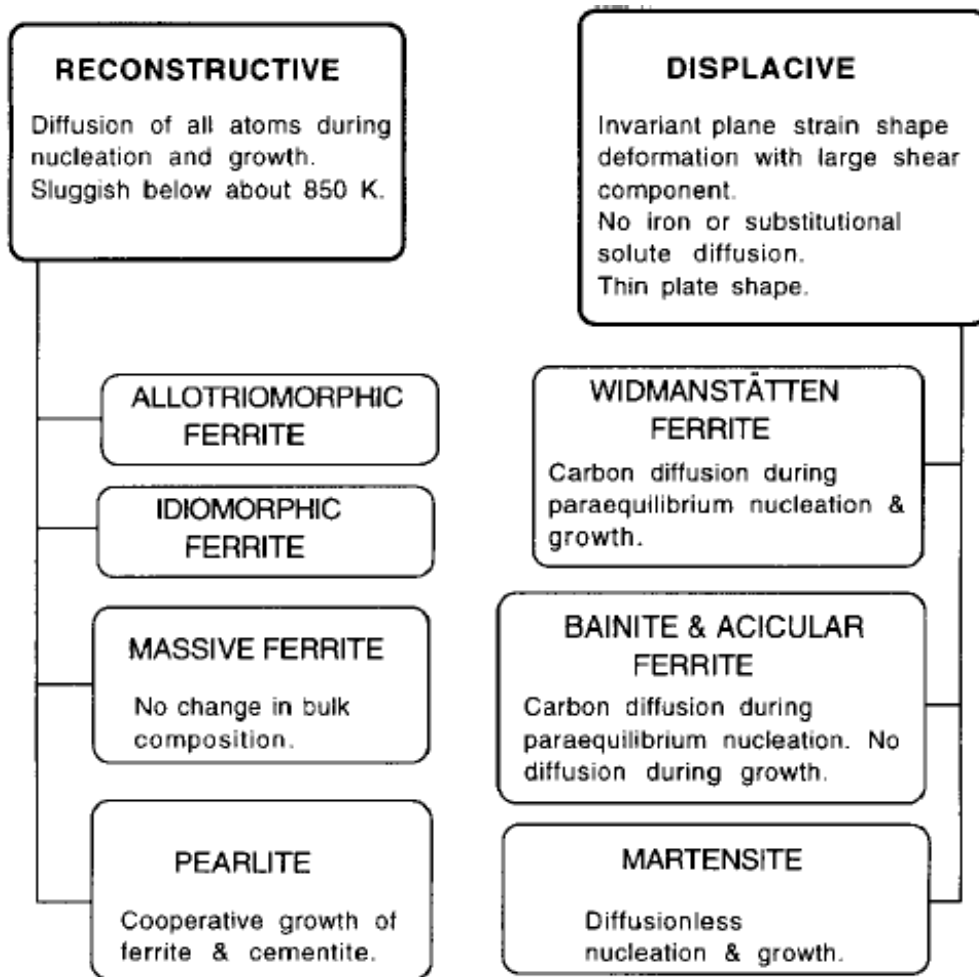Diffusionless nucleation & growth.

Fig.2.9. Summary of the variety of phases generated by the decomposition of austenite [15,19,84].
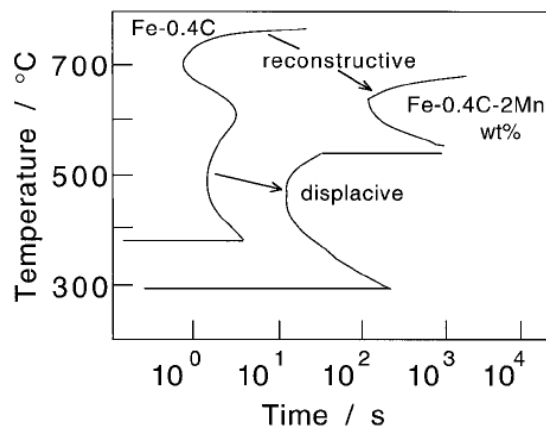

Fig.2.10 TTT diagram showing the larger retarding effect that manganese has on a reconstructive transformation compared with displacive [15].

2.3.1. PRO-EUTECTOID FERRITE

Grain boundary allotriomorphs are the first morphology to appear over the whole range of composition and temperature and has a shape which does not reflect its internal crystalline symmetry. This is because it tends to nucleate at the austenite grain surfaces, forming layers which follow the grain boundary contours (Fig. 2.11a).The allotriomorph is in contact with at least two of the austenite grains and will have a random orientation with one of them, but an orientation which is more coherent with the other. It may, therefore, be crystallographically facetted on one side but with a curved boundary on the other side. However, at the highest temperatures (above 800 $^{\circ}$C), they predominate by growing along the boundaries, and also into the grains to give a well-defined grain structure, generally referred to as equi-axed ferrite. The allotriomorphs nucleate having a reproducible orientation relationship such as the approximate Kurdjumov–Sachs orientation with one austenite grain (γ_1) [15, 19]:

$$\{111\}_{\gamma_1} \parallel \{110\}_\alpha,$$

$$\langle 1\bar{1}0 \rangle_{\gamma_1} \parallel \langle 1\bar{1}1 \rangle_\alpha.$$

As well as during the isothermal transformation processes, the formation of proeutectoid ferrite from austenite occurs by a diffusionally controlled reaction which consists of subsequent events:

$$\textbf{Incubation} \rightarrow \textbf{Nucleation} \rightarrow \textbf{Growth} \rightarrow \textbf{Impingement}$$

Incubation

The incubation can be defined as the minimum time at which it is not possible to find some ferrite nucleated at the austenite grain boundary.

Nucleation of Proeutectoid Ferrite

Many studies have been done on nucleation of proeutectoid ferrite [85-87]. In general, twoнјьењtypes of nucleation are possible during the phase transformation [85]: homogeneous and heterogeneous. Proeutectoid ferrite nucleates heterogeneously in recrystallized austenite, the most probable nucleation sites will be grain surface, edgesand corners, as shown in Fig. 2.11(g).
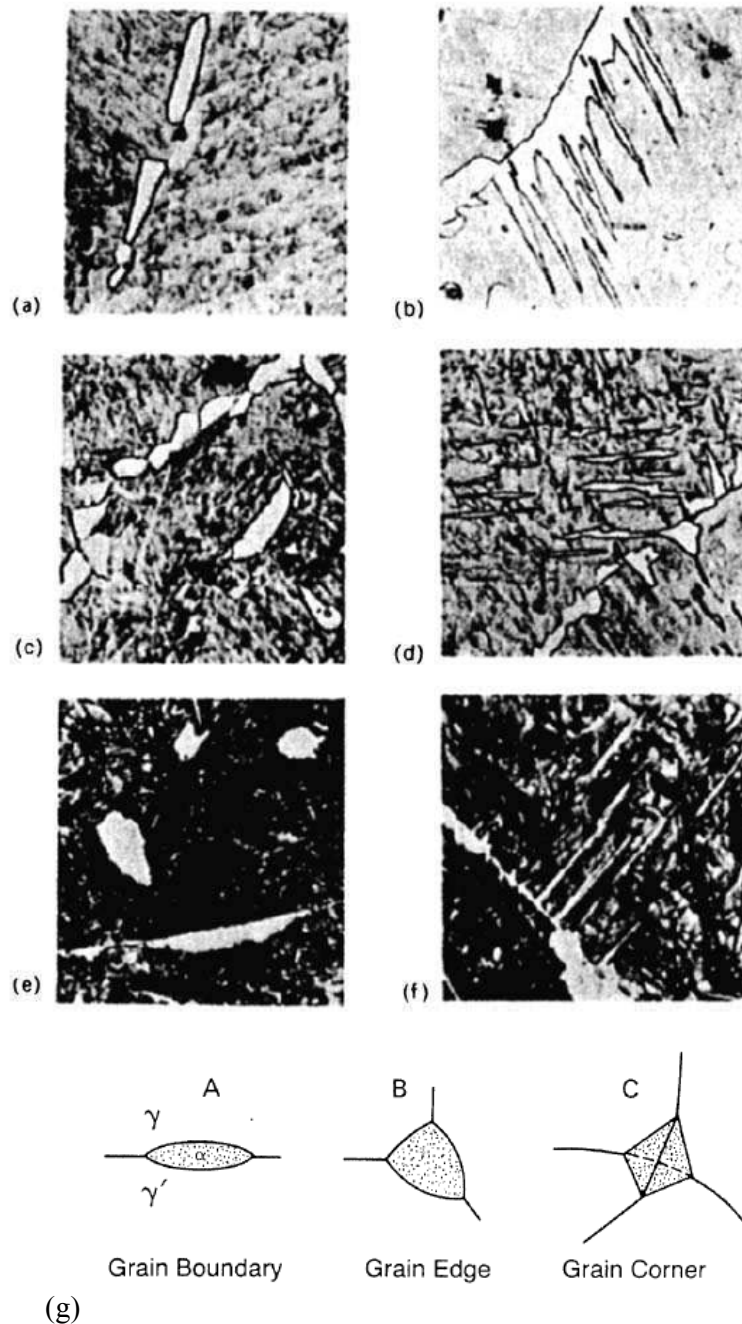
Fig. 2.11(a)Grain boundary allotriomorphs of ferrite. (b)Widmanstätten ferrite growing from grain boundary ferrite. (c)Grain boundary allotriomorphs and intragranular idiomorphs of ferrite. (d)Intragranular Widmanstätten ferrite plates. (e)Grain boundary allotriomorphs and intragranular idiomorphs of cementite. (f)Widmanstätten cementite: optical micrographs, (a)–(d) ×500, (e) and (f) ×350 [19]. (g) Heterogeneous nucleation sites in fully recrystallized austenite [85].
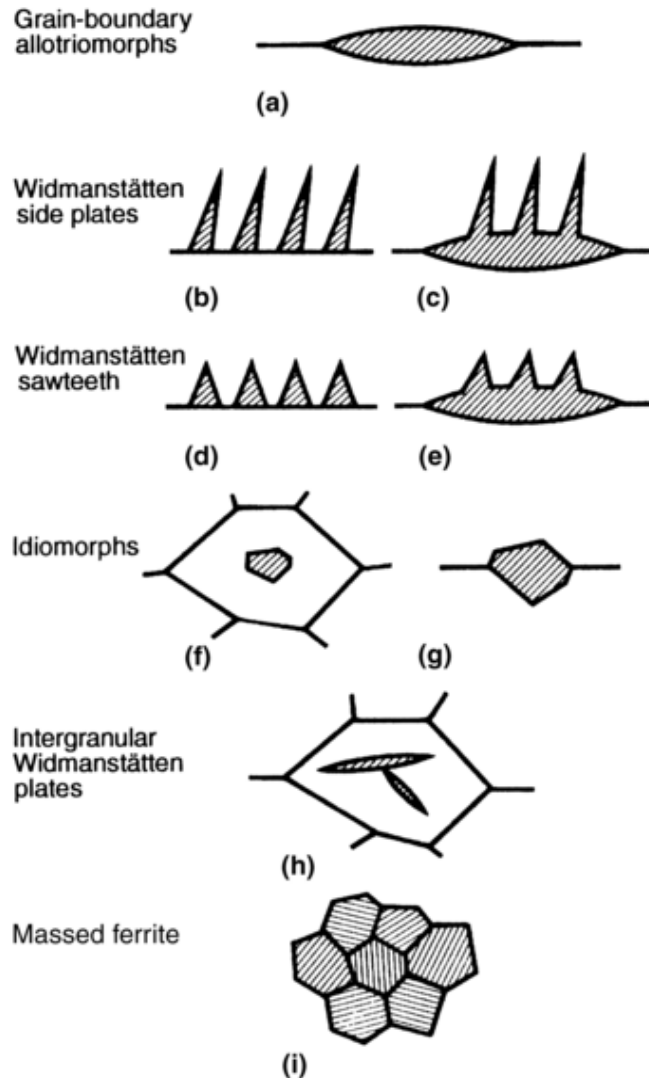
Fig. 2.11-continued. Schematic illustration of ferrite morphologies (i) Grain-boundary allotriomorphs,(b) Primary Widmanstätten(c) Secondary Widmanstätten (d) Primary Widmanstätten sawteeth grow from grain boundaries with a triangular appearance(e) Secondary Widmanstätten sawteeth (f) Idiomorphs that are equiaxed but faceted ferrite form almost entirely in the interior of parent austenite grains. (g)Grain-boundary idiomorphs are not normally observed in steels. (h) Intergranular Widmanstätten plates in parent grain of austenite. (i) Massed ferrite [123]

Growth

Once ferrite nucleated at boundary sites, growth of ferrite will proceed, being driven by the difference in free energy between the austenite and ferrite phases.The kinetics can be divided into thickening and lengthening (Fig.2.12). As reported by Simonen et.al. [88]. Lengthening kinetics of proeutectoid ferrite provides results indicating that the planar interface-carbon-controlled and edge mechanisms takes place during transformation. Since

the lengthening of ferrite is much faster than thickening, and austenite grain boundaries are usually completely covered by ferrite grains before apprecible growth by thickening has occurred [89].
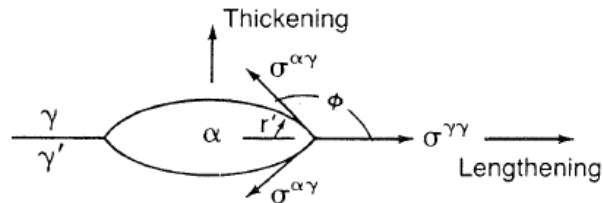

Fig. 2.12 Thickening and lengthening of grain boundary allotriomorphic [90].

Impingement

At the later stages of the transformation, the carbon diffusion field from adjacent ferrite grains, each being created by rejection of carbon into remaining austenite,overlap.The process reduces the carbon gradient at the interface and thus slows down the carbon diffusion.The phenomenon is called soft impingement, another type of impingement which occurs when ferrite grains impinge on each other is known as hard impingement.The parabolic growth law does not hold anymore when either type of impingement occurs [88].

2.3.1.1 Widmanstatten Ferrite Morphology

Widmanstätten ferrite plates or laths: These plates grow along well-defined planes of the austenite and do not grow across the austenite grain boundaries. Primary Widmanstätten ferrite grows directly from the austenite grain surfaces, whereas secondary Widmanstätten ferrite develops from allotriomorphs of ferrite already present in the microstructure (Fig. 2.11b).However as shown in figure 2.13. Primary Widmanstatten ferrite either directly grows from the austenite grain surfaces, whereas secondary Widmanstatten ferrite develops from any allotriomorphic ferrite that may be present in the microstructure [45]. Hillert pointed out that ferrite could inherit the content of alloying elements from austenite even if it partitions at the interface [91,92].The Widmanstatten ferrite can form at temperatures below to the Ae_3 temperature when

$$\Delta G^{\gamma \to \dot{\gamma} + \alpha} < - G_{SW} \ \ (\Delta Gm < GN)$$

Where G_{SW} is the stored energy of Widmanstatten ferrite and hence can occur at very low driving forces; the under cooling needed amounts to a free energy change of only 50 J.mol^{-1}.This is much less

than required to sustain diffusionless transformation and $\Delta G^{\gamma \rightarrow \dot{\gamma} + \alpha}$ is the free energy change associated with the paraequilibrium growth of Widmanstatten ferrite [15,45,93].
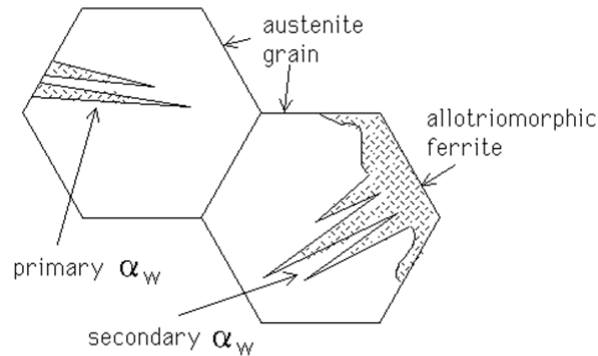
austenite
grain

allotriomorphic
ferrite

primary α_W

secondary α_W

Fig 2.13. Morphology of primary and secondary Widmanstatten ferrite [45].

2.3.1.2. Idiomorphic Ferrite Formation

The idiomorphic ferrite or intragranular idiomorphs ferrite are equi-axed crystals which nucleate inside the austenite grains (Fig. 2.11c), usually on non-metalic inclusions present in the steel. An idiomorph forms without contact with the austenite grain surfaces and has a shape which some shows crystallographic facets.These type of ferrite,which grows by diffusional mechanisms, can be classified into two main forms: allotriomorphic ferrite and idiomorphic ferrite [94,95].Allotriomorphic ferrite nucleates at the prior austenite grain boundaries and tends to grow along the austenite boundaries at a rate faster than in the normal direction to the boundary plane (Figure 2.14). By contrast, idiomorphic ferrite nucleates at the inclusions inside the austenite grains and can be identified in the microstructure by its equiaxed morphology (Figure 2.14). Consequently, the balance between the number of intragranular nucleation sites and the number of sites at the austenite grain boundarie is a very important factor in the competitive process of allotriomorphic-idiomorphic ferrite formation.
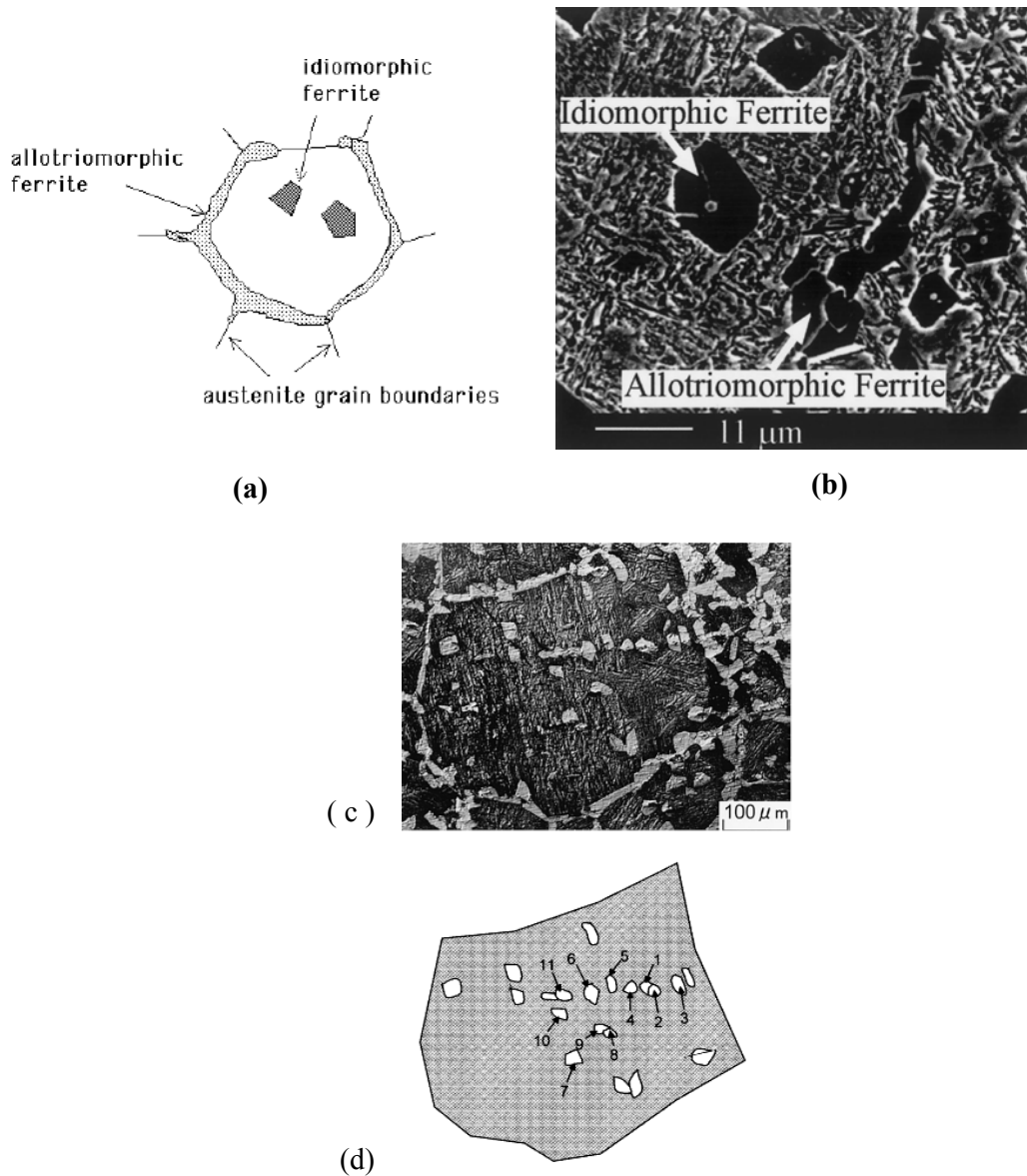
Fig. 2.14 (a.b) Idiomorphic and Allotriomorphic ferrite: (a) Schematic illustration [45]; (b) SEM micrograph [94]; (c,d) Optical microstructure of the Fe–1.5Mn–0.2C alloy transformed at 973 K for 240 s; (b) schematic representation of intragranular ferrites in (a) [96].

It is well known that an increase in the PAGS leads to a reduction in the number of nucleation sites at the austenite grain boundaries. Therefore, an increase in the PAGS indirectly favors the intragranular nucleation of ferrite: then, the formation of idiomorphic ferrite, rather than allotriomorphic ferrite, is enhanced. Likewise, as the PAGS increases, the number of inclusions trapped inside the austenite grains increases, which promotes the intragranular nucleation of ferrite.

2.3.1.3. Intragranular plates

These plates are similar to those growing from the grain boundaries, but they nucleate entirely within the austenite grains (Fig. 2.11d).

2.3.1.4. The Effect of Alloying Elements on the Ferrite Reaction

The alloying elements can be divided into three categories [19]:

(1) Elements which enter only the ferrite phase; such as nickel, copper, phosphorus and silicon, which, in transformable steels, are normally found in solid solution in the ferrite phase.

(2) Elements which form stable carbides (carbide-forming elements) and also enter the ferrite phase. Typical examples are manganese, chromium, molybdenum, vanadium, titanium, tungsten and niobium. At higher concentrations most will form alloy carbides, which are thermodynamically more stable than cementite. Manganese carbide is not found in steels, but instead manganese enters readily into solid solution in Fe3C. The carbide-forming elements are usually present greatly in excess of the amounts needed in the carbide phase, which are determined primarily by the carbon content of the steel.The remainder enter into solid solution in the ferrite with the non-carbide-forming elements nickel and silicon. Some of these elements, notably titanium, tungsten and molybdenum, produce substantial solid solution hardening of ferrite. The majority of alloying elements used in steels fall into there category.

(3) Elements which enter only the carbide phase. Nitrogen is the most important element and it forms carbonitrides with iron and many alloying elements. However, in the presence of certain very strong nitride-forming elements, e.g. titanium and aluminium, separate alloy nitride phases can occur.

Two basically different modes of growth of pre-eutectoid ferrite in austenite have been observed. The actual mode observed is dependent on the composition of the alloy but the two modes may occur at different temperatures in the same alloy. The modes are:

(a) Growth with partition of the alloying element between α and γ under local equilibrium conditions.

(b) Growth with no partition of alloying element between α and γ under local equilibrium conditions.

In the first mode, the ferrite grows at a slow rate determined by the diffusivity of the alloying element in the γ phase. This behaviour is sensitive to alloy composition. The mode where no partition occurs gives rise to a narrow zone of enrichment or depletion, depending on whether alloying element is a γ - or α -stabilizer, which moves ahead of the α / γ interface. In the no-partition regime the observed growth rates are relatively high, being determined by the diffusivity of carbonwhich diffuses several orders of magnitude faster than the metallic alloying elements.

A third approach to the ferrite reaction was introduced by Hultgren [19], who proposed a state of para-equilibrium at the γ/α boundary. In this, the transformation occurs at such a rate that the substitutional solutes are unable to partition.

2.3.1.5. Structure Changes Resulting From Alloying Addition

The addition to iron–carbon alloys of elements such as nickel, silicon, manganese, which do not form carbides in competition with cementite, does not basically alter the microstructures formed after transformation. However, in the case of strong carbide-forming elements such as molybdenum, chromium and tungsten, cementite will be replaced by the appropriate alloy carbides, often at relatively low alloying element concentrations. Still stronger carbide-forming elements such as niobium, titanium and vanadium are capable of forming alloy carbides preferentially at alloying concentrations less than 0.1 wt% [19].It would, therefore, be expected that the microstructures of steels containing these elements would be radically altered.

2.3.1.6. Effect of Ti on Grain Size Control

In commercial V-microalloyed steels small amounts of Ti (~ 0.01%) are commonly added to prevent excessive grain coarsening at high temperatures [8,9,42,97,98].Because, Ti reacts with the nitrogen in the steel to form a fine dispersion of very stable TiN. However, to attain the fine TiN size necessary for effective grain growth control fast cooling is needed during the solidification of the steel, as in continuous casting of slabs [8,42,97].A general conclusion is that the stability of TiN itself is not expected to change by additions of other microalloying additions, such as V or Nb [8,42,97] Ti as a result of its much lower solubility compared to V or Nb.

2.3.1.7. Effect of Mn and Mo on the Kinetics of the Ferrite Reaction

As reported by Kinsman and Aaronson [99], and as can be clearly seen in Fig. 2.15, ferrite still grows much more slowly than in Fe–C alloys, even when no partition of alloying element is observed. For Mn, some of this retardation is because the substitutional solute affects the thermodynamic stability of γ relative to α. But for molybdenum containing alloy the α/γ boundary collects atoms during the transformation and, as a result, experiences an impurity drag.
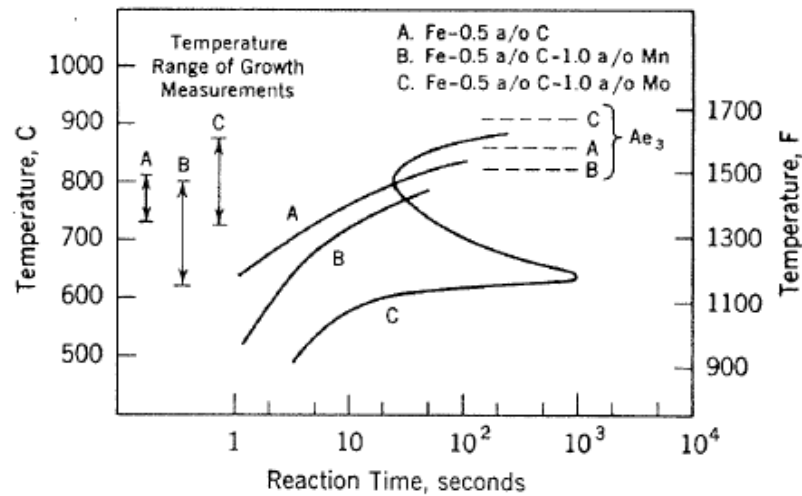
Fig 2.15 Effect of manganese and molybdenum on the kinetics of the ferrite transformation [19,99].

2.3.1.8. Toughness Improvement

Improvement of these steels toughness is vital. By microalloying with Ti or alternatively raising the Al-content somewhat above normal levels and with close control of N it is possible to reduce the austenite grain size to below 50 μm. This refines the final ferrite-pearlite microstructure and thereby increases toughness. By combining this method with a reduction of the C-content and an increase of the Mn-content to dilute the pearlite with respect to cementite, it has been possible to double the Charpy impact toughness of the standard V-microalloyed steel while maintaining the level of strength[100,101]. Fig. 2.16 shows examples of predicted microstructure steels having different levels of vanadium, niobium and nitrogen, when subjected to the same rolling schedule [102].As evident from Fig. 2.16, the steel with high vanadium and nitrogen is characterised by the most effective microstructural refinement..
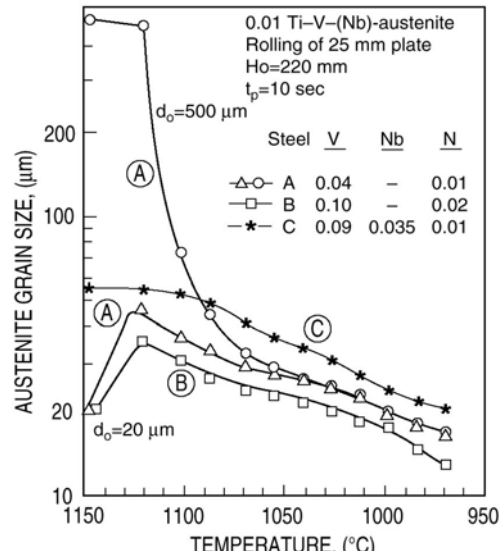
Fig. 2.16 Development of austenite microstructure for Ti-V-(Nb)-N-steels during simulation of industrial hot rolling of plates [102].

2.3.1.9. Effect of Reheating Temperature

The yield stress and tensile strength decrease because lower reheating temperature reduces the amount of dissolved vanadium (or niobium) in the austenite and accordingly the potential for precipitation hardening after cooling. For Ti-V-N microalloyed steels it was found that a reduction in reheating temperature from 1250 to 1100C○ reduced the yield stress by about 40MPa while at the same time decreasing the ductile-brittle transition temperatureby about 15C ○ [42].The carbon steels are the most frequently produced and used steels. More than 85% of the steels produced are carbon steels. Variation of carbon has the greatest effect on the mechanical properties of steels. Carbon steels contain up to 2 % total alloying elements and can be subdivided into ultra low carbon, low carbon , medium carbon , high carbon and ultra high carbon steels.The medium carbon microalloyed steels are designed to meet the specific requirements of mechanical properties.These steels are similar to low carbon steels except that carbon content in these steels are higher and normally in the range of 0.25 to 0.60 % and the manganese from 0.60 to 1.65% (up to 2% also used), in order to provide adequate deep drawing and welding properties with small quantities of chromium, nickel, molybdenum, copper,nitrogen. In these steels small amounts of vanadium, niobium and/or titanium is also present. Individual elements generally less than 0.10% and total microalloying elemants generally less than 0.15% are added for refinement of grain size as well as precipitation hardening.

The medium carbon steels may also have small addition of calcium, rare earth elements or zirconium for sulfide inclusion shape control.However the steels can be classified based on different systems depending upon:

The composition: Carbon, micro alloy, low alloy, high alloy or stainless steels.

The manufacturing processes: basic oxygen process, energy optimizing furnace or electric arc furnace.

The finishing methods: Hot rolling, cold roling or forging etc.

The type of product: Flat such as plate,sheet,strip,long such as wire rods, reinforcement bars, rounds and shapes,pipes and tubes or forged products.

The de oxidation method: Killed, semi-killed, rimmed or capped steels.

The microstructure: Ferrite, austenite, pearlite, bainitic or martensitic.

The strength levels: HSS, HSLA or normal strength to meet standard requirement heat.

The treatment process: Annealing, normalizing, thermo mechanical treatment, quenching and tempered etc.

Quality defining designations: Forging quality, Commercial quality, drawing quality or welding quality etc.

2.3.2 PEARLITE TRANSFORMATION

Pearlite is a diffusional transformation. All experimentall data show that the pearlite grows with the diffusion of substitutional solute atoms. Pearlite has never been shown to grow by the para-equilibrium transformation of austenite [82,83]. Hillert and co-workers [19], were able to show that pearlite could be nucleated either by ferrite, or by cementite, depending on whether the steel was hypo- or hyper-eutectoid in composition. Mehl and co-workers [19], took the view that pearlite nodules are formed by sideways nucleation and edge-ways growth (Fig. 2.17). Modin [19], indicated that nucleation of pearlite also took place on clean austenite boundaries. Hillert has shown that nucleation also occurs on ferrite, C. S. Smith [19], first

pointed out that the mobile pearlite interface in contact with austenite was an incoherent high-energy interface growing into a grain with which the pearlitic ferrite and cementite had no orientation relationship.
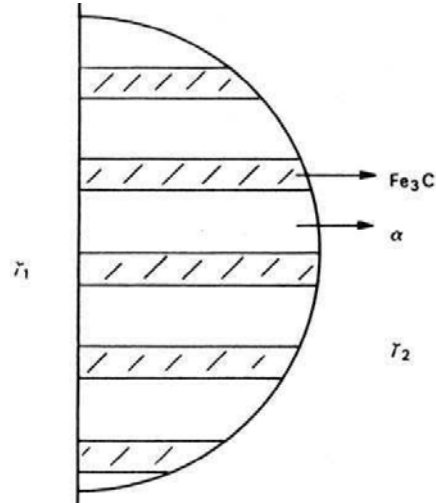

Fig. 2.17 Idealized pearlite nodule at austenite grain boundary [19].

Therefore, the nodules which nucleated on pre-existing grain boundary cementite and ferrite would choose the higher energy interfaces across which the boundary phase had no orientation relationship with the adjacent austenite, while on the low-energy interfaces Widmanstätten growth of ferrite (or cementite) was usually observed. The spacing of the lamellae in pearlite is a sensitive parameter which, in a particular steel, is larger the higher the transformation temperature.The spacing was first measured systematically for a number of steels by Mehl and co-workers [19],who demonstrated that the spacing decreased as the degree of undercooling, ΔT, below the eutectoid temperature increased. Growth of the lamellae can only occur if the increases in surface energy is less than the decrease in energy resulting from the transformation. Therefore, the condition for growth can be found from Equation (2.15):

$$\Delta H \, (T_e - T) \, / \, (T_e) \, \rho \, S_0 = 2\sigma. \qquad (2.15)$$

Where

T_e = Eutectoid temperature

T = Transformation temperature

ΔH = latent heat of transformation.

σ = Interfacial energy per unit area.

S_0 = Interlamellar spacing or pearlite spacing and ρ is the density.

The equation predicts three important aspects of the transformation:

1. The pearlite spacing S0 decreases with transformation temperature.

2. The fineness of the spacing is limited by the free energy available from the transformation.

3. A linear relation should exist between the reciprocal of the spacing and the degree of undercooling.

It is only possible for cementite, ferrite and austenite to coexist in equilibrium at the eutectoid temperature in plain carbon steels. Therefore, fully pearlitic steels in which all of the austenite is consumed.

2.3.2.1 Divergent Pearlite

However, when substitutional solutes are present they may partition between the phases so that the austenite may become enriched or depleted as the transformation proceeds, leading to a decrease in the driving force for transformation.This in turn leads to an increase in the interlamellar spacing as the pearlite grows, a phenomenon known as divergent pearlite [19].

2.3.3.2 The Kinetics of Pearlite Formation

The pearlite nucleates at preferred sites in the austenite and the nuclei then grow until they impinge on each other.The process is both time and temperature dependent, as it is controlled by the diffusivity of the relevant atoms. Johnson and Mehl [19],first applied a detailed analysis of nucleation and growth to the pearlite reaction, which assumed that the fraction of austenite transformed (X) could be expressed in terms of a rate of nucleation $\dot{N}$ defined as the number of nuclei per unit volume of untransformed austenite formed per second, and a rate of growth of these nuclei G, expressed as radial growth in cm s - 1. An expression was obtained for the fraction of austenite transformed X, in time t:

$$X = 1 - e^{-(\pi/3)\dot{N}G^3 t^4}$$

(2.16)

where: $\acute{N}$ is the rate of nucleation and G is the rate of growth. In practice, however, the pearlitic reaction does not conform to the simple nucleation and growth model referred to above, because of [19]:-

1. Ń is not constant with time.

2. *G* can vary from nodule to nodule and with time.

3. The nuclei are not randomly distributed.

4. The nodules are not true spheres.

For that reason Cahn and Hagel [19], suggest a new theoretical approach which fully recognized the inhomogeneous nature of nucleation in the pearlite reaction. It was pointed out that not all grain boundary nucleation sites were equivalent, that grain corners would be more effective than edges, and that edges would be better than grain surfaces. The expression for the fraction of austenite transformed assuming site saturation of grain corner sites is [19]:

$$X = 1 - e^{-(4/3)\pi\eta G^3 t^3}$$

(2.17)

where η is the number of grain corners per unit volume. The time for completion of the reaction, t_f, is simply defined as [19]:

$$t_f = 0.5d/G,$$

(2.18)

where d is austenite grain diameter and d/G is the time taken for one nodule to absorb one grain, so the presence of only several nodules per grain will meet the above criterion for t_f. The nucleation rate, where measured, does seem to vary with time according to the relation: where *k* and *n* are constants. However, for most experimental conditions, the

$$\dot{N} = kt^n,$$

(2.19)

where *k* and *n* are constants. However, for most experimental conditions, the rate of growth G is the dominant quantity. The rate of growth of pearlite nuclei can be measured by reacting a series of samples for increasing times at a particular temperature. It has been found that *G* is structure insensitive [19], i.e. structural changes such as grain size, presence or absence of carbide particles have little effect. However,G is markedly dependent on temperature, specifically the degree of cooling ΔT below Te, and increases with increasing degree of undercooling until the nose of the *TTT* curve is reached,G is also strongly influenced by the concentration of alloying elements present [19].
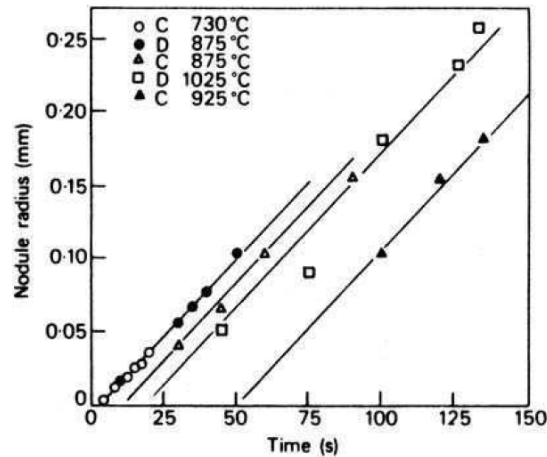
2.3.2.3   The Growth of Pearlite Nuclei

The rate of growth of pearlite nuclei G, can be measured by reacting a series of samples for increasing times at a particular temperature.As a result of measurements on polished and etched sections, the radius of the largest pearlite area, assumed to be a projection of the first nodule to nucleate, can be plotted against time. Normally a straight line is obtained, the slope of which is G (Fig. 2.18). It has been found that G is structure insensitive [19], i.e. structural changes such as grain size, presence or absence of carbide particles have little effect. However, G is markedly dependent on temperature, specifically the degree of cooling ΔT below Te, and increases with increasing degree of undercooling until the nose of the TTT curve is reached, G is also strongly influenced by the concentration of alloying elements present.

Fig. 2.18 Growth of pearlite in two 0.8C 0.6Mn wt% steels [19].

The growth of pearlite was proposed by Mehl and Hagel [19],and proposed the following relationship for G:

$$G = \frac{K D_c^{\gamma}}{S_0}$$

(2.20)

Where D_c^{γ} the diffusion coefficient of carbon in austenite, S_0 is the interlamellar spacing and K is a constant. The growth rate increases as the transformation temperature is lowered, because the driving force of the reaction is increased [15,19].

2.3.2.4   The Effect of Alloying Elements on the Pearlite Reaction

The work of Mehl and coworkers [19], showed that many alloying elements reduce both rates of nucleation N and rates of growth G. For example, in molybdenum steels of eutectoid composition both N and G were decreased, and nickel steels behaved in a similar manner. The growth rate G as a function of atomic concentration of alloying elements in several groups of steels is shown in Fig. 2.19.
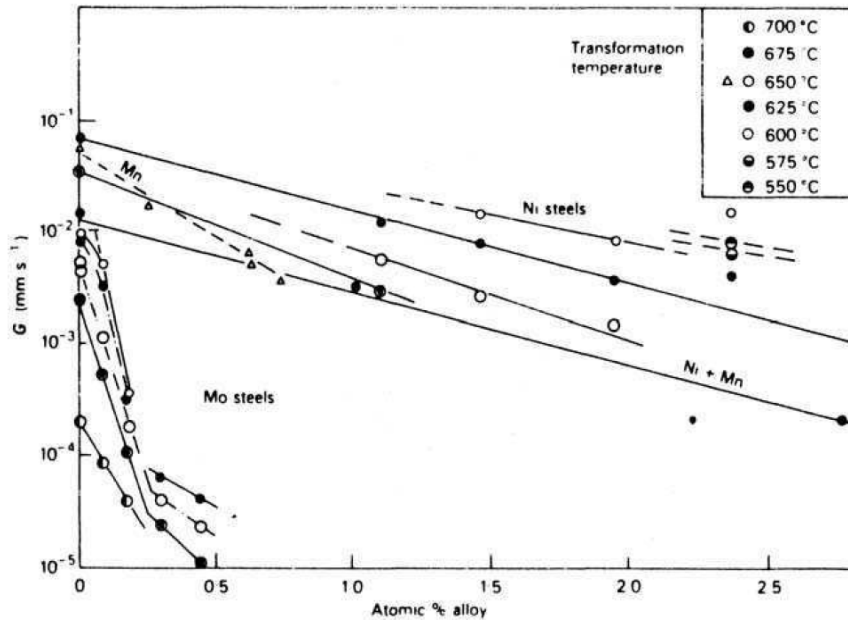
Fig. 2.19. Effect of alloying elements on the rate of growth of pearlite in the range
550–700°C[19].

The change in slope for Mo steels was correlated with the substitution of cementite by a molybdenum-rich carbide. Certain elements, notably cobalt, increased both N and G for the pearlite reaction. The rates of growth of pearlite nodules at 660 °C in cobalt steels are compared with that of a cobalt-free steel in Fig. 2.20.

Recent work [19], on chromium steels has shown that the addition of 1wt% Cr to an eutectoid steel results in substantially lower growth rates of pearlite. It follows that in general the C-curve for a pearlitic steel will be moved to longer times as the concentration of alloying element is increased.
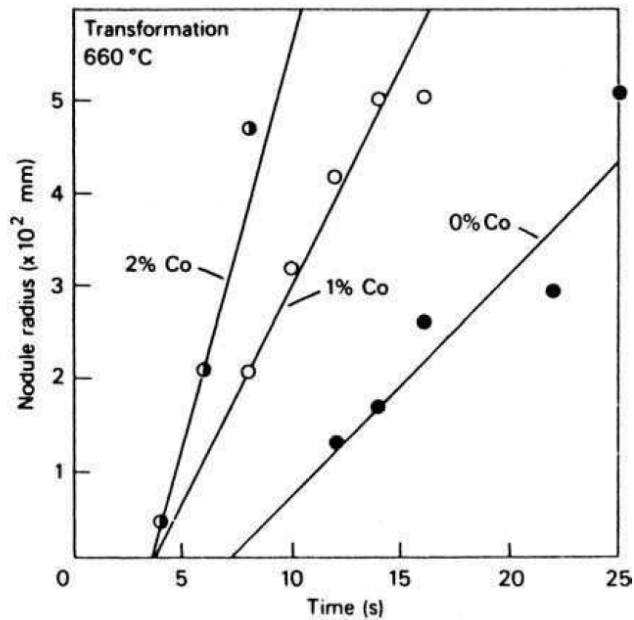
Fig. 2.20. Effect of cobalt on pearlite growth rate [19].

2.3.2.5 Mechanical Properties of Pearlite

The strength of pearlite would be expected to increase as the interlamellar spacing is decreased [19]. Pearlite has an adverse effect on ductility and toughness. The presence of pearlite in the microstructure provides sites of easy nucleation of cracks, particularly at the ferrite–cementite interfaces. The result is low energy absorbed due to the fact that many crack nuclei can occur at the pearlitic interfaces which, together with the high work hardening rate associated by presence of pearlite, restricts plastic deformation in the vicinity of the crack. The result is that there is a wide transition temperature range (Fig. 2.21) [19].Also impact transition temperature is raised substantially as the carbon content is increased (Fig. 2.21), and quantitative studies have shown that 1wt% by volume of pearlite raises the transition temperature by about 2 °C [19].Hugo and Woodhead [19], confirmed that the yield strength and the ultimate tensile stress (UTS) could be linearly related to the reciprocal of the square root of the interlamellar spacing or of the degree of undercooling. Steels of lower carbon contents, i.e. down to 0.3 wt%, gave similar results, but situation is different for lower carbon steels, i.e. below 0.3 wt%, where pearlite occupies a substantially smaller volume of the microstructure. In these steels the yield stress is not markedly affected as the proportion of pearlite is increased, provided other factors, e.g. ferrite grain size.
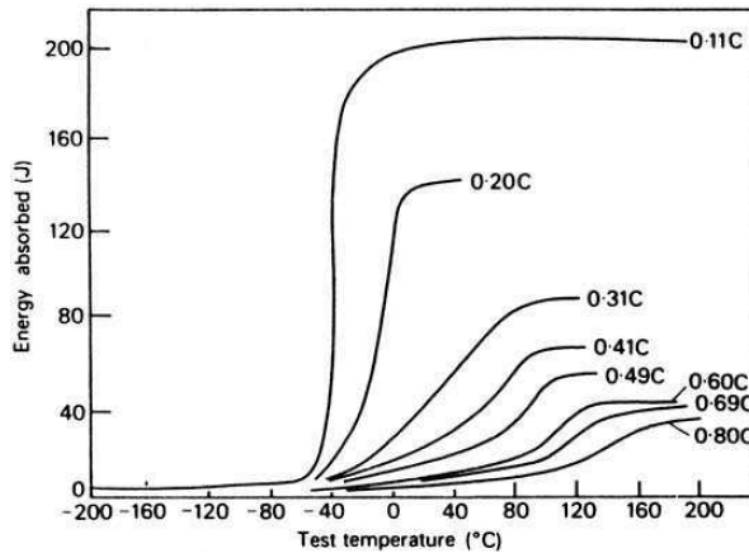
Fig. 2.21 Effect of pearlite on toughness measured by Charpy impact transition temperature
[19].

2.3.3. BAINITE TRANSFORMATION

The first theory based on the mechanism of the bainite reaction, which emerged incorporated the following principles.

(i) An individual platelet grows without diffusion. Any excess carbon is then partitioned into the residual austenite [103].

(ii) The size of each platelet is limited by a breakdown in interface coherency due to the plastic accommodation of the shape deformation [104]. The growth of a cluster of platelets therefore requires the nucleation of new platelets.

(iii) Classical nucleation theory is inappropriate for the bainite reaction [52]. Nucleation is governed instead by the dissociation of three-dimensional arrays of dislocations.

The essential kinetic features of the bainite transformation are illustrated schematically in figure 2.22. All the available theories has been reviewed in [15].
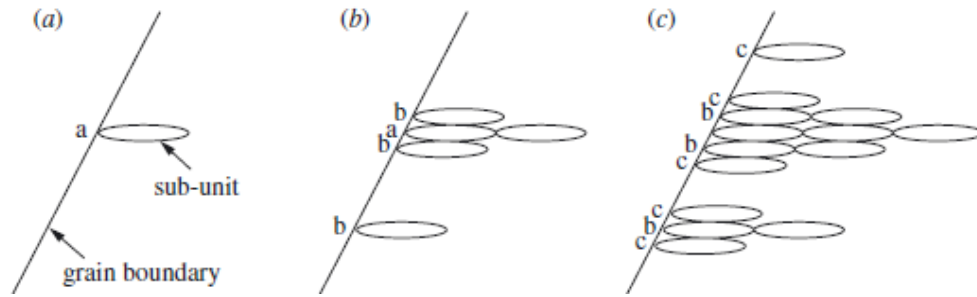
Figure 2.22: Schematic illustrating the growth of sheaves by propagation of successive sub-units for bainitic microstructure [15,42,105].

2.3.3.1 Thermodynamics of Bainite Formation

The equilibrium is said to exist in a system when it reaches a state in which no further change is perceptible i.e (system sinks into a very deep free energy minimum or lowest free energy state), no matter how long one waits [106].However metastable equilibrium is in minimum free energy but does not exclude the existence of deeper minimum. A bainite microstructure is far from equilibrium. The free energy change accompanying the formation of bainite in Fe-0.1 C wt% at 540 °C is - 580 $Jmol^{-1}$, whereas that for the formation of an equilibrium mixture of allortiomorphic ferrite and martensite at the same temperature is - 1050 J mol^{-1} (excess 470 $Jmol^{-1}$). Also, when compared against highly metastable materials such as rapidly-quenched liquids which solidify as supersaturated solutions, or multilayered structures containing a large density of interfaces. This bainite steels can be welded, where all the other materials listed in table (2.2) with high stored energies would not survive the weld process [15].

Table (2.2). Excess energies of metastables materials

Materials	Excess energy in units of RT_M
Highly supersaturated solution	1
Amorphous solid	0.5
Artificial multilayers	0.1
Bainite	0.04
Cold-deformed metal	0.003

Where R is the gas constant and T_M the absolute melting temperature

It has been demonstrated that bainite does not follow classical nucleation theory involving heterophase fluctuations, but rather follows a theory similar to that of martensite where the activation energy for nucleation is related directly to the driving force [43,105]. Bainite nucleates like martensite but with the partitioning of the interstitial carbon [52,107]. The chemical driving force for nucleation is defined as the free energy changes that accompanies the formation of a nucleus from the matrix [39,40,42,43].The free energy changes that occur as result of the formation of a ferrite nucleus, when the austenite partly decomposes into ferrite (formation of a ferrite nucleus hardly affects the composition of remaining austenite) is given by Fig. (2.23a).The formation of bainite becomes possible at a temperature where the conditions for nucleation and growth are satisfied simultaneously. To achieve a detectable nucleation rate i.e

$$\Delta G\text{m} < G\text{N},\qquad\qquad (2.21)$$

Where, $\Delta G\text{m}$ as shown on figure 2.23 6(a), is the maximum free energy available for para-equilibrium nucleation in which only carbon is partitioned between the parent and product phases (maximum possible free energy change for nucleation), G_N is a universal nucleation function which expresses the minimum free energy required to obtain a detectable amount of Widmanstatten ferrite or bainite. $\Delta G\text{m}$ is calculated using the parallel tangent construction as shown in Fig. 2.23(a), and described by [45,108].G_N has been determined experimentally by [109], and found it equal:

$$G\text{N} = 3.637(T - 273.15) + 2540 \text{ J / mol}\qquad (2.22)$$
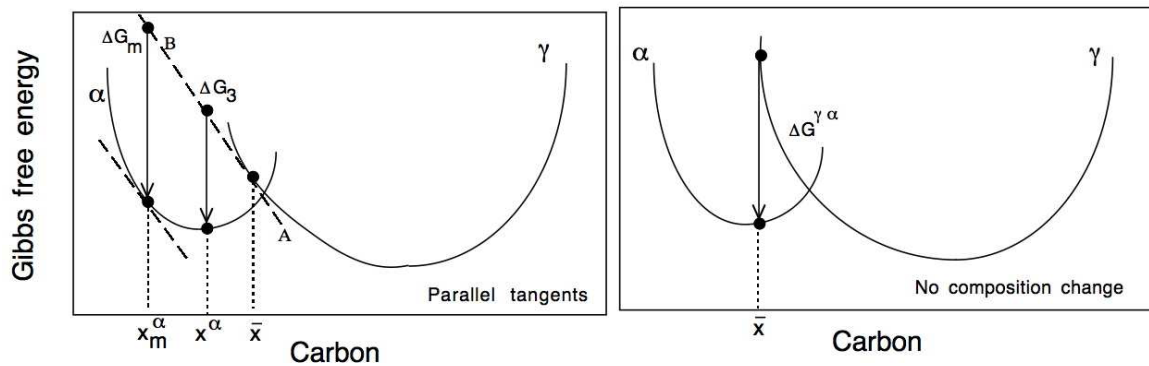
Fig. 2.23 Free energy diagrams illustrating (a) the chemical free energy changes during the nucleation and(b) the growth of bainitic–ferrite from austenite of composition x [45].

For temperature range (670-920 K$^\circ$), where T is the absolute temperature.The nucleus can only evolve into bainite if there is sufficient driving force available for growth without a

composition change as shown in Fig. 2.23b. Authors [52,110], has been estimated to be 400 J / mol, so that the condition for growth becomes

$$\Delta G\,\gamma \rightarrow \alpha < -400 \text{ J / mol} \tag{2.23}$$

where $\Delta G\gamma \rightarrow \alpha$ is the free-energy change for the transformation of austenite into ferrite of the same composition as shown in Fig. 2.23b.

2.3.3.2 Kinetics of Bainite

As shown in Figure 2.22, a sub-unit nucleates at an austenite grain boundary and lengthens at a certain rate before its growth is stifled by plastic deformation within the austenite. New sub-units then nucleate at its tip, and the sheaf structure develops as this process continues. The volume fraction of bainite depends on the totality of sheaves growing from different regions in the sample. Carbide precipitation events also influence the kinetics, primarily by removing carbon either from the residual austenite or from the supersaturated ferrite. Little is known about the nucleation of bainite except that the activation energy for nucleation is directly proportional to the driving force for transformation [19, 52]. However, unlike martensite, carbon must partition into the austenite during bainite nucleation, although the nucleus then develops into a sub-unit which grows without diffusion. The individual plates of ferrite is too small to be resolved adequately using optical microscopy, which is capable only of revealing clusters of plates.However the higher-resolution techniques such as photoemission electron microscopy (Fig. 2.24), it has been possible used to study directly the progress of the bainite reaction. Not surprisingly, the lengthening of individual bainite platelets has been found to occur at a rate which is much faster than expected from a diffusion controlled process. The growth rate is nevertheless much smaller than that of martensite, because the driving force for bainite formation is smaller due to the higher transformation temperatures involved. The platelets tend to grow at a constant rate but are usually stifled before they can traverse the austenite grain.
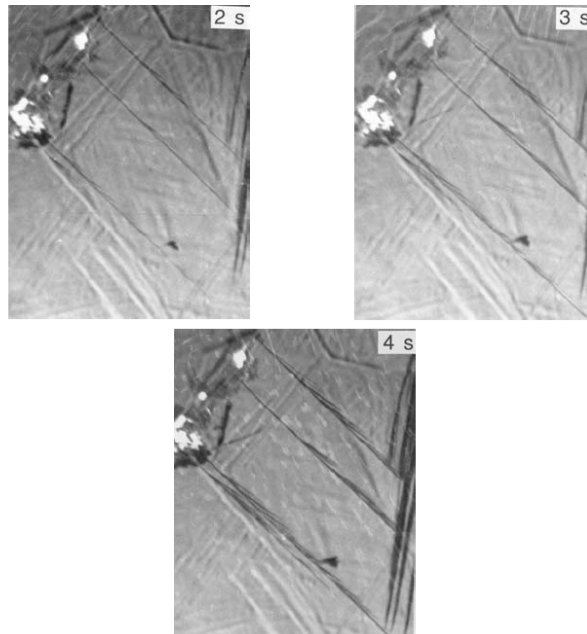
Fig. 2.24 Photoemission electron microscope observations on the growth of individual sub-units in a bainite sheaf [111]

The lengthening rate of a sheaf is slower still, because of the delay caused by the need to repeatedly nucleate new sub-units. Nevertheless, sheaf lengthening rates are generally found to be about an order of magnitude higher than expected from carbon diffusion-controlled growth. Also using thin-foil electron microscopy, the thickening of bainite sheaves was measured. The result is thickening process depends on the rate at which sub-units are nucleated in adjacent locations within a sheaf. The bainitic reaction takes place isothermally, starting with an incubation period during which no transformation is detected followed by an increasing rate of transformation to a maximum and then a gradual slowing down. As reported by [112-116,280], the temperature and transformation time determine the phase fractions andthe carbon content of the retained austenite, which in turn determine the mechanical properties.These features are illustrated in Fig. 2.25. For three transformation temperatures and for the same holding time, the fraction of bainite transformed was greater when transforming at higher temperatures.
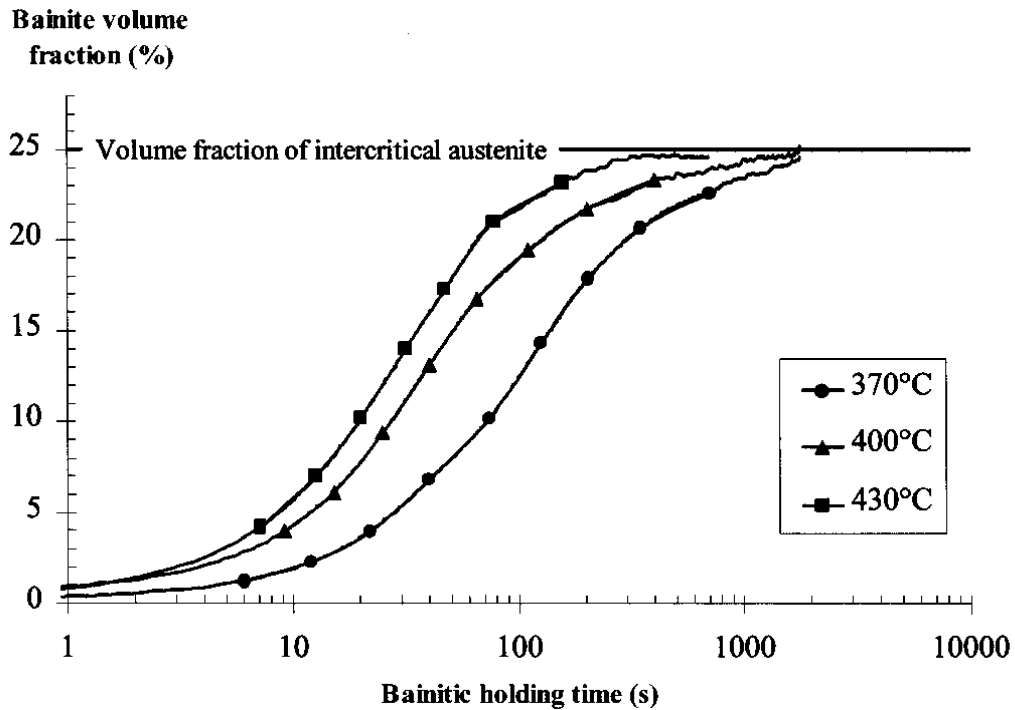
Fig 2.25: Volume fraction of bainite as a function of transformation time and temperature, for Fe-0.29C-1.4Mn-1.5Si (wt%) [117].

The overall transformation characteristics, i.e. the change in the fraction of bainite with time, temperature, austenite grain structure and alloy chemistry are therefore best considered in terms of a TTT diagram (Fig. 2.26).The TTT diagram tend to have two separable C-shaped curves becous the reaction rates are slow at high and low temperatures. In this effect, the diffusion of atomes becomes difficult at low temperatures whereas the driving force for transformation is reduced as the temperature is raised [15].The one at higher temperatures describes the evolution of diffusional transformation products such as ferrite and pearlite, whereas the lower C-shaped curve represents displacive reactions such as Widmanstätten ferrite and bainite [19]. In lean steels which transform rapidly, these two curves overlap so much that there is apparently just one curve which is the combination of all reactions. As the alloy concentration is increased to retard the decomposition of austenite, the two overlapping curves begin to become distinct, and a characteristic 'gap' develops at about the Bs temperature in the TTT diagram. This gap is important in the design of some high-strength (ausformed) steels which have to be deformed in the austenitic condition at low temperatures before the onset of transformation [19].There are two major effects of alloying additions on transformation kinetics. Solutes which decrease the driving force for the decomposition of

austenite retard the rate of transformation and cause both of the C-curves to be displaced to longer times. At the same time they depress the martensite-start temperature as illustrated in Fig. 2.27. The retardation is always more pronounced for reconstructive reactions where all atoms have to diffuse over distances comparable to the size of the transformation product [15].
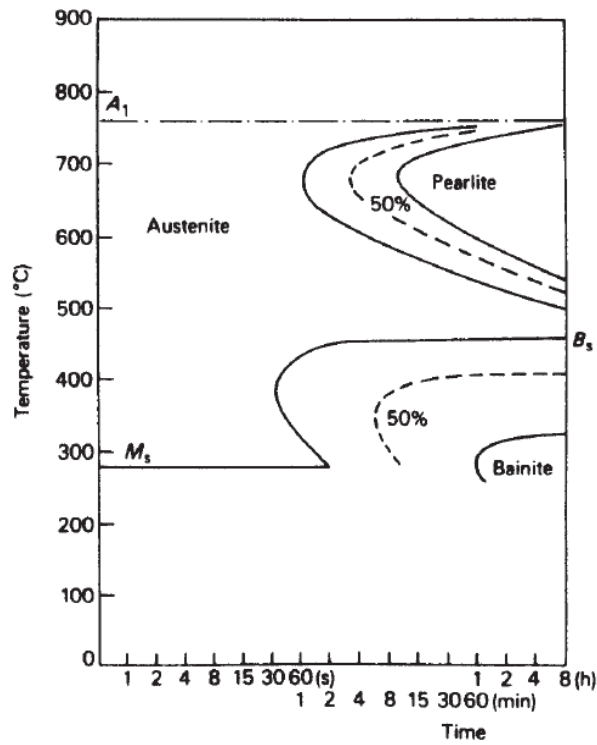
Fig. 2.26 TTT curves for a Fe–3Cr–0.5C wt% steel [118].
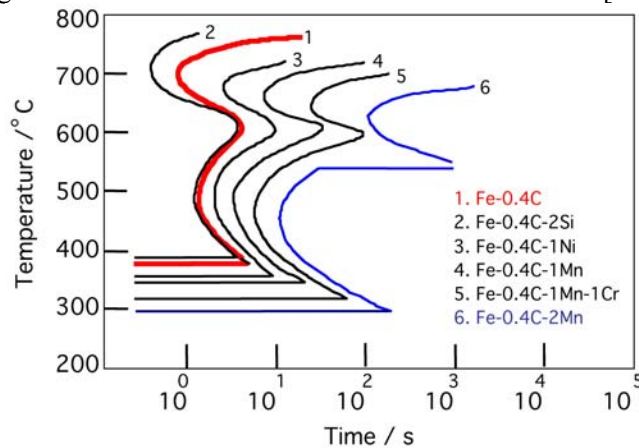
Fig. 2.27 Calculated TTT diagrams showing the C-curves for the initiation of reaction for a variety of steels [15,43,45,108]

2.3.3.3 Kinetics of Growth

There are two processes to consider in the evolution of the bainitic microstructure:

(1) Independent nucleation of a sub-unit at an austenite grain surface and

(2) Subsequent autocatalytic nucleation of sub-units on pre-existing platelets. The latter process is essential in the generation of the sheaf structure.

As shown in figure 2.22. A sub-unit nucleates at an austenite grain boundary, and lengthens at a certain rate. So the sheaf can continue to grow by the sub-unit mechanism until the T_0 condition is achieved (growth is stifled by plastic deformation within the austenite) as illustrated in figure 2.42. New sub-units then nucleate at its tip, and the sheaf structure develops as this process continues [15,45,105].The nucleation rate, I, is dependent on the activation energy i.e

$$I_V \propto \nu \exp\{-G^*/RT\}$$

(2.24)

where $\nu = kBT/h$ is the attempt frequency factor, kB and h are the Boltzmann and Planck constants respectively, G* is the activation energy for nucleation, and R is the universal gas constant. The activation energy for the nucleation of bainite is proportional to the driving force for transformation [52].

In respect to the nucleation rate its possible also, the lengthening rate of sub-units can be calculated as predicted theoretically by Trivedi [119], or measured by using hot-stage photoemission electron microscopy. Electrons are excited from the surface of the sample using incident ultraviolet radiation, and these photo-emitted electrons which form the image. The technique can resolve individual sub-units of bainite as demonstrated in Fig. 2.24. The volume fraction of bainite depends on the totality of sheaves growing from different regions in the sample. Carbide precipitation events also influence the kinetics, primarily by removing carbon either from the residual austenite or from the supersaturated ferrite. Little is known about the nucleation of bainite except that the activation energy for nucleation is directly proportional to the driving force for transformation. This is consistent with the theory for martensite nucleation. However unlike martensite, carbon must partition into the austenite (carbon must be allowed to partition during nucleation) during bainite and Widmanstatten ferrite nucleation [15,45,52,105], although the nucleus then develops into a sub-unit which grows without diffusion.

2.3.3.4   Estimation of Bainite Dislocation Density

Bainite has a high dislocation density ρ_d (more dislocation than allotriomorphic ferrite), even when they form at similar temperatures, it is depends on the shape of deformation, and the density of defects increasing as the transformation temperature decreases. Results are summarised in Fig 2.28. However the X-ray line profile measurements also show an increase in the lattice strain due to dislocations as the transformation temperature is reduced.This can be used to estimate the dislocation density, latter it is influence strength of the parent and product phases. The isothermal transformation to bainite at 300, 360 and 400 °C gave dislocation densities 6.3×10^{-15}, 4.7×10^{-15} and 4.1×10^{-15} m^{-2} respectively. A full description of this behaviour is given in Ref. [15,104].
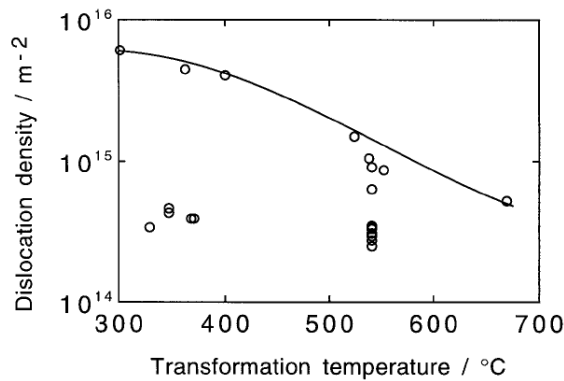
Fig 2.28 Dislocation density of martensite, bainite acicular ferrite and Widmanstatten ferrite as a function of the transformation temperature [120].

The empirical relationship which is valid for all displacive transformation (martensite, bainite and Widmanstatten ferrite), over the range 570-920 K°:

$$\log \rho_d = 9.28480 + \frac{6880}{T} - \frac{1780360}{T^2}$$

$$(2.25)$$

Where ρ_d is the dislocation density in m^{-2}, and T is the reaction temperature in Kelvin [120]. For martensite the transformation temperature is taken to be M_S temperature. The strengthening σ_d (MNm^{-2}) due to dislocations is given by:

$$\sigma_d = 0.38 \, \mu \, b \, (\rho_d)^{-0.5} = 7.34 \times 10^{-5} (\rho_d)^{-0.5} \qquad (2.26)$$

where μ is the shear modulus and b is the magnitude of the Burgers vector.

2.3.3.5 Bainite Morphologies

Bainite is defined as the product of a nonlamellar, non-cooperative mode of eutectoid decomposition [121,122].Bainite describes the resultant microstructure in steels of the decomposition of austenite (γ) into ferrite (α) and cementite (Fe_3C) in the temperature range above the martensitic transformation and below that for pearlite [123].Bainitic steels are used in a number of applications in industry because bainite structures can have good mechanical properties. They are stronger and harder than pearlite and have greater toughness than martensite.

All the proposed models for the transformation fall into two categories:

1) Displacive Tansformation (martensitic) is like shear process, because it is often associated with a change in crystal structure.

2) Diffusional Transformations. This is some times called a reconstructive transformation.

The transformation was believed to be martensitic if it conformed to the requirements of the Phenomenological Theory of Martensite Crystallography (PTMC [121].These can be summarized as follows:

Precipitates formed by a martensitic mechanism must have a plate or lath morphology and exhibit an invariant plane strain surface relief.

The prent and product phase are related by an atomic correspondence.

The orientation relationship between the parent phase and the product phase is irrational (except for fcc: hcp transformations).

Internal heterogeneities are required to produce a lattice invariant deformation (except fcc: hcp transformations).

There is no composition difference between the precipitate and matrix (except, perhaps , in interstitial alloys)

There is no difference in long-range order between the parent and the product phases.

For a transformation to take place martensitically, all of these requirements must be met [121].On the other hand, many of these requirements are also fulfilled by dissusional transformation. In order for a transformation to take place by a shear mechanism, the interphase boundary must be glissile and capable of moving in a conservative fashion. It does

clearly distinguish between bainite and lamellar pearlite. In fact, observations of roughly equiaxed bainite nodules in both Ti-Cr alloy and in steels [121].Led to the recent proposal that such equiaxed shapes are the fundamental morphology of bainite, and that Widmanstatten bainite structures form as a result of the dominating influence of one of the proeutectoid phases (e.g proeutectoid ferrite plates or laths)) [121].
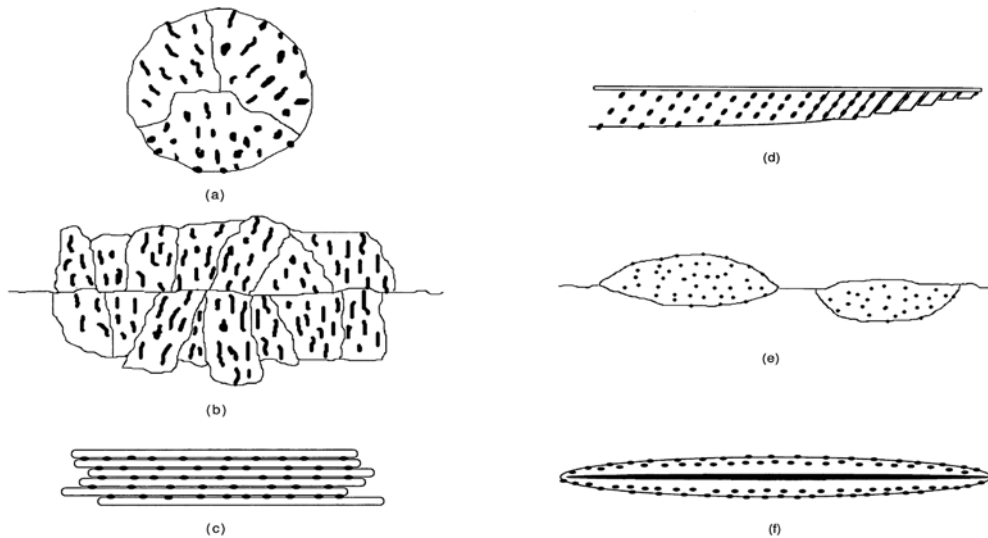
Fig.2.29. Schematic illustration of various bainite morphologies [121]; (a) Nodular bainite; (b) Columnar bainite; (c) Sheaf of upper bainite laths; (d) Lower bainite; (e) Grain boundary allotriomorphic bainite. f) Inverse bainite

2.3.3.6   Upper and Lower Bainite

Bainite nucleates on parent austenite grain boundaries (Fig. 2.30). Its growth completely takes place within the parent austenite grain. When the carbide precipitation occur in thin austenite regions between ferrite plates or laths (ferrite plates or laths precede the formation of carbide) converting the microstructure to upper bainite as shown in Fig. 2.29(c). This classic bainite morphology Fig. 2.31(a) consists of fine plates of ferrite (also called subunits) as shown in Fig. 2.31 (b,c) that grow in clusters called sheaves Fig. 2.31(d) with further reduction in reaction temperature [15,121,123]. Plates in each sheaf are separated by low-angle boundaries or cementite particles. These ferritic structures are parallel to each other and have identical crystallographic orientation. In upper bainite the excess carbon is then rapidly partitioned into the austenite from which it precipitates as coarse cementite during the progress of the transformation. However for lower bainite, the partitioning of carbon is somewhat slower

because of the lower temperature so that there is an opportunity to precipitate some fine carbides within the ferrite. There is nevertheless some precipitation of cementite from carbon-enriched austenite. By contrast in the martensite, the carbon remains within the supersaturated plate until a tempering heat treatment can be given to precipitate fine carbides [124].

The microstructure of upper bainite consists of fine plates of ferrite, as shown in Fig. 2.5 [15,19,45,125-127].It is also possible to measure the thickness of sub-units (individual platelets) by empirically modeled formula [127], as $0.2 \times (T - 528) / 150$ μm , based on experimental data by Chang & Bhadeshia [128] ,for steels containing 0.095–0.5 wt% C, transformed isothermally between 523 and 773 K°, then it follows that the sub-unit volume is given by

$$Vu = \left(100.0 \times 10^{-6} \times T - 528 /150\right)^{2} \times 0.2 \times 10^{-6} \times (T - 528 / 150)$$

$$= 2.0 \times 10^{-17} \times \left(T - 528 / 150\right)^{3} \quad m^{3} \tag{2.27}$$

The plates grow in clusters called sheaves. Within each sheaf the plates are parallel and of identical crystallographic orientation, each with a well-defined crystallographic habit. The individual plates in a sheaf are often called the 'sub-units' of bainite. They are usually separated by low-misorientation boundaries or by cementite particles [19,46], so that a low angle boundary arises whenever the adjacent platelets touch. The ferrite always has a Kurdjumov-Sachs type orientation relationship with the austenite in which it grows [19].
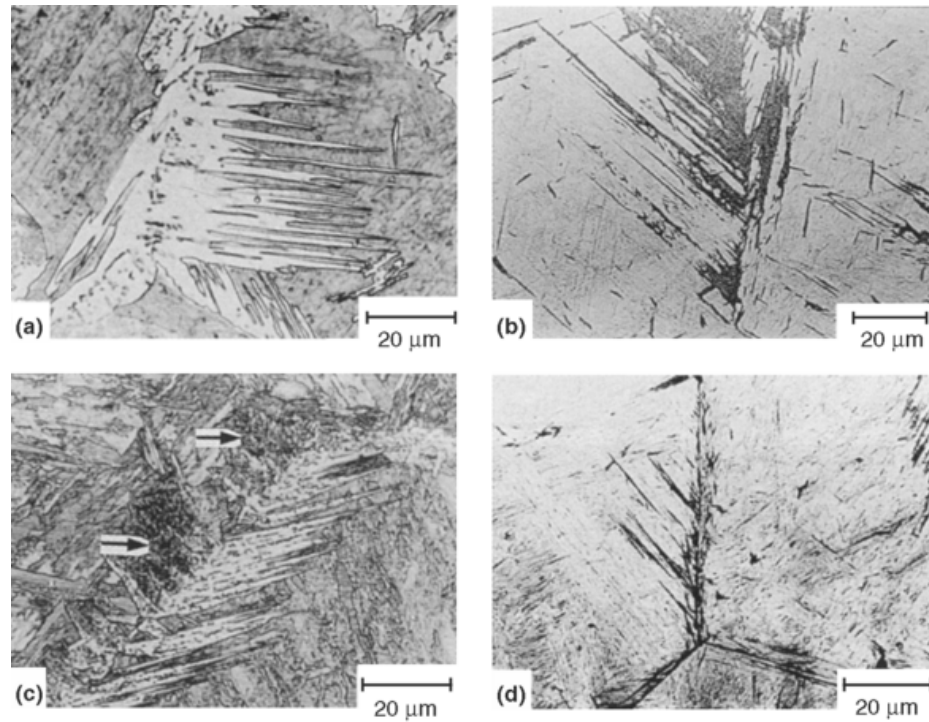
Fig. 2.30 Optical micrographs of (a) the structure formed by transformation (b) typical upper bainite formed by the decomposition (c) the upper bainite laths (d) the bainitic structure formed by the isothermal decomposition [123].
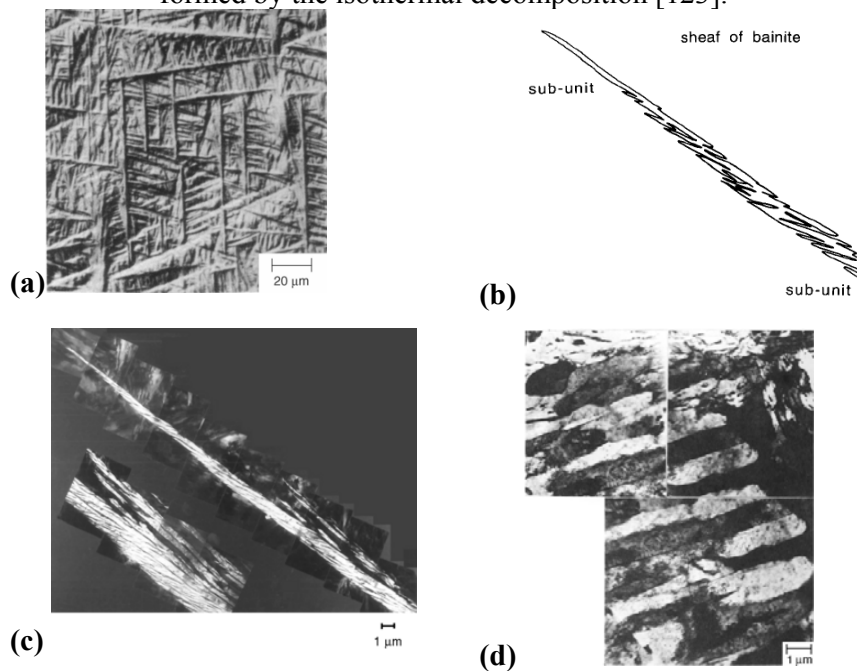
Fig. 2.31(a) General surface displacements due to upper bainite (b) Corresponding outline of the sub-units near the sheaf tip (c) TEM micrograph of a sheaf of upper bainite (d)TEM micrograph illustrating the substructure of upper bainite plates (2340 steel) [15,19,123].

The elongated cementite particles usually decorate the boundaries of these platelets as shown in Fig. 2.5. The amount and continuity of the cementite layer depending on the carbon concentration of the steel [45], i.e that will be the main difference between the low-carbon and medium carbon microalloyed steel.At figure Fig. 2.22, each sheaf is itself in the form of a wedge-shaped plate on a macroscopic scale. The sheaves inevitable nucleate heterogeneously at austenite grain surfaces [19,129, 49], this can be harmful to mechanical properties because cleavage crack can propagate readily across the packets [15,19, 130], or nucleated with one austenite grain (individual) and grow in the different direction [13,131]. The ferrite plates are so much fine, each about 10 μm long and about 0.2μm thick, making the individual plates invisible in optical microscope [19,45].

Lower bainite has a microstructure and crystallographic features which are very similar to those of upper bainite. The major distinction is that cementite particles also precipitate inside the plates of ferrite. There are, therefore, two kinds of cementite precipitates: those which grow from the carbon-enriched austenite which separates the platelets of bainitic ferrite, and others which appear to precipitate from supersaturated ferrite. These latter particles exhibit 'Petsch' orientation relationship with the austenite from which they precipitate [19].

$$[0\ 0\ 1]_{\mathrm{Fe_3C}} \| [\bar{2}\ 2\ 5]_{\gamma},$$
$$[1\ 0\ 0]_{\mathrm{Fe_3C}} \| [5\ \bar{5}\ 4]_{\gamma},$$
$$[0\ 1\ 0]_{\mathrm{Fe_3C}} \| [\bar{1}\ \bar{1}\ 0]_{\gamma}.$$

The carbides in the lower bainite are extremely fine, just a few nanometres thick and about 500 nm long. Because they precipitate within the ferrite, a smaller amount of carbon is partitioned into the residual austenite. This in turn means that fewer and finer cementite particles precipitate between the ferrite plates, when compared with an upper bainitic microstructure. An important consequence is that lower bainite is usually found to be much tougher than upper bainite, in spite of the fact that it also tends to be stronger.The coarse cementite particles in upper bainite are notorious in their ability to nucleate cleavage cracks and voids [15,19,45].

(a)   (b)

(c)
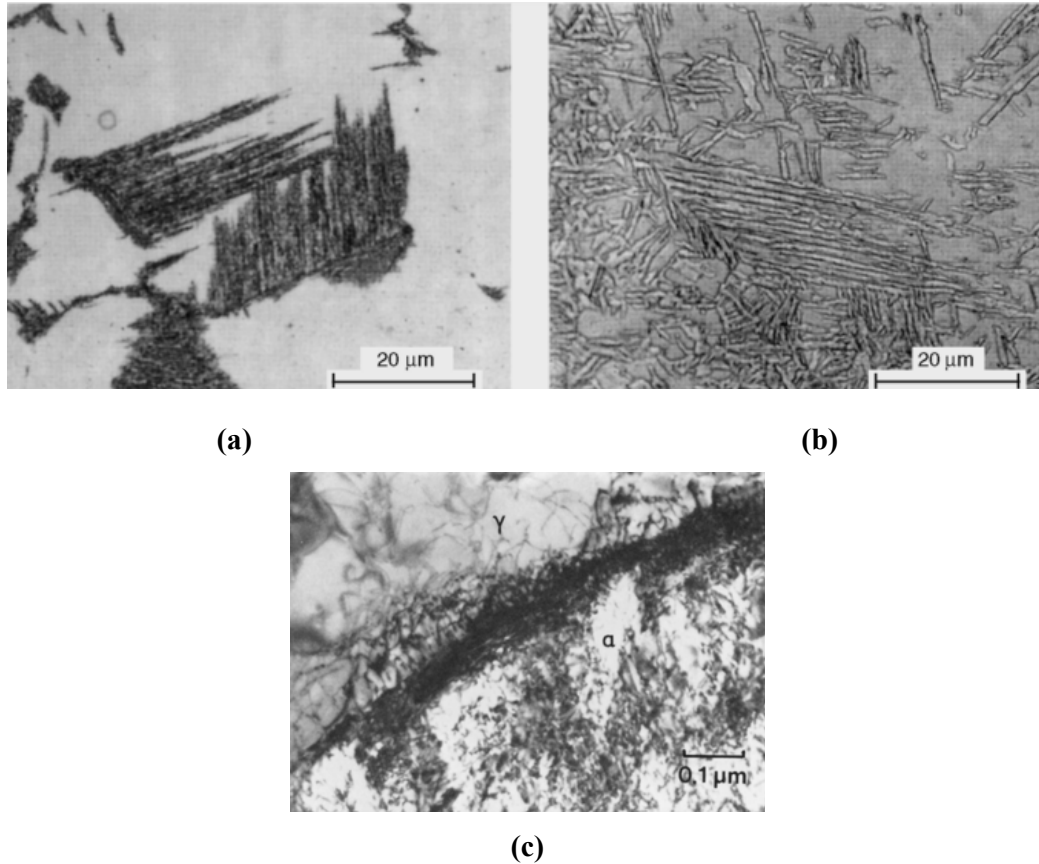
Fig. 2.32 (a) Bainite with cementite (b) Bainite without cementite (c) Intense dislocations both at the bainite/austenite and in the vicinity of interface [19,123].

The addition of sufficient quantities of alloying elements, such as silicon or aluminum, can even completely suppress the nucleation of cementite, resulting in an upper bainite microstructure consisting of just bainitic ferrite and carbon-enriched retained austenite [19,123].In the stabilization of carbon-enriched austenite surrounding the transformed plates of bainitic ferrite, as shown in Fig. 2.32(a, b). However the reduced strength of austenite at the elevated transformation temperature range of upper bainite and the shape change associated with the bainite transformation cause deformation of the parent austenite matrix, resulting in the buildup of dislocations at the γ/α interface Fig. 2.32 (c). The tangles of dislocations at the interface produce a workhardening effect, reducing interface mobility and halting the growth process, thereby limiting the size of each platelet within the sheaf [123].

2.3.3.7. Transition from Upper to Lower Bainite

The transition between upper and lower bainite is believed to occur over a narrow range of temperature. It is possible for both forms to occur simultaneously during isothermal

transformation near transition temperature [15].On a recently proposed diffusional mechanism for the formation of lower bainite [122], a largely carbide-free ferrite plate forms first and secondary ferrite plates then form predominantly at one broad face of the initial plate or (spine) by edge-to-face sympathetic nucleation [121], as shown in Fig. 2.33 (a, b). However at elevated temperatures the diffusion is so rapid that there is no opportunity to precipitate carbides in the ferrite, giving rise to an upper bainitic microstructure. A full description of this behaviour is given in Fig. 2.34(a). As the isothermal transformation temperature is reduced below Bs temperature so the time for decarburization increases, some of the carbon has an opportunity to precipitate as fine carbides in the ferrite, whereas the remainder partitions into the austenite, eventually to precipitate as inter-plate carbides (upper bainite sheaves are replaced by sheaves with a different morphology), as shown in Fig. 2.33 (a, b). Its called lower bainite microstructure. Because only a fraction of the carbon partitions into the austenite and the inter-plate carbides are much smaller than those associated with upper bainite as shown in Fig. 2.34 (b). Both carbide (lath like) and cementite are observed to precipitate within lower bainite. These lathlike carbides frequently adopt a unique variant within a ferrite grain, usually oriented at a characteristic55 to 60° angle to the long axis of the bainitic ferrite plate Fig.(c)[15,19,121-123].The broad faces of the secondary plates lie at an acute angle with respect to the longitudinal axis of the spine and carbides form along these broad faces in usually very narrow austenite regions remaining between adjacent secondary plates as schematically illustrated in Fig. 2.29(d) [121]. This is why lower bainite with its highly refined microstructure is always found to be much tougher than upper bainite, even though it usually has a much higher strength [19,45].It is also possible to obtain mixtures of upper and lower bainite by isothermal transformation. As upper bainite forms first, the residual austenite becomes richer in carbon and the tendency to form lower bainite increases as the transformation progresses [19,45].

(a)

(b)
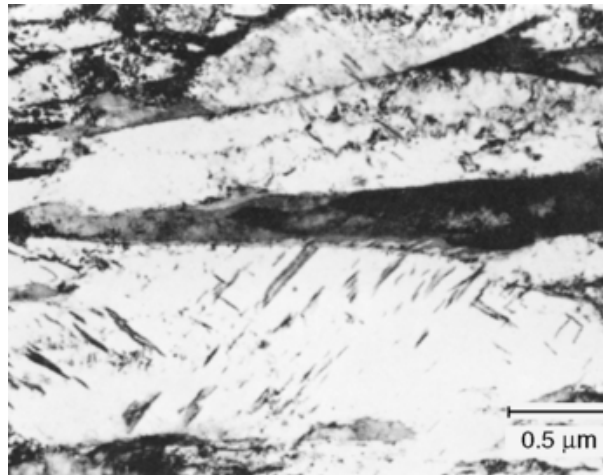
(c)

Fig. 2.33 Ligth Micrograph (a) sheaves of lower bainite (b) Lower bainite- 4360 steel (c) TEM lower bainite showing the precipitation of several variants of carbide particles within the plate of bainitic ferrite [15,19,123].
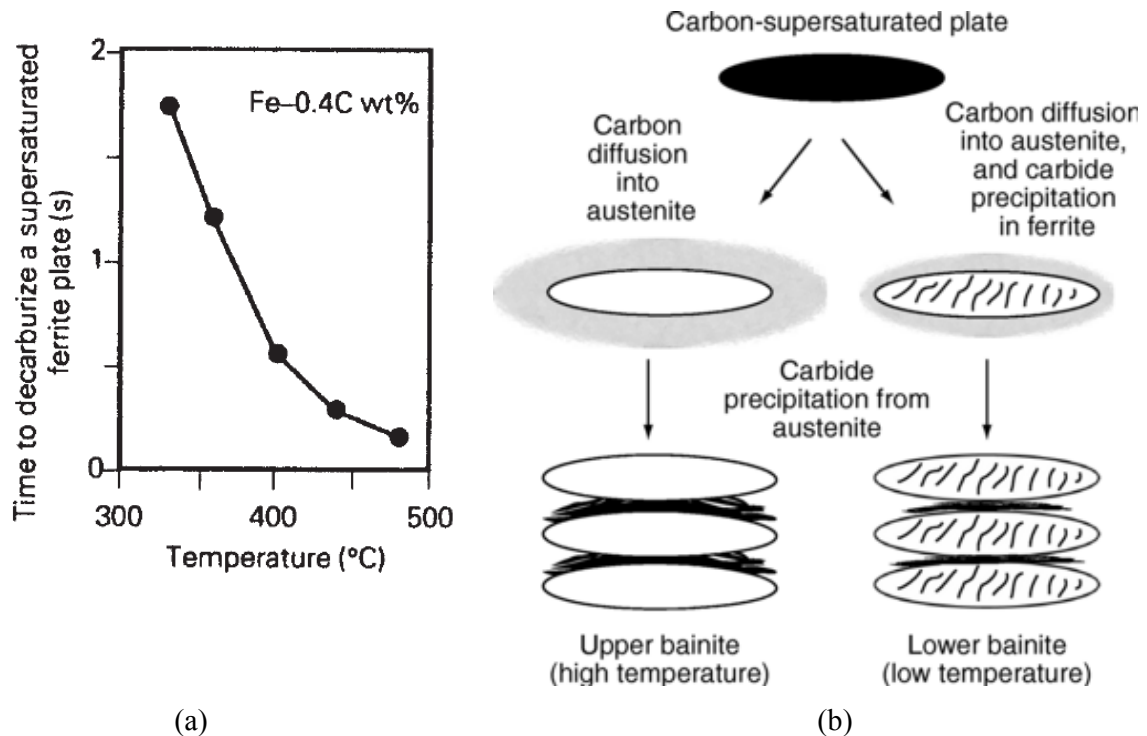
Fig. 2.34 (a). The approximate time required to decarburize a supersaturated plate of bainite [19]. (b) Stages in the development of a bainitic microstructure [15,19,45,51,84,123,124].

2.3.3.8 Nodular (Granular) bainite

Granular bainite (Fig. 2.35a) is a term frequently used to describe the bainite that occurs during continuous cooling transformation. This terminology is used widely in industry, where most steels undergo non-isothermal heat treatments [15,19,45].The nodular bainite formed in hypoeutectoid steels after precipitation of a considerable volume fraction of proeutectoid ferrite allotriomorphs and sideplates [121].The term used to describe bainite is external morphology. The two eutectoid phases play a nearly equal role in the evolution of the external morphology is the growth of bainite nodule and shape of eutectoid mixture is approximately a sphere as shown in Fig. 2.29(a) [121], this form of bainite is only observed in low- or medium-carbon steels [121], also bainite nodules have been observed in hyper-eutectoid Ti-Cr, Fe-C, Fe-C-Mo and Fe-C-Ni, [121] and Fe-C-Mn alloys [122].Because the transformation occurs during cooling, the sheaves of bainite are coarse, giving the resultant microstructure a blocky or granular appearance as shown in Fig. 2.35(a). A characteristic feature of granular bainite is the lack of carbides in the microstructure, because the carbon partitioned from the bainitic ferrite stabilizes the residual austenite so the final microstructure contains both

retained austenite and some high-carbon martensite in addition to the bainitic ferrite [15,19,123].

(a)   (b)
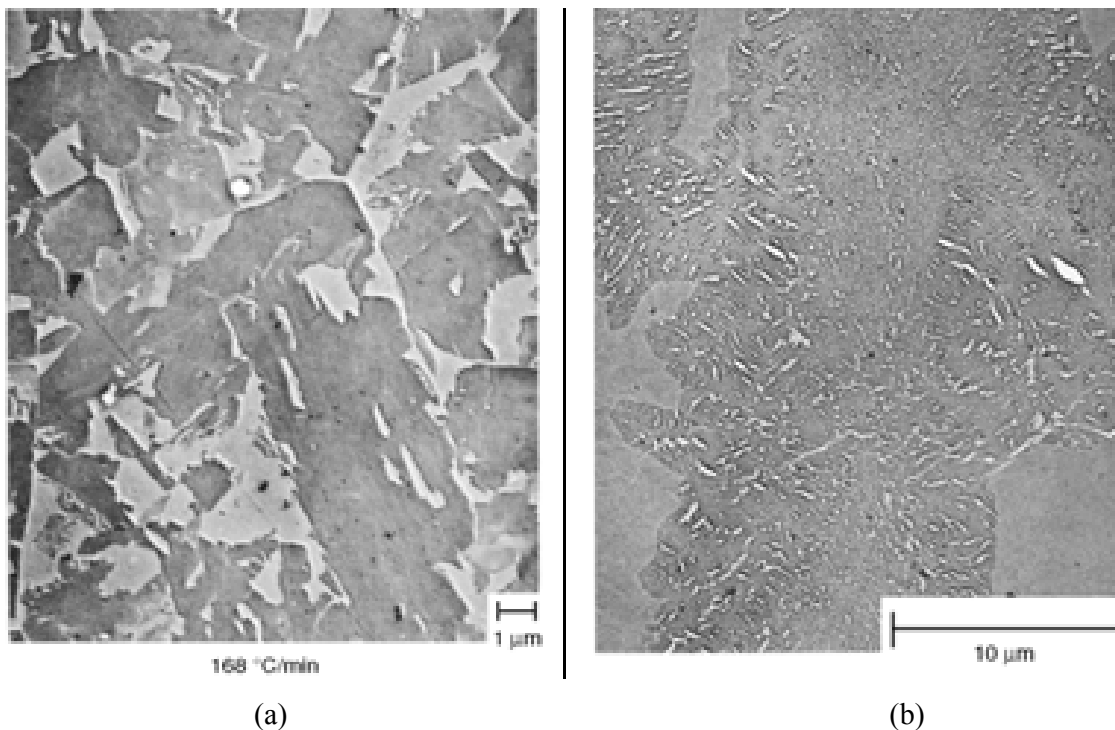
Fig. 2.35 Electron Micrograph (a) mixed microstructure (granular bainite, austenite, and martensite), with the parent austenite boundaries delineated by irregularly (b) blocky, or columnar-shaped, regions generally nucleated at grain boundaries that contain a coarse dispersion of carbides in a steel, austenitized and isothermally transformed at 290 °C [123].

2.3.3.9   Columnar Bainite

Columnar bainite is a modification of nodular bainite i.e the nodular internal morphology develops between preciously formed bainite elongates along austenite grain boundaries [121,122].as in Fig. 2.29(b), instead of adopting the nearly spherical shape of nodular bainite. This bainite morphology consists of nonacicular ferritic grains containing cementite precipitates formed in the bainitic temperature range at very high pressures. This microstructure is most often observed in medium- and high-carbon steels as illustrated in Fig. 2.35 (b) [123].

2.3.3.10   Grain Boundary Allotriomorphic Bainite

 Below the widmanstatten start temperature, (Fig 2.4) the first ferrite to form adopts the grain boundary allotriomorph morphology and supplemented by intragranular plates or laths when

the austenite grain size is sufficiently large (usually ASTM 0-1 or larger), and replaced by allotriomorphic bainite with decreasing austenite grain size at a given temperature [15,121]. The extenal shape of this form of bainite is thus obviously dictated by the proeuectoid ferrite allotriomorphs as schematically illustrated in figure (2.29d).

2.3.3.11   Inverse Bainite

In these cases, the carbide phase nucleates first, resulting in a different microstructural appearance than normally observed. The external morphology of this microstructure was originally reported by M. Hillert [121].Is dominated by the proeutectoid cementite reaction. Proeutectoid cementite plates or grain boundary allotriomorphs initiate inverse bainite formation [122]. The cementite is soon surround by a rim of ferrite, and a non-lamellar eutectoid mixture of carbide and ferrite then develops from the ferrite rim as schematically illustrated in figure 2.29 (f) [122]. The initial cementite precipitates as lath or plate but is quickly engulfed by a sheath of ferrite, as shown in Fig. 2.36(a).This formation causes the decomposition of adjacent austenite into larger ferrite laths that grow and coarsen by a more classical bainite reaction (Fig. 2.36b). The greater volume fraction and higher growth velocity of ferrite regions ensures that the volume fraction of inverse bainite will be relatively small; consequently, a large portion of the normal bainitic structure nucleates independently of the formation of inverse bainitic structures [123].

(a)   (b)
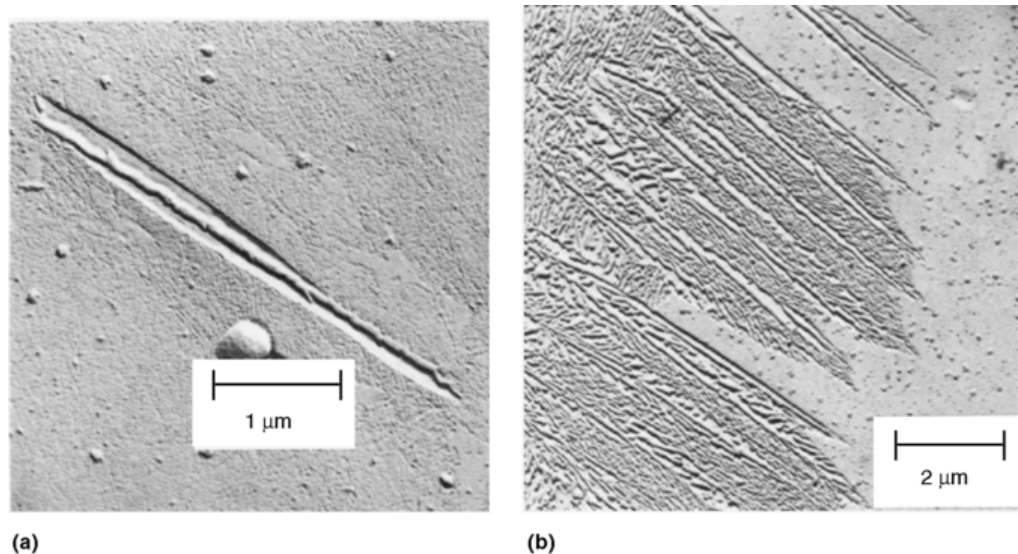
Fig. 2.36. Replica electron micrograph (a) showing the microstructural unit of inverse bainite (b) showing the evolution of a normally bainitic structure from initially formed units of inverse bainite [123].

2.3.3.12   Pearlitic Bainite

In the case of alloyed steels, especiallywhen steel contain strong carbide forming elements, it is possible to obtain pearlite, in which carbide phase is an alloy carbide such as M_7C_3 instead of cementite, it is forms at $T > B_S$, or some below B_S, but only after holding for very long time (many days) as illustrated in Fig. 2.37. The pearlite etches as dark nodules as can be seen in Fig. 2.37 (a) whereas on TEM, the colonies tend to have crystallographic facets Fig. 2.37 (b) (rather than rounded colonies for normal pearlite) i.e it consist parallel ferrite plates with intervening carbides (its similar to upper bainite).

(a)   (b)
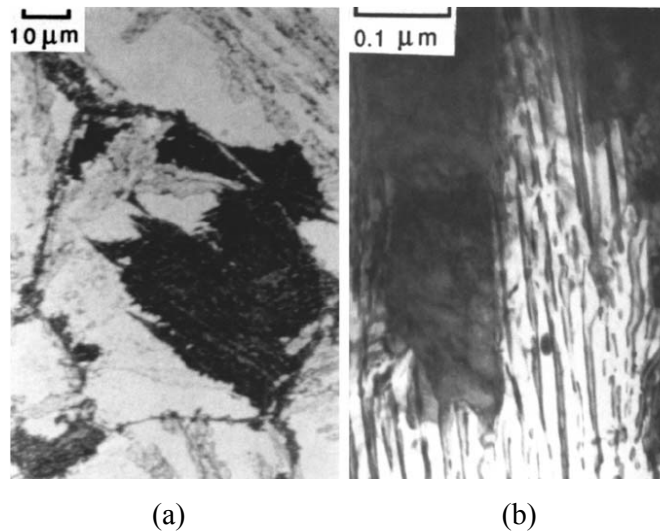
Fig. 2.37 Pearlitic bainite (a) light micrograph (b) transmission electron micrograph [15]

2.3.3.13 Effect of Pressure on Bainite Morphologies

Nilan obtained under condition of high hydrostatic pressure in (0.44%C and 0.82%C) [121]. At a pressure of one atmosphere, the 0.44%C steel is hypoeutectoid while 0.82%C is a near eutectoid composition [121] As the pressure is increased to 270 k bar, both alloys become hyperutectoid. This is reflected in the change from an upper or lower bainite morohology at 315 and 290 $^\circ$C to a columnar bainite microstructure [121].Increasing the pressure has the same effect as increasing the carbon concentration. The increased pressure raises the driving force for the nucleation and growth of cementite relative to that of ferrite, thus α_α / α_c and ΔG v^α/ ΔG v^c decrease, her favoring a transition from upper or lower bainite to nodular bainite.

2.3.3.14   Heat Affected Zone in Bainitic Steels

As reported by [15] the heat affected zone (HAZ) regions, which have been austenitized by the heat pulse may transform during cooling into untempered martensite or to some other hard microstructure. These hard regions are susceptible to cold-cracking due to hydrogen embrittlement and other impurity effects. This is the main reason why hardenable steels are difficult or impossible to weld {Fig. 2.38).
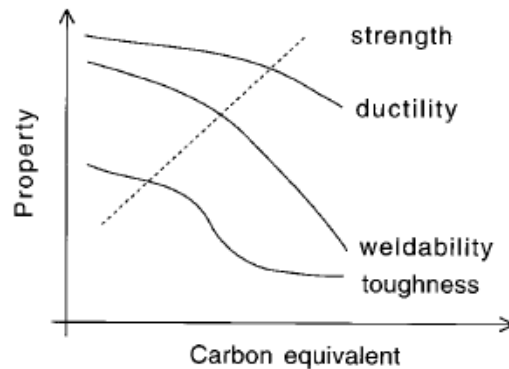
Fig. 2.38 Variation in mechanical proerties of HAZ as function of C.E [15].

Therefore, to avoid martensite formation in the HAZ, the cooling rate must be reduced during welding and it can be done by heating the steel before welding begins (preheating), but this processes adds cost of manufacture. So the cold cracking susceptibility of the weld HAZ is directly related to the composition of steel [132] As weel as, one common criteria of weldability is the carbon equivaent C.E (measure of hardenability) which gives information of the risk for hydrogen induced cracking in heat affected zone (HAZ), and results which are summarized in table 2.3. Whereas if (CE) ≤ 0.41 the risk of cracking is negligible for the sheet thickness of interest (3−8 mm) [133]. However the strengthening due to grain refinement and precipitation hardening by microalloying permits a reduction in (CE) to the result that the net effect is an imporvement in cold cracking susceptibility [3]. Whereas the lower carbon contents in MA steels also led to improved weldability and weldment properties. Graville has shown that the susceptibility to underbead or cold cracking of the weld HAZ is directly related to the composition of the base plate as shown in Fig (2.39).
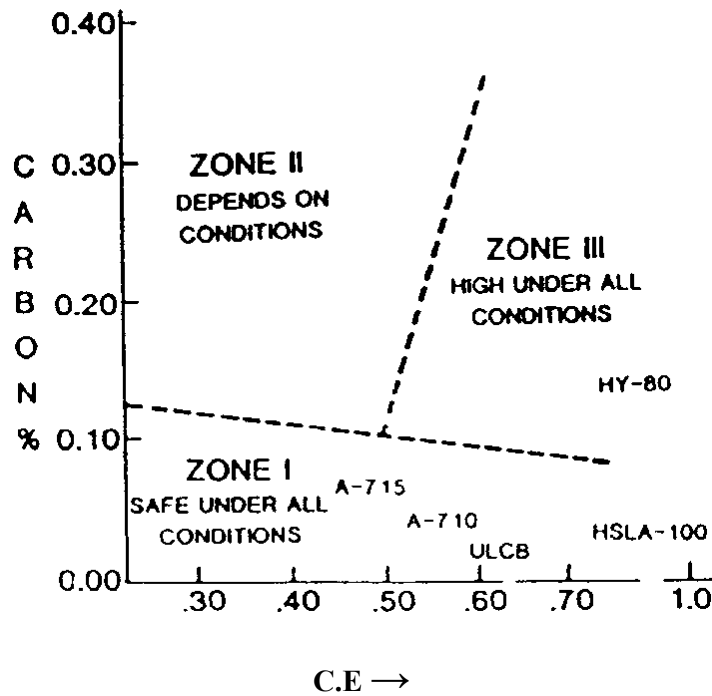
Figure 2.39 Influence of steel composition on the susceptibility of the heat affected zone to cold cracking. Carbon concentration and carbon equivalent (CE) values are represented by weight % [132].

There are two popular formula for C.E caculation [15]:

$$CE = C + \frac{Mn + Si}{6} + \frac{Ni + Cu}{15} + \frac{Cr + Mo + V}{5} \quad wt\%$$

(2.28)

is applied to steels containing less than 0.18 wt% of carbon. The other equation:

$$CE = C + \frac{Si}{30} + \frac{Mn + Cu + Cr}{20} + \frac{Ni}{60} + \frac{Mo}{15} + \frac{V}{10} + 5B \quad wt\%$$

(2.29)

and it is accepted for steels containing higher than 0.18 wt% of carbon.

Table 2.3. Effect of the carbon equivaent C.E on weldability

C.E	Weldability
< 0.4	Excellent
0.41-0.45	Good
0.46-0.52	Fair
> 0.52	Poor

2.3.4   ACICULAR FERRITE MORPHOLOGY

By inoculating molten steel with controlled additions of non-metallic particles, bainite can be induced to nucleate intragranularly on the inclusions, rather than from the austenite grain surfaces. This intragranularly nucleated bainite is called 'acicular ferrite'. It is a much more disorganized microstructure with a larger ability to deflect cracks[15,134]   Several authors showed that the presence of a uniform layer of allotriomorphic ferrite along the austenite grain boundaries as shown in Fig. 2.47 induces the transformation of austenite to acicular ferrite instead of bainite[15,50,95,98,121,135].The plates of acicular ferrite nucleate heterogeneously on small non-metallic inclusions and radiate in many different directions as shown in figure 2.40(a,b). It is believed that propagating cleavage cracks are frequently deflected as they cross an acicular ferrite microstructure with its many different orientations. This gives rise to superior mechanical properties, especially toughness. Acicular ferrite is therefore widely recognized to be a desirable microstructure [14,15].The suppressing of the grain boundary reaction preventing the nucleation of coarse boundary plate structure, BS or blocky ferrite BLF and promote the nucleation of acicular ferrite [15,45,56].Acicular ferrite microstructure, which provides effective grains (structural) refinement, is one of the most desired microstructure that improves both strength and toughness [15,49,98,136,137]. In early days most of the work on acicular ferrite has been carried out on welds, the high density of inclusions present in steel weld deposits ensures a high density of nucleation sites, which favors the development of an acicular ferrite microstructure instead of a bainite one[48,49]. The process of nucleation on the inclusions, together with the autocatalytic nucleation, leads to a chaotic arrangement of plates and fine-grained interlocking microstructure characteristic of acicular ferrite. Acicular ferrite has also been developed in a medium carbon forging steel or a low carbon steel following a conventional processing route .The main factors affecting the formation of AF have been summaraized as follows [56]:

1) Non-metallic inclusions are preferential sites for AF, but their nucleation potential vary with composition, crystal structure and dispersion (number, size and spacing).

2) An increase in austenite grain size can act to decrease the γ/α transformation temperature. This can increase intragranular nucleation potential until an intermediate grain size range is reached at which the potential is optimized.

3) Alloy hardenability (cooling rate control) must be such to provide the necessary transformation temperature range whereby AF can be formed.

So it should be possible to switch between these two morphologies by controlling the nucleation site. A bainite microstructure can be replaced by one containing acicular ferrite by increasing the number of particles [15]. A cicular ferrite does not grow in sheaves because their development is stifled by impingement between plates nucleated independently at adjacent sites [49,138].The larger prior austenite grain diameter (PAGD), as shown in Fig. 2.45 enhances the transformation austenite-to-acicular ferrite in detriment to reconstructive and bainite transformation [49,94,136,139,140,141,142,143,144]. The large austenite grains are required for the preferential formation of acicular ferrite relative to bainite [15,49,94,130]. The plates of acicular ferrite nucleate heterogeneously on small nonmetallic inclusion as shown in figure 2.40(a,b).and radiate in many different directions [15,49,98].The acicular ferrite is in fact intragranularly nucleate bainite [15,46,48,49,130,136,139,140,145].The morphologies of acicular ferrite and conventional bainite differ in that the former nucleates intragranularly at inclusions inside large austenite grains. The microstructure of acicular ferrite is less organized when compared with the ordinary bainite, the acicular ferrite have chaotic arrangement of plates and fine grains interlocked, such microstructure are better suited to deflect propagation cleavage cracks and therefore more desirable from toughness point of view in comparison to BS [15,46,56,131].The crystallographic data show highly misoriented plates nucleated on the same inclusion, propagation cracks are then deflected on each encounter with a differently oriented acicular ferrite plate. A full description of this behaviour is given by Gourgues et al [146].This give rise to superior mechanical properties especially toughness (improve toughness without compromising strength). In some recent studies, an improved toughness, observed in medium-carbon steels is associated with AF [56,98].In acicular ferrite microstructure, four points are critical for the achievement of optimum strength and toughness properties [46]:-

1. Refining the ferrite lath size.
2. Eliminating pearlite.
3. Minimizing the development of interlath carbides.
4. Control of the amount and distribution of retained austenite

(a)

(b)

(c)
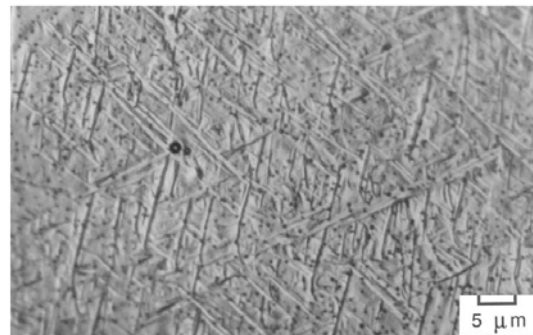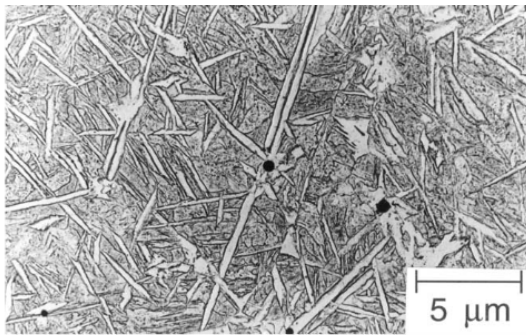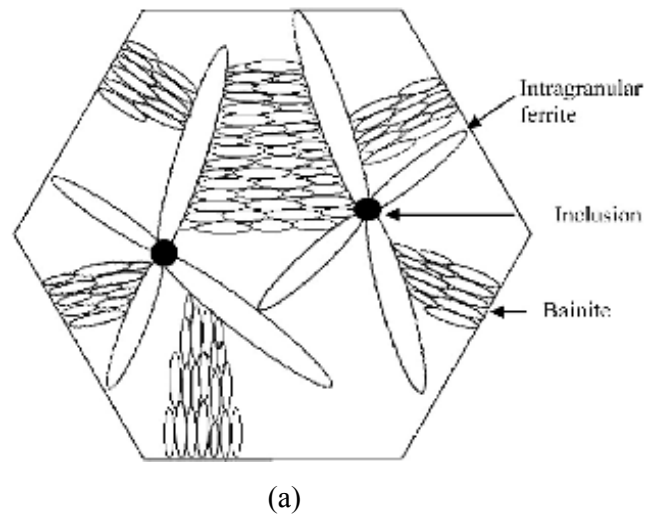
Figure 2.40(a). Schematic presentation showing the formation mechanism of a fine mixed microstructure of intragranular ferrite and bainite [147](b).Replica transmission electron micrograph of acicular ferrite plates in a steel weld deposite[15,19] (c) Surface displacements associated with the formation of acicular ferrite [15].

The resulting dislocations are inherited by the acicular ferrite as its grows giving dislocation at 10^{14} m^{-2}, whereas it contribute some of 145 MPa to its strength [15]. Acicular ferrite clearly grow by a displacive mechanism, so as reported in Ref. [148],there is no long-range partitioning of substitutional solutes during forming of acicular ferrite, where as the size of the acicular ferrite plates increases with transformation temperature.

2.3.4.1   Mechanism of AF Formation

It was emphasized that the transformation mechanism for acicular ferrite is identical to that for bainite, so the acicular ferrite is intragranularly nucleated bainite, whereas it is possible to switch between two morphologies by controlling the nucleation sites. There fore acicular

ferrite and bainite forms at some what higher temperatures where the carbon can escape out of the plate within a fraction of a second. Its original composition cannot therefore be measured directly. There are three possibilities [15,19,45].The carbon may partition during growth so that the ferrite may never contain any excess carbon. The growth may on the other hand be diffusionless with carbon being trapped by the advancing interface. Finally, there is an intermediate case in which some carbon may diffuse with the remainder being trapped to leave the ferrite partially supersaturated. As shown on Fig, 2.41. Austenite with a carbon concentration to the left of the T_0 boundary (Which is the thermodynamic boundary below which there is a driving force for the diffusionless transformation) can in principle transform without any diffusion. The diffusionless transformation is thermodynamically impossible if the carbon concentraction of the austenite exceeds the T_0 curve.
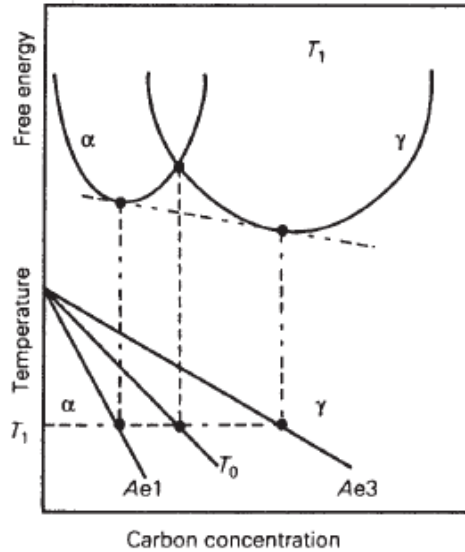
Fig, 2.41: Schematic illustration of the origin of the T_0 construction on the Fe–C phase diagram [15,19,45,84].

During isothermal transformation and suppose that the plate of bainite grows without diffusion, as shown in Fig.2.42 then partitions its excess carbon (excess carbon rejected) into the residual austenite. The next plate therefore has to grow from carbon-enriched austenite. However this process must cease when the austenite composition eventually reaches the T_0 curve (Transformation in fact ceases before the austenite achieves its equilibrium composition). The reaction is said to be incomplete [15,19,45,121].This characteristic is known as incomplete reaction pheneomenon. This is because the regions of austenite with the highest carbon concentration ($X\gamma > X\ T_0$) are unable to transformation to bainite. An obvious one is the fact that incomplete reaction pheneomenon is not general in steel. Recent findings

indicate that it depends upon the types of alloying elements present and their concentrations [121].However as reported by Bhadeshia[149,150],and illustrated in Fig. 2.43, two different reconstructive reactions occur after the bainitic reaction is stopped by continued holding at the isothermal transformation temperature for long time (days). Decomposition of residual austenite at an incredity slow rate lead either to pearlite which nucleates at the austenite grain boundaries or the original bainite/austenite interfaces move to produce ferrite growing eiptaxially from bainite plates .

(a)

(b)

Fig.2.42 (a) Illustration of the incomplete-reaction phenomenon. (b) Experimental data showing that the growth of bainite stops when the austenite carbon concentration reaches the T0 curve [15,19,45].

(a)   (b)
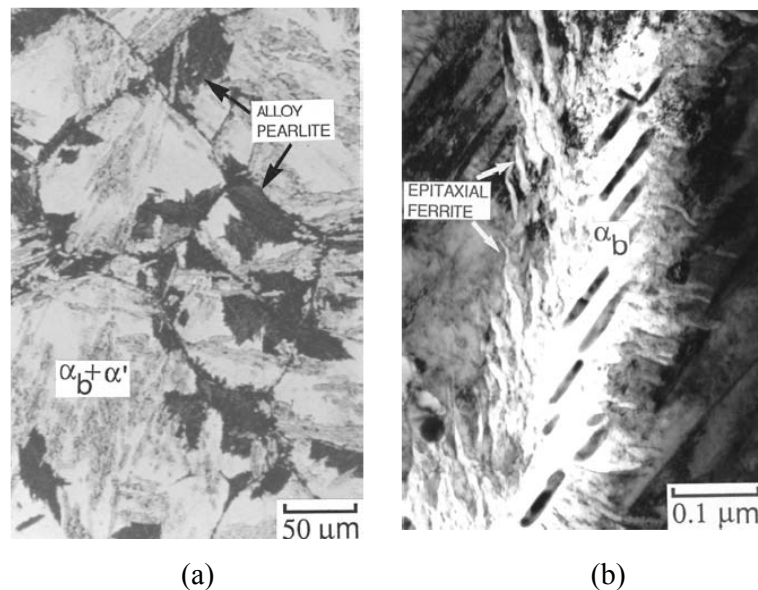
Fig. 2.43 The decomposition of residual austenite once the bainite reaction has stopped. (a) pearlite colonies, (b) ferrite growing epitaxially from bainite plates [ ].

2.3.4.2   Paraequilibrium Transformation Mechanism

The carbon, which is a fast diffusing element in iron, partitions to an extent which allows it to achieve local paraequilibrium at the interface. This is a metastable mode of transformation, which allows the growth of ferrite to be controlled by the diffusion of carbon, without any partitioning of alloying element. Paraequilibrium carbon concentration causes the residual austenite to become enriched in carbon, the enrichment of austenite with carbon should eventually cause the paraequilibrium precipitation of cementite from austenite in a region adjacent to the bainitic ferrite. Hulgren [15],proposed, (without any evidence,) that bainitic cementite should be randomly oriented to the austenite in which it precipitated. This process of ferrite and subsequent cementite precipitation then repeated, giving rise to bainitic sheaves.Therefore considered upper bainite to be similar to pearlite but growing under paraequilibrium condition and different in the orientation with austenite.

2.3.4.3   Factors Effecting Acicular Ferrite Formation

2.3.4.3.1   *Effect of Isothermal Transformation Temperature*
 As shown in Fig. 2.44. Quenching from 600°C produced a thin band of grain boundary ferrite and higher number density of intragranulary nucleated polygonal ferrite crystal as shown in Fig.2.44 (a). Isothermal transformation at 550°C as shown in Fig. 2.44(b) produced a very little grain boundary nucleated allotriomorphs and high density of small ferrite side plates nucleated within the prior austenite grains. According to Fig. 2.44(c) a very fine acicular ferrite structure was formed in V-steels when the the isothermal transformation temperature was lowered to 450°C.

(a) 600°C   (b) 550°C   (c) 450°C
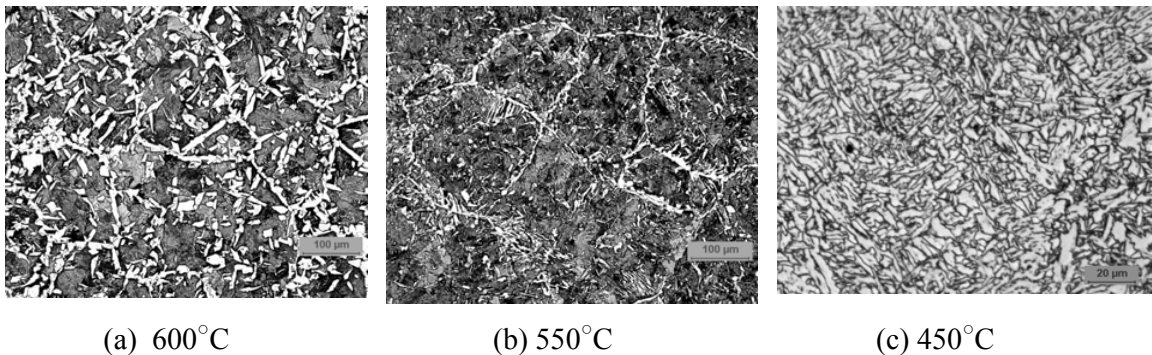
Fig. 2.44 Microstructure of 0.10%V steel isothermally transformed between 700-450°C prior to gas quenching to room temperature [39,40].

2.3.4.3.2   Effect of Inclusions

The reduction in inclusion density leads to a transition from acicular ferrite to bainite [145,281-82].Non-metallic inclusions steel are the most potent nucleants if they have a good lattice match with ferrite. There may then exist reproducible orientation relationships between inclusions and the ferrite plates that they nucleate [15].The steels with relatively free of non-metallic inclusions as shown in figure 2.45 , bainite nucleates initially in austenite/austenite grain surfaces and grows by repeated formation of sub-units as shown figure 2.22 to generate the classical sheaf morphology [49,130,145].Acicular ferrite content is always very small in absence of inclusions. Supporting experiment is when the inclusions are removed by vacuum remelting a weld. Therefore when steel cools, it transforms into bainite instead of acicular ferrite microstructure. A full description of this behaviour is given in Ref. [151].
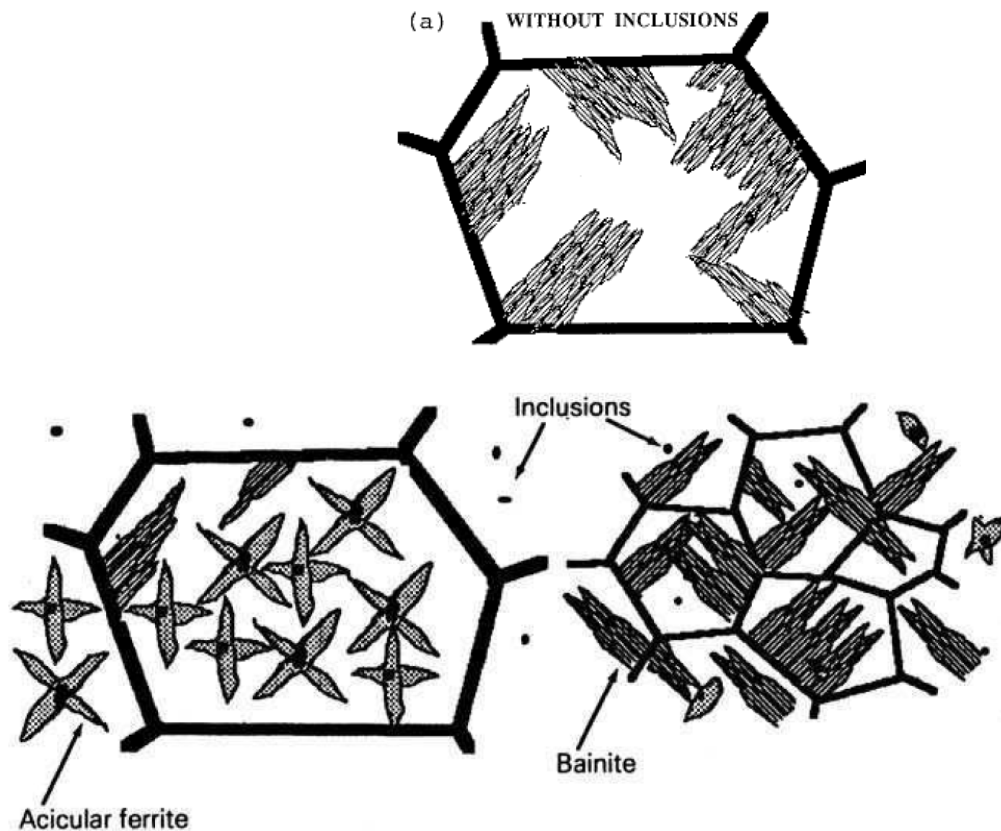
Figure 2.45 The effect of inclusion density, since the sample with smaller inclusion density transformed to bainite [15, 49,145].

2.3.4.3.3. Effect of Reheating Temperature

The austenite grain size control and precipitation strengthening are important factors in development of the final mechanical properties of the product [9,129].As reported by [288]

, and illustrated in Fig 2.46(a), the austenite grain size for Nb-V Microalloyed steel slightly increase when T_{rh} = 900-1150°C, whereas for the V micro-alloyed steel, it is effective as grain size inhibitor only below 950°C, above this temperature the grains coarsen rapidly. This is attributed to the precipitation dissolution temperature. After the precipitate is in the solid solution, it acts as solute drag (weak pinning), but if temperature lower than precipitation dissolution temperature, the MEA will precipitate and retard grain growth (grain size inhibitor) i.e acts as (strong pinning) as shown in Fig. 2.46 (b). However for Nb-V the higher increase in grain size was observed when T_{rh}=1250 $^{\circ}$C, because the niobium is an effective grain refining element [3,9,152].Whereas the lower end and upper end dissolution temperature of (Nb)(C,N) precipitate which was in the vicinity of 1200°C ,and in the close to 1250 $^{\circ}$C as predicted based on Johansen, Hudd and Narita relations [46].However at higher reheating temperature, the increase in the amount of AF, due to higher austenite grain size because austenite grain boundaries are preferred sites for the nucleation pearlite and bainite [15,49,94,138].Therefore ,with larger austenite grains fewer nucleation sites will be available for the above phases , as a result , intragranular nucleation will be promoted in expense of grain boundary transformation products.

(a)   (b)
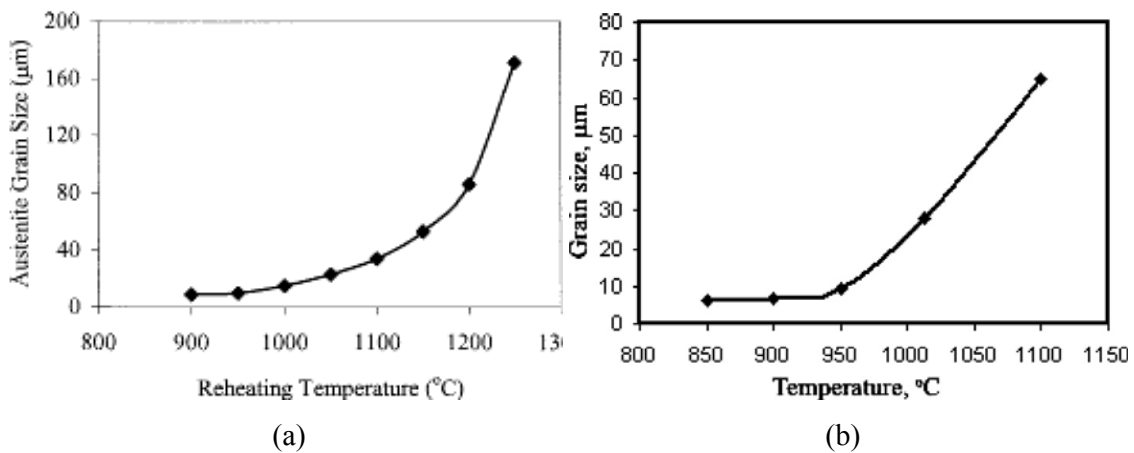
Fig. 2.46 Average austenite grain size variation with reheating temperature (a) Nb-V
Microalloyed steel [46], (b) V Microalloyed steel [288].

It has been known for many years that particles can restrain the growth of austenite grains [46,153,154,288].Several theoretical interpretations of grain growth in particle-containing materials have been put forward. The model developed by Zener [155] produces a simple relationship:

$$R_Z = \frac{4r}{3f}$$

(2.30)

Between the grain radius R, the particle volume fraction f and particle radius r. He considered that both grains and particles could be approximated to spheres.

Gladman [156] adopted a more realistic approach by considering the pinning force exerted by a single particle on a planar boundary and then derived the driving force for grain growth. An important feature in this model is the ratio of the radii of growing grains to matrix grains, Z.

$$R_G = \frac{\pi r}{6f}\left(\frac{3}{2} - \frac{2}{Z}\right)$$

(2.31)

where Z lies between $\sqrt{2}$ and 2.

Hellman and Hillert [157] considered the curvature in the grain boundary and introduced into Zener's equation a correction factor β which equalled to $(0.12540.\text{Ln}(40R/r)$,and for abnormal grain growth the equation was derived as

$$R_{H_1} = \frac{4r}{3f\beta}$$

(2.32)

where β was normally between 1.3 to 1.6.

In recent years, computer modelling has been developed to predict particle-size / grain-size relationships. Hillert [158] compared these models with both two and three dimensional approaches. He concludes that in three dimensional systems

$$R_c = \frac{4r}{9f^{0.93}}$$

(2.33)

is recommended, except for large values of f, where the exponent decreases to lower values. Rios [159] derived an equation to predict grain growth in systems in which particles are coarsening and dissolving where

$$R_R = \frac{r}{6f}$$

(2.34)

Another model, developed by Elst *et al*, [160] can be modified to accommodate elongated particles, a bimodal particle distribution and a distribution of grain boundary precipitates. Here

$$R_E = \frac{4r}{3f\beta}\left(\frac{3}{2} - \frac{2}{Z}\right)$$

(2.35)

where β is an increasing function of R/r and R_E approximated to 0.056~0.067 (r/f) [161]

2.3.4.3.4   *Effect of Allotriomorphic Ferrite Formation*

 Since the allotriomorphic ferrite is the first phase to grow on cooling from the austenite phase field.The formation of an allotriomorphic ferrite layer on the pervious austenite grain boundaries as shown in (Fig. 2.47). It is expected to cause a reduction in the density of austenite grain boundary nucleation sites and, hence, promote the preferential formation of acicular ferrite at the expense of bainite i.e the promotion of grain boundary ferrite will encourage intragranular acicular ferrite nucleation [15,49,56,98,94,136,145,162,163].
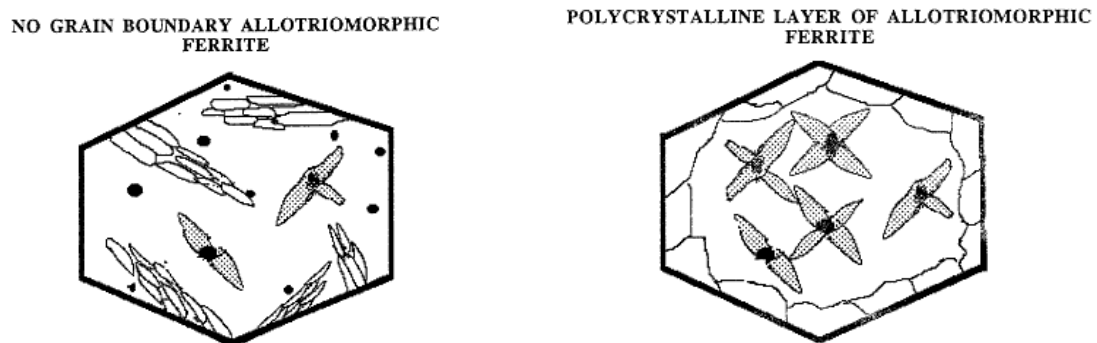
Fig. 2.47. The growth of a layer of inert allotriomorphic ferrite at the austenite grain surfaces causes a transition from bainite to a cicular ferrite [15,49,145].

2.3.3.3.5. *Effect of Boron*

The boron retards the heterogeneous nucleation of allotriomorphic ferrite at the austenite grain surfaces, to a greater degree than that of bainite as can be seen in Fig. 2.48. Boron segregates to austenite grain boundaries, so it reduces the grain boundary energy i.e makes it less effective as heterogeneous nucleation sites (render austenite grain boundary nucleation sites impotent and hence to promote acicular ferrite). A typical addition of ≈ 0.002 wt% is

sufficient to have a profound effect on transformation kinetics [15], although the exact amount must clearly depend on the austenite grain size. Too much boron precipitates as borides which stimulate the nucleation of ferrite. Boron is only effective in enhanching hardenability when present in solid solution, not when precipitate as oxides or nitrides as illustrated in Fig. 2.49. It's the reason why boron-containig steels are usually deoxidized with aluminium
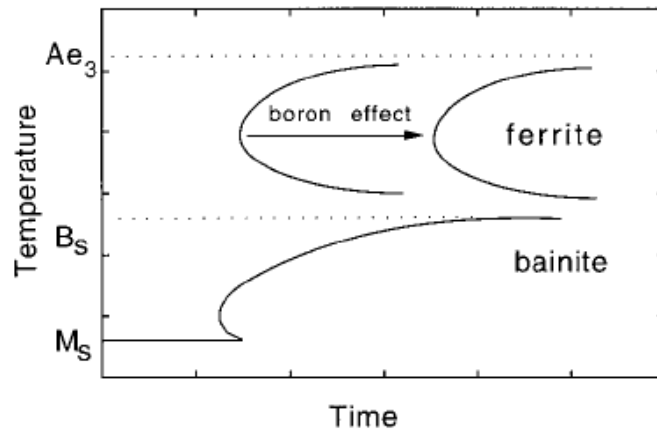
Fig. 2.48. The effect of boron. There is a pronounced effect on the allotriomorphic ferrite Transformation but only a minor retardation of bainite reaction [15].
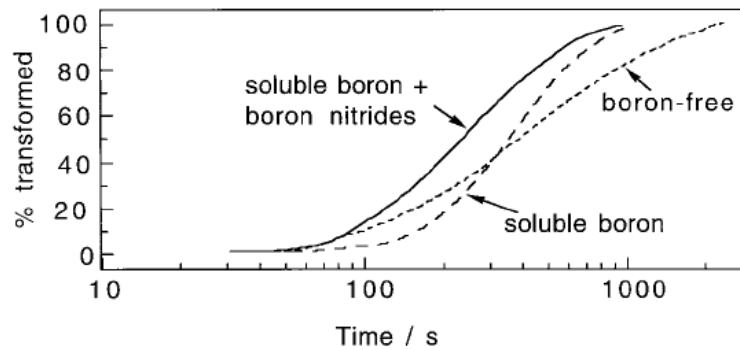
Fig. 2.49. The rate of reaction is fast in steel containing boron nitride, compared with Boron free,where as the rate is slow in solouble boron steel [15].

2.3.4.3.6 *Effect of Sulfur and Managanese*

Manganese sulphide (MnS) particles are commonly present in commercial steel, ther can act as substrate nucleation sites of primary ferrite plates. The presence of MnS core covered or at least partially covered with vanadium nitride (VN) and vanadium carbide (VC) or both of them, promotes the nucleation of idiomorphic ferrite as illustrated in Fig.2.50(a,b) and Fig.2.51.By contrast and as reported by [164],the presence of MnS at the surface of oxides

particles inhibits the nucleation of ferrite. In some studies it is suggested that, for titanium containing steel, the MnS is found to be precipitate on titanium oxides and stimulaing the nucleation of acicular ferrite [15].The formation of bainite or intragranular ferrite will found [131] dependend on the amount of sulphur added to the steel. So small concentration of sulphur (S ≈ 0.005 wt %) can sometimes stimulate the nucleation of bainite and resulting decrease in absorved energy [131,165].Moreover, the formation of intragranular ferrite plate IFP is promoted by increasing amount of sulfur (0.06-0.07 wt% S) due to increase the number of MnS particles as an effect off sulfur addition , resulting an increase in absorved energy (Fig.2.50-C), due to increase the resistance to the propagation of brittle fracture which is dominant in fracture mode at lower temperature, however as the amount of sulfur addition in large quantities, the MnS particles coarsened and acts as crack initiation points, there by promoting brittle fracture [46,131].Some researches indicate that the intragranular ferrite is caused by the formation of Mn depleted zone around inclusions [147].The precipitation of MnS at oxide was reported to promote the formation of intragranular ferrite [147].Recent experimental results clearly demonstrate that intragranular ferrite plates can easy nucleate on VN [166].This has been related to the atomic matching between (100)vn // (100)α planes which allow the growing ferrite to maintain coherent, low energy interfaces with respect to vavadium nitride, in order to obtain intragranular ferrite the active VN particles must first form in austenite [166].

(a)   (b)
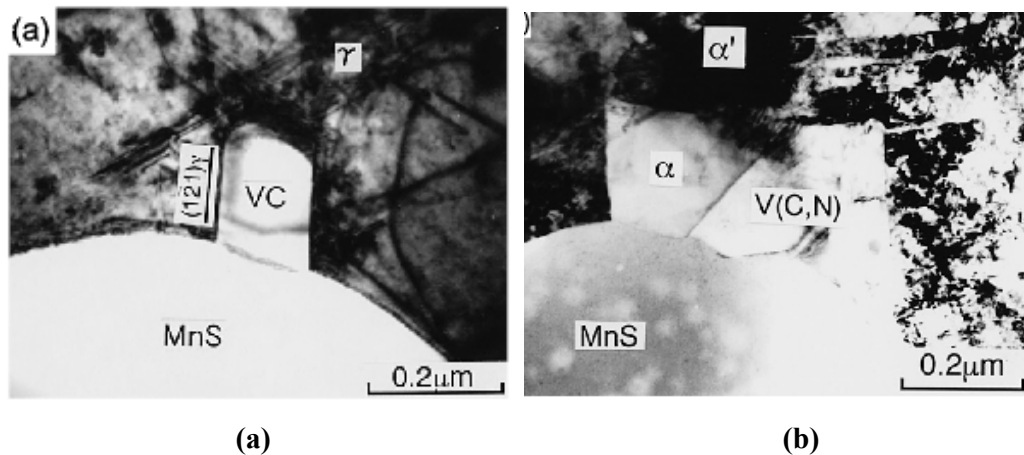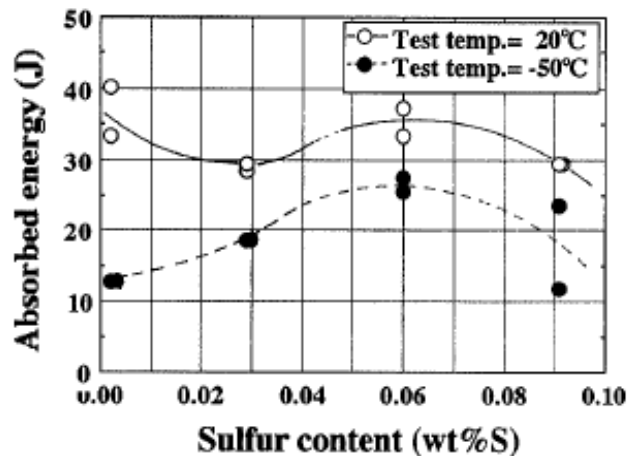
(c)

Fig.2.50 (a) TEM micrograph-VC nucleated at incoherent MnS,(b) TEM micrograph. Itragranular nucleated ferrite at MnS + V(C,N) complex precipitate [96],(c) Effect of sulfur content on impact absorbed energy at -50 $^\circ$C and 20 $^\circ$C [131].

2.3.4.3.7. Effect of Nitrogen and Vanadium

Previous data strongly indicate that the role of nitrogen is clear. The positive effect of higher nitrogen content in V-microalloyed steel on the yield strength, notch toughness and weldability is given in Ref. [102,167].However as reprted by[8,42],the nitrogen in V-microalloyed steel is conducive to improved grain refinement and raised yield stress.The recent experimental results clearly demonstrate that intragranular ferrite plates can easy nucleate on VN [39,40].As shown on the Fig. 2.51 VN start to grow on the existing MnS inclusions. So it is concluded that nitrogen is a very reliable alloying element, increasing the yield strength of V-microalloyed steels by some 6 MPa for every 0.001% N [168].
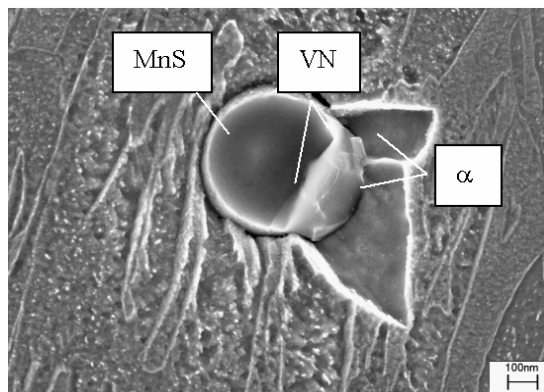
Fig. 2.51 Intragranular ferrite nucleus in 0.12%V-steel, water quenched from 660°C after ≈ 5% transformation [39,40,169].
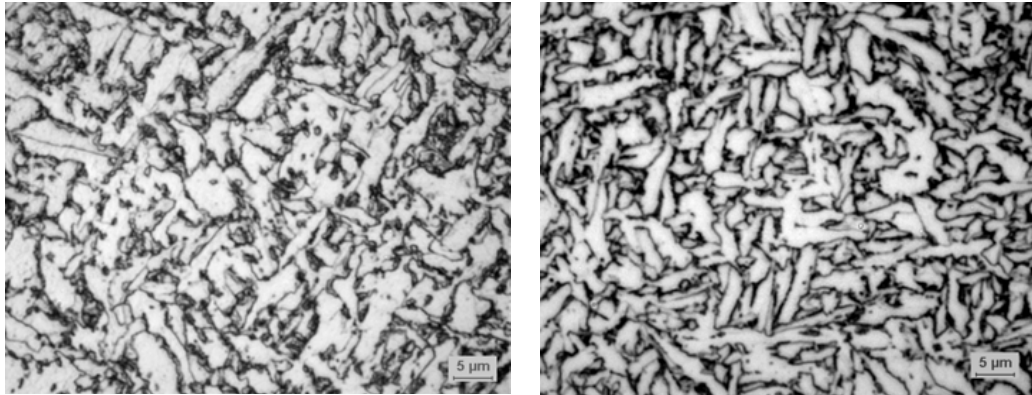
| (a) 0.22C-0.12V-0.0015N | (b) 0.1C-0.12V-0.025N |

Fig. 2.52. Microstructure of low N-steel, and high N-steel isothermally transformed at 450°C [39,40].

However the V is the most effective microalloying element for nucleation of intragranular ferrite. The formation of intragranular polygonal ferrite requires the presence of active VN particles in austenite [39,40].But the effect of V in promoting the formation of intragranular polygonal ferrite is more profound in high N steels, because as the N content is increased the chemical driving force for precipitation is increased and VN particles become coarser and more numerous, thereby increasing the nucleation rate of intragranular ferrite. However the tendency for the formation of acicular ferrite was observed in the V-microalloyed steel with a very low nitrogen content as shown in Fig. 2.52. This suggests that vanadium on its own promotes the formation of the acicular ferrite microstructure. If it is assumed that V alone is responsible for the formation of AF i.e in this case the driving force for nucleation of ferrite determined by the interaction of V with other alloying elements [39,40],as e.g VC. By contrast the vanadium is selected due to its precipitation hardening capability, with a view to improve the toughness properties [98,179,171].As reported by [15],presence of small concentrations of nitrogen in ferrite steel, it is unlikely that nitrogen has any significant thermodynamic effect on the $\gamma \rightarrow \alpha$ transformation, its influence must be kinetic, perhaps via some interaction with the inclusion phases. Authors [162],found that intragranular ferrite predominant morphology were nucleated at VN or VC which was precipitated on MnS particles in austenite grains resulting in a fine ferrite-pearlite microstructure, because vanadium free steel, containing only MnS inclusion which implies that these MnS inclusions are not an effective nucleant for ferrite or only a weak nucleant, based on this finding the success was achieved in improving of toughness of hot-forged products with a strength of

800-900 MPa with no subsequent heat treatment can by widely used for automobile structural parts [46,131].It has been suggested [162],that presence of V can enhance the nucleation potential of inclusions by precipitation of VN at the inclusion surface due to it produce low energy interface [15,131,172].Authors [166],explain two ways in which the precipitation of VN in austenite can be enhanced. The first alternative is to modify the steel composition to obtain a high density of MnS inclusions or other particles which may act as nucleation sites for VN in austenite. The second alternatives a strain-induced precipitation of VN in austenite during hot rolling in the temperature range of VN precipitation. It is clarified that the addition of both vanadium and nitrogen is indispensible for the formation of intragranular ferrite plates [49,131,147].The presence of high V and N in steel that lead to vanadium nitride VN can precipitate on manganess sulfide particles (MnS) before austenite is transformed to ferrite acts as nucleation sites of intragranular ferrite [56,131,166].As the nitrogen content is increased the chemical driving force for precipitation is increased and the VN particles become coarser and more numerous, thereby increasing the nucleation rate of intragranular ferrite [166] Fig.2.50 (a) which show typical example of VC nucleated at incoherent MnS i.e (VC/MnS) in Fe-12Mn-0.8C-0.3V, since VC grows only into austenite, it is usually considered that VC should hold a low-energy orientation relationship with respect to austenite [96], fig.2.50(b) shows an intergranular ferrite nucleated at MnS+V(C,N) complex precipitates.

2.3.4.3.8. Effect of Ti addiation

Titanium is added with the aim of refining the microstructure through the inhibiting effect to grain coarsening exerted by small TiN precipitates [98,173-175].To suppress this grain coarsening, a addition of 0.010 – 0.015 % Ti will provide TiN precipiton on grain boundaries [1,8,9] Therefore Ti additions, on the order of 0.01%, which cause the precipitation of fine TiN particles in austenite, are very effective in maintaining fine austenitic grain sizes during forging. It is important not to add too much Ti in order to prevent the formation of coarse TiN particles in liquid steel. Coarse particles are ineffective in restraining austenite grain growth and are detrimental to toughness and fracture. Ti is a very strong nitride forming element, and titanium nitride particles are stable at the high temperatures of forging. Fig. 2.53 ranks austenite grain coarsening behaviour of steels containing V, Al, Nb and Ti and shows that grain coarsening in Ti-containing steels does not occur at temperatures around 1200ºC or higher [85].Titanium and vanadium microalloyed steels are of common use in the manufacture of automotive components [27,98,176].Moreover the intragranular nucleation of acicular ferrite can be

promoted by inoculating the steel with TiN particles, and by rendering the austenite grain boundaries inactive in respect to nucleation of bainitic sheaves [15,56].The small TiN – particles existing after strand casting of Ti – microalloyed steels, not only engender effective grain – growth inhibition between rolling passes and during colling following the termination of rolling, but are also useful for restricting HAZ – grain coarsening in association with subsequent welding [177].The maximum level of fine TiN precipitation from supersaturated solid solution occurs when the levels of Ti and N in the steel are at the stoichiometric ratio [178,179] i.e the increasing levels of TiN precipitation with increasing Ti in the steel , only a part of this precipitation is fine enough to be effecive in controlling grain size i.e the use of Ti–based microalloy precipitates reveals an attractive means of controlling the coarse grain size in high heat input welding application [178].
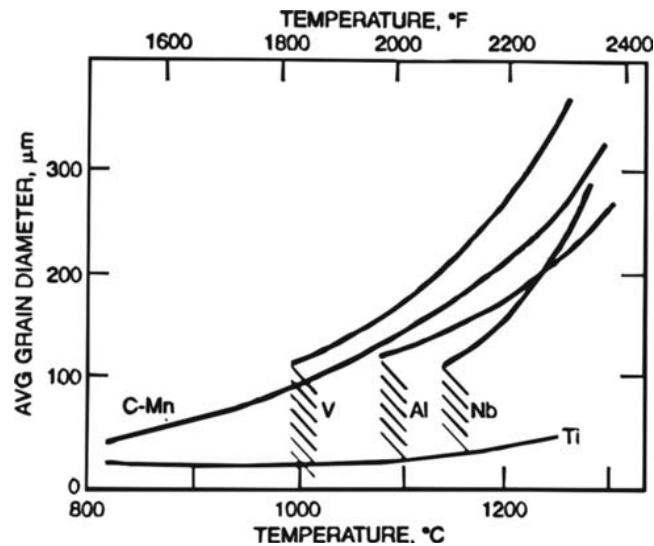
Fig. 2.53   The effect of various microalloying elements on austenite coarsening [85].

 However as given in Ref.[147], TiN particles served as nucleation sites for proeutectoid ferrite preferentially and also accelerated its formation in low-carbon alloy steels. TiN is regarded as an effective nucleation sites for intragranular ferrite owing to low interfacial energy between ferrite and TiN. Morikage et al [147] also reported that the critical size of a TiN particle for the formation of ferrite decreased with the amount of undercooling in low carbon steels, that is ≈140 nm at 750C and ≈ 50 nm at 650C. The intragranular nucleation of acicular ferrite can be promoted by TiN particles.

2.3.4.3.9. Effect of the Crystallographic Relationship between the Phases

The crystallographic relationship between the phases affects greatly the nucleation kinetics of intragranular ferrite. The factor governing the formation of intragranular ferrite plates is the presence of precipitates which can develop coherent, low energy interphase boundaries with ferrite in austenite for that reason toughness of medium carbon steel with tensile strength higher than 1000 MPa were shown to be improved through the formation of intragranular ferrite plates i.e formation of low energy boundaries interface seems to promote the nucleation [96,131].The interfacial energy are considered to be strongly depended on the lattice mismatch of interphase boundary [131].Acicular ferrite is not found when the density of intragranular nucleation sites is small. Alternatively, an increase in the density of austenite grain boundary nucleation sites leads to the same transition [49,145].This lead to formation of low-energy ferrite/V(C,N) interface seems to promote the nucleation of ferrite in this case [49].Recent experimental results [166], clearly demonstrate that intragranular ferrite plates can easy nucleate on VN. This has been related to the atomic matching between $(100)_{VN}$ // $(100)\alpha$ planes which allow the growing ferrite to maintain coherent, low energy interfaces with respect to vanadium nitride, in order to obtain intragranular ferrite the active VN particles must first form in austenite [166].Since the misfit ratio of VN, which is for (001) planes estimated at 1.37% is lower than others (For TiN =3.8% and for MnS = 8.8%) i.e VN particles should be more potent nucleation sites than the latter [56].As it is shown in fig.2.54 that the interfacial energy between ferrite and vanadium nitride VN is very small if the B-N relationship holds.
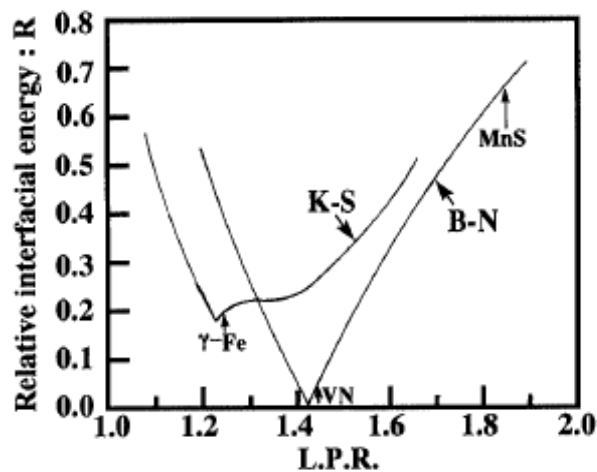
Fig.2.54 The relative interfacial energy, R, as function of the lattice parameter ratio, L.P.R [131].

These results suggest that intergranular ferrite plate is nucleated while maintaining, low energy interfaces with respect to vanadium nitride [131].Also Ishikawa et.al [86] reported that the presence of low energy ferrite/V(C, N) interface with the Baker-Nutting (B-N) orientation relationship promotes intragranular ferrite transformation. The low degree of misfit between the ferrite matrix and the substate lattices and a large strain field build up in austenite around inclusions are both assumed to increase the nucleation potential of inclusions, and to favour nucleation at higher temperatures [56,172].

2.3.4.3.10. Effect of Molybdenum and Chromium

The addition of suitable amount of chromium and molybdenum prevent the formation of allotriomorphic ferrite at high concentrations and, hence, lead to the promotion of classical bainite at the expense of acicular ferrite [15,145].In some quantitative data [145,180] have been reported that as the chromium or molybdenum is increased, the volume fraction of acicular ferrite goes through a maximum as a function of concentration as illustrated in Fig. 2.55, whereas at relatively large concentrations of chromium and /or molybdenum, its prevents the growth of allotriomorphic ferrite and acicular ferrite is replaced by classical bainite, until the microstructure becomes almost entirely bainitic. However as reported by [145],this effect cannot be attributed to any drastic changes in the austenite grain structure, nor to the inclusion content of the weld deposits, but may be related to the reduction in the coverage of austenite grain boundaries by layers of allotriomorphic ferrite as the solute concentration exceeds a certain value.
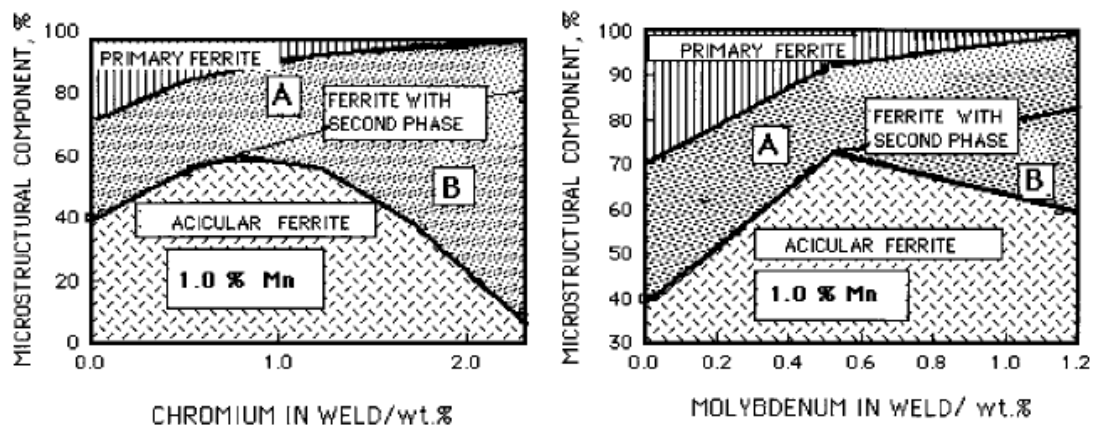
Fig. 2.55 .Change in microstructure of steel weld as a function of chromium and molybdenum concentration [145,180].

Concurrently below that concentration, the steel hardenability is low enough to ensure that the austenite grain surfaces are completely covered by uniform layers of alltriomorphic ferrite, consequently allowing the development of acicular ferrite by intragranular transformation. However the chromium or molybdenum its called also strong carbides forming element, it has been suggested by [145,177],that it can reduce the rate of growth of ferrite, as well as proeutectoid ferrite, by a solute-drag effect on the moving γ/α interface. It is generally accepted that austenite decomposition is delayed in molybdenum containing steels leading to an increase in hardenability [136] (decrease rates of transformation) i.e two c-curves in TTT diagram are separated, and as the hardenability of steel decreases, the two curves tend to overlaps so it appears like the TTT diagrams contains just one curve with complicated shape. The alloys utilize chromium and molybdenum, which serve to enhance hardenability but also, during subsequent heat-treatment, cause the precipitation of alloy carbides which greatly improve the creep resistance [45].Whereas isolating of the bainite reaction in low-carbon steels has been found by adding small amounts of boron and molybdenum to suppress allotriomorphic ferrite formation.While the straight molybdenum steel encourages the bainite reaction [45].

2.3.4.3.11. *Effect of Stress on the Acicular Ferrite Transformation*
As reported by [181], the stress has little influence on the overall fraction of acicular ferrite. Nevertheless, an extermally applied stress accelerates transformation and alters the morphology of acicular ferrite [15].

2.3.4.3.12. *Effect of Strain*
The growth of ferrite plates results in carbon enrichment of the remaining austenite which may remain untransformed or transformed to martensite. Upon the application of strain, the untransformed austenite is converted to martensite, which would increase strain hardening and residual compressive stresses bringing higher resistance to necking and crack arrest properties respectively [46].So the effect of deforming austenite prior to its transformation is illustrated in Figs. 2.56.The outer part of the sample recrystallise whereas the center remains unrecrstallised (deformed). The acicular ferrite/binite microstructure are the main component in the outer part of the sample (recrystallised region), allotriomorphic ferrite and pearlite are the major component of microstructure in the center as showen in Figs. 2.56 (b) and 2.56 (c), respectively.This is attributed to the increase deformation promotes the formation of

allotriomorphic ferrite inside austenite grains as shown on fig. 2.56.(d) and indicated by white arrow[176].Authors [166] revealed that the precipitation of VN in undeformed austenite is very sluggish and requires long holding time near the temperature of maximum precipitation in order to produce effective VN particles [166].
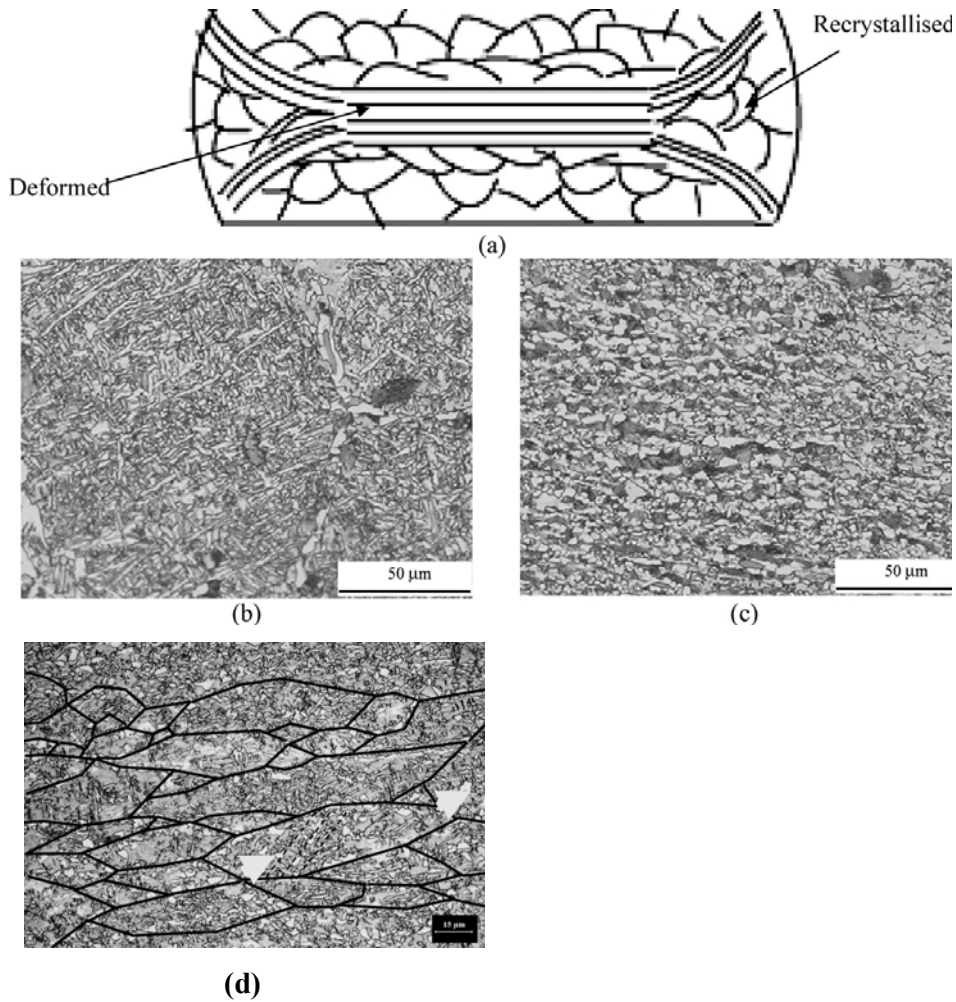
Fig.2.56. (a) Scheme of prior austenite grain structure, (b) outer and (c) center of steel (d).Formation of intragranular proutectoid ferrite in steel (see arrows). Black solid lines indicate the prior deformed austenite grain [136].

2.3.4.3.13. Effect of strain rate

The strain rate has a strong effect on acicular ferrite formation as shown on fig. 2.57 on the same deformation level and cooling condition, the volume fraction of acicular ferrite increased for high strain rates as compared with lower ones that was due to increase the shear bands at higher strain rates i.e intragranular nucleation sites increases [136].
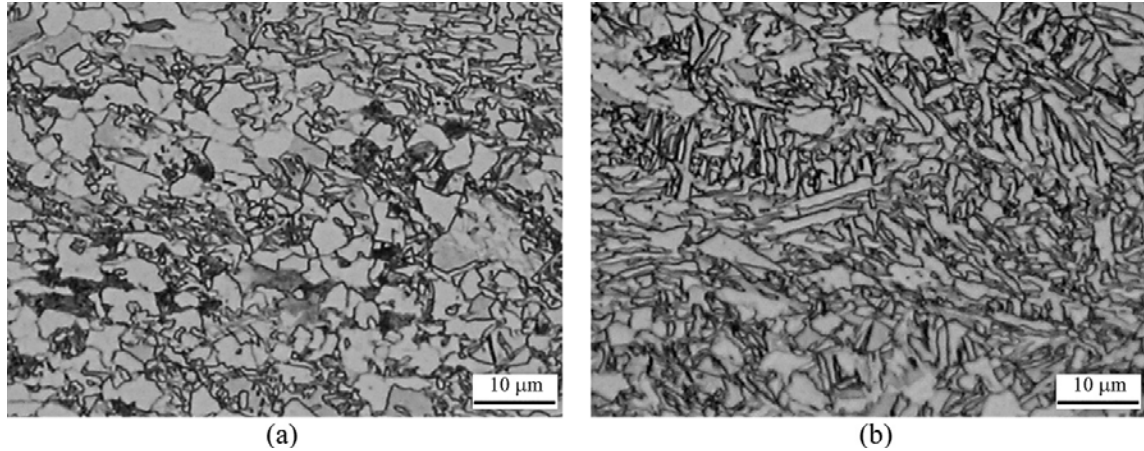
Fig 2.57 Microstructure of steel obtained after deformation at ε =1,and cooled at 2C/s (a) 1/s (b) 10/s strain rate [136].

2.3.5. MARTENSITE TRANSFORMATION

The fundamental requirement for martensitic transformation is that the shape deformation accompanying diffusionless transformation be an invariant–plane strain; all the characteristics of martensite will be shown to be consistent with this condition. The transformation starts only after cooling to a particular temperature called the martensite start (Ms) temperature. The fraction transformed increases with the undercooling below Ms.

2.3.5.1. Nature of Martensitic Transformations

Martensitic transformation is diffusionless [15,19,182].The formation of martensite can occur at very low temperatures where atomic mobility may be inconceivably small. Even when martensite forms at high temperatures, its rate of growth can be so high that diffusion does not occur. Plates of martensite in iron based alloys are known to grow at speeds approaching that of sound in the metal [183].

2.3.5.2. Orientation Relationships

Since there is no diffusion during martensitic transformation, atoms must be transferred across

the interface in a co-ordinated manner (Ref. 184]. All martensite transformations lead to a reproducible orientation relationship between the parent and product lattices. Typical examples of orientation relations found in steels are given below [19,185].

1-Kurdjumov–Sachs:

$$\{1\ 1\ 1\}_\gamma \| \ \{0\ 1\ 1\}_\alpha$$
$$<1\ 0\ \bar{1}>_\gamma \| \ <1\ 1\ \bar{1}>_\alpha$$

2-Nishiyama–Wasserman

$$\{1\ 1\ 1\}_\gamma \| \ \{0\ 1\ 1\}_\alpha$$
$$5.3° \ \text{from} <1\ 1\ \bar{1}>_\alpha \ \text{towards} \ <\bar{1}\ 1\ \bar{1}>_\alpha$$

3-Greninger–Troiano

$$\{1\ 1\ 1\}_\gamma \quad \text{about } 0.2° \text{ from} \{0\ 1\ 1\}_\alpha$$
$$<1\ 0\ \bar{1}>_\gamma \quad \text{about } 2.7° \text{ from} <1\ 1\ \bar{1}>_\alpha \ \text{towards} \ <\bar{1}\ 1\ \bar{1}>_\alpha$$

The Kurdjumov–Sachs is found in plain carbon and low alloy steels up to about 0.5 wt% carbon [19]. When the carbon content is increased, the orientation relationship changes from Kurdjumov–Sachs to Nishiyama. The change is not detectable microscopically. Although the addition of metallic alloying elements causes Nishiyama it to occur at much lower carbon contents [19].

2.3.5.3. The Shape Deformation due to Martensite Transformation

It is clear from Fig. 2.58, that the martensitic transformations are always accompanied by a change in shape of the parent crystal, this shape deformation always has the characteristics of an invariant–plane strain (IPS), when examined on a macroscopic scale. All martensitic transformations involve co-ordinated movements of atoms and are diffusionless [185]. The formation of martensite (due to its IPS shape deformation), cause a distortion of the parent lattice. The strain energy due to this distortion, per unit volume of martensite, is approximately given by [186]:

$$E = \frac{c}{r}\mu(s^2 + \delta^2)$$

(2.36)

where μ is the shear modulus of the parent lattice, c/r is the thickness to length ratio of the martensite plate and s and δ are the shear and dilatational components of the shape deformation strain. E usually amounts to about 600 J / mol for martensite in steels [186]. The typical energies associated with martensitic transformation are given in table 2.4.

Table 2.4: Typical energies associated with martensitic transformation [187,283].

	$\mathrm{J\,mol^{-1}}$
Strain energy	600
Twin interface energy	100
γ/α' interface energy	1
Stored energy due to dislocations	20
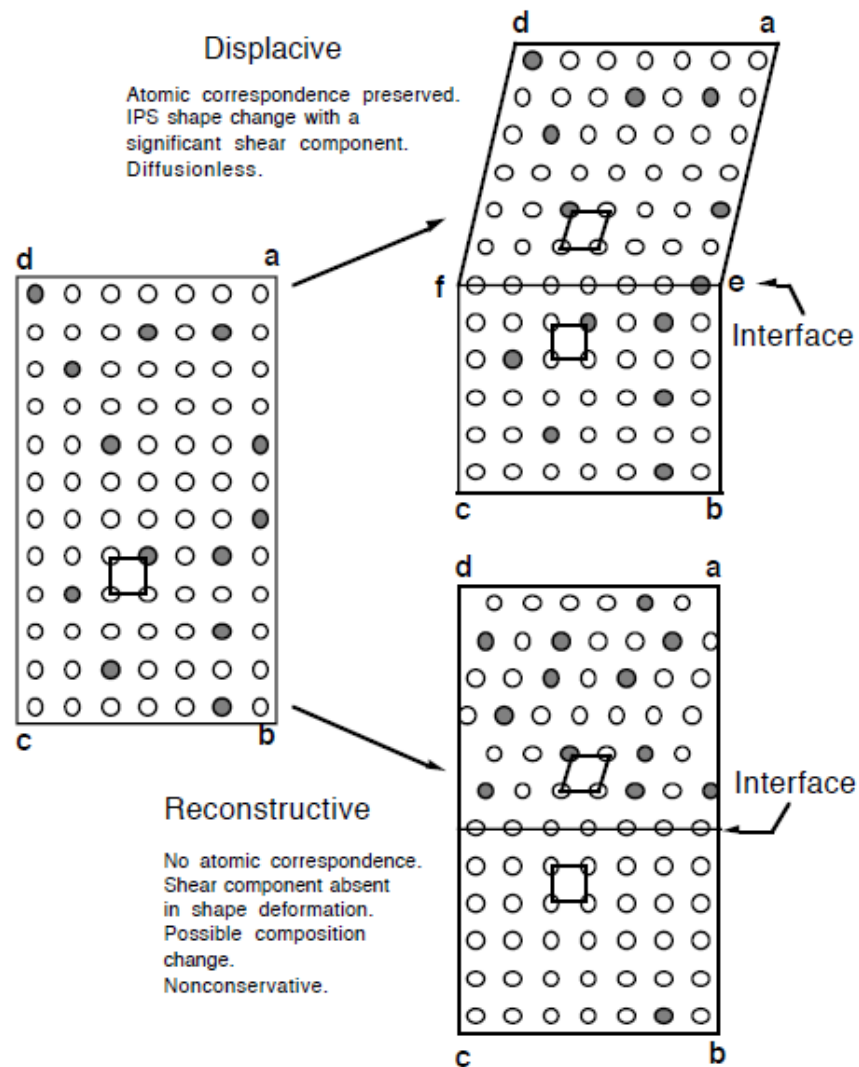
Fig.. 2.58 Schematic illustration of the mechanisms of diffusional and shear Transformations Transformations [185]

By contrast, in the case of the diffusional transformation illustrated in Fig. 2.58, it is evident that the product phase can be of a different composition from the parent phase. In addition, there has been much mixing up of atoms during transformation and the order of arrangement of atoms in the product lattice is different from that in the parent lattice - the atomic correspondence has been destroyed. Because the transformation involves a reconstruction of the parent lattice, atoms are able to diffuse around in such a way that the IPS shape deformation (and its accompanying strain energy) does not arise. The scratch ab remains straight across the interface and is unaffected by the transformation.

2.3.5.4. **Thermodynamics of Martensitic Transformations**

Martensite is not represented on phase diagrams because the latter deal with equilibrium. Martensite deviates from equilibrium in two important ways:

(i) Martensite grows without diffusion, so it inherits the chemical composition of the parent austenite. In an equilibrium transformation the chemical elements partition into the parent and product phases in a manner which leads to a minimisation of free energy.

(ii) The shape deformation associated with martensitic transformation causes strains; the resulting strain energy has to be accounted for before the transformation can happen. These deviations can be represented on a free energy plot as illustrated in Fig. 2.59.

The relationship with the phase diagram is illustrated in Fig 2.41. Martensitic transformation is only possible below the T_0 temperature.

The distance **ac** in figure 2.59 represents the free energy decrease when austenite of composition $\bar{x}$ decomposes into an equilibrium mixture of ferrite and austenite of compositions $x^{\alpha\gamma}$ and $x^{\gamma\alpha}$ respectively .The distance **ab** is the smaller decrease in free energy when martensite forms without any composition change, taking into account the stored energy associated with the transformation [45].
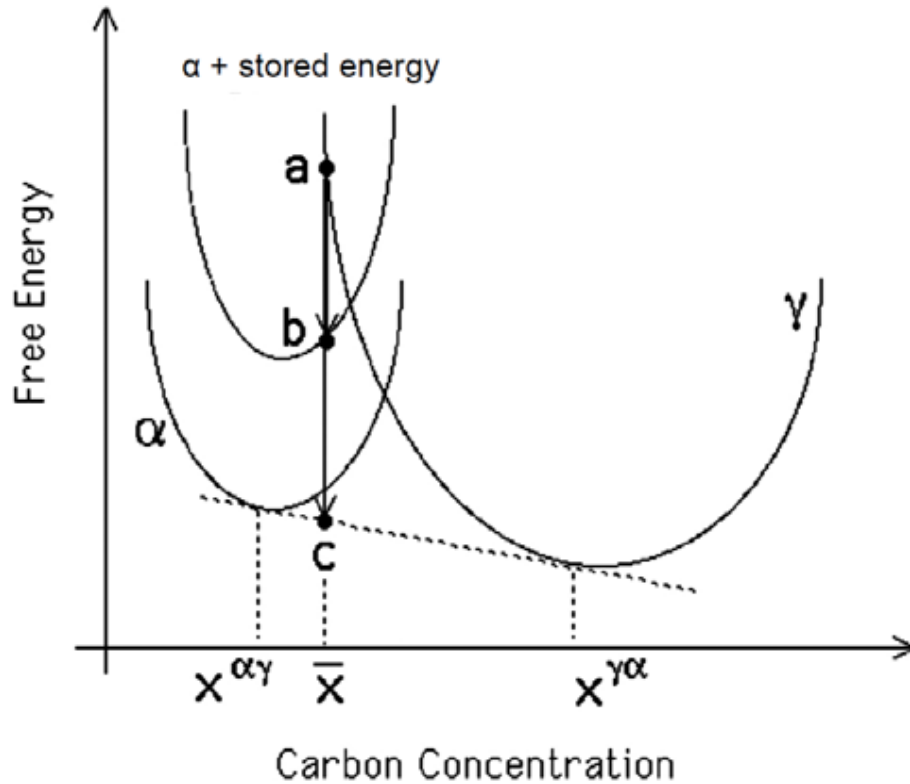
Fig. 2.59. Dependence of free energy on carbon concentration [45]

2.3.5.5. MARTENSITE Morphology

Two different morphologies are observed in ferrous martensite microstructures: plate martensite and lath martensite, as shown in Fig. 2.60 [188]

2.3.5.5.1 Plate Martensite

A characteristic of plate martensite is the zigzag pattern of smaller plates,as shown in Fig. 2.60 (b) and Fig. 2.61 (a), which is formed later in the transformation. Smaller planes are bounded by adjacent larger plates that were formed at the beginning of the transformation. An important feature of plate martensite is the presence of microcracks (see Fig. 2.61 a). These cracks occur when adjacent martensite crystals impinge on each other. Due to the shear-type mechanism, the transformation velocity of martensite can approach 10^6 mm/s, and thus growing martensite plates can achieve a significant amount of momentum. Impacts between moving plates create these microcracks [189].The substructure of plate martensite consists of transformation twins, as a result of the shear mechanism that occurred during the transformation.The regions in between the martensite plates in these micrographs are leftover

parent phase that did not transform to martensite, called retained austenite, (the region between these packets is retained austenite). Retained austenite between martensite plates is easily resolvable by the light optical microscope.
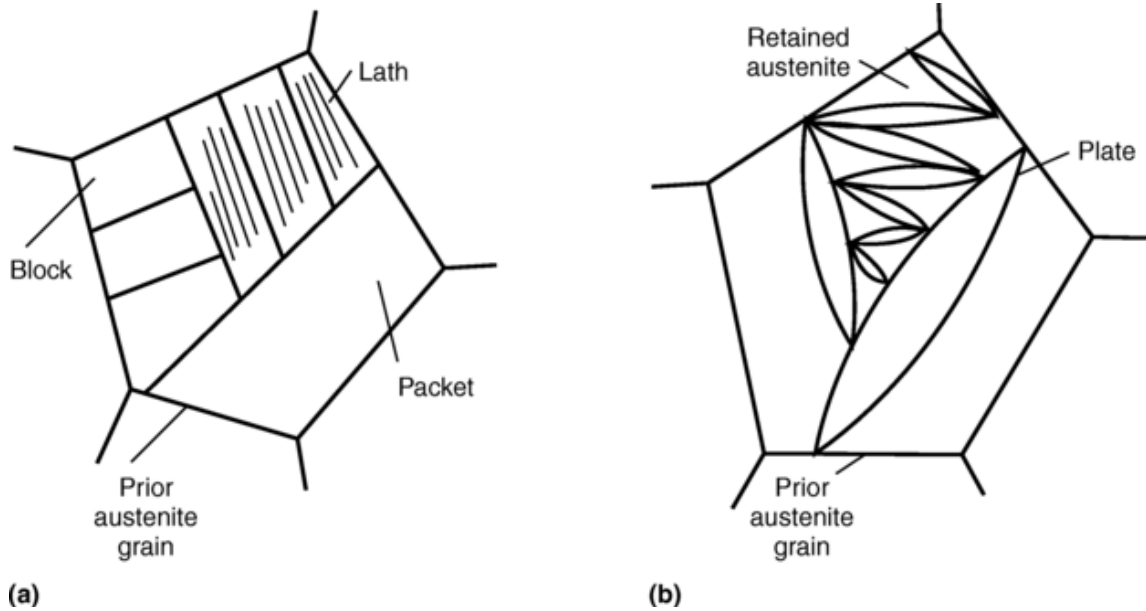
Fig. 2.60. Martensites. (a) Lath. (b) Plate [189].
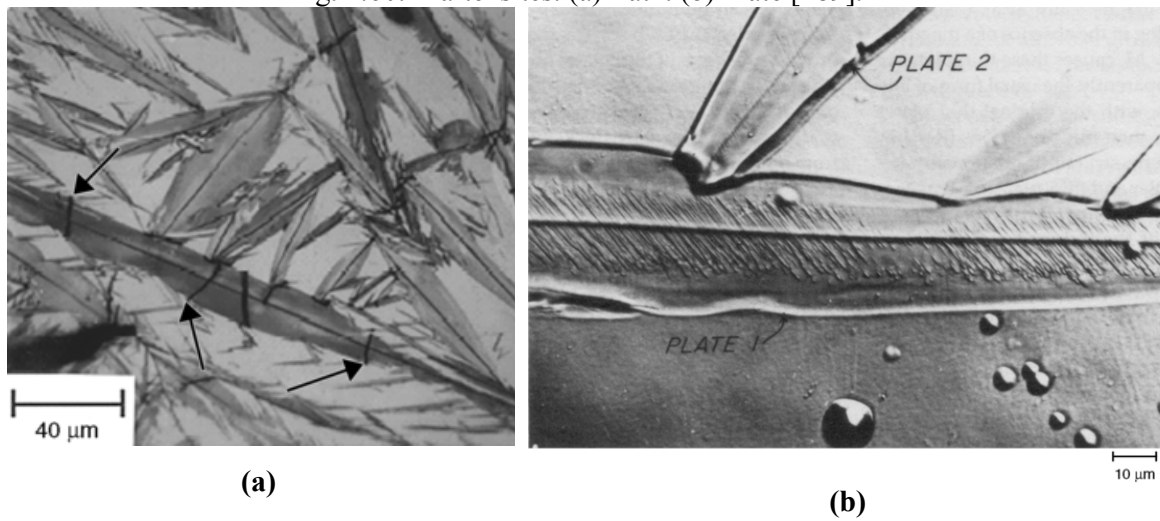
Fig. 2.61. **(a)** Plate martensite. Arrows indicate microcracks [191], **(b)** Martensite plates. Note the presence of midrib in both plates. Plate 1 shows fine structure consisting of twins [190].

2.3.5.5.2   *Lath Martensite*

The other major martensite morphology is lath martensite (Fig. 2.60 a), some times referred to as packet martensite. The structure of most hardened steels is lath martensite. Figure 2.62 (a) is a micrograph of lath martensite in Fe-0.2C alloy. The dashed lines trace out prior austenite

grain boundaries and the dark regions labeled A, B, and C are martensite laths.The term lath refers to the fine structure of the martensite crystal i.e lath martensite is much finer than plate martensite. As shown in Figure 2.62 (b), laths tend to align themselves into groups with the same orientation; these groups are termed packets.and transmission electron microscopy (TEM) is often necessary to resolve the laths.The substructure of lath martensite consists of a network of dislocations, a result of the shear processes during transformation. As with plate martensite, retained austenite can be present in lath martensite, both in between packets and between individual laths. Due to the difference in martensite morphology scale, the quantity of retained austenite in lath martensite is significantly less than that for plate martensite [191].

(a)   (b)
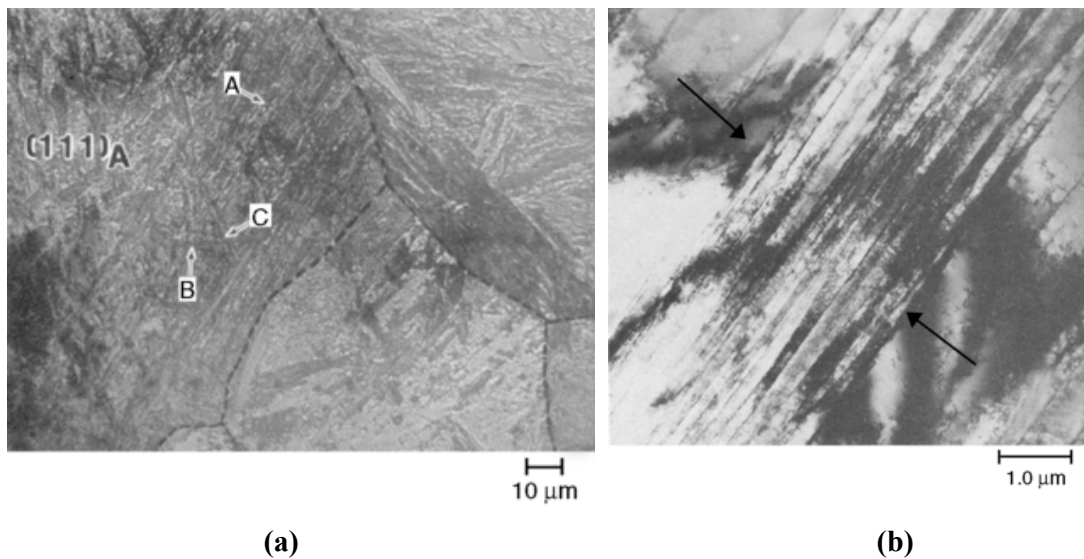
Fig. 2.62(a) Optical micrograph showing martensite laths in Fe-0.2%C alloy (b)TEM showing a packet of martensite laths (between arrows) [189].

2.3.5.6. Effect of Carbon on Martensite Morphologies

Most low-carbon steels form lath martensite, while higher-carbon steels form plate martensite. Figure 2.63 shows which martensite morphology exists for a wide range of carbon contents. Note that it is also possible to obtain microstructures with a mixture of both plate and lath martensites.
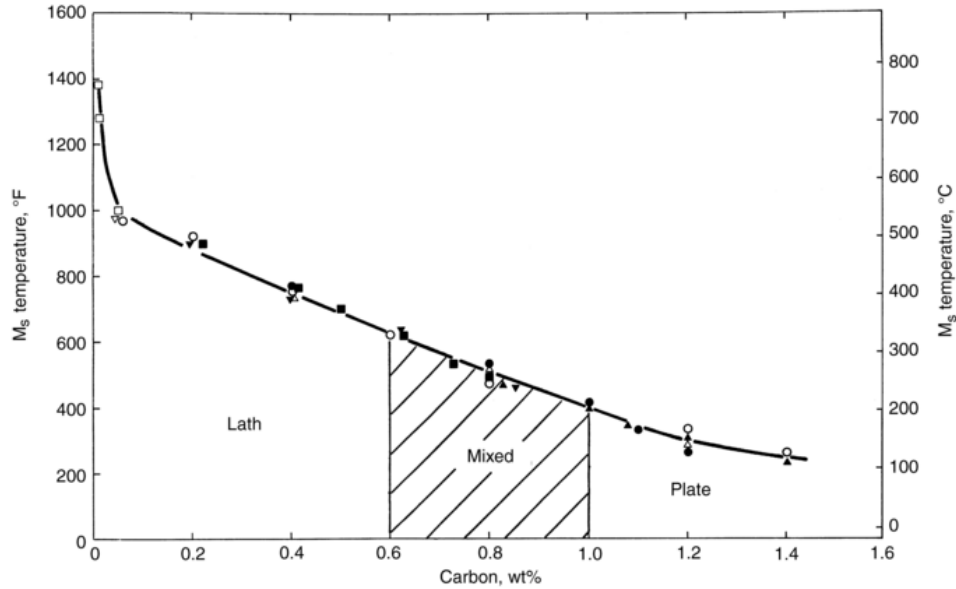
Fig. 2.63   Martensite transformation start temperatures versus carbon content [189].

2.3.5.7. Martensite Start Temperature

The martensite start (Ms) temperature generally features on a TTT or CCT diagram as a horizontal line parallel to the time axis. The martensite–start temperature (Ms) is the highest temperature at which martensite forms on cooling the parent phase [15,19,182].The microstructure, (dislocation, vacancies, grain, twins, inter-phase boundaries, and precipitates), external stress and plastic deformation, may sometimes play an important role, but the chemical composition of a steel seems to be a main factor in affecting its M_S [192].It can be estimated by two formulas:-

1) The statistical formulas in the general linear form of:

$$Ms = k_0 + \sum k_i w_i$$

$$Ms = 545 - 470.4 w_C - 3.96 w_{Si} - 37.7 w_{Mn}$$
$$- 21.5 w_{Cr} + 38.9 w_{Mo}, \quad °C.$$

(2.37)

2) A new empirical model taking into effects of binary interactions. By adding interaction terms into eq. (4) for C-Si, C-Mn, C-Cr, C-Mo, Si-Mn, Si-Cr, Si-Mo, Mn-Cr, Mn-Mo, and Cr-Mo, a more accurate regressive equation has been obtained [192].

$$Ms^{BR} = 540 - 584.9w_C - 23.1w_{Si} - 117.7w_{Mn} - 42.5w_{Cr}$$
$$+ 49.9w_{Mo} - 62.5w_{C-Si} + 178.3w_{C-Mn}$$
$$- 10.0w_{C-Cr} + 52.5w_{C-Mo} + 117.2w_{Si-Mn}$$
$$+ 50.9w_{Si-Cr} - 142.2w_{Si-Mo} - 29.2w_{Mn-Cr}$$
$$- 9.7w_{Mn-Mo} + 69.9w_{Cr-Mo}, \quad °C \qquad (2.38)$$

The effect of carbon on both Ms and Mf is shown in Fig. 2.64(a) from which it can be seen that, as the carbon content is lower both M_S and M_f increase. A better approach is to express Ms in terms of the driving force for transformation. It was found that the driving force $\Delta G\alpha' \rightarrow \gamma$ at the Ms temperatures of the alloys was practically constant, approximately 1250 J/mol, independent of carbon content. However, work on iron–nickel alloys [19], has shown that the driving force increases with increasing nickel content, i.e. as the Ms is depressed.
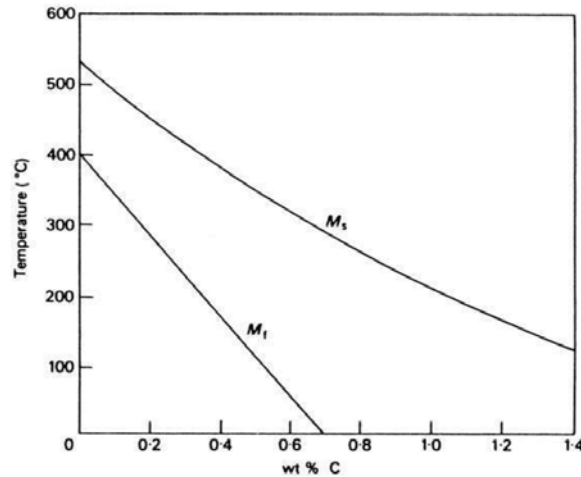
Fig. 2.64(a) The effect of carbon on Ms and Mf [19].

Austenite Grain Size and (Ms)Temperature. There have been several studies on the dependence of the martensite–start temperature (Ms) onthe austenite grain size [193].The austenitisation temperature also affects Ms [194].The results presented in Fig. 2.64(b); consistent with previous work [193], there is a large dependence of Ms as a function of the austenite grain size.
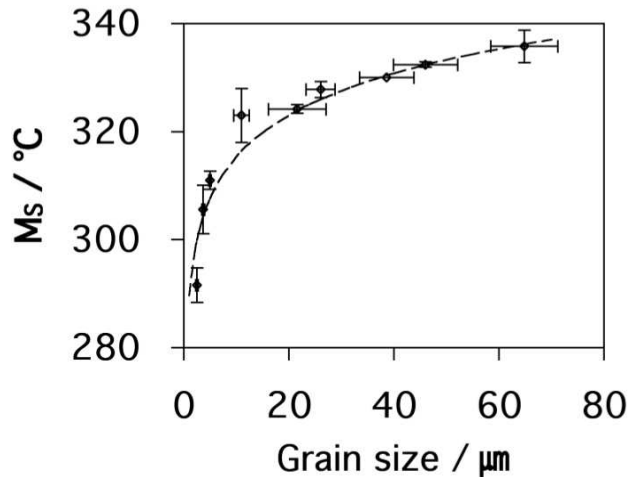
Fig. 2.64(b) Measured variation in the (Ms) temperature as function in the grain size [193].

2.4 STRENGTHENING MECHANISMS

As we known the strength is a basic engineering specification, steels can be made stronger by transforming the austenite at ever decreasing temperatures (Fig. 2.65), or by increasing hardenability, whereas the toughness does not necessarily increase with strength, by the same time the ultra high strength steels are difficult to be welded.
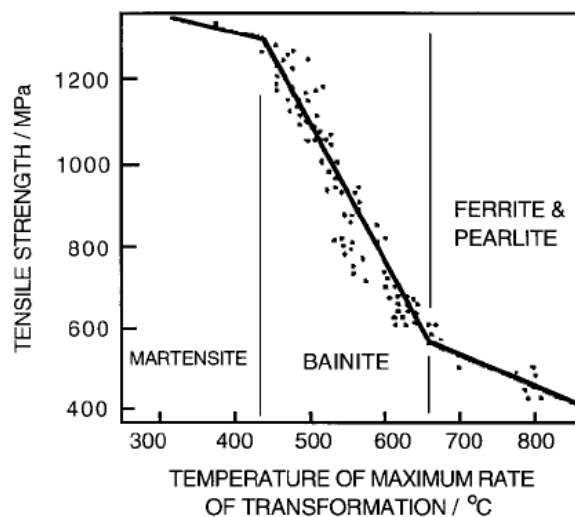
Fig. 2.65 Variation of the tensile strength as function of the temperature at which the rate of transformation is greatest [15].

The strengthening of structural steels by increased C was unacceptable because of low toughness and poor weldability, for that reason the development of microalloyed steels is

needed [42].The microalloying steels with small amounts of strong carbide and nitride forming elements such as Nb, Ti and V have achieved a great improvement in their mechanical properties. These improvements in mechanical properties are a result of many factors. The microalloying elements (MAE) Nb ,Ti and V are widely appreciated and exploited for their ability to increase the strength and toughness of structural steel . The MAE are known to impede the motion of crystalline defects such as grain boundaries, recrystallization boundaries and dislocations when the MAE are present either as solute (weak pinning) or as precipitate (strong pinning) . Hence, the MAE can suppress grain coarsening, static recrystallization and the motion of dislocations [132].However as reported by [14,195].The strengthening mechanisms applied in MA steels include : –

1. Grain refinement;
2. Precipitation;
3. Dislocation substructure;
4. Solid solution strengthening;
5. Strain aging.

Grain refinement is the preferred mode of strengthening in steels because it is the only mechanism that improves both strength and toughness [15] and consequently the precipitation in the ferrite will provide additional strength to the microalloyed steels [9, 195] A small addition of microalloying elements, MAE (0.1wt%), such as Nb, V, and Ti, can provide sufficient microstructure control, that produces a fine –grained steel with good combination of strength and toughness, whereas the post–process heat treatment is not necessary. The elimination of heat treatment is cost reduction factor that provides the driving force for the development of MA steel for forgings .[9,13,20-23].Grain refinement is unique in that it adds both strength and toughness to the steel whereas microalloy precipitation increases strength at the expense of some loss in toughness [42].Also the particles which precipitate during or after transformation to ferrite are nessary to produce the very fine particles that are responsible for dispersion strengthening [9,39,40,197] As reported by R . K .Amin,[196] the value of ($\Delta\sigma_{ph}$) for any given rolling condition increased with increasing reheating temperature up to the stoichiometric Nb : C_{Eq} ratio . The increase in ($\Delta\sigma_{ph}$) with increasing reheating temperature was due to the increaserd solubility of precipitate. So the composition of the steel with respect to the ratio Nb :C, Ti : C or V : C is also important. The maximum temperature–dependence of the solubility of the precipitate occurs at stoichiometric composition [27,178,179], so that ,

at this composition, the maximum amount of precipitate will be formed. In most structural steels, the ratio Nb : C, Ti :C or V : C is much lower than the stoichiometric ratio, and consequently increasing the metallic alloy addition will increase the strengthening due to precipitation [9,27,178,179].The value of precipitation hardening was taken from the work of Irvine [198] However the contribution to strength from dislocations was evaluated from the standard relationship [198] :

$$\sigma_{dh} = \alpha \, G \, b \sqrt{\rho} \qquad\qquad (2.39)$$

$$= 14.4 \cdot 10^{-4} \sqrt{\rho}$$

where α is a numerical factor dependent on crystal structure , G the shear modulus , b the Burgers vector , and ρ the dislocation density (lines$/$cm^2).

In general, decreasing the transformation temperature by either alloying or increasing the cooling rate, both refines the grain and increases the dislocation density. This increased dislocation density increases the yield stress [27].The yield strength is expressed by the Hall – Petch [8,197] relationship : –

$$\sigma_y = \sigma_0 + K_y \, d^{-1/2} = (\sigma_{LH} + \sigma_{Sh} + \sigma_{dh} + \sigma_{ph} + \sigma_{th}) + K_y \, d^{-1/2} \qquad (2.40)$$

where σ_{Lh} = intrinsic lattice hardening ,

$\quad$ $_{sh}$ = solid solution hardening ,

$\quad$ $_{dh}$ = dislocation hardening ,

$\quad$ $_{ph}$ = precipition hardening ,

$\quad$ $_{th}$ = texture hardening , and

$K_y \, d^{-1/2}$ = hardening due to grain refinement.

The dislocation hardening $\Delta\sigma_{dh}$ and texture hardening $\Delta\sigma_{th}$ will depends on the % of deformatiom and as given in Ref.[197] are negligibly small by 10 % reduction due to quite similar structure with no deformation observations. Since there is no dislocation and texture hardening ($\sigma_{dh} = 0$, $\sigma_{th} = 0$), equation (2.40) is reduced to :

$$\sigma_y = \sigma_{Lh} + \sigma_{sh} = \sigma_{ph} + K_y \, d^{-1/2} \qquad\qquad (2.41)$$

With increasing amounts of deformation up to 30 % or more, ferrite grains are elongated, texture is more strongly developed, and dislocation density becomes high. All of these factors contribute to the increase in strength [196,197].The microalloyed steels are strengthened by a combination of grain refinement, subgrain formation, and precipitation hardening. The amount of strengthening from columium carbonitride precipitates depends upon the amount of columbium added, finishing rolling temperatures, and amount of deformation [9,199].

2.5. TOUGHNESS

Because of the difference in the mechanism of transformation, bainitic steels have always been second–best when compared with tempered martensite [124].As we noted earlier bainite grows without diffusion causes large regions of austenite to remain untransformed (Blocky regions of austenite) as shown in figure 2.66(a ,b,c). The blocks are relatively unstable and transforms into high-carbon, untempered, brittle-martensite under the influence of stress, its acts as largs inclusions render the steel brittle (Lack of Toughness). The blocky regions of austenite can be eliminated by promoting further transformation to bainite by displacing the T 0 curve to larger carbon concentration i.e strong and tough bainitic steel can be designed. This has led to the development of novel ultra-high strength steels with strength and toughness combinations which match or exceed more expensive alloys [19,200,201].Or by reducing the average carbon concentrations as shown in figure 2.67. Both of these new steels have much better impact properties because the modifications allow more bainitic ferrite to form at the expense of blocky austenite, so the better toughness is achieved without any sacrifice to strength [15,19,45,124,200,201].

(a)   (b)   (c)
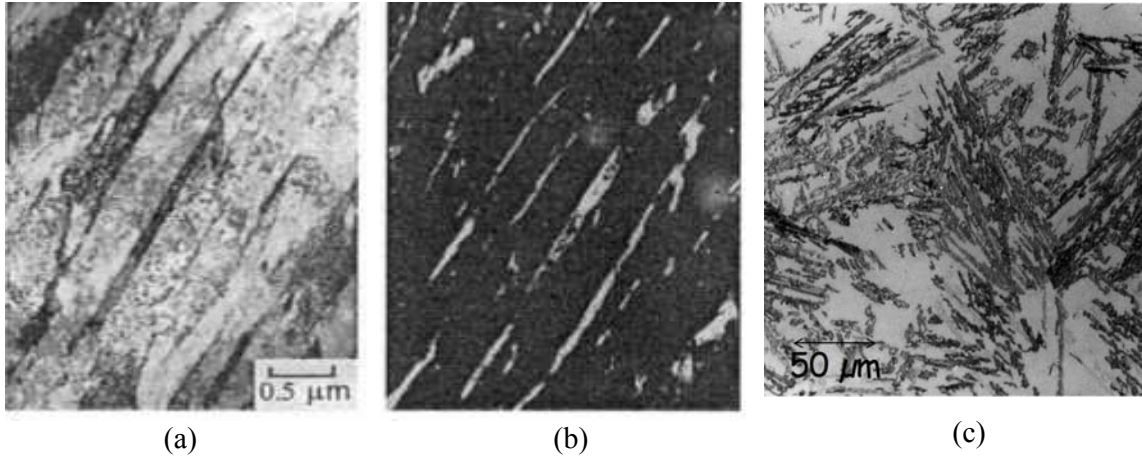
Figure 2.66 : (a, b) Transmission electron micrograph of a mixture of bainitic ferrite and stable austenite. (b) Optical micrograph of upper bainite in an Fe–0.43C–3Mn–2.02Siwt% showing the blocks of retained austenite between sheaves of bainite [45,124].

(a)

(b)
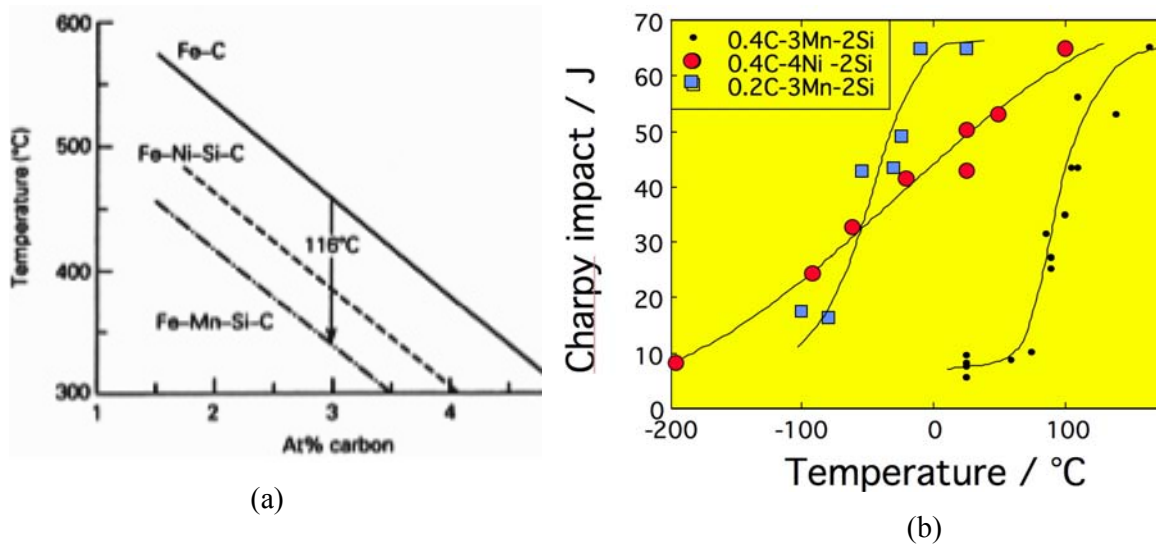
Figure 2.67: (a) Calculated T0 curves for the Fe-C, Fe-Mn-Si-C and Fe-Ni-Si-C steels. (b) Experimentally determined impact transition curves [45,124].

2.4.2   INFLUENCE OF CHEMICAL COMPOSITION ON TOUGHNESS

2.4.2.1   Effect of Silicon

The diffusion of carbon atoms from the ferrite to austenite after the transformation without formation of carbide due to the presence of silicon [202], so the carbides in the ferrite need not always be cementite. As reported by [45,134,187], steels containing more than about 1wt% silicon (which retards cementite formation) or it is possible to suppress the formation of

94

cementite altogether. Reasults which are given in Ref.[124,134,187,203], show that the addition of suitable amount of silicon (e.g. 1.5 wt %), has an effect on toughness (Lack of toughness can be eliminated). Due to the cementite precipitation from austenite can be prevented by increasing the silicon concentration to about 1.5 wt%. Because silicon is insoluble in cementite (Silicon has a negligible solubility in cementite and hence greatly retards its precipitation). Silicon rich bainite steels can have very good toughness because of the absence of brittle cementite i.e there are no cementite particles to nucleate cleavage cracks or voids [104,124,134,187,202,203]. However as reported by Sakuma et al [204], the increase of silicon content is beneficial for enhancing the combination of strength and ductility, and effectively retards the pearlite formation, but prolongs the bainitic transformation time required for the optimum mechanical properties. Also and as reported by [205], small amount addition of both aluminium and phosphorus retard cementite precipitation during bainitic transformation and hence can substitute for silicon because aluminium, like silicon, is not soluble in cementite and phosphorus reduces the kinetics of cementite precipitation. However the aluminium is less potent in retarding the formation of cementite than silicon at the same weight concentration [206].

2.4.2.2 Effect of Titanium

Another approach to increase toughness is to add titanium as a microalloying element. Ti is a very strong nitride forming element, and titanium nitride particles are stable at the high temperatures of forging. The titanium nitride particle dispersions prevent austenite grain growth, and as a result more grain boundaries are available for pearlite nucleation and pearlite colony size is reduced. The finer pearlite colony size increases impact toughness [4, 24].

2.4.2.3.   Effect of Sulfur

Another approach [131].to increasing toughness of microalloyed forging steels is to increase sulfur content to suitable amount as shown in Fig.2.50. Authors [207,208] have shown that in vanadium-microalloyed steel ferrite nucleates and grows on manganese sulfide particles due to vanadium nitride and carbides precipitate on the sulfides and stimulate the nucleation of ferrite as shown in fig 2.50 (a,b) and figure 2.68. As a result, ferrite forms not only on widely spaced austenite grain boundaries in steels forged at high temperatures, but also within austenite grains. The intragranularly nucleated ferrite breaks up the structure of coarse colonies of pearlite, effectively decreasing pearlite colony size and improving toughness. As well as the addition of 0.1 wt% phosphorus leads to an increase of about 75 MPa in the strength of ferrite [27].
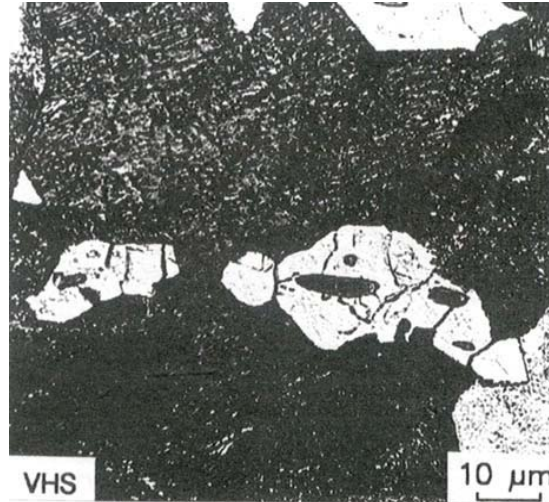
Figure 2.68.   Intra-granular ferrite formed in MnS particles. The ferrite is surrounded by pearlite which appears black in the light micrograph [207].

2.5. PRECIPITATION IN MICROALLOYED STEELS

The precipitation process proceeds at perceptible rate only if there is driving force , that is , a free energy difference between the product and parent phase. The chemical driving force for nucleation is defined as the free energy changes that accompanies the formation of a nucleus from the matrix [39,40,42] Fig. 2.69 illustrates the chemical driving force for nucleation of V(C,N) in austenite, during γ-α transformation and in ferrite. It can be seen that , as the temperatures is decreased the driving force increases monotonically and changes slope after the austenite to ferrite transformation i.e the chemical driving force for precipitation in austenite is low but increases suddenly and strongly as γ is transformed to α , reflecting the solubility drop associated with the widely different solubilities in the two phases.

(a)   (b)
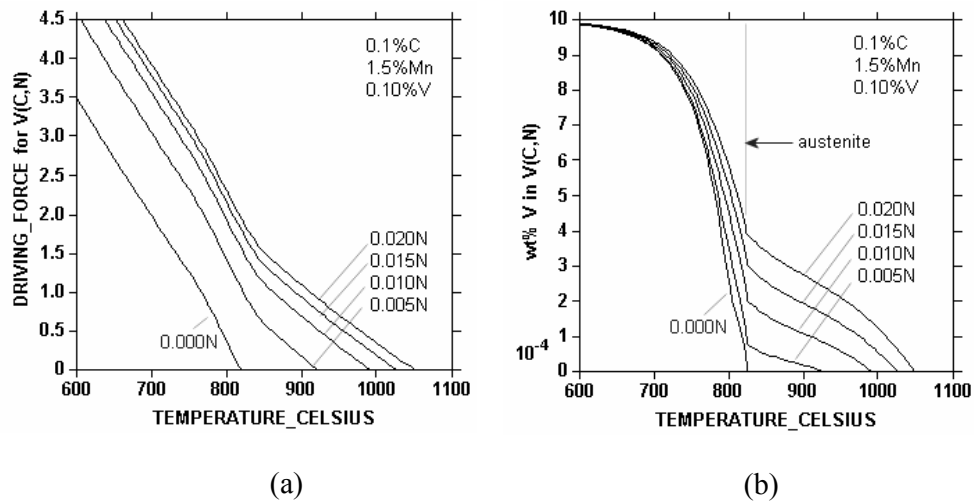
Fig. 2.69 Chemical driving force , $\Delta G_m / KT$, for nucleation of V(C,N) as a function of temperature (a) and the solubility drop of V during γ-α transformation (b) [39,40].

2.5.1 EFFECT OF NITROGEN AND VANADIUM ON DRIVING FORCE FOR PRECIPITATION

The nitrogen in small contents adds significantly to precipitation strengthening as shown in Fig. 2.70(c) due to the larger driving force in the high-N steels than in the low-N steels becouse it will cause a denser precipitates and electron microscopy has clearly confirmed this, as shown in Fig.2.70 (a,b).

(a)   (b)
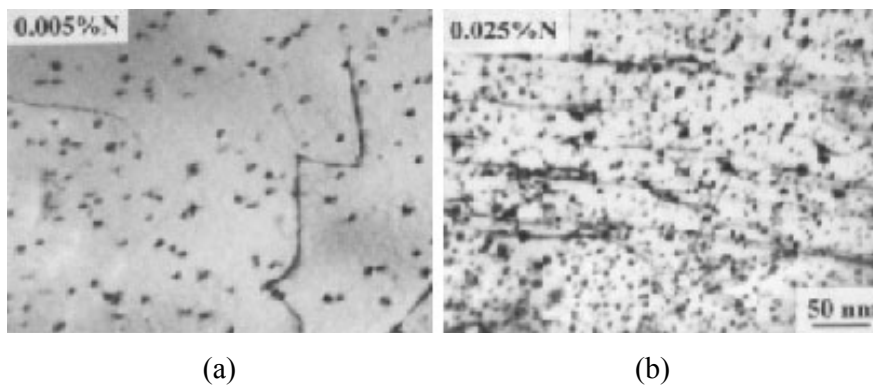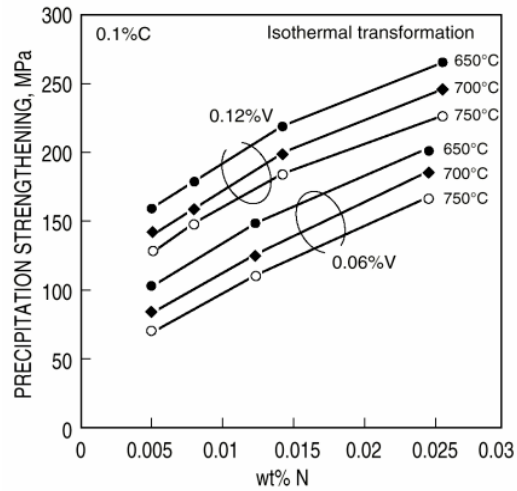
(c)

Fig. 2.70.(a,b) Electron micrographs illustrating the effect of N on the density of V(C,N)-precipitates during isothermal transformation,(c) Nitrogen effect on the precipitation strengthening of V-steel [39,40,42].

The dominating effect of N on the driving force for V(C,N) is also clearly seen in the figure 2.71. Hence, the strong effect of N in increasing this driving force [39,40,42].The V is usually the preferred element when precipitation strengthening is wanted. A modest addition of 0.10%V can bring about a strength increase beyond 250 MPa, and in special cases even up to 300Mpa [209].It should be noted, however, that the driving force can also be raised by V-addition but the effect per concentration unit is much less. Moreover, V-additions increase alloying costs significantly whereas the usage of N at the present levels is free [39].As shown in figure 2.71. Since the nitrogen contents of commercial structural steels , up to 200 ppm , are generally below the solubility limit in both ferrite and austenite , for that reason all the nitrogen is available for precipitate formation and however the nitrogen is always present in a form where it can react efficiently with microalloy elements [39,40].
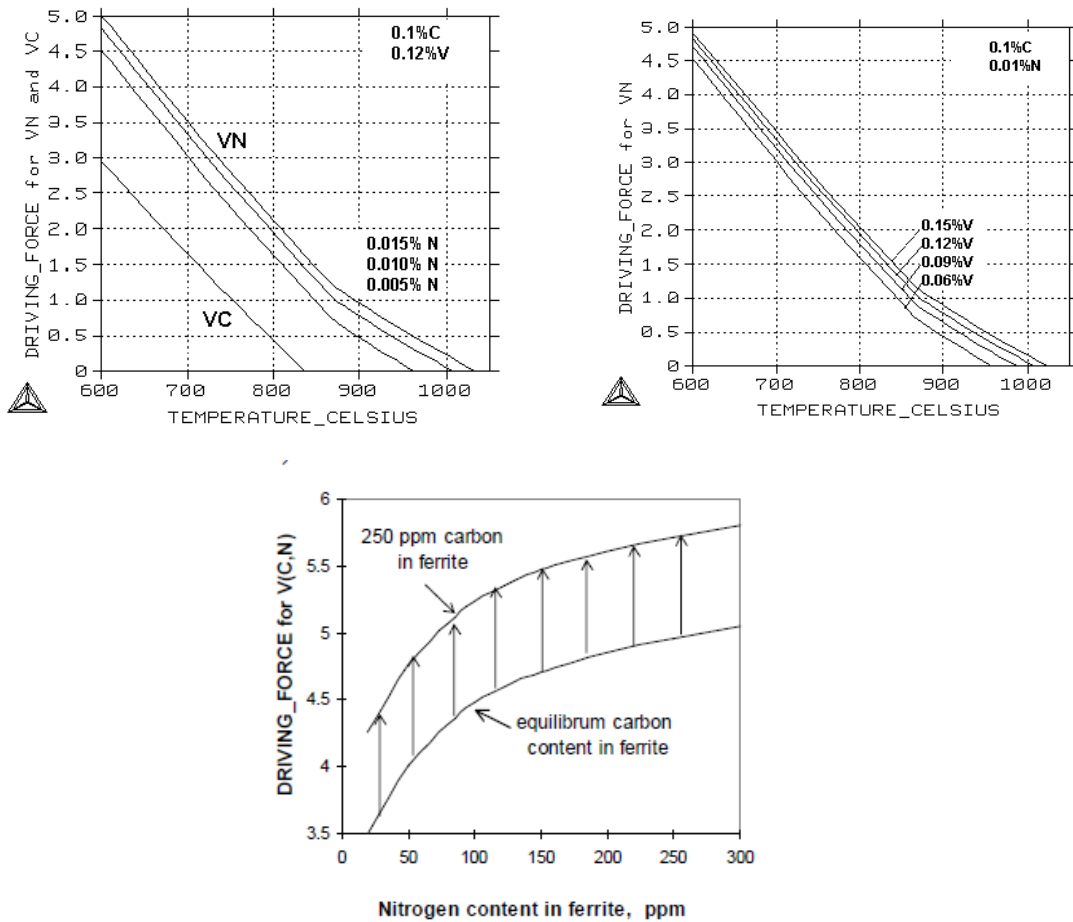
Fig. 2.71 (a) Chemical driving force, $\Delta G_m/RT$, for precipitation of VC and VN in 0.12% V steel. (b) Effect of equilibrium and metastable carbon content in ferrite on driving force for precipitation of V(C,N) at 650°C [39,42].

The effect of V- and N-additions for precipitation strengthening of steels is clearly demonstrated in Fig. 2.72 [84]. According to these results 5 parts per weight of N are equivalent to one part of V. Enhanced cooling is an efficient method to increase precipitation strengthening; raising the cooling rate from 1°C/s to 4° C/s increases the tensile strength of a 0.4C-1.2Mn-0.10V steel by 120 Mpa [100,210].The most significant properties of V as compared to Nb and Ti are [42]:-

1) The solubility of V(C,N) is much larger i.e larger amounts of V can be dissolved at a given temperature.

2) This implies that N as a microalloying element has a decisive role in V-microalloye steels, especially for the enhancement of their precipitation strengthening .
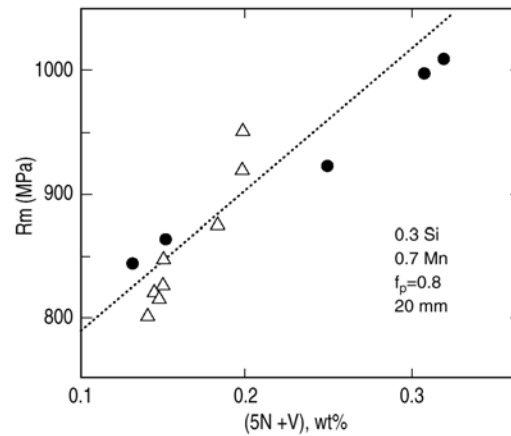
Fig. 2.72 Effect of precipitation strengthening by V and N on R_m. All steels contain 0.7%Mn and were austenized at 1200-1250°C [101].

The nucleation and morphology of V(C, N) particles at dislocations and microtwins have been reported in Ref. [211]. Previous work [212], has examined precipitation behaviour and found, the precipitates of V(C,N) obeyed the Baker-Nutting (B-N) orientation relationship with the pearlitic ferrite as given below.

$$(001)\alpha // (001)_{V(C,N)}$$
$$(010)\alpha // (\bar{1}10)_{V(C,N)}$$
$$(100)\alpha // (110)_{V(C,N)}$$

However when precipitation takes place it may do so in two different ways. One of these is so called inter-phase precipitation and as reported by [129,213,214], the mechanism.of interphase precipitation is fall broadly into two categories: ledge mechanisms and solute-depletion model based on solute diffusion control. In this case the particles are alingned in rows in the same phase boundary all possess the same orientation, a unique variant of the B-N orientation relationship . By contrast in the case of the random precipitate, the particles are not alingned in rows but are randomly distributed and also are characterised by the occurance of different variants of the B-N orientation relationship [215].

2.5.2   KINETICS OF CEMENTITE PRECIPITATION

Speich [15] reported that the change in hardness of martensite in iron-carbon steels after time of tempering at temperature above 320 °C, includes significant contributions from recovery, recrystallisation and coarsening of cementite particles as illustrated Fig. 2.73
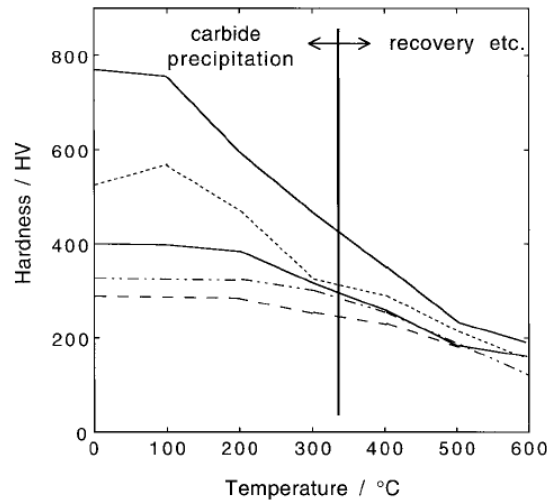
Fig. 2.73.Hardness curves changes for five steels (different in C wt %), tempered for 1 h [15].

The change in hardness is attributed dut to precipitation of carbides, in left of vertical line, where as at right the change is due to recovery or coarsening processes [15]. Since it is assumed that the volume fraction of cementite $\xi\{t\}$ is related at any time to hardness of the martensite, $H\{t\}$, it follows that:

$$\xi\{t\} = (H_0 - H\{t\})/(H_0 - H_F)$$

(2.42)

H_0 is the hardness of the as-quenched virgin martensite, H_F is its hardness when all the carbon has precipitated but before any significant recovery, recrystallisation or coarsening has occurred. The assumption here is that the amount of carbon precipitated is related linearly to the change in hardness during the early stages of tempering or isothermally treated. However the H_F can be expressed empirically as a function of the initial hardness and average carbon concentration $\bar{x}$ (mole fraction) as follows:

$$H_F = H_0[1 - 1.731\bar{x}^{0.34}]$$

(2.43)

This equation is valid plain carbon steels containing less than 0.4 wt% Carbon, the value of H_F becoming constant thereafter. The hardness H_0 of plain carbon martensite (< 0.4 wt% carbon) before tempering or isothermally treated (as quenched) can be also deduced from the data reported by Speich:

$$H_0 = 1267(\text{weight } \% \quad \text{carbon})^{0.9} + 240$$

(2.44)

This equation gives the hardness of virgin martensite in plain carbon steels as a function of dissolved carbon. By contrast, there is evidence that the effect of carbon tends to eventually to saturate, so H_0 should be set not exceed about 800 HV. However the yield strength of martensite σ_y is expressed as a combination of the intrinsic yield strength, the effect of the dislocation cell structure, and precipitation hardening by cementite [216]:

$$\sigma_y = \sigma_0 + k_\epsilon \epsilon_1^{-1} + k_p \Delta^{-1}, \mathrm{MPa}$$

(2.45)

Where σ_0 is the intrinsic strength of martensite (including solid solution strengthening), ϵ_1 is the average transverse thickness of the cell structure, and Δ is the average distance between a particles.

3. EXPERIMENTAL PART

3.1 CHEMICAL COMPOSITION OF STEELS

The chemical composition of steel studied in the present work is given in Table 3.1. The steels were made by ingot casting and fabricated into 22 and 19 mm diameter bar by full-scale forging and hot-rolling. Representative hot-rolled steel bars were homogenized at 1250 °C for 4 hours, in the presence of argon as protective atmosphere, to minimize any effect of chemical segregation. After annealing, the samples were oil quenched. Specimens with 12mm height were cut from 22 and 19mm diameter bars.

Table 3.1: Chemical composition of the experimental steels (wt %)

Element	Chemical composition (wt %)	
	Ti-V-N Steel	V-N Steel
C	0.309	0.256
Si	0.485	0.416
Mn	1.531	1.451
P	0.0077	0.0113
S	0.0101	0.0112
Cr	0.265	0.201
Ni	0.200	0.149
Cu	0.232	0.183
Al	0.017	0.038
Mo	0.041	0.023
Ti	0.011	0.002
V	0.123	0.099
Nb	0.003	0.002
N	0.0221	0.0235
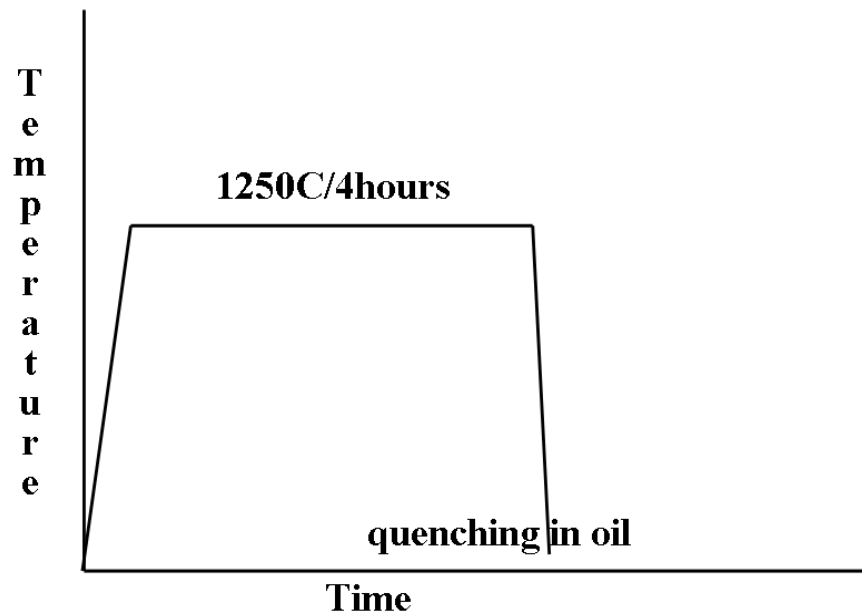
Figure 3.1. Thermal schedule for elimination as-received microstructure.

3.2. PRIOR AUSTENITE GRAIN SIZE

Evaluation of prior-austenite grain size (PAGS), involved heat treatment, etching and grain size measurement.

3.2.1 HEAT TREATMENT

The samples with 19 and 22 mm diameter and 12mm in length of the two steels were used to reveal austenite grain boundaries by thermal etching (TE) method. Samples were heat-treated in radiation furnace at different heating temperatures to the austenitization condition listed in table 3.2., in order to yield distinct prior-austenite grain size (PAGS). After that the samples were quenched in water and afterwards tempered at 450 °C for 24 h, and then slowly cooled in natural air to room temperature. A scheme of this heat treatment is shown in Fig. 3.1.

Table 3.2 : Austenitization condition (Tγ is austenitization temperature and tγ is austenitization time).

Steel	Tγ ($^{\circ}$C)	tγ (s)
Ti-V-N	950, 1050, 1100,1150,1250	600
V-N	950, 1050, 1150,1150,1250	600
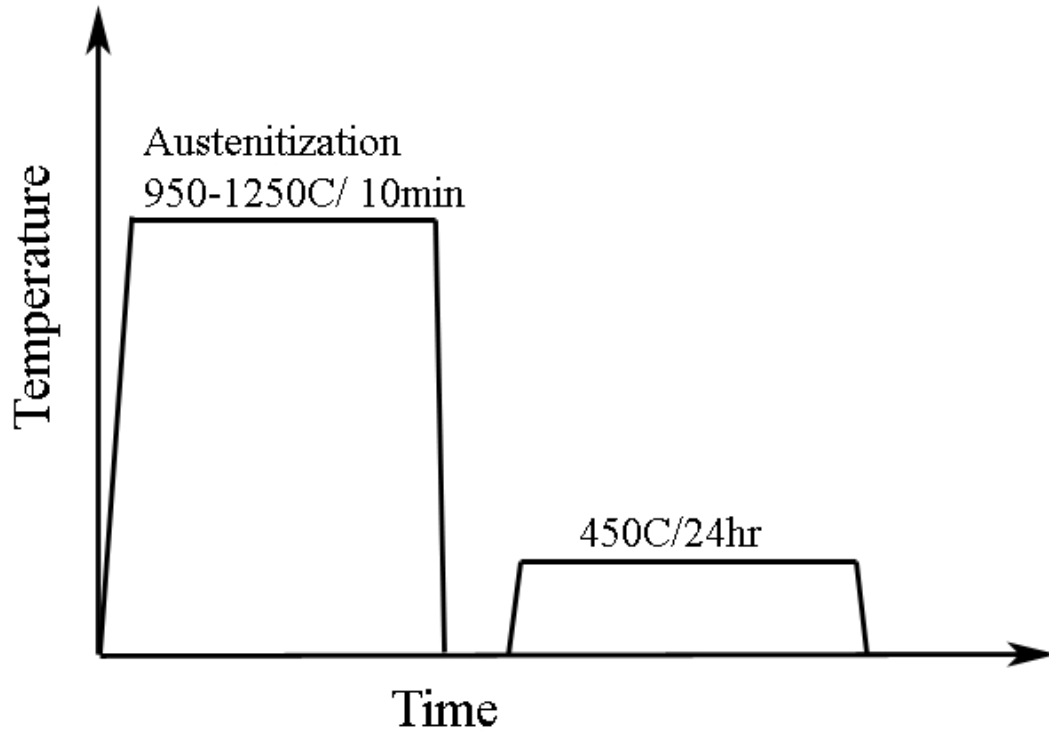
Fig.3.2 Thermal tesing procedure in order to reveal prior-austenite grain size.

3.2.2. ETCHING

The etching reagents based on saturated aqueous picric acid plus a wetting agent seem to give the best results in quenched and tempered steels [141,217].The chemical etchant that gave positive results for these steels revealing the prior-austenite grain boundary at all austenitization temperatures was a solution formed by100 ml of distilled water, 10 g of picric acid ($C_6H_3N_3O_7$), 50 ml of sodium alkylsulfonate (Teepol), 1 ml of HCl. However, it is relevant to point out that this solution is used hot (90 $^{\circ}$C), then immerse the polished specimen into the solution. Eaching time is usually in the range of 25 seconds.

3.2.3. GRAIN SIZE MEASUREMENTS

Grain size determination (linear intercept) was conducted via standard methods on samples etched in aqueous picric acid containing a wetting agent as mention before. The standards for the determination of grain size are set in ASTM E112 and DIN EN ISO 643 [218-220]. Linear intercept technique involving at least 50 intercepts, which made it possible to count the number of grains intercepted by the grid line. The austenite grain size control are important factor in development of the final mechanical properties of the product [129].There are three types of error that can influence grain size estimates. The first arises from experimental limitation for example limited resolution, poor grain boundary delineation, over-etching, inaccurate test line length measurement, miscounting. The second error type is due to improper sampling and the third error type arise from the representativeness of the chosen areas and specimens to the entire material, the last two error types are usually the greatest source of error [221].

3.2.4. ISOTHERMAL TREATMENTS

A Scheme for isothermal testing treatments is given in figure 3.3. Samples were austenitized for 600 second at 1100 $^{\circ}$C and quickly cooled to test temperature. After austenitization, specimens of both steels were isothermally transformed at different temperatures ranging from 350 $^{\circ}$C to 600 $^{\circ}$C at different times between 2 and 1200 s. A full description of scheme of isothermal treatments is mentioned in table 3.3, finally after the isothermal holding time, the specimens were water quenched to room temperature. The samples were cut, mechanically ground and then polished to 1μm diamond finish paste using standardized metallographic techniques and subsequently etched in 2 % nital for their observation by optical and scanning electron microscopy (SEM).

Table 3.3: A scheme of isothermal treatments

Isothermal treatments, $^{\circ}$C	Holding time,(s)
350	10,20,30,60,120,600,1200
400	2,5,10,20,30,60,120,600,1200,1800

450	2,5,10,20,30,60,120,600,1200,1800
500	5,10,20,30,45,60,80120,600,1200
550	5,10,20,30,45,60,80120,600,1200
600	5,10,20,30,60,80,100,120,600,1200
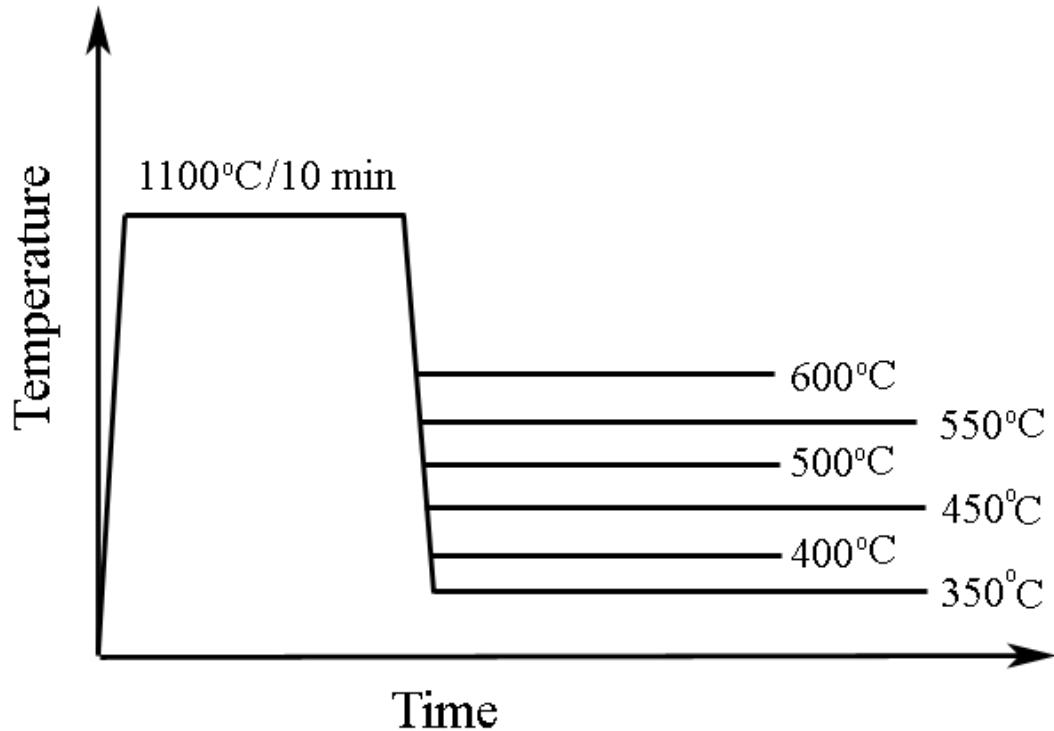
Figure (3.3) Schematic Presentation of Testing conditions at different temperatures performed in order to evaluate isothermal decomposition.

3.2.5. M_S TEMPERATURE

The martensite start (Ms) temperature in present work has been examined by analyzing the result predicted experimentally by use of optical microscopy. Moreover large numbers of experimental data are required and used for complete analysis and predict the Ms temperature in present work. Testing details are given in table 3.4, while schedule of testing is shown in figure 3.4.

Table 3.4. Testing temperatures performed in order to determine Ms temperature

Steel	Testing temperature, $^{\circ}C$	Holding time, s
Ti-V-N	330, 320, 310, 300, 290, 280,270	45
V-N	340, 330, 320, 310, 300, 290, 280,270	45
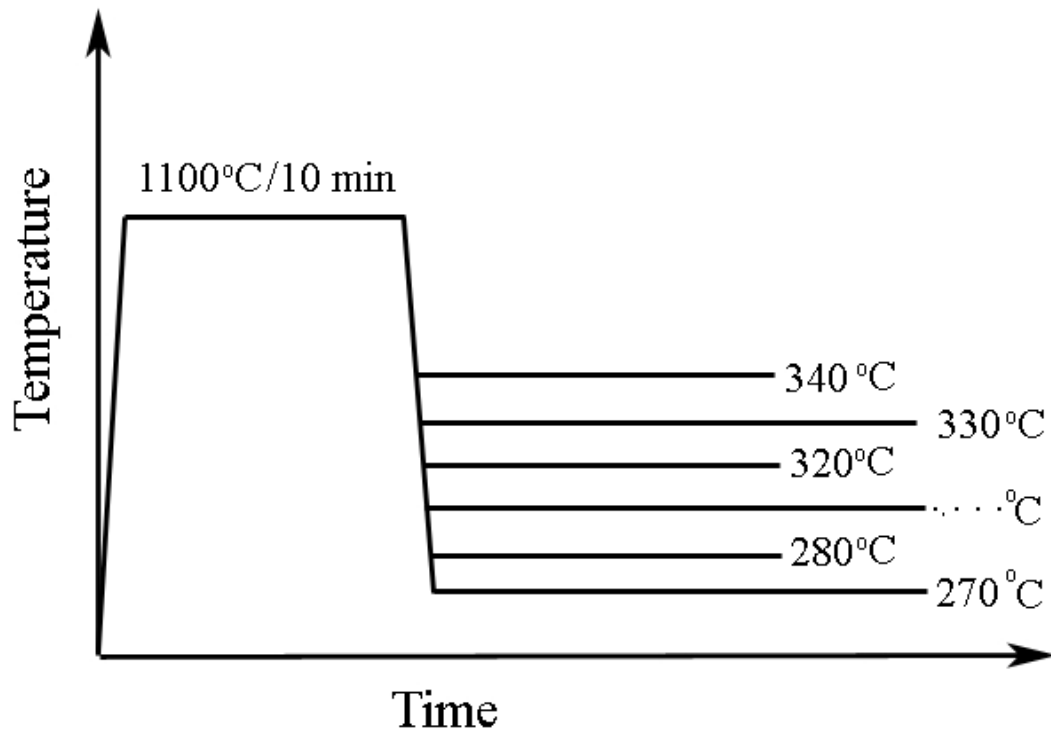
Figure 3.4. Schematic Presentation of Test conditions performed in Order to determine Ms temperature.

3.3 HARDNESS MEASUREMENTS

Hardness is the property of a material that enables it to resist plastic deformation, usually by penetration. Hardness test is practical and provide a quick assessment and the result can be used as a good indicator for material selections, because it is very sensitive to change in microstructure.

For each specimen, the Vickers hardnes was measured using a 30 Kg/mm^2 as indentation load. The hardness measurement was carried-out at five points in the region of specimen where microstructure observation was made.

3.4 COMPRESSION TESTING

Compression tests were carried out at room temperature on specimens transformed isothermally at isothermal treatment was carried out at 350, 400, 450, 500, 550 and 600 $^{\circ}$C for different isothermal times.The compression equipment used in the present study is built up around a 100 KN maximum capacity of (Instron Servo-Hydraulic Testing Machine. Model 1332) A detailed description of the machine has been given in appendix 1. The compression specimens of 5mm in diameter and 5mm in length-cylinder machined from the metallographic samples were tested in accordance with ASTM E9-89a [203,222].These test methods cover the apparatus, specimens, and procedure for axial-load compression testing of metallic materials at room temperature. Also as reported by [Ref. 131,223], compression specimens with different sizes were also used. Compression tests were performed for evaluation of the offset yield strength, $R_{p0.2}$ at plastic strain of 0.2 %. The deformation speed was 0.5mm min^{-1} corresponding to a strain rate of approximately 4×10^{-4} S^{-1}.

4. RESULTS

4.1 AUSTENITE CONDITIONING

4.1.1. PRIOR AUSTENITE GRAIN SIZE

Typical microstructures showing revealed prior austenite grain boundaries are shown in Figure 4.1. On the other hand more images showing the prior austenite grain boundaries in this work are given in appendix A. Grains are generally homonegeous in size and equiaxed in shape.

V-N -Ti steel   V-N steel

(a)   (b)

(c)   (d)
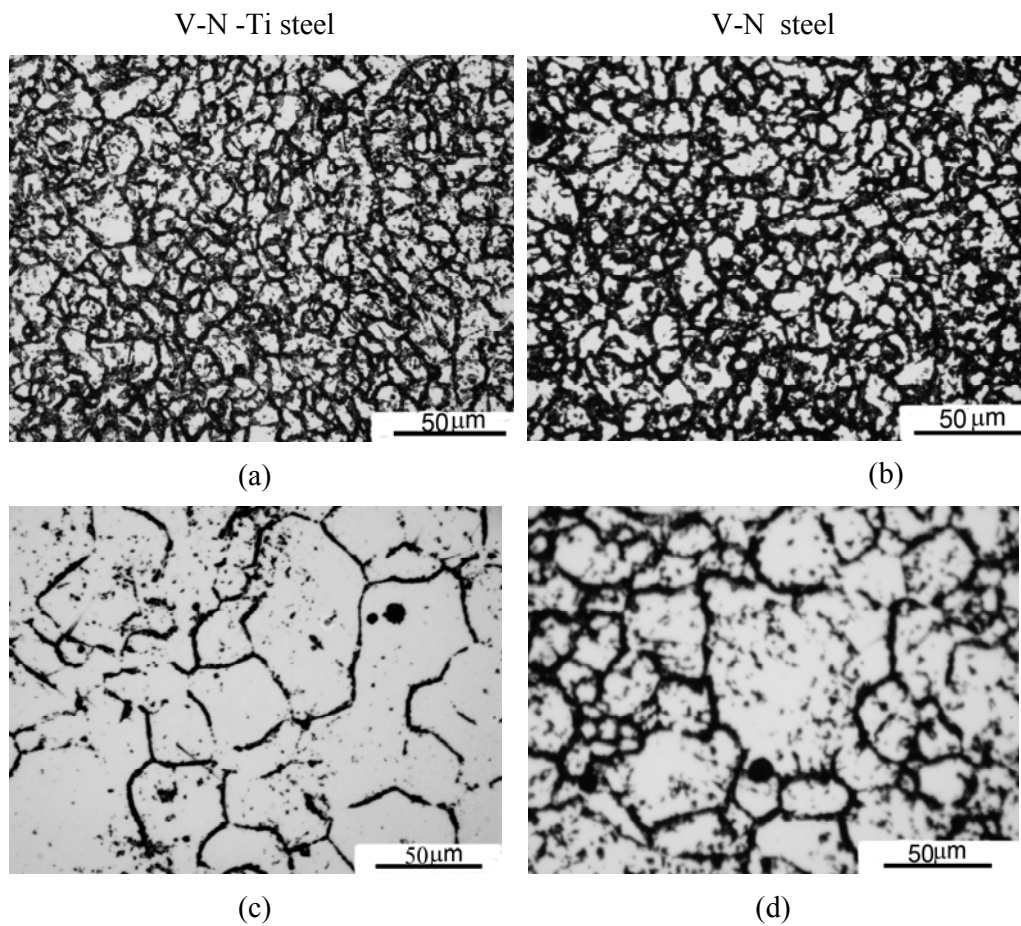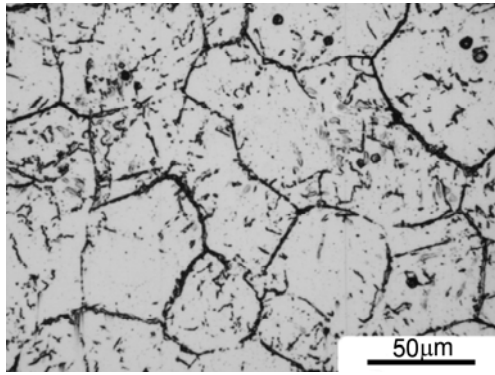
(e)
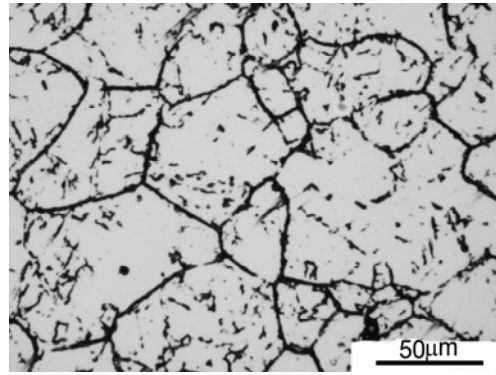
(f)
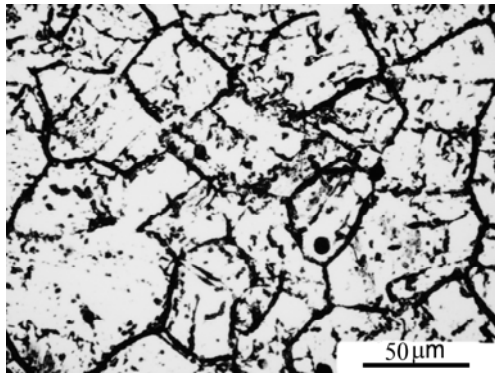
(g)
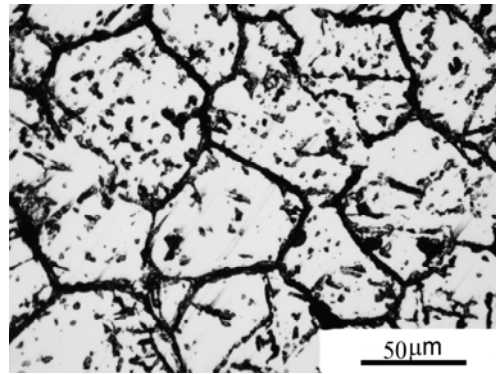
(h)
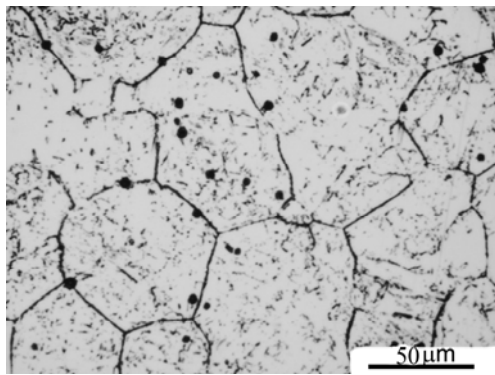
(i)
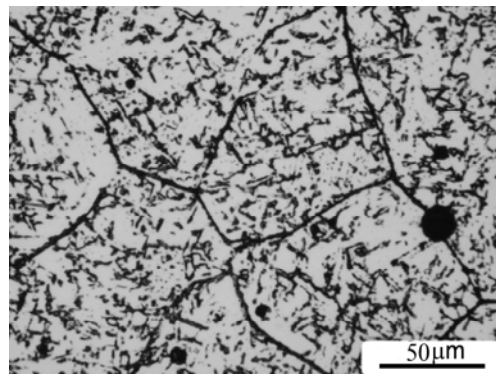
(j)
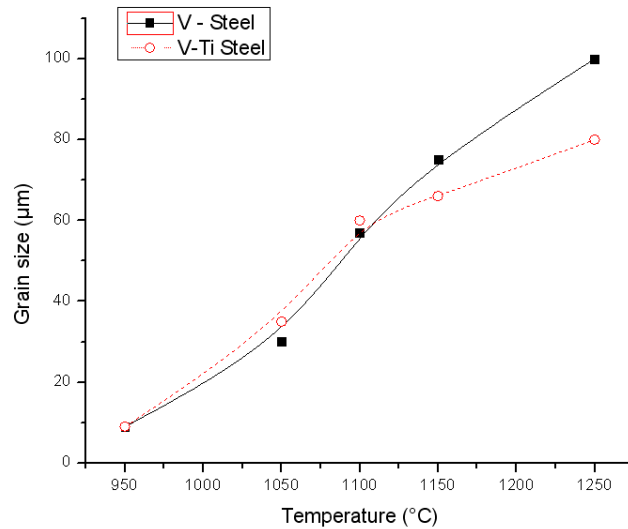
Figure 4.1. Typical microstructures showing revealed prior austenite grain boundaries (a, b) 950 °C, (c, d) 1050 °C, (e, f) 1100 °C, (g, h) 1150 °C and (k, l) 1250 °C; (m) the grain size as a function of austenitization temperature

The grain size was measured using traditional intercept method that included more than 50 visual fields. The values of average prior austenite grain size are given in table 4.1 and shown in figure 4.1m.

Table 4.1. Prior Austenite Grain Size (PAGS) estimated in this work.

Austenitization temperature Tγ, °C	Prior austenite grain size (PAGS), μm	
	Ti-V-N steel	V-N steel
950	9 ± 1	9 ± 1
1050	35 ± 5	28 ± 3
1100	60 ± 5	50 ± 5
1150	64 ± 3	75 ± 5
1250	80 ± 10	100 ± 10

Two steels show very similar behaviour, i.e., grain size increases with increase of austenitization temperature. At temperatures below 1100°C, measured grain sizes in both

steels have close values, but at temperatures above 1100°C, the grain size increase is more pronounced in VN steel in comparison to TiVN steel.

4.1.2 DIRECT QUENCHING

Several samples were either directly quenched or quenched after a spot second in salt bath, from reheating temperature of 1100 °C, in order to clarify if the austenite decomposition starts during continuous cooling from reheating temperature to temperature of isothermal treatment. After thorough search, no sign of any microstructure but martensite was recorded.

4.1.3 ALLOYING ELEMENTS DISTRIBUTION

Taking the solubility product of alloying elements into consideration the distribution of vanadium and nitrogen in austenite is rationalized in terms of the temperature for complete dissolution of VN and VC, according to the equation (2.1) and (2.2) [53-56]. Results are given in Table 4.2. It is assumed that the total amount of Ti is within TiN particles, which are insoluble at the reheating temperatures.Using stochiometric ratio Ti:N $=$ 3.4 it could be calculated that titanium ties 6 ppm of nitrogen for V-N and 32 ppm for V-Ti. Therefore, available amount of nitrogen left in solid solution is slightly reduced in comparison to chemical composition, Table 4.2.

Table 4.2. Distribution of alloying elements and temperature for complete dissolution of VN and VC.

Steel	[N], (ppm)	$[N]_{TiN}$, (ppm)	$[N]_{free}$, (ppm)	T_{VN}, (°C)	T_{VC}, (°C)
V-N	235	229	6	1111	1088
Ti-V-N	221	189	32	1114	1084

4.1.4. SELECTION OF REHEATING TEMPERATURE

Reheating temperature was selected to be 1100C, based on two reasons:

  (i) At 1100°C microstructure consists only of austenite, avoiding influence of other microconstituents on further austenite decomposition;

(ii) The grain size in both steels is large enough to enhance AF formation instead of bainite by increasing the ratio between intragranular and grain boundary nucleation sites [142,143].

4.2. MARTENSITE START (MS) TEMPERATURE

The martensite–start (M_S) temperature is of vital importance for engineering practice. Therefore great efforts have been made in predicting the M_S temperature of both steel investigated in present work.

4.2.1. PREDICTING MS TEMPERATURE BY EMPIRICAL METHODS

The martensite–start (M_S) temperature calculated by use of different empirical equations for both steel investigated in present work and the calculation results have shown that, it occure at temperature 337 ± 20 °C [192,224-230]. The details of Ms temperature calculated by use of different empirical equation for different authors are given in table 4.3

Table 4.3: Methods for predicting the Ms Temperature.

Ms – (Ti-V-N Stee)l	Ms – (V-N Steel)	Source
336	365	[Eq.4]. [192]
346	373	[Eq.5]. [192]
344	366	[225]
353	377	[226] [227]
335	361	[192]
357	383	[192]
351	379	[228]
355	381	[227]
343	366	[229]
340	361	[230]
318	359	[230]
355	381	[230]

Ms: Start Temperature of the Martensitic Transformation [°C]

4.2.2 MS TEMPERATURE EXPERIMENTALLY ESTIMATED

Start Temperature of the Martensitic Transformation (M_S Temperature) was estimated in this work using optical and SEM microscopy. Ms temperature was detected as the highest temperature at which only martensite was present, as shown in Fig.4.2. i.e., when no grain boundary ferrites (GBF) were recorded because the GBF is diffusion processes. The specimens were treated for 45 seconds on each testing temperature, in order to avoid influence of possible temperature gradient in specimens. The Ms temperatures estimated in this work are given in table 4.4 and are plotted in Fig. 4.30 by a horizontal line parallel to the time axis. Results show that Ti-V-N steel has lower Ms Temperature. The experimentally estimated (M_S Temperature) results in rather good agreement with the similar steel given in Ref. [231].
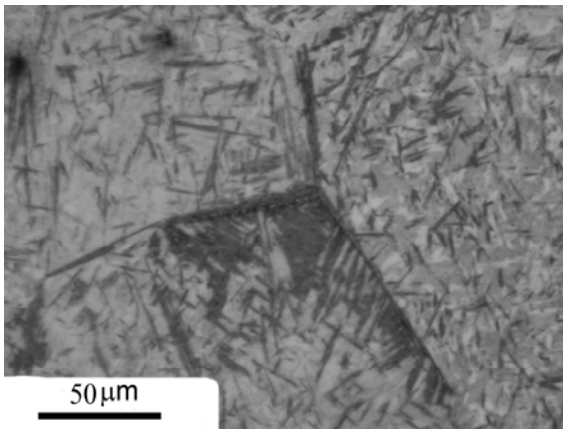
a) TiS-330 °C –BS phase onset nucleated at G.B triplepoint
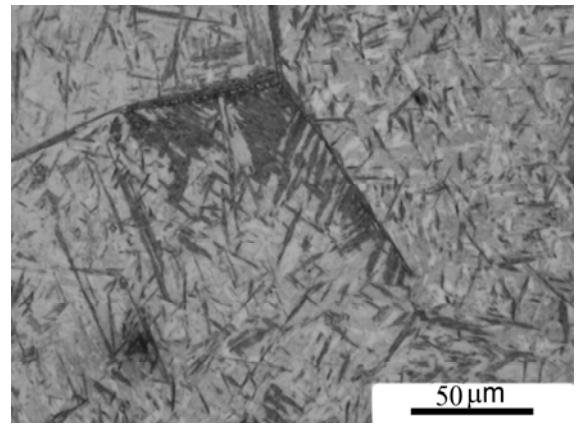
b) TiS-330 °C –BS phase onset nucleated at G.B triplepoint
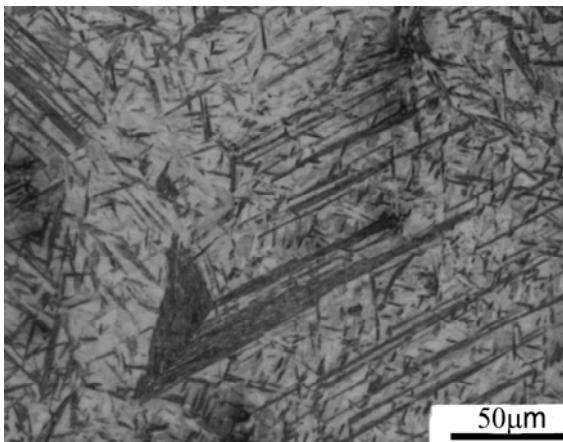
c) TiS-330 °C –BS phase onset nucleated atG.B
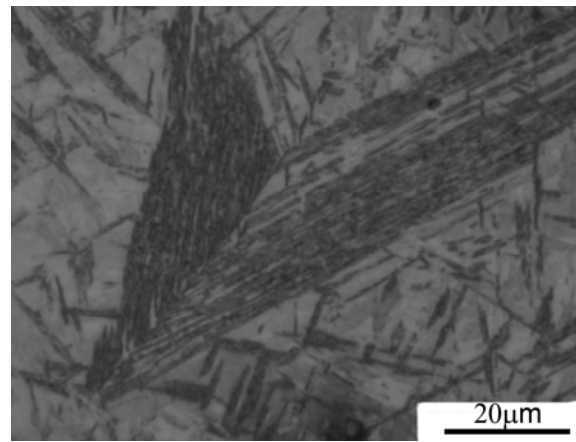
d) TiS-330°C –BS phase onset nucleated at G.B
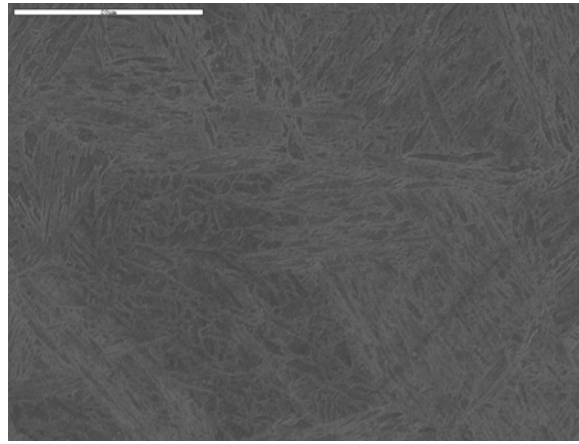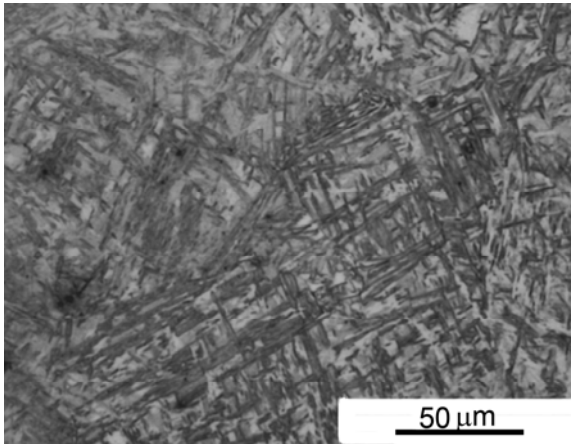
(e)TiS -320°C-No any clear phase nucleated-
All Martensite

f) TiS -320°C -SEM-No any phase nucleated-
All Martensite

Figure 4.2..Typical microstructures showing revealed M_S Temperature, of Ti-V-N steel at 330°C/45s (a-c) 200X, (d)500X, where (e) 320°C/500X, and (f) SEM /320°C.

Table 4.4. Martensite Start Temperature experimently estimated for TiVN and VN steels, °C

Steel	Ti-V-N	V-N
Martensite Start Temperature, °C	320	330
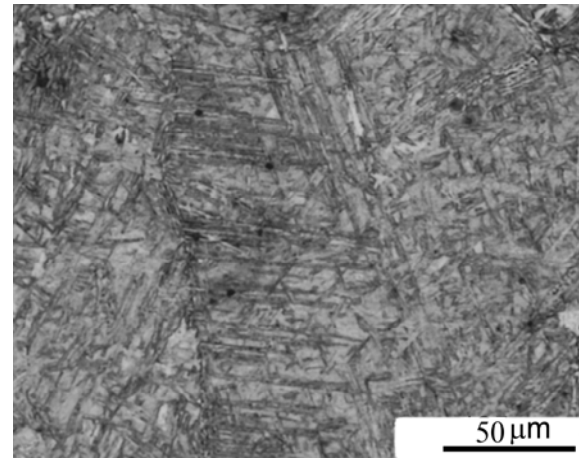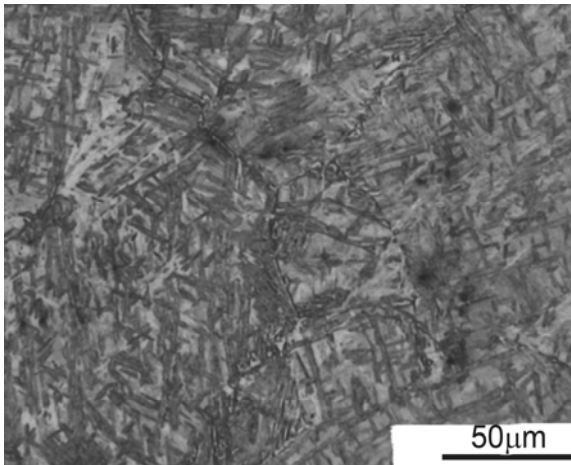
a) TiF-340 °C-BS onset(1252– 200X)

b) TiF-340 °C –BS onset (1257-200X)
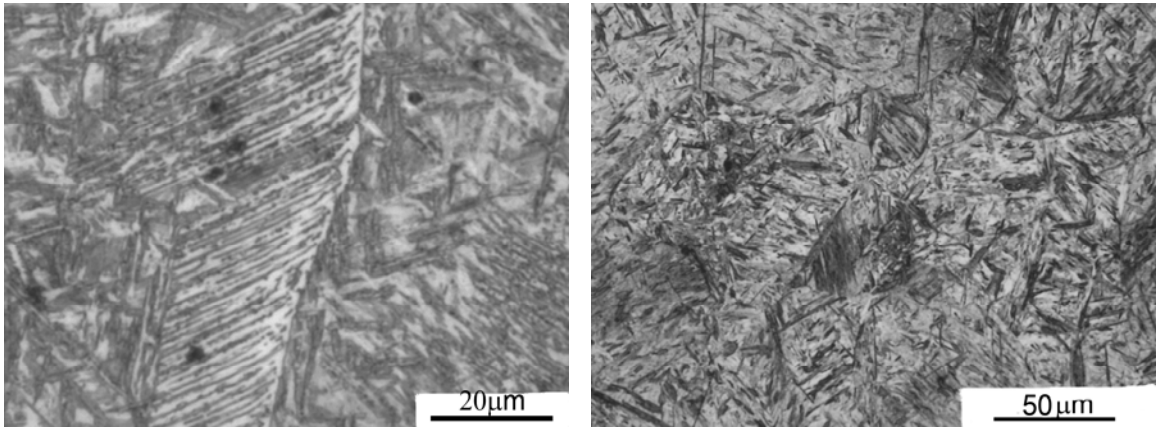
c) TiF-340 °C –BS phase onset nucleated at
G.B (1253– 45s – 500X)

d) TiF- 330°C-200X-No any clear phase
nucleated-All Martensite.

Figure 4.3..Typical microstructures showing revealed M_S Temperature, of V-N steel at 340°C/45s, when (a, b) 200X, (c) 500X, where (d) 330°C/500X.

4.2.3   DETERMINATION OF T_0 FROM M_S TEMPERATURE

The T_0 describes the critical temperature for athermal decomposition of austenite. T_0 is defined as the temperature at which the ferrite and austenite phases with the same composition have an equal Gibbs free energy. The T_0 represented based on equation (8) given in Ref. [192], and the results have shown that, it occure at temperature 637 °C for Ti-V-N steel and 646 °C for V-N steel respectively.

4.2.4. INFLUENCE OF CARBON ON M_S TEMPERATURE

Undoubtedly, carbon plays the strongest role in decreasing the Ms.This is consistent with results shown in Ref. [192,231]. In present case, the decrease rate of Ms temperature reduces when the C concentration in the steel increases.

4.3. BAINITIC TRANSFORMATION START TEMPERATURE (B_S)

The temperature corresponding to the upper part of the shear transformation C curve is often called the bainite-start temperature Bs [108,231]. The Bainitic Transformation Start

Temperature (B_s) calculated by use of different empirical equations for different authors and experimentally measured for both steel in present work are given in table (4.5). It is clear from table (4.5) that the predicted results in rather good agreement with the experimental for both steel investigated. The experimentally estimated (B_S Temperature) results is rather good agreement with the similar steel given in Ref. [231].

Table (4.5) B_s : Start Temperature of the Bainitic Transformation ($^\circ$C) for steels studied calculated by use some authors sources.

B_s for Ti-V-N Steel	B_s for V-N Steel	Source
534	549	Kirkaldy, [224]
522	548	Suehiro, [224]
526	537	Zhao, 2002,[224]
534	549	[232]
520	550	Experimentally measured

4.4   ISOTHERMAL TRANSFORMATION

The transformation behaviour was evaluated in temperature range 350-600°C after isothermal treatment. Phases were evaluated on bases explained in chapter 2. Identification of phases was based on the shape of new phase, temperature range and place of nucleation, using OM and SEM. Identified phases are: grain boundary ferrites in high and lower temperature range, acicular ferrite (needle type and sheaf type), bainitic sheaves and pearlite.

4.4.1. GRAIN BOUNDARY FERRITES

Grain boundary ferrites obtained during isothermal decompositions are allotriomorphic and Widmanstatten ferrite.

4.4.1.1 Allotriomorphic Ferrite

Allotriomorphic ferrite is the first phase to be nucleated during isothermal treatment in temperature range 500-600°C. Allotriomorphic ferrite nucleates on the austenite grain boundaries as shown in Fig. 4.4 and Fig. 4.5 for both types of steels. On the other hand more Grain Boundary Ferrite (GBF) images present in this work by optical and SEM images are given in appendix B. After the first grains are produced, allotriomorphs continue to decorate

austenite grains. Further growth in the direction inside grains is not pronounced. Therefore, it can be summarized in Fig. 4.4   and Fig. 4.5 at highest temperatures, they predominate by growing along the boundaries, and also into the grains to give a well-defined grain structure, generally referred to as equi-axed ferrite. However the allotriomorphic ferrite obtained after increase treatment time are shown in Figure 4.4 (k-n) and Figure 4.5 (a,m,n). The proeutectoid ferrite start to decoreate all the austenite grain boundary as treatment time increased.

Table 4.6 Nucleation onset time for Allotriomorphic ferrite in both steels

Isothermal transformation Temperatures, °C	Allotriomorphic Ferrite nucleation time, s	
	V-N steel	V-N-Ti steel
450	2	2
500	3	5
550	5	7
600	7	10
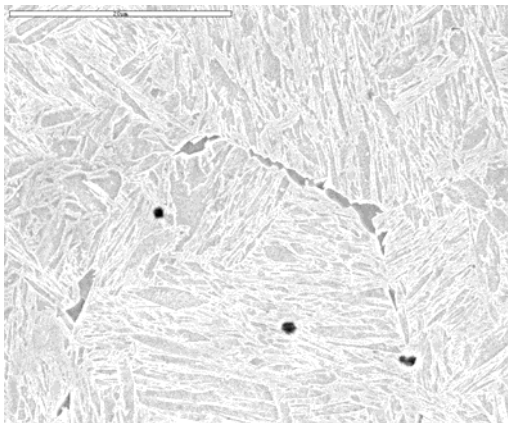
a) SEM/ 600°C /10s /(S6x2500-2)
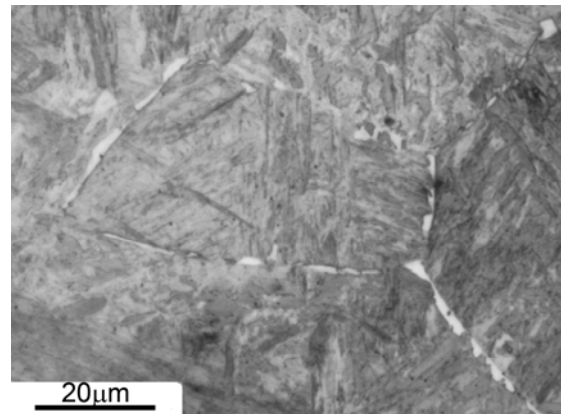
b) OM/600°C /10s/500X
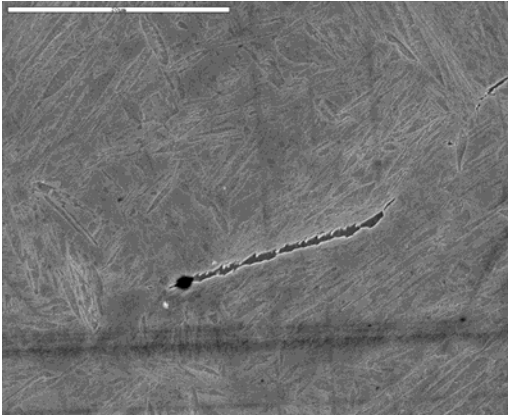
c) SEM /550°C /5s/ S5x2500-2
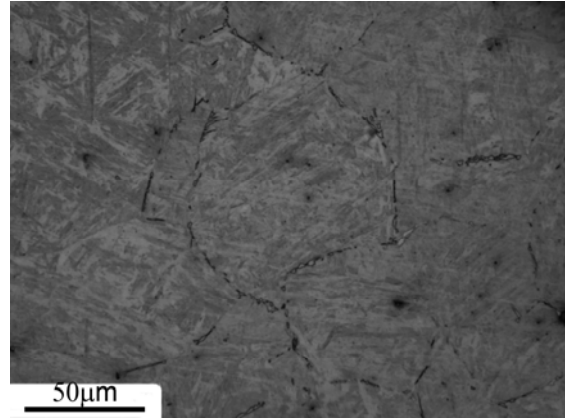
d) OM/550°C /10s/200X
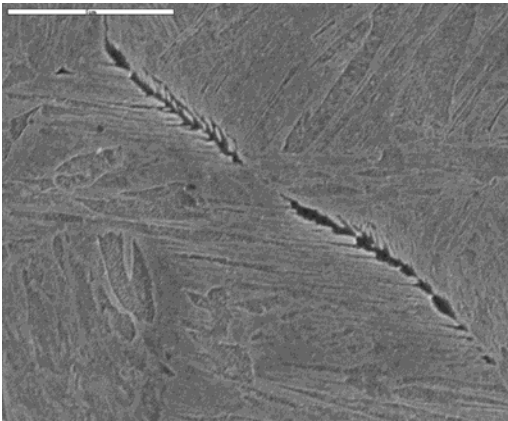
e) SEM/500°C /03s /(S4x7500-2).
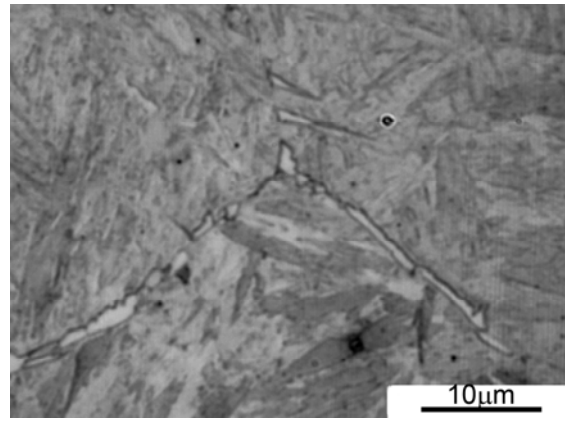
f) OM/500°C /5s/1000X
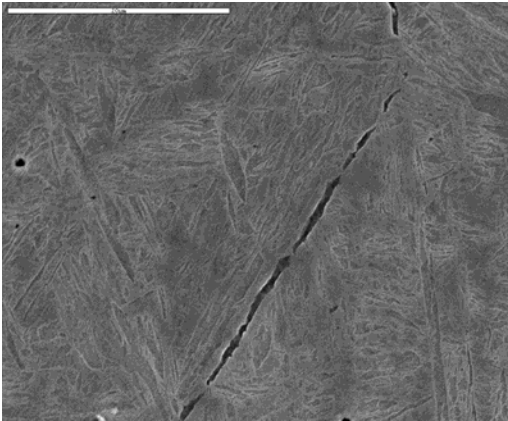
g) SEM /450°C/ 2s / (S3x2500)
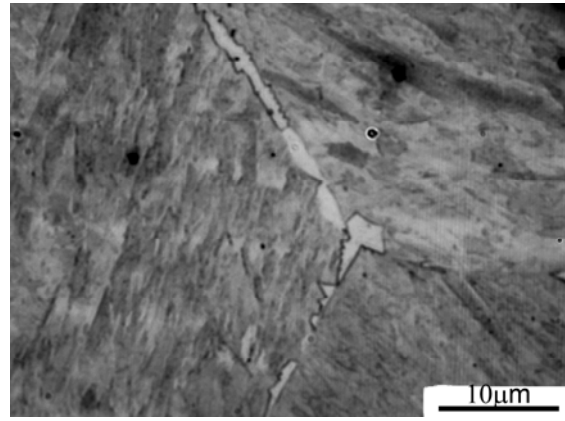
h) OM/450°C/ 2s/1000X
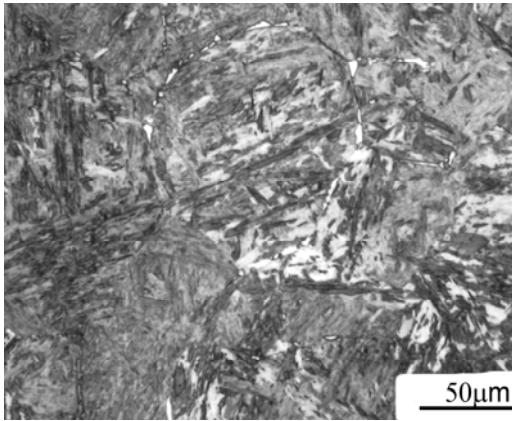
k) OM/600°C/ 10s/200X(04)
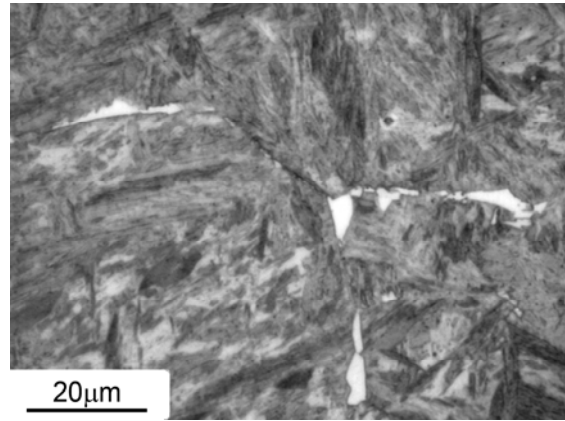
l) OM/600°C/ 10s/500X(06)
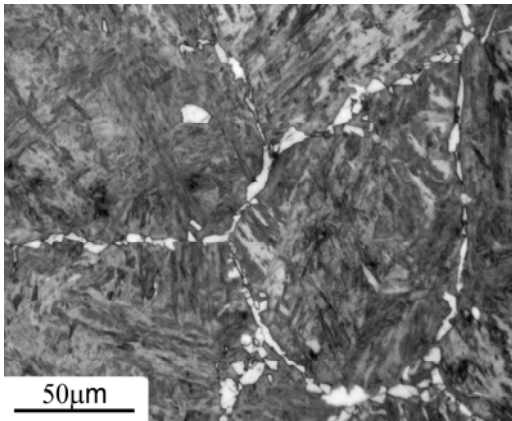
m) OM/600°C/ 20s/200X(027)
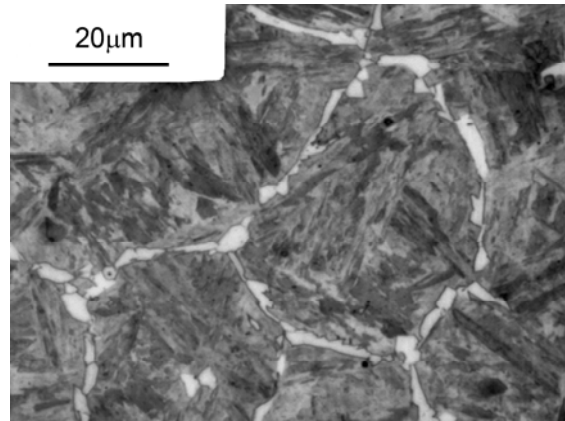
n) OM/600°C/ 20s/500X(1032)

Fig. 4.4 SEM images and optical micrographs of Grain Boundary Ferrite GBF for V-N steel.
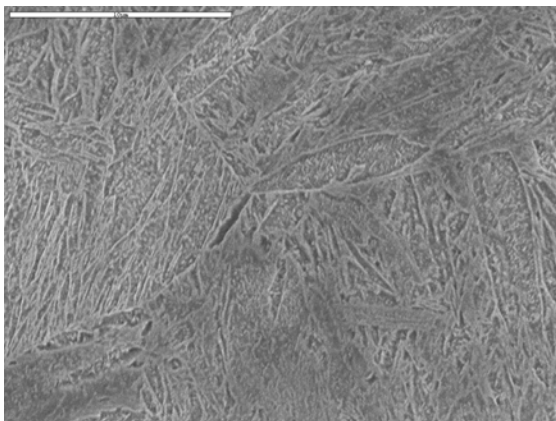
a) SEM/600°C /10s /(S11x5K-1).
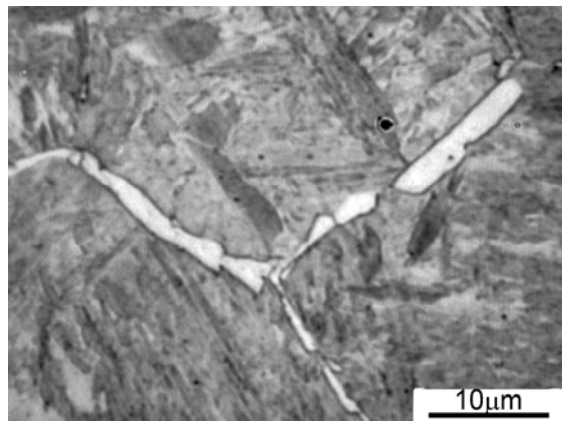
b)OM/ 600°C /30s/1000X/ (1049)
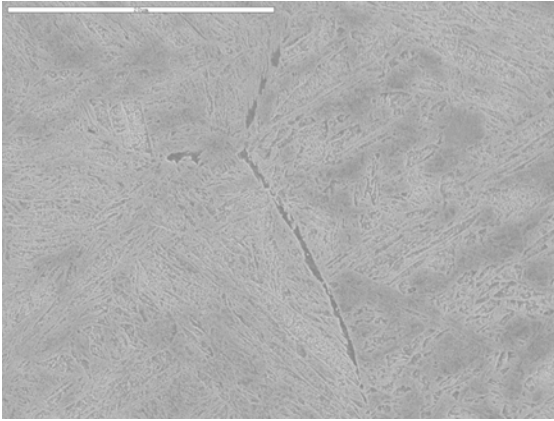
c) SEM/550°C /10s /S9x3k-1
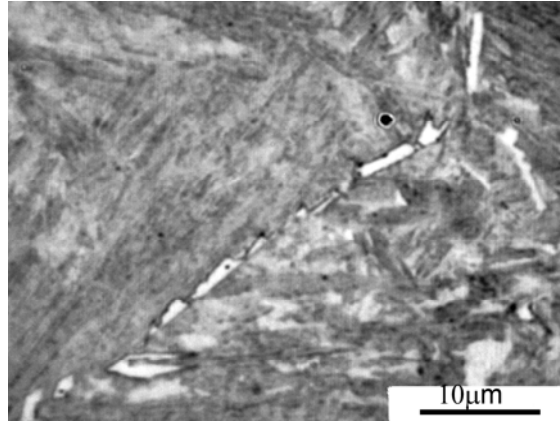
d) OM/550°C /20s/1000X
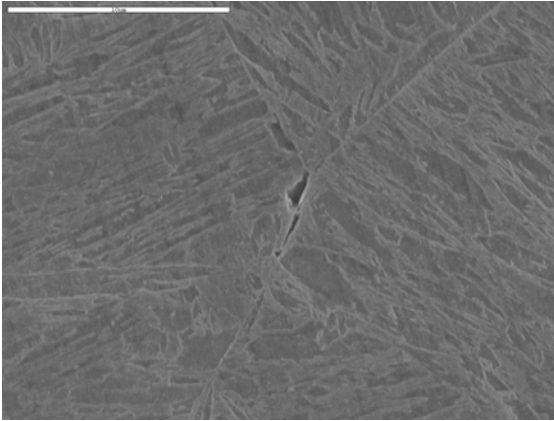
e) SEM/500°C /5s /(S6x5k-1).
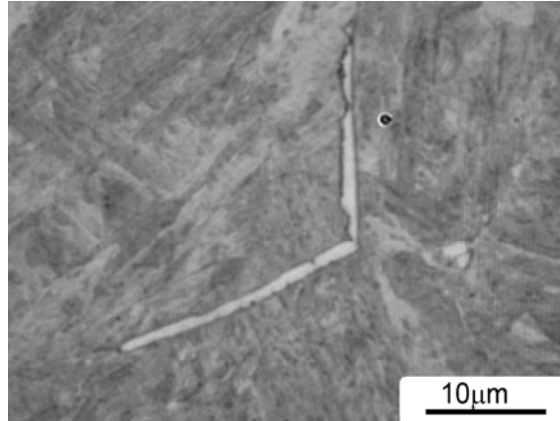
f) OM/500/°C 5s/1000X/ (704).
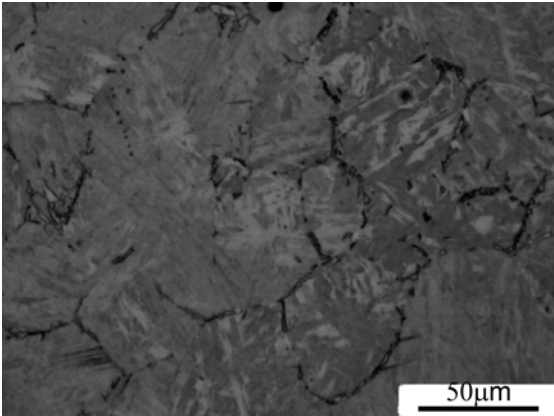
g) OM/500°C /10s/ (719 – 10s – 200X).
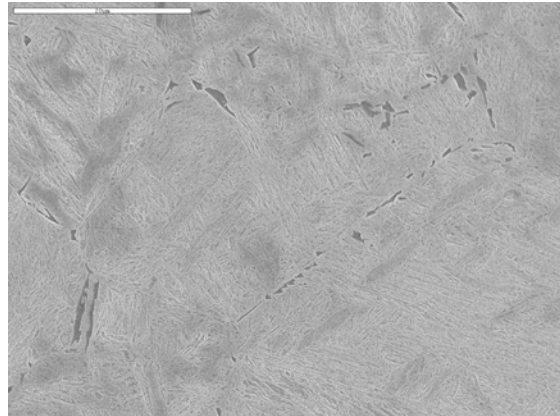
h) SEM/500°C /10s/ (S7x2k-1).
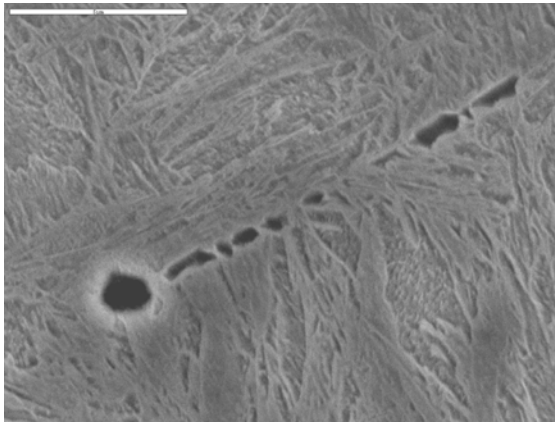
k) SEM/ 450°C / 2s/ (S4x8k-1)
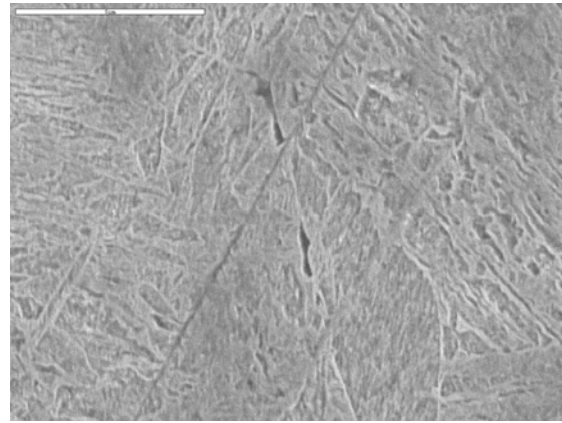
l) SEM/ 450°C / 5s /(S5x8500-1)
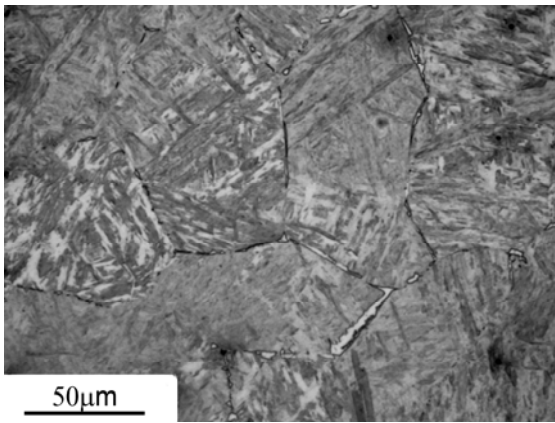
m) OM/600°C /30s/200X (1294).
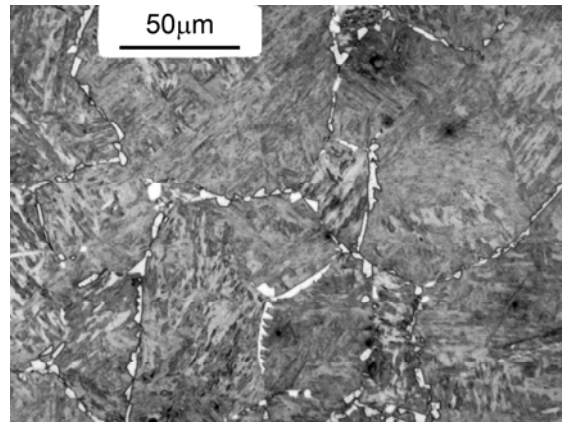
n) OM/600°C /60s/200X (1299).

Fig. 4.5 SEM images and optical micrographs of Grain Boundary Ferrite GBF for Ti-V-N steel.

4.4.1.2. Widmanstätten ferrite

These laths (narrow plates) of ferrite are nucleated on grain boundaries and grow along crystallographically defined planes of the austenite; these grains do not grow across the austenite grain boundaries, but in one of austenite grains. Primary Widmanstätten ferrite grows directly from the austenite grain surfaces, whereas secondary Widmanstätten ferrite develops from allotriomorphs of ferrite already present in the microstructure as illustrated in Fig. 4.6. It occurs in temperature range below 500 °C and it is also exist on isolated sites at higher temperature as illustrated in Fig. 4.6 (x, w and z). The incubation time for Widmanstätten ferrite formation WSF is given in table 4.7

Table 4.7 Nucleation onset time for WSF by sec. For both steel investigated.

Isothermal Transformation Temperatures, °C.	Widmanstaetten Ferrite start time, s	
	V-N steel	V-N-Ti steel
500	Nil	Isolated
450	2	10
400	2	10
350	10	10

Incubation time for WSF in this temperature range is shorter for V-N-Ti free steel, in comparison to Ti steel.
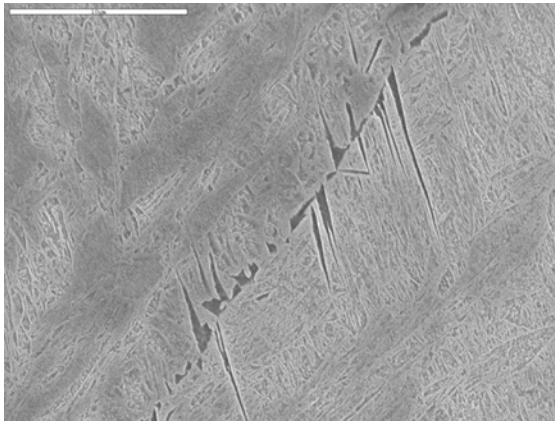
a) SEM/WSF / Ti-V-N steel /500°C /10s
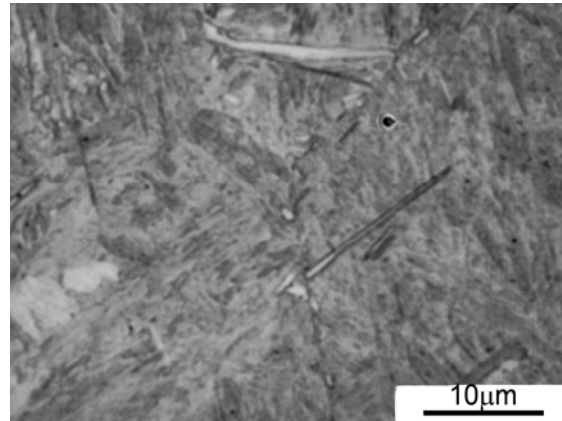
b) OM/WSF Onset/ Ti-V-N steel/ 350°C/10s
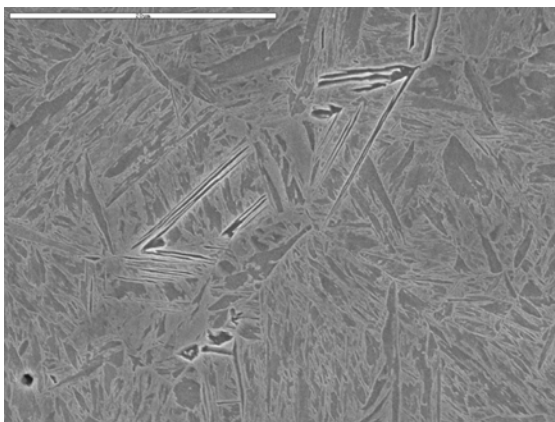
c) SEM/Ti-V-N steel /350°C / 10s

d) OM/WSF-Onset / Ti-V-N steel /450/°C/ 10s/1000X
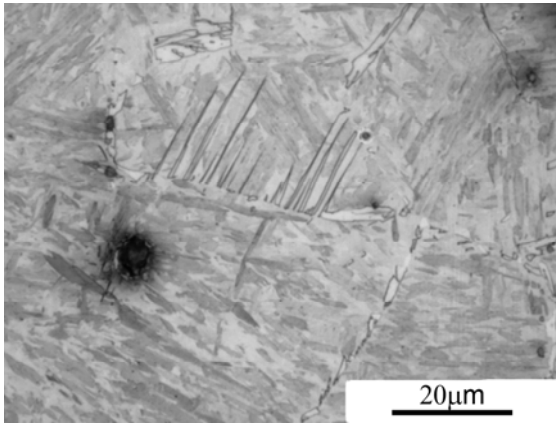
e) OM/WSF / Ti-V-N steel/ 450/°C10s
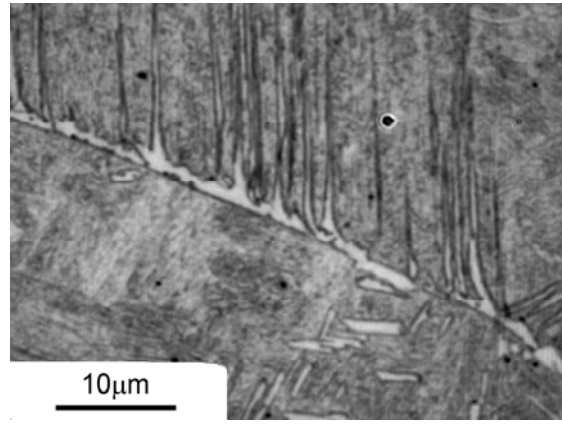
f) OM/WSF /V-N steel/ 400°C /10s
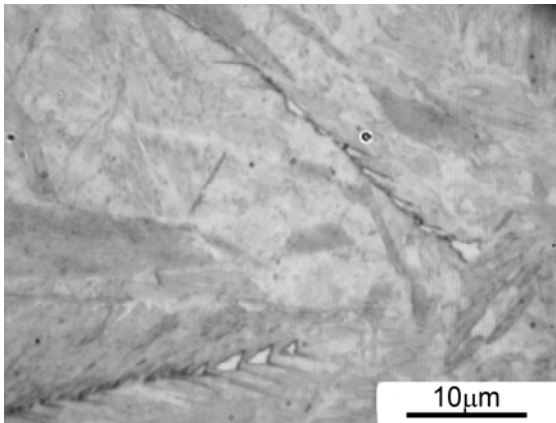
g) OM/WSF/ V-N steel 450°C /2s
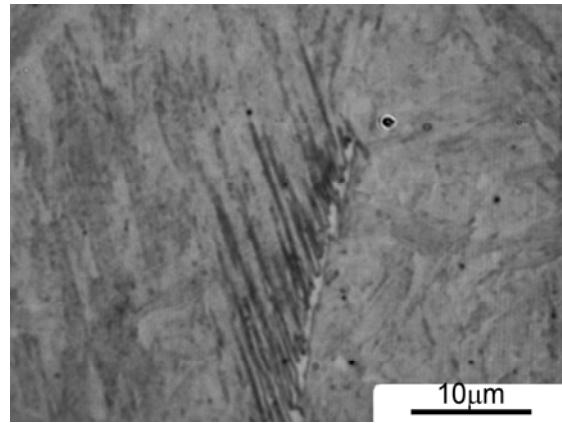
h) OM/WSF/V-N steel /450°C /5s
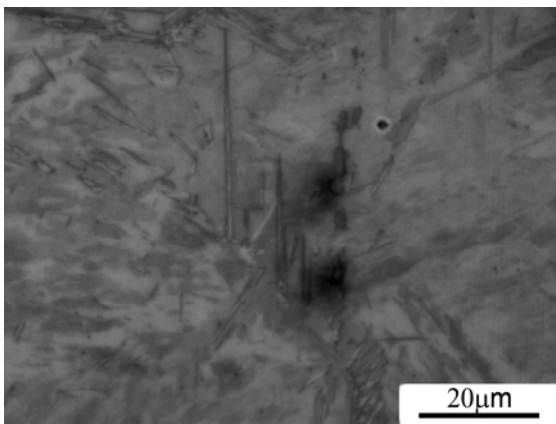
k) OM/WSF/ V-N steel /350°C /10s
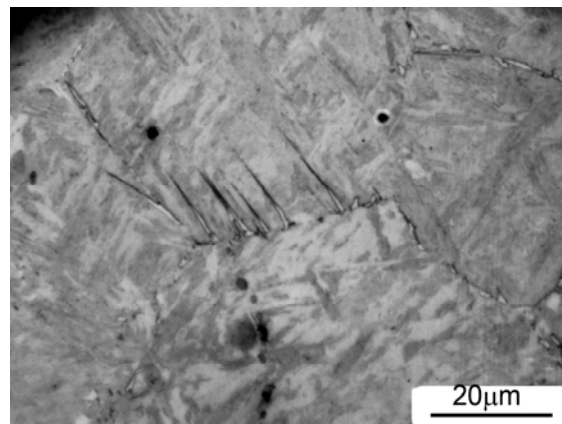
(l)OM/WSF/ Ti-V-N steel /500°C /10s
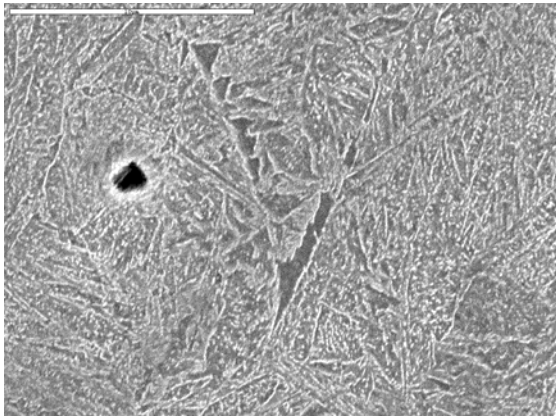
m) SEM/V-N steel/ 400°C /2s SEM
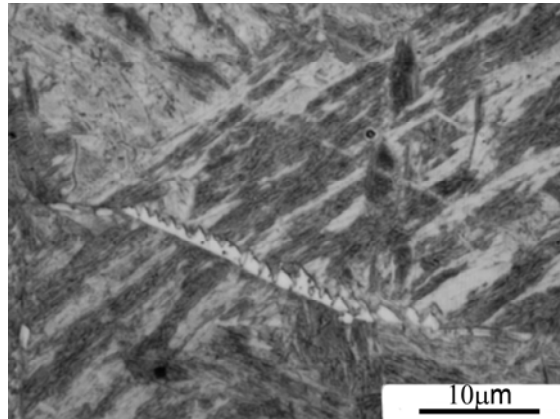
(n)OM/WSF/ V-N steel /450°C /5s
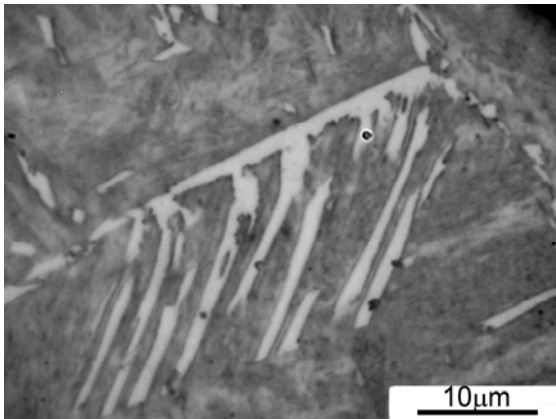
(x)OM/WSF/ V-N steel/ 550°C /20s
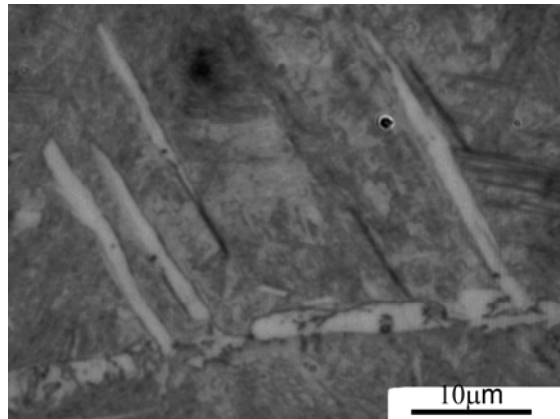
(y)OM/WSF/ V-N steel/ 450°C /10s
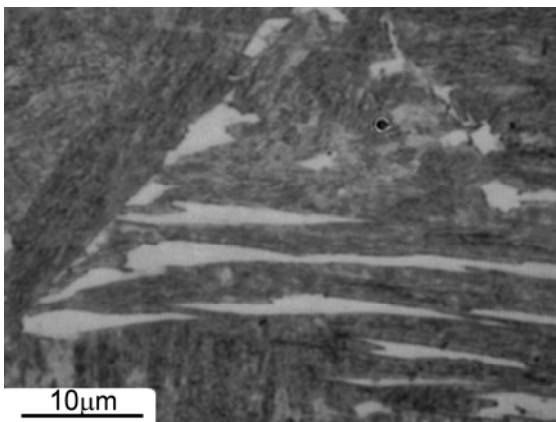
(w)OM/WSF/ Ti-V-N steel /550°C /80s
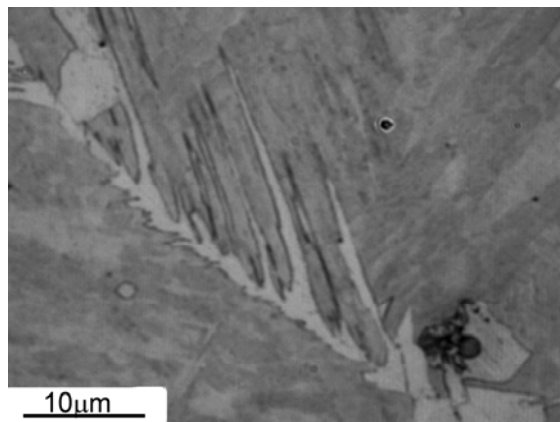
(z)OM/WSF/V-N steel /600°C /120s

Figure 4.6. SEM and OM images showing the nucleation of Widmanstätten ferrite

4.4.2 INTRAGRANULARLY NUCLEATED PHASES

Intergranularly nucleated phases classified in this chapter are: (i) Intragranular idiomorphs; (ii) Intelocked acicular ferrite and (iii) Sheaf type acicular ferrite. Intragranular cementite and intragranular plates are listed in 4.4.3.1 and 4.4.4 respectively. Acicular ferrite formation is a mechanism competitive with bainite formation. Acicular ferrite is usually considered as intragranularly nucleated bainite. Both microstructures develop in the same range of temperature: below the high temperatures where pearlite onset form, but above the martensite start temperature. The identifying difference between acicular ferrite and bainite is related to the nucleation sites. The acicular ferrite is always nucleated intragranularly, usually at nonmetallic inclusions. There are two types of acicular ferrite, depending on the morphology: (a) interlocked type - chaotic arrangement of interlocked plates, or (b) sheaf type - sheaves of intragranular parallel ferrite plates

4.4.2.1.   Polygonal Ferrite (IGF)

These are equiaxed crystals which nucleate inside the austenite grains as demonstrated in Table 4.8, usually on non-metalic inclusions present in the steel. An idiomorph forms without contact with the austenite grain surfaces and has a shape which some shows crystallographic facets as shown in Figure 4.7 (a-l). On the other hand more images showing the Intragranular Idiomorphs in this work are given in appendix D.

Table 4.8 Nucleation time for Polygonal Ferrite or Intragranular Idiomorphs for both steels.

Temperatures	Intragranular Idiomorphs start time, s	
°C.	V-N steel	V-N-Ti steel
500	10	10
550	20	30
600	30	60
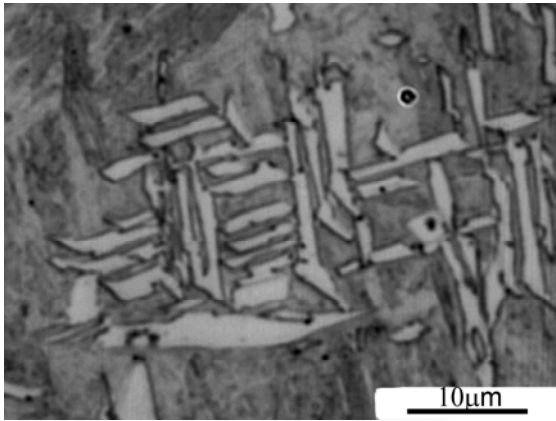
a) TiF/ 500°C /20s
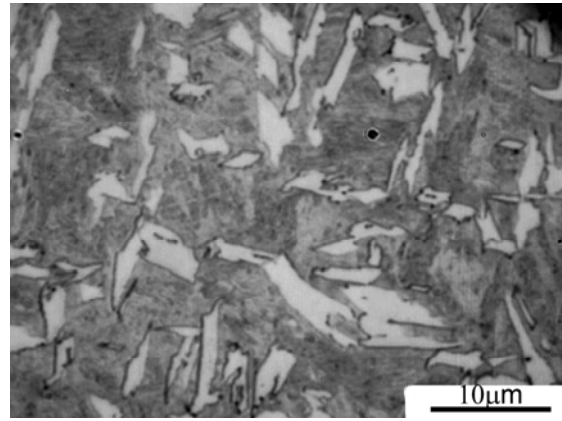
b)TiS/ 500°C /80s
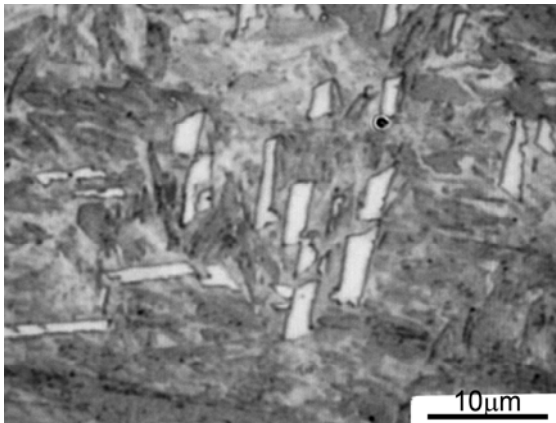
c)TiF/ 550°C /30s/1000X-929
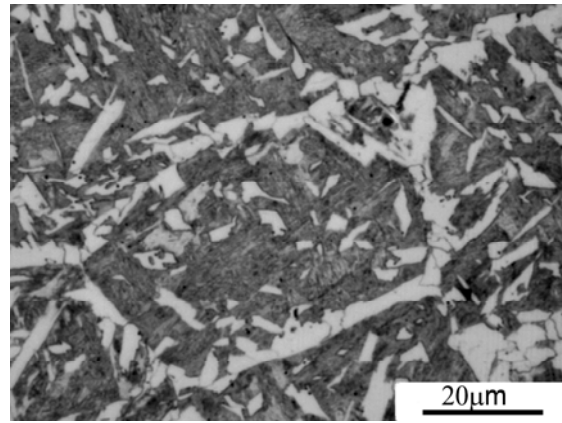
d) 550/°C 60s/500X(645)-Ti free Steel
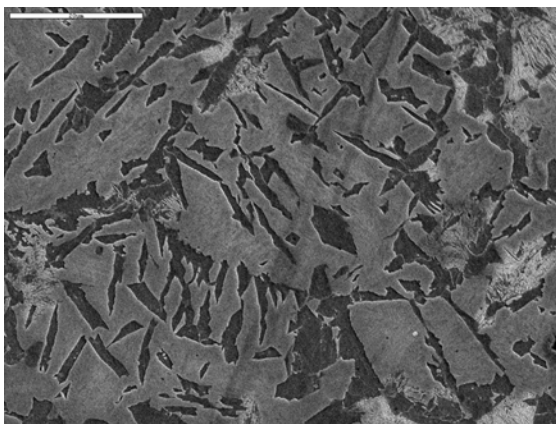
e) 550°C /120s SEM) –Ti-F(1500-2)
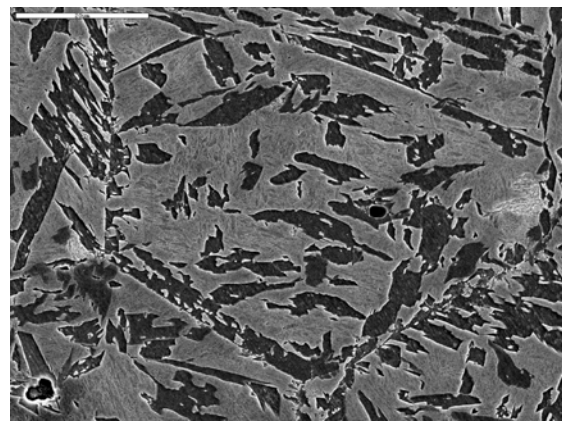
f) 550/°C 420s SEM) -TiS(1500-2)
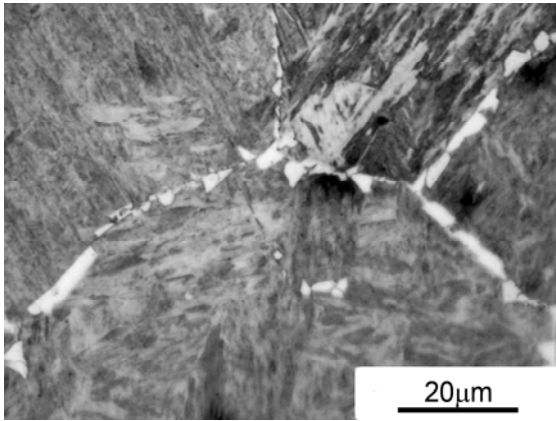
g) 600°C /60s/500X (1052)-Ti Steel   h) 600°C /60s/1000X (1051)-Ti Steel
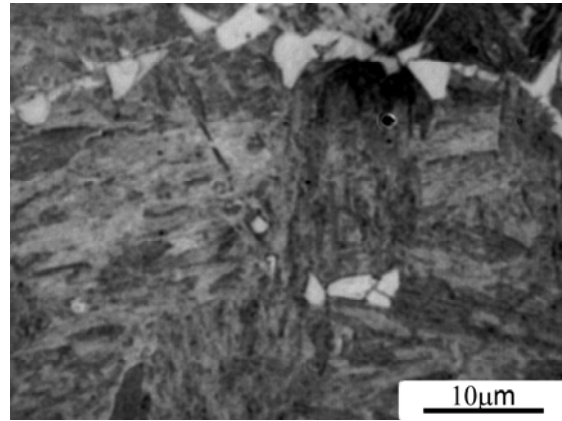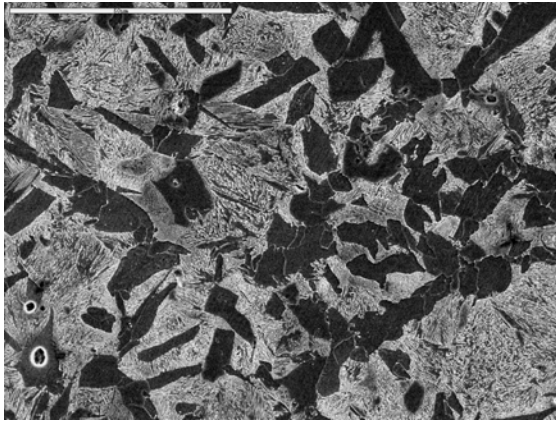
k) Ti free 600°C /120s/SEM/1000-1   l) 600°C /120s/200X (058)-Ti free.
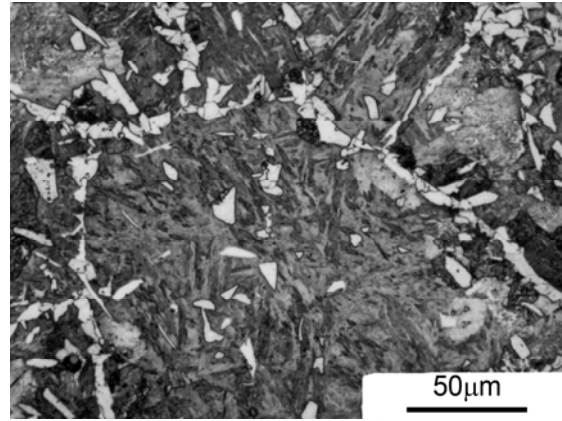
Figure 4.7(a-l) SEM and OM images showing the Intragranular Idiomorphs formation

4.4.2.2. Interlocking Acicular Ferrite

(i) Nature of Inclusions and Nucleation at Particles

At the initial stages, the nucleation of the primary ferrite plates takes place intragranularly at second phase particles present in the austenite and not at grain boundaries. Nucleation time for primary acicular ferrite is given in Table 4.9. Examples of different particle stimulated nucleatin are presented in figure 4.8. Second phase particles in this work are nonmetallic inclusions, as identified on figure 4.9. The times for the onset of Interlocked type AF are seems tobe very similar for both steels as indicated in table 4.9. Also, with prolonged time,

the amount of interlocked type AF increases up to the moment when pearlite transformation occurs.

Table 4.9 Interlocking Acicular Ferrite start time

Temperatures °C.	Interlocking Acicular Ferrite start time, s	
	V-N steel	V-N-Ti steel
450	10	10
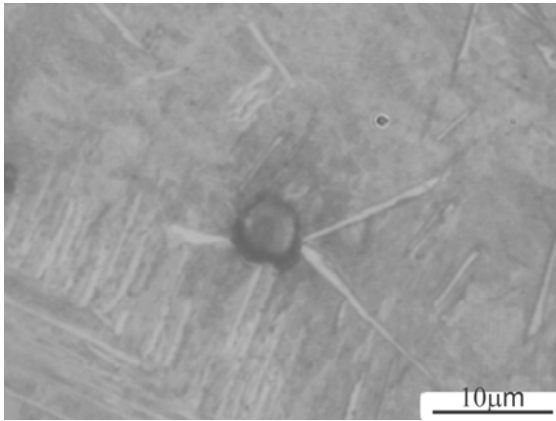
a) OM / 450°C /20s-TiS
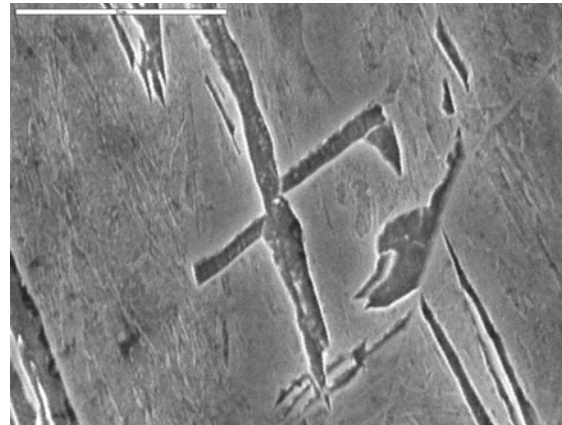
b) SEM / 450°C /20s/10k TiS)
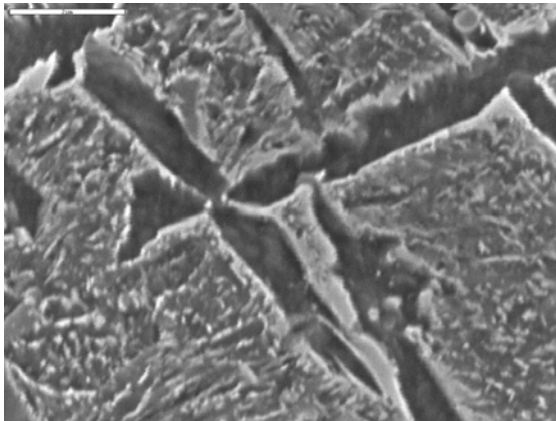
c) SEM / 450°C /20s/13k TiF
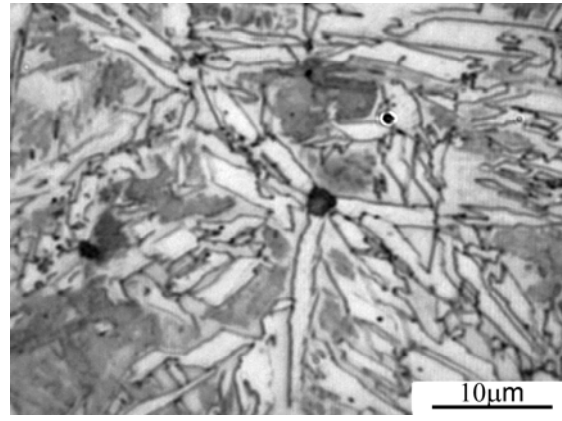
d) OM / 500°C /30sTiS
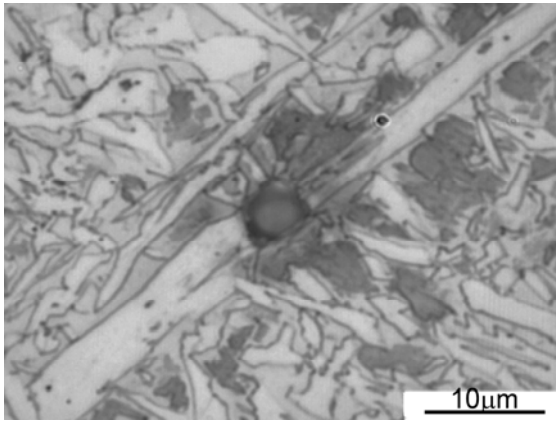
e) OM / 500°C /30s/TiF
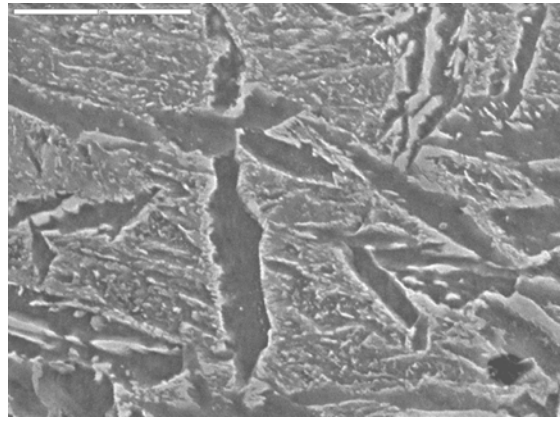
f) SEM / 450°C /20s/TiF
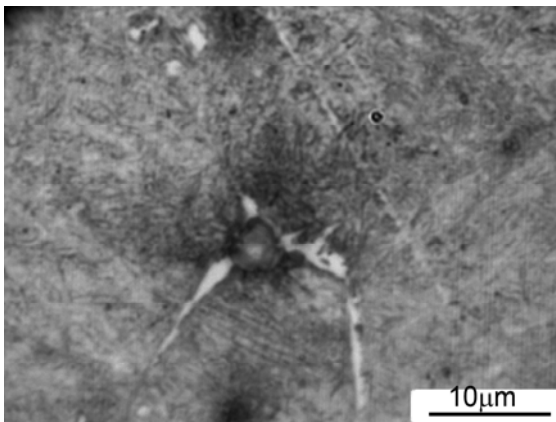
g) OM / 550 °C /10s TiF
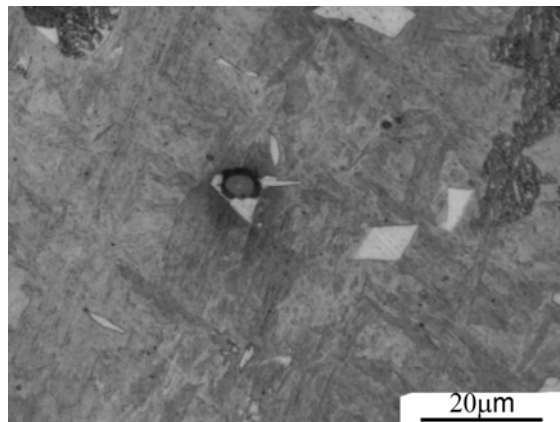
h) OM / 600 °C /100s/TiF
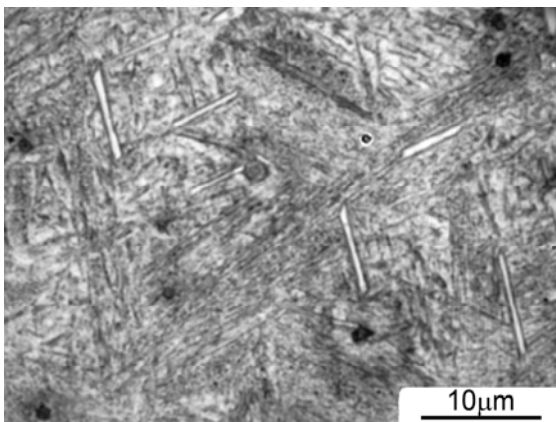
k) OM / 450°C /10s/ Ti F
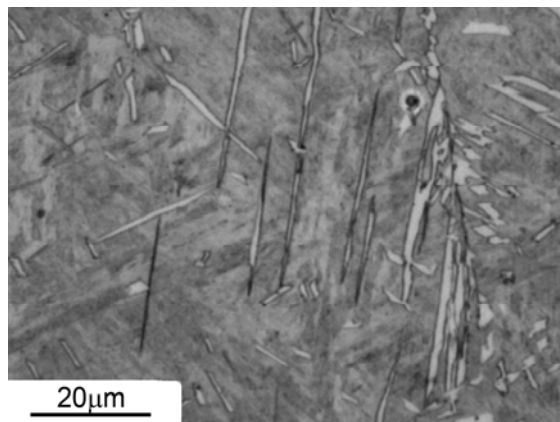
l) OM / 500°C /30s/ Ti S
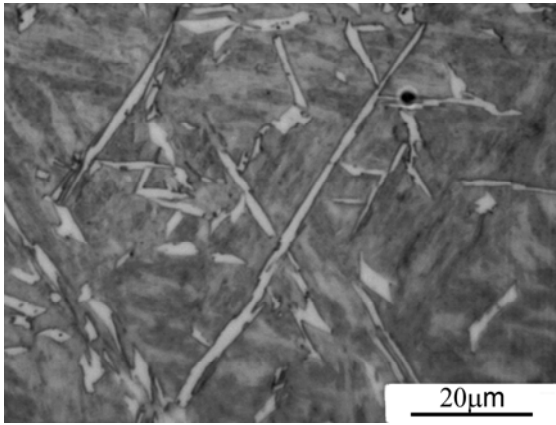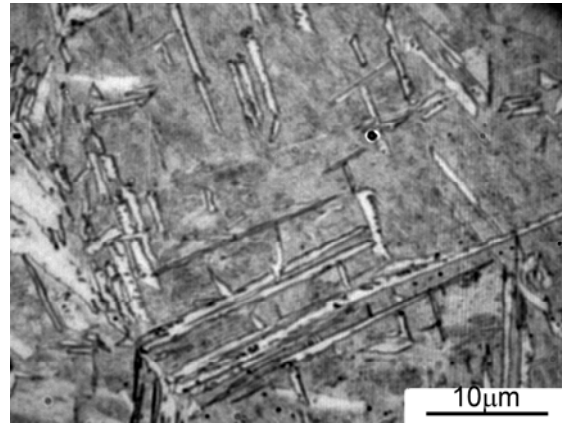
m) OM / 500 °C /45s / TiS   n) OM / 450 °C /20s/TiS
Figure 4.8 (a-n) SEM and OM images show nucleation at particle.
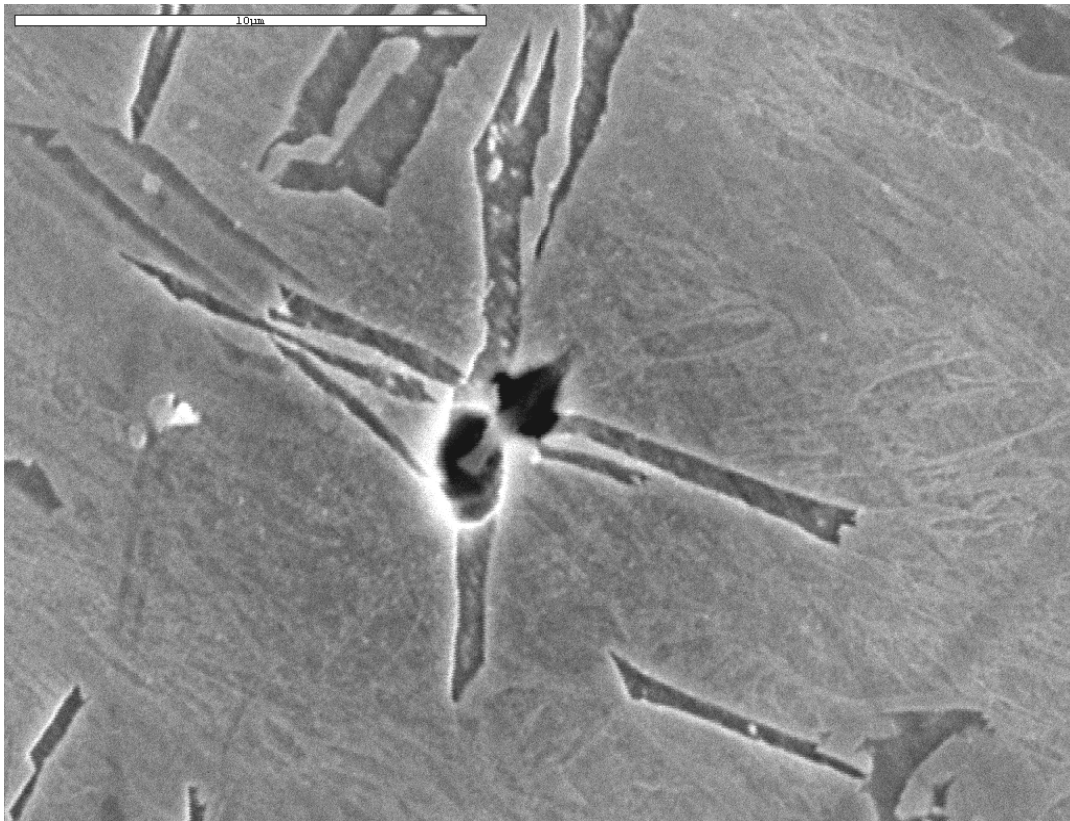
Full scale = 1.69 k cps   Cursor: 9.5675 keV
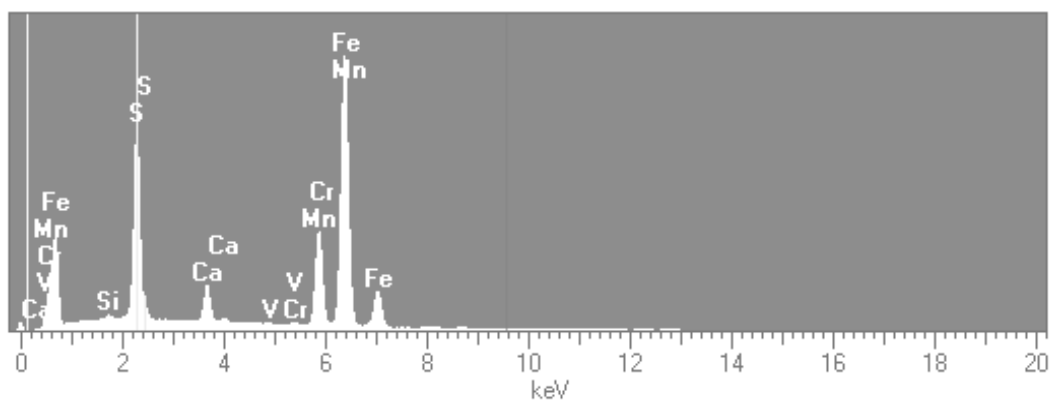
(a)
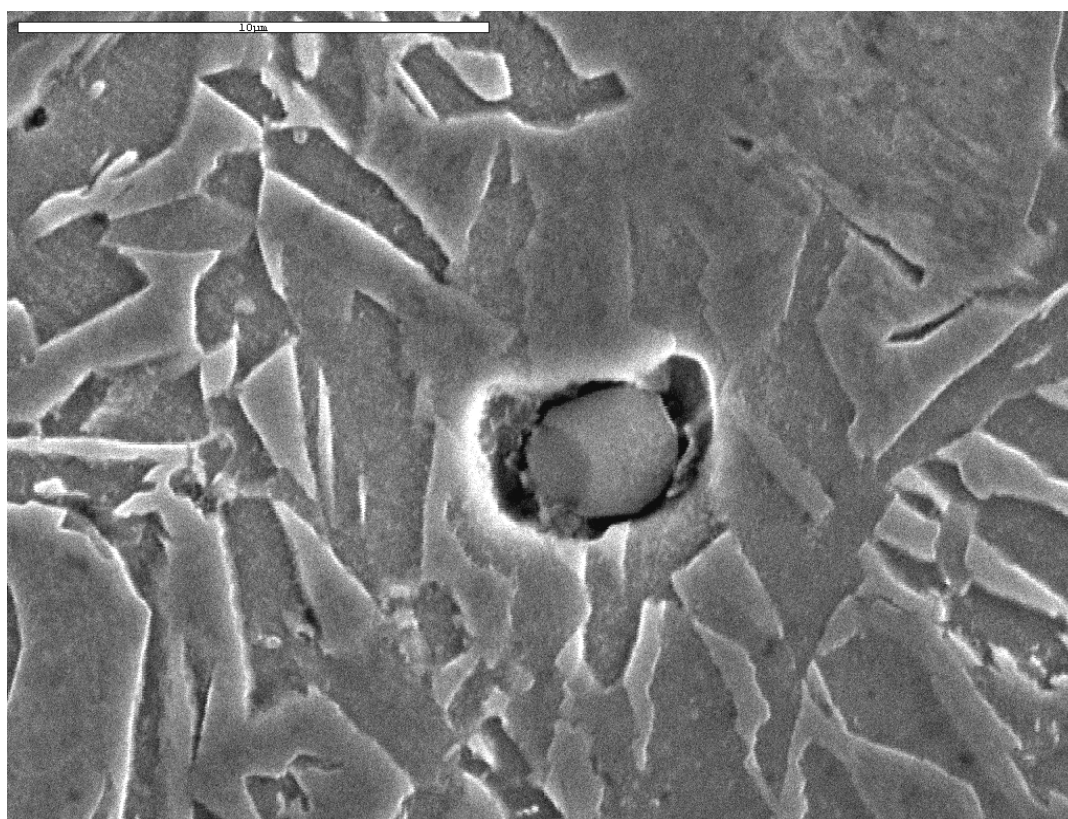
(b)
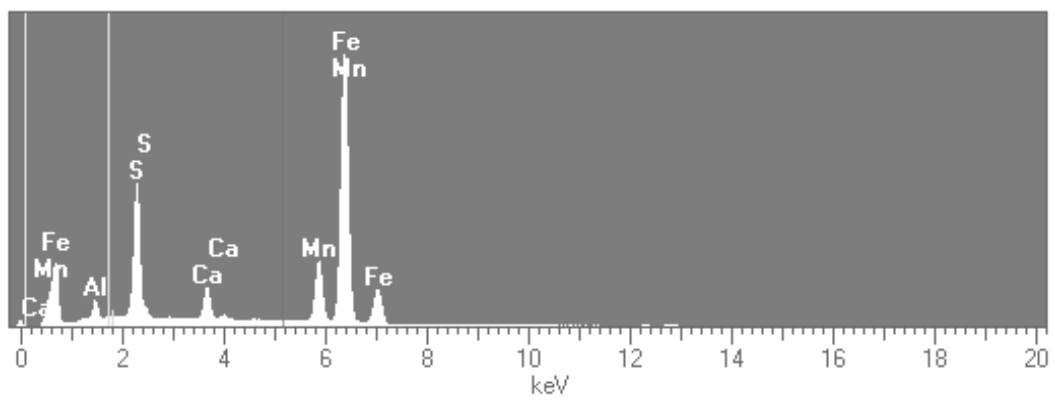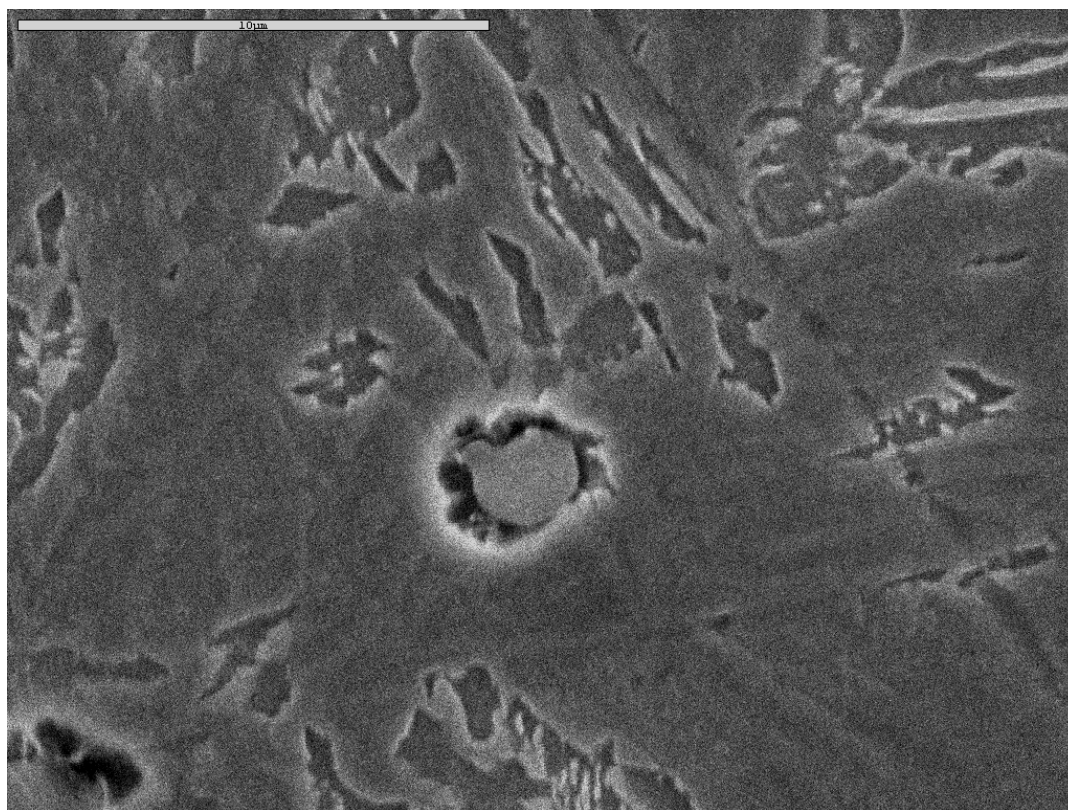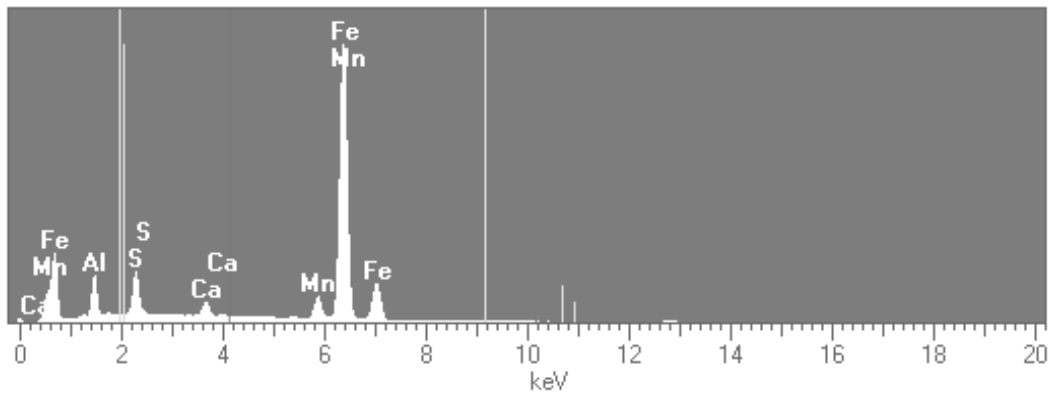
(c)

Fig.4.9 (a-c) SEM image showing the beginning of the nucleation of acicular ferrite at an inclusion and EDX spectrum of an inclusion (a) 500°C /30s (Ti-V-N steel).(b) 500°C /30s and (c) 450°C /30s (V-N steel).

The micrograph present in Figure 4.9 and an energy dispersive X-ray (EDX) spectrum analysis illustrate a typical active inclusion, with the corresponding chemical analysis at different points of the particle, which reveals the existence of Ca-treated manganese sulfides inclusion (Ca,Mn)S core covered or at least partially covered with VC or V(C,N) complex precipitates.

(ii)   Formation of Interlocked Structure

In regards to the nucleation of the first acicular unites takes place intragranularly at non-metallic inclusions present in the austenite and after the initiation of the first generation of plates from inclusion as can be seen in Fig. 4.8, the second generation of plates nucleated on the face of a substrate plate (sympathetically) must have a different habit plane and orientation. The result of multiple sympathetic nucleation is an interlocking ferrite network, and after sufficient time, it results into a complex interlocking ferrite microstructure, characteristic of acicular ferrite, such as that shown in Figure 4.10 (k-n).

In Figure 4.10.The sympathetic nucleation of secondary acicular ferrite plates has been observed to occur at the austenite/primary acicular ferrite interface and continue to grow within the austenite matrix until impingement occurs with other plates. However the acicular ferrite does not normally grow in sheaves because the development of sheaves is stified by hard impingement between plates nucleated independently at adjacent sites [233].A typical

example of impingement processes is illustrated in the SEM and optical micrographs as clearly shown in Figure 4.11.
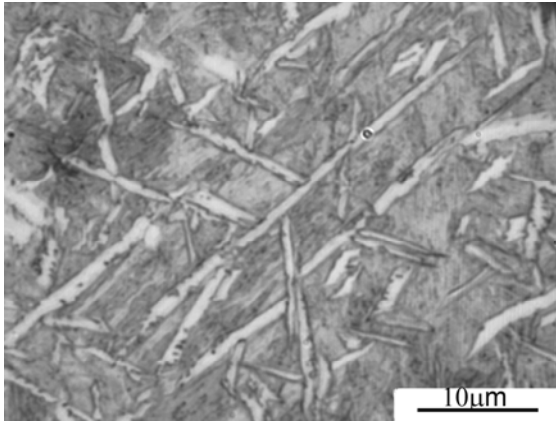
a)OM /V-N steel/ 450°C /20s
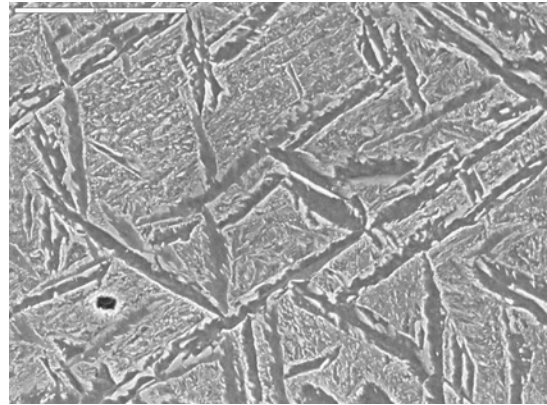
b) SEM/ V-N steel 450°C /20s
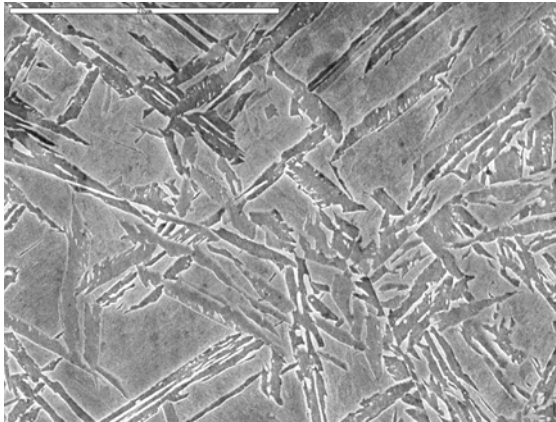
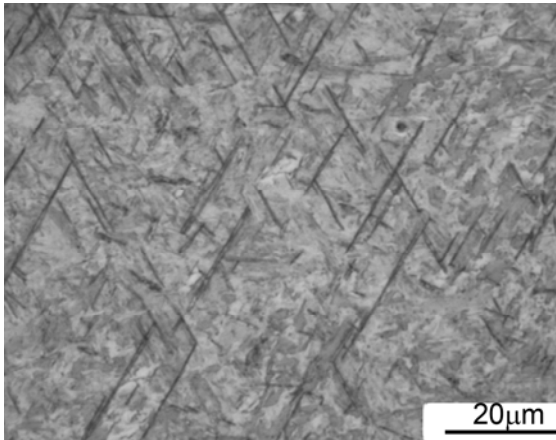c) SEM/Ti-V-N steel /450°C 20s(7S02x3k).
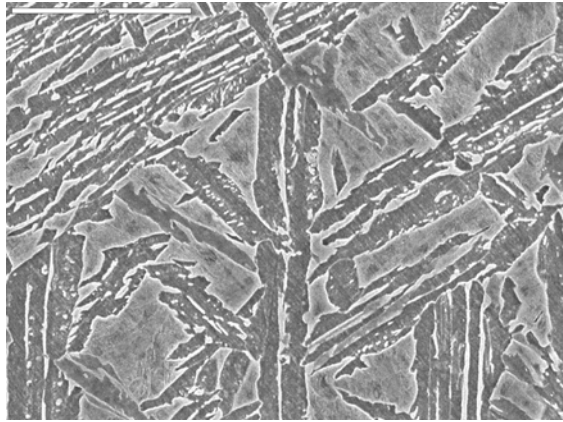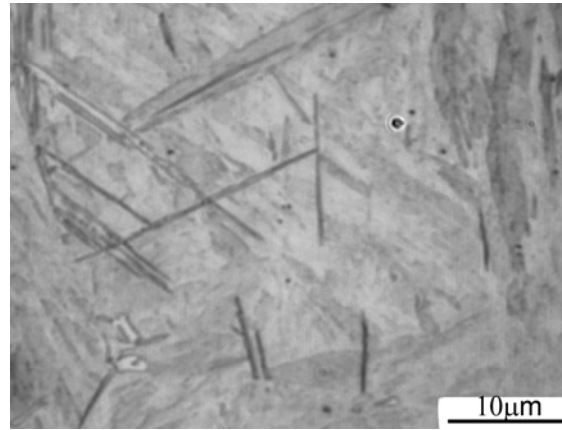
d)SEM/ Ti-V-N steel/ 450C/30s (6S02x4k)
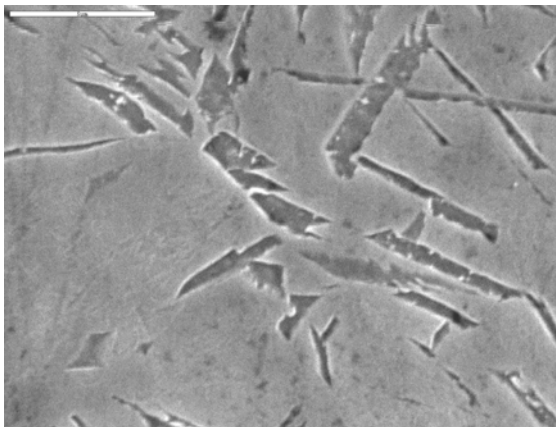
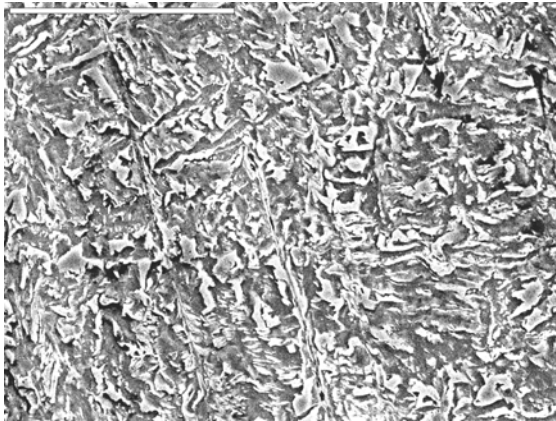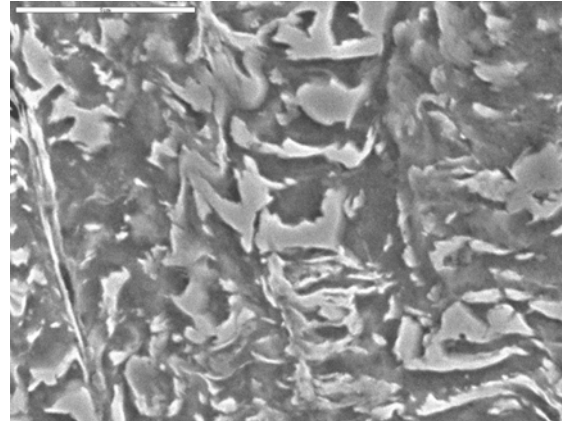e)-SEM/ Ti-V-N steel /450°C /20s(2245201)
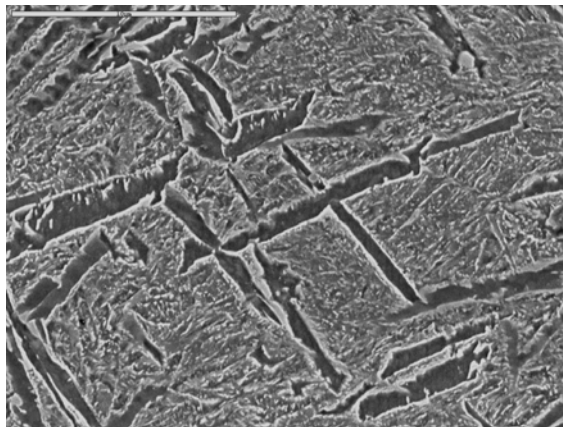
f)-SEM/V-N steel/ 450°C /20s(1S09X5K).

(g) OM/Ti-V-N steel /350°C /20s/500X

(g)OM/350°C /10s/1000X (1525)/V-N steel
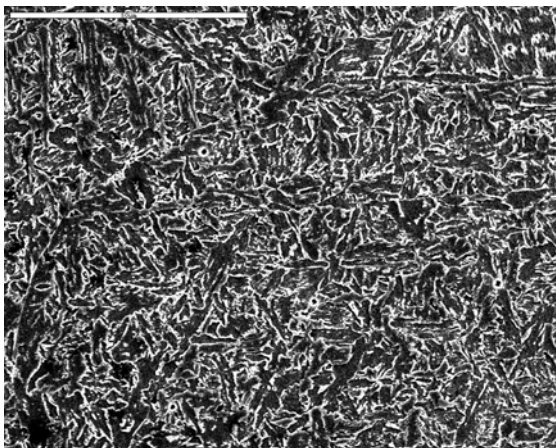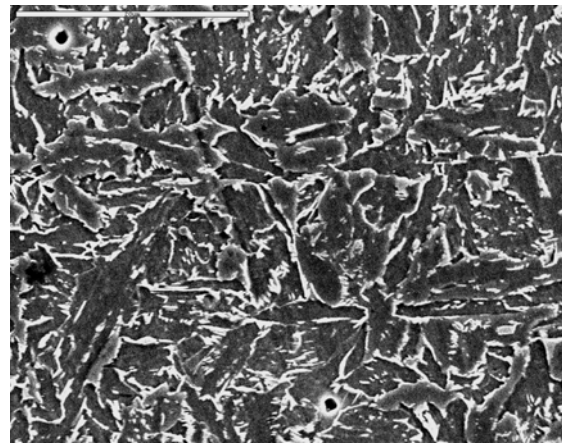
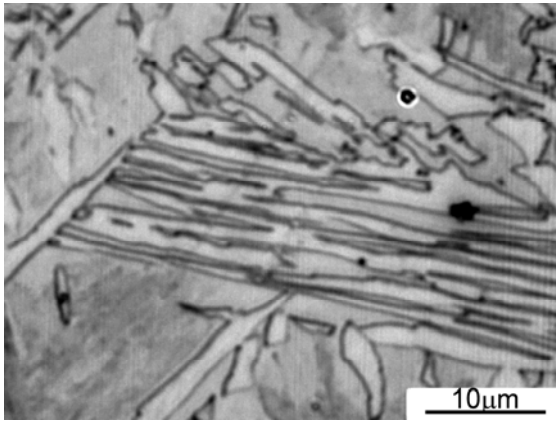k) SEM/ Ti-V-N /450/°C/600s(S4x2500-1)

L) SEM/450°C /600s (S4x23k-3)/ Ti-V-N steel.

M)SEM/V-N /450°C /1200s (S5x1000-1).

N) SEM/V-N steel/450°C /1200s (S5x2500-2).

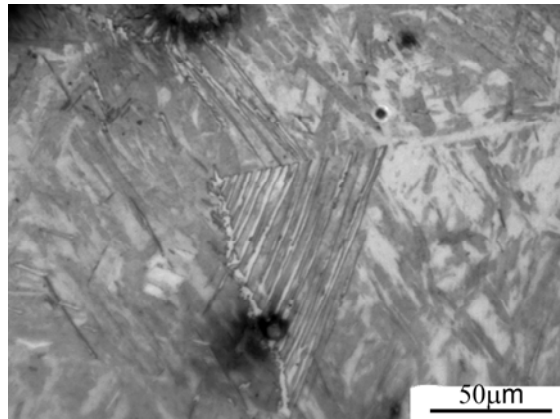Figure 4.10. SEM and OM images showing the sympathetic nucleation and AF interlock structure formation.
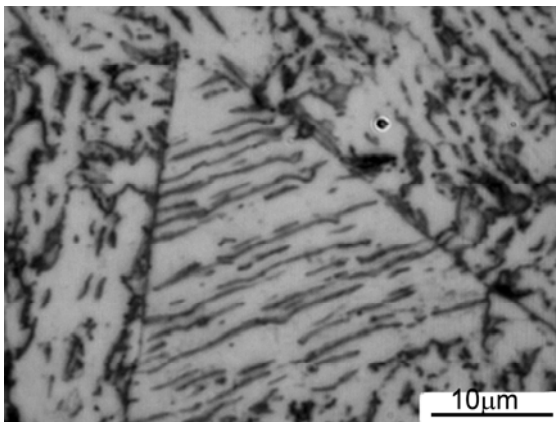
a) OM/V-N steel/500°C /30s
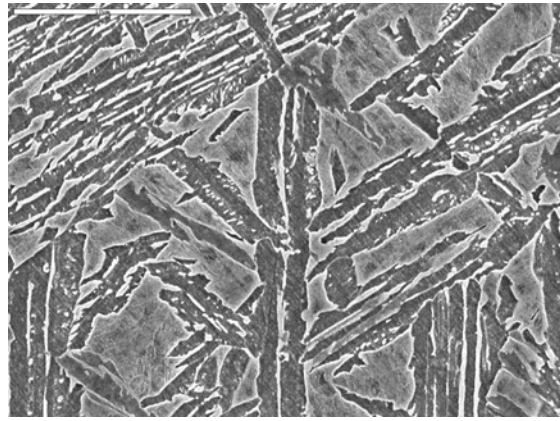
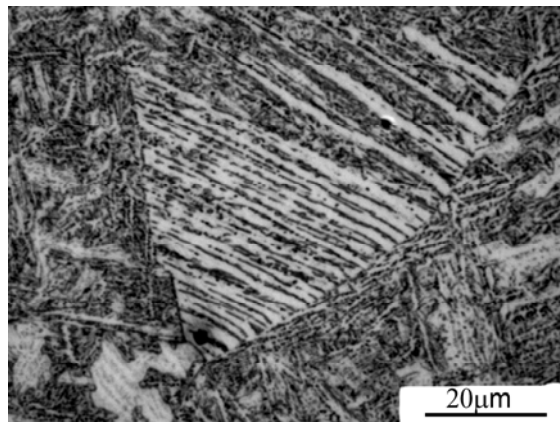b) SEM 450°C /30s/ Ti-V-N steel.
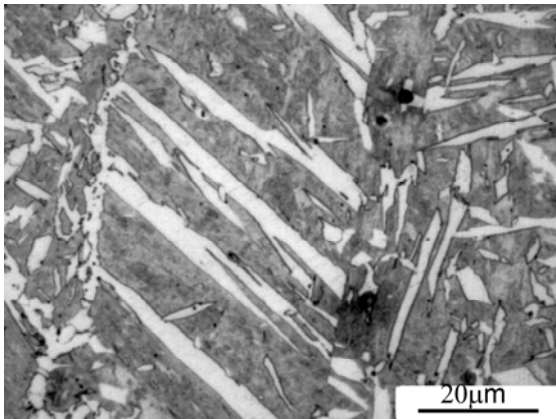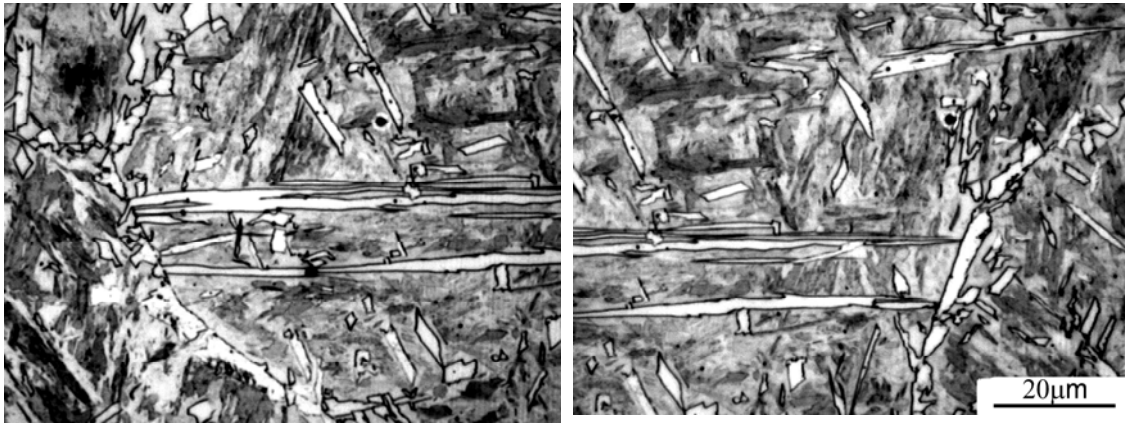
c) OM/550°C /45s/500X/V-N steel (630).

d) OM/350°C /10s/200X/ V-N steel

e) OM/450°C/1800s/1000X/ Ti-V-N steel

f) OM/350°C /600s/500X/ V-N steel (1485)

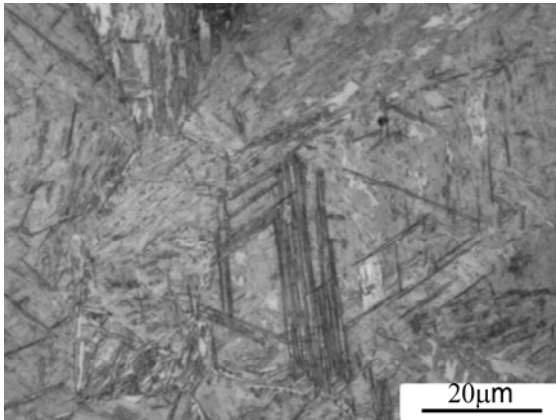g) OM/550/°C /30s/500X/ V-N steel   g) OM/550/°C /30s/500X/ V-N steel
Figure 4.11 Examples of impingement processes.

## 4.4.2.3. Sheaf Type Acicular Ferrite (STAF) Morphology

Main characteristic of sheaf type AF is presence of intragranularly nucleated microstructure composed by sheaves of parallel ferrite plates, Figure 4.12. After nucleation, it transformed to sheaf type acicular ferrite (STAF) or generation of plates developed in a parallel sheaf formation i.e there is more tendency to form sheaves composed by parallel plates, but the origin is not the grain boundaries and the final microstructure is composed of packets of plates following the same growth direction, as is shown in Figure 4.12 and it is called sheaf morphology or sheaf type acicular ferrite (STAF). Nucleation time for sheaf type acicular ferrite for both steels are given in Table 4.10. In regards to the nucleation of the first acicular unites takes place intragranularly at non-metallic inclusions present in the austenite and by comparing the micrographs corresponding to 10 seconds of isothermal at 450 °C and 400 °C, it can be seen that at initial stages, the transformation proceeds identically in both cases. The difference in the microstructure obtained at the two temperature become pronounced as the transformation progressed beyond 10 seconds, i.e., after the initiation of the first generation of plates from inclusion as can be seen in Figure 4.10. At 400 °C, the second generation of plates developed in a parallel sheaf formation. By contrast the transformation at 450 °C progressed with non parallel plates. As illustrated in Figure 4.10, the plates nucleated on the face of a substrate plate must have a different habit plane and orientation, leading to a chaotic microstructure. By contrast, a plate nucleating at the tip of the substrate plate must be identical variant with the same habit plane and orientation, giving rise to a sheaf microstructure as illustrated in Figure 4.12.

Table 4.10 Sheaf type acicular ferrite start time formation for both steel.
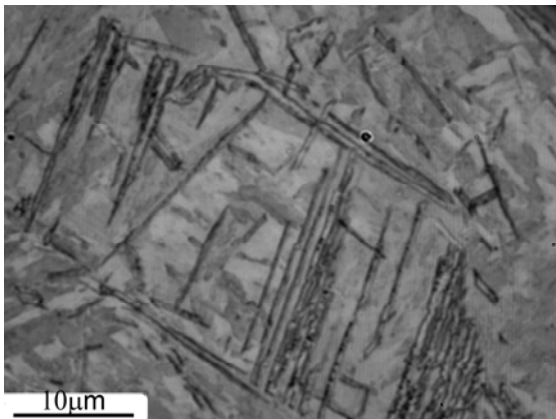
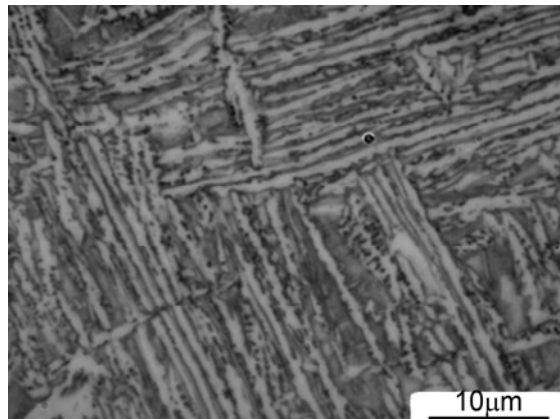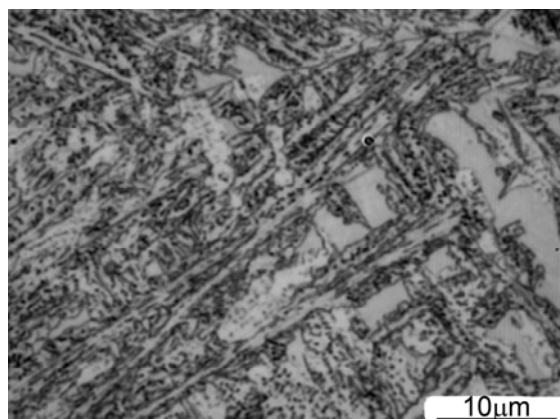| Temperatures | Sheaf Type Acicular Ferrite start time, s | |
| °C. | V-N steel | V-N-Ti steel |
| 400 | 10 | 20 |

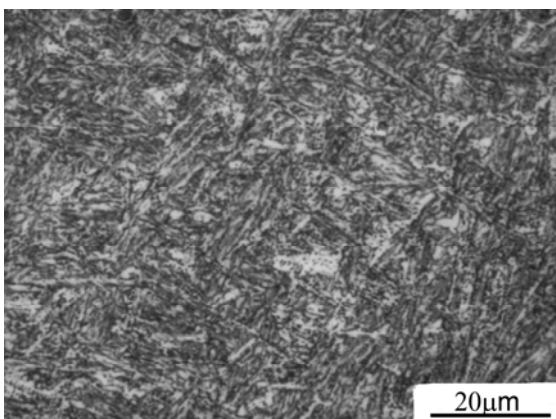a) OM/350°C /20s/500X/ V-N-Ti steel
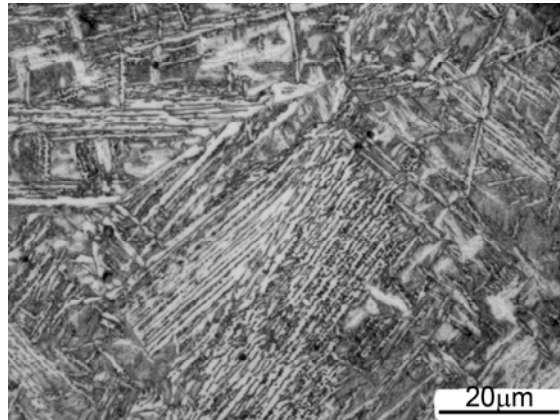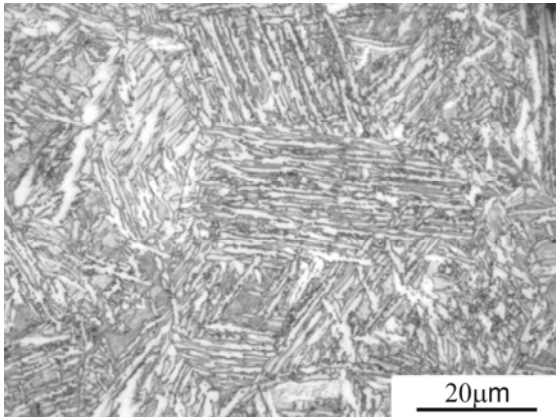

b) OM/ 400°C /20s/500X. / V-N steel.

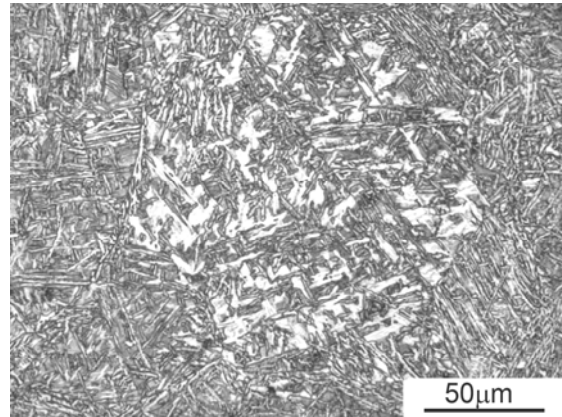c)OM/400°C /20s/1000X/ V-N-Ti steel/561

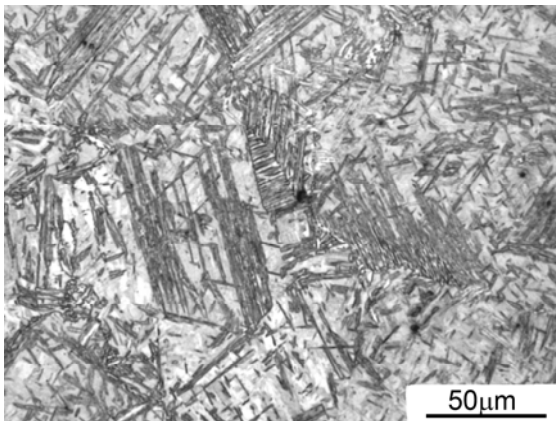
d) 400/°C 30s/1000X (294)/ V-N steel

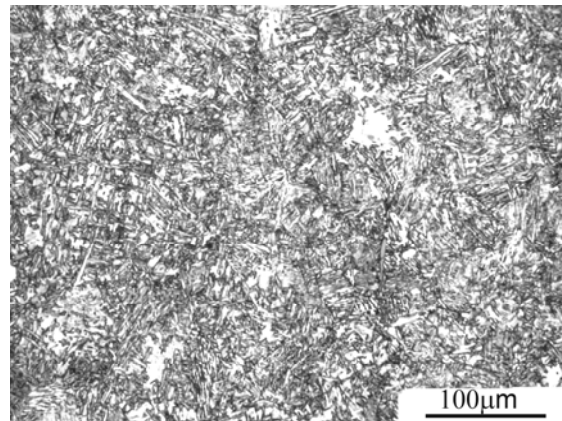e)OM/ 400°C /120s/ V-N-Ti steel   f)OM/400°C /120s/1000X / V-N-Ti steel

g)OM/ 400°C /30s/500X/ V-N steel (517).   h)OM/ 400°C /30s/200X/ V-N steel (292).

k) OM/350 °C /20s/200X/ V-N steel(1443).   l) OM/400 °C /30s/100X/ V-N steel (295).

Figure 4.12 (a-l) OM images showing the sheaf type acicular ferrite (STAF) formation

4.4.3 FORMATION OF CARBIDES

Carbides formed during austenite decomposition are cementites. Various morphologies of cementite are polygonal cementite or Intragranular Idiomorphs of Cementite and Widmanstätten cementite. As in the case of ferrite, most of the side plates originate from grain boundary allotriomorphs, but in the cementite reaction more side plates tend to nucleate at twin boundaries in austenite.

4.4.3.1 Intragranular Idiomorphs of Cementite

Results which are summarized in Fig. 4.13 show that there was some tendency for Grain boundary allotriomorphs and intragranular cementite to occur at the same condition. However

Grain boundary allotriomorphs are the first morphology to appear over the whole range of temperature as demonstrated Figures 4.4 and Figures 4.5; cementite is usually located at GBF grain surface.
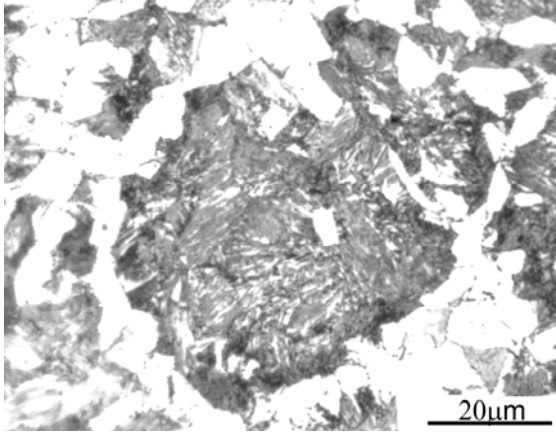
a) OM/ 600°C /1200s/500X/ V-N steel
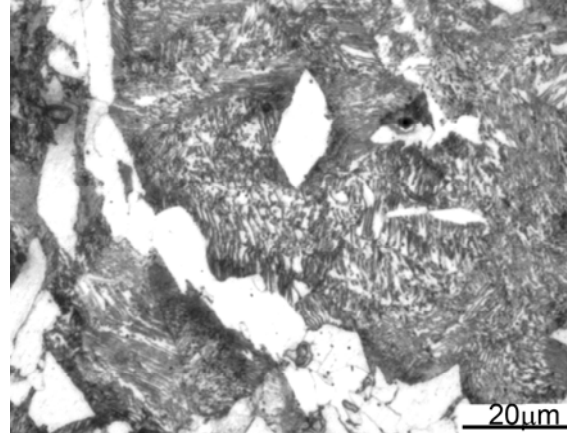
b) OM/ 600°C /600s/500X/ V-N steel
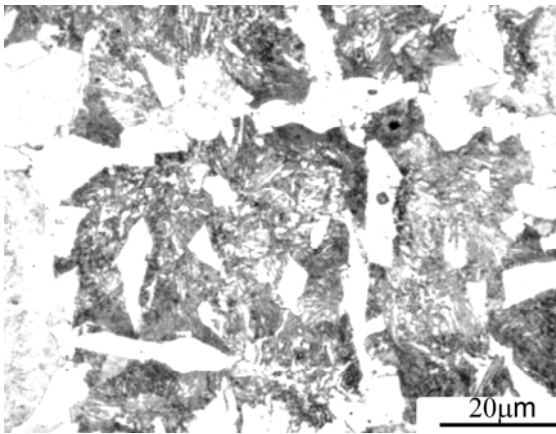
c)OM/ 600/°C /120s/500X/ V-N steel
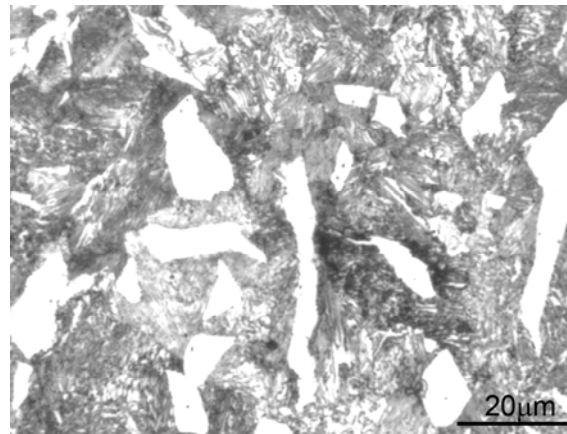
d) OM/600°C/ 600s/500X/ V-N steel
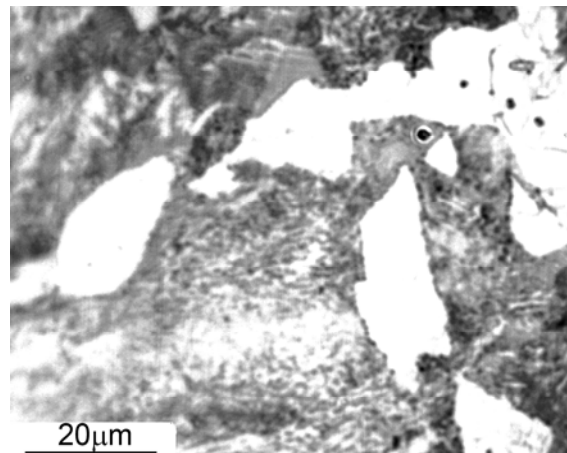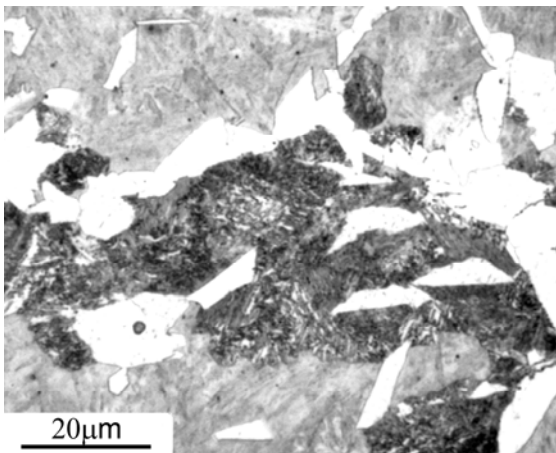
e)OM/600°C /100s/500X/ V-N steel   f)OM/600°C /600s/500X/V-N steel
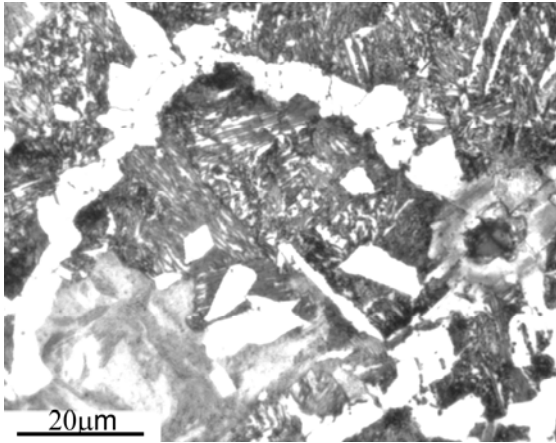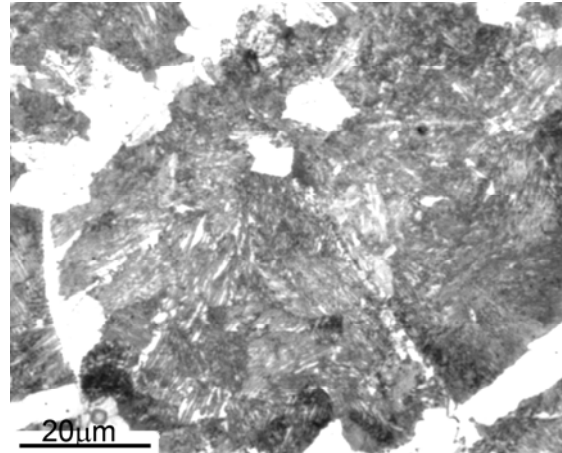
g)OM/ 600°C /120s/500X/ V-N steel   h)OM/ 600°C /600s/500X/ Ti-V-N steel
Figure 4.13 (a-h) OM images showing GBF and intergranular cementite exist at the same condition.

4.4.3.2 Widmanstätten Cementite

Following the growth of side plates or Widmanstätten ferrite, cementite follows the same pattern as ferrite. On the figures is clear very strong relationship with ferrite grains, figure 4.13 and figure 4.14
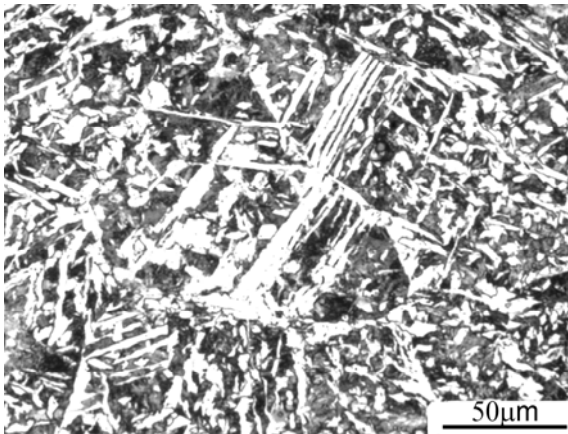
(a) 550°C /600s/200X/ V-N steel(1081)   (b) 550°C /600s/500X/ V-N steel(1082)
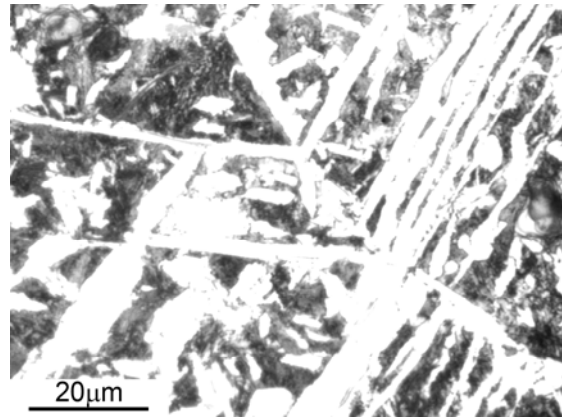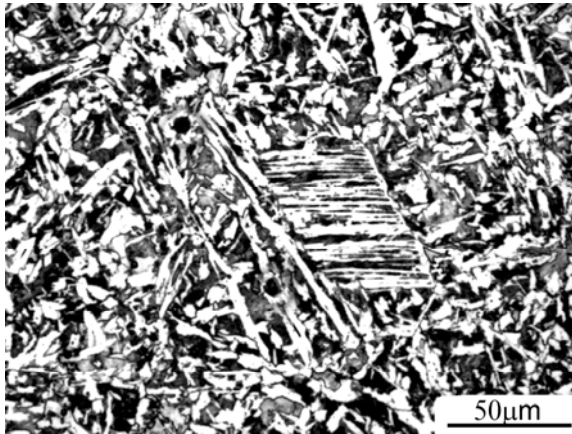
(c) 550°C /1200s/200X/ V-N steel
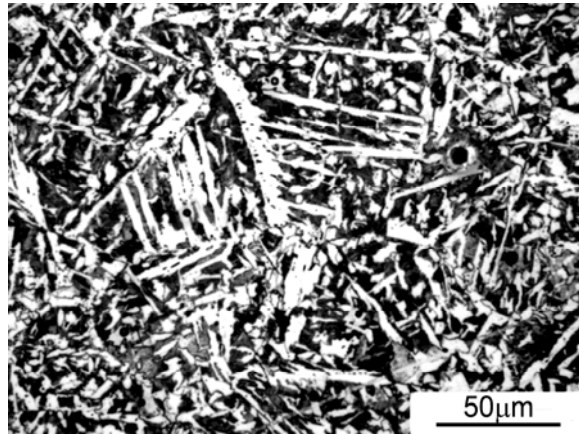
(d) 550°C /1200s/200X/ V-N steel
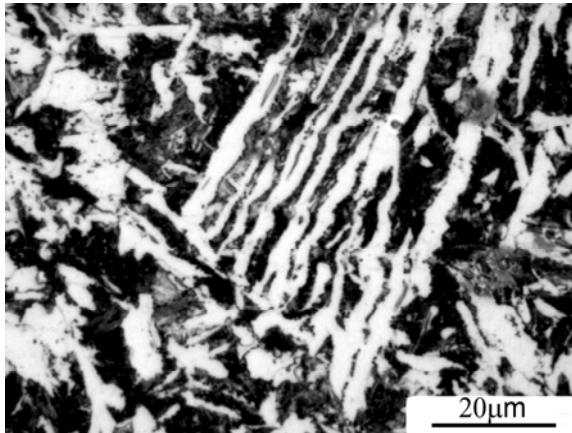
(e) 550°C /600s/500X/ V-N steel

(f) 550°C /1200S/500X/ V-N steel

Fig. 4.14(a-f) Optical micograph showing presence of Widmanstatten Cementite in some cases.

4.4.4. INTRAGRANULAR PLATES

These plates are similar to those growing from the grain bundaries, but they nucleate entirely within the austenite grains (Fig. 4.15). They occur in wide temperature region, showing crystallographic orientation. They look very much a like bainitic sheaves, but they are nucleated within the grain and also, in contrast to sheaf type AF, they are much thicker.

(a) 550°C /45s/500X/ Ti-V-N steel(619)
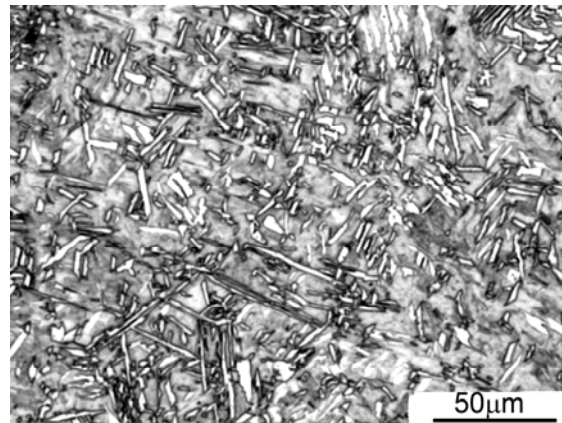
(b) 500°C /20s/200X/ V-N steel(745)
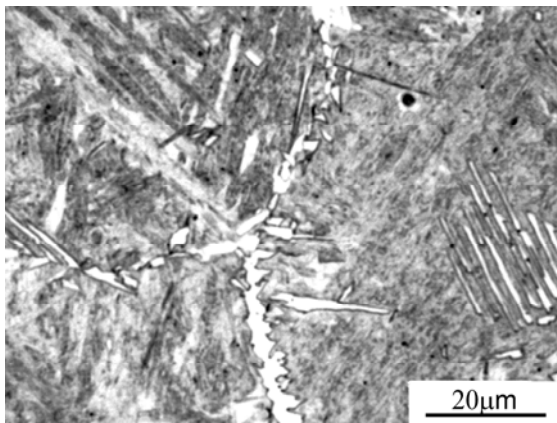
(c) 500°C /20s/500X/ V-N steel (725)
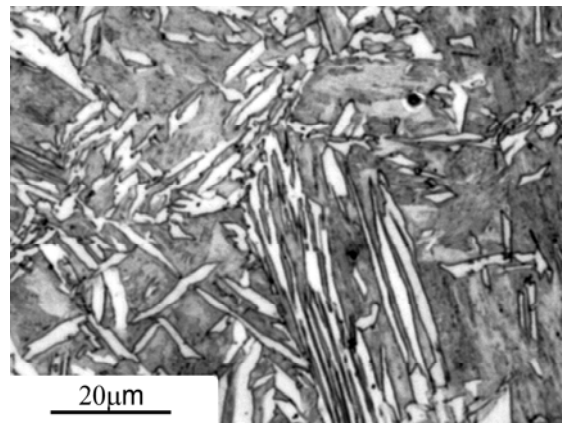
(d) 500°C /20s/500X/ V-N steel(740)

Fig. 4.15(a-d) Optical micograph showing presence of Intragranular plates in some sites.

4.4.5 BAINITIC SHEAVES AND PLATES

Bainitic plates are similar to bainitic sheaves both growing from the grain bundaries, but differ in thickness. The bainitic plates are thicker than bainitic sheaves as can be seen in (Fig. 4.16) and Fig. (4.17). The bainite seem to be exists without presence of cementite (Fig. 4.16).
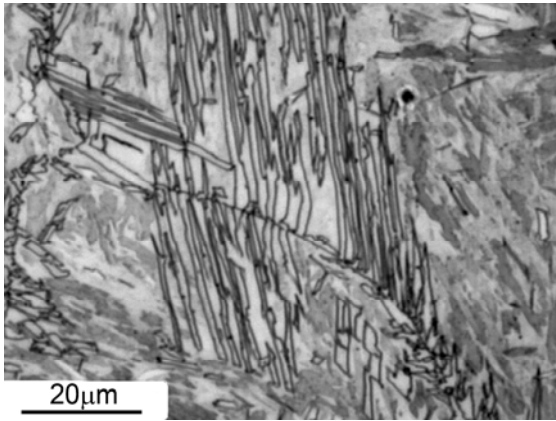
(a) 500°C /20s/500X/ Ti-V-N steel
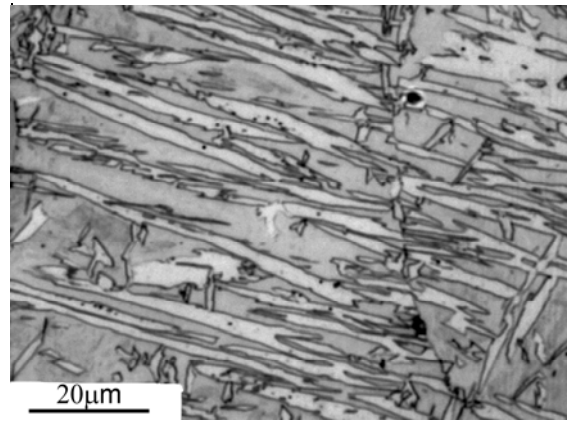
(b) 500°C /60s/500X/ Ti-V-N steel
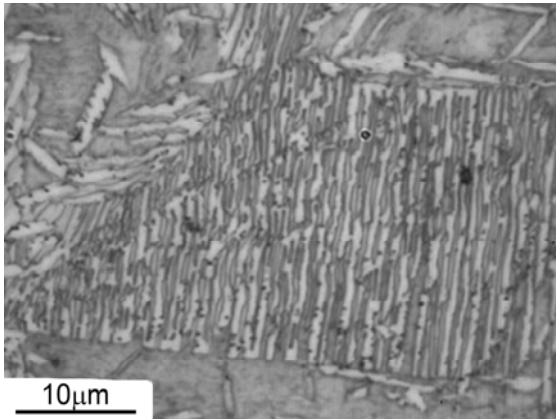
(c) 450°C /20s/1000X/ V-N steel
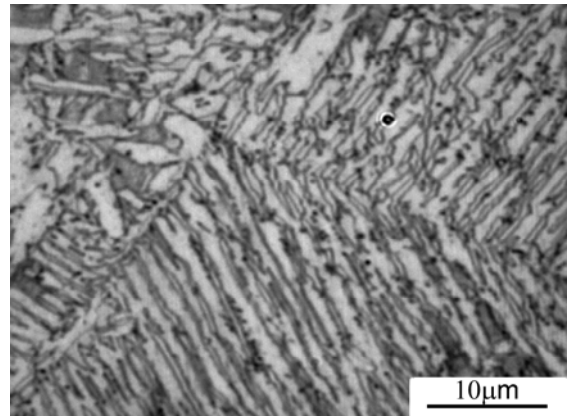
(d) 450°C /30s/1000X V-N steel
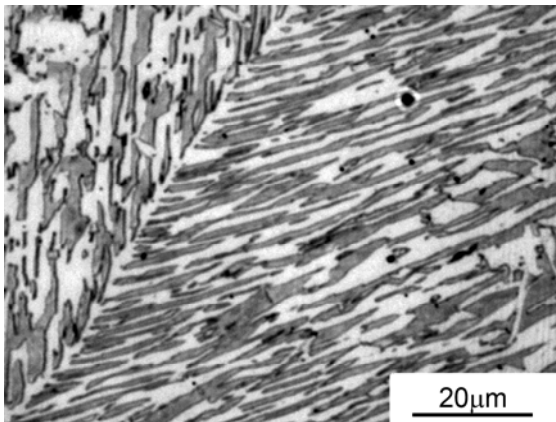
(e) 500°C /120s/500X/ V-N steel(806)
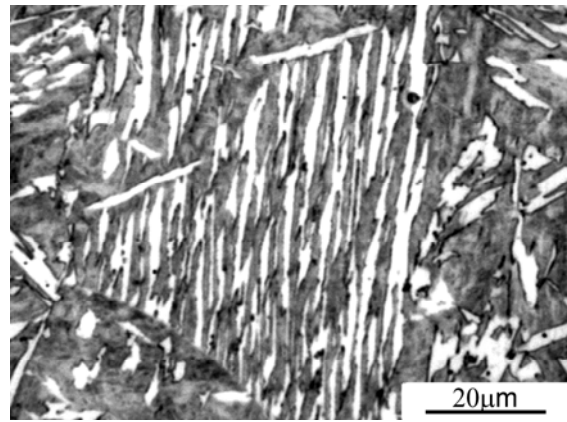
(f) 500/°C 80s/500X/ Ti-V-N steel (
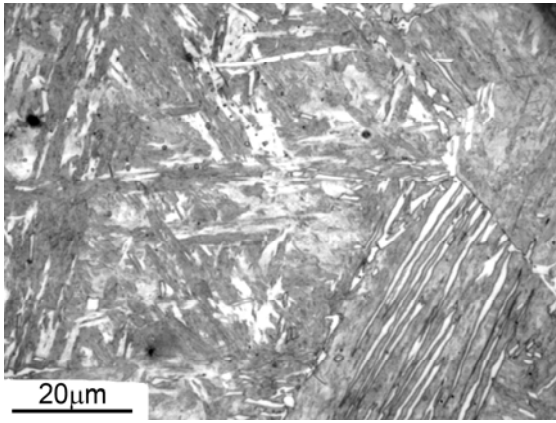
(g) 550°C /20s/500X/ V-N steel   h) 450°C /60s/1000X/Ti-V-N steel .
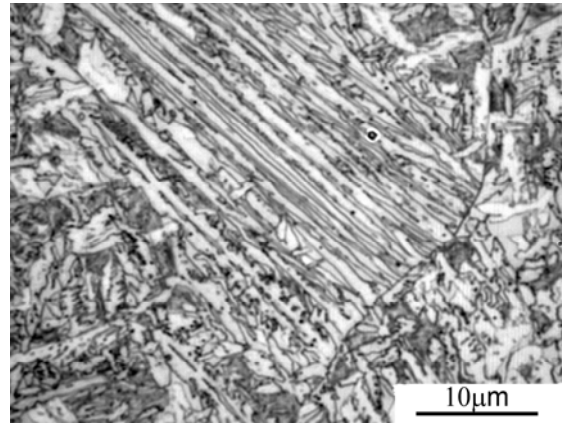
Fig. 4.16(a-h) Optical micograph showing Bainitic Plates
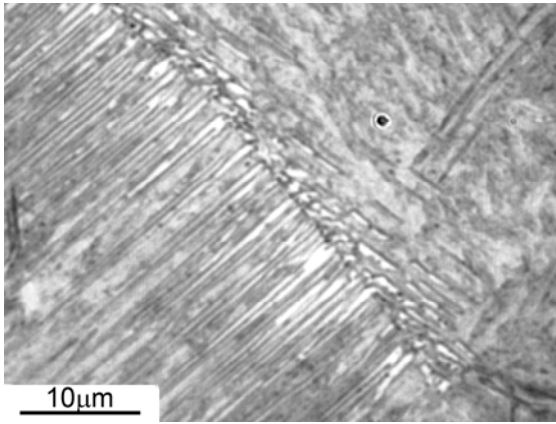
(a)350°C /10s/1000X/ Ti-V-N steel
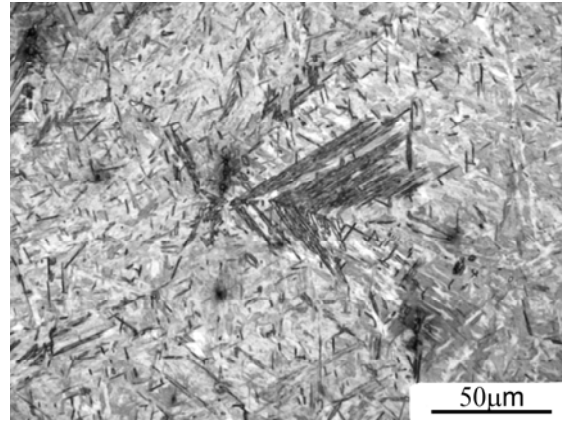
(b)400°C /20s/200X/ Ti-V-N steel
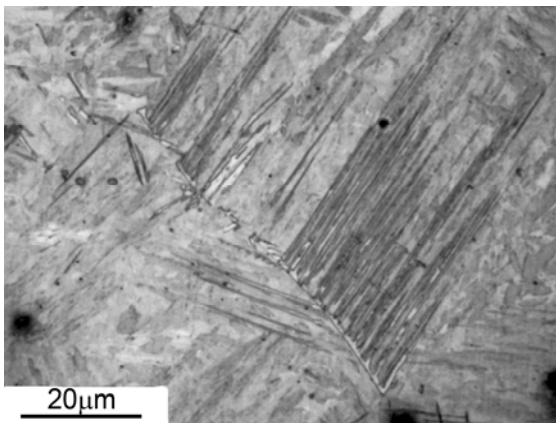
(c) 350°C /10s/500/V-N steel
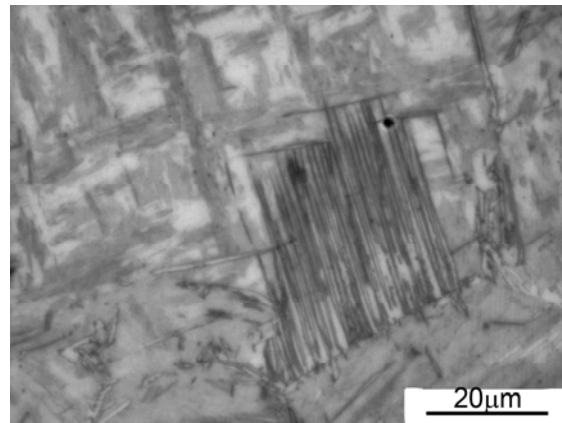
(d) 350°C /10s/500X/V-N steel
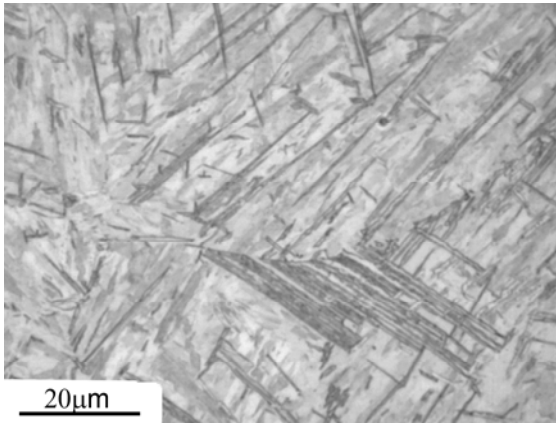
(e)400°C /20s/500X/ Ti-V-N steel (083)
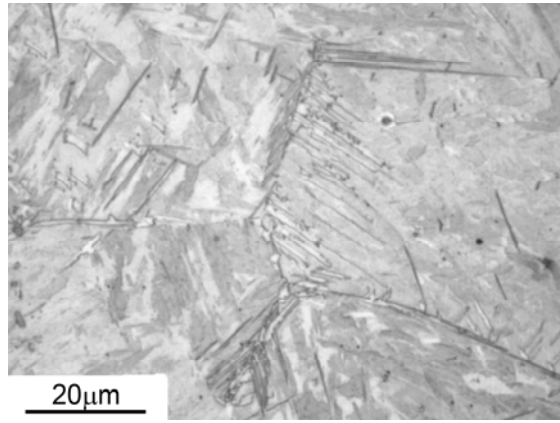
(f) 350°C /10s/500X/ V-N steel.(1436)
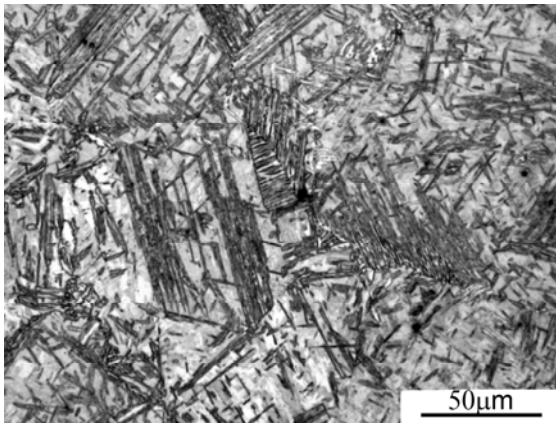
(g) 350°C / 20s /200X/ V-N steel
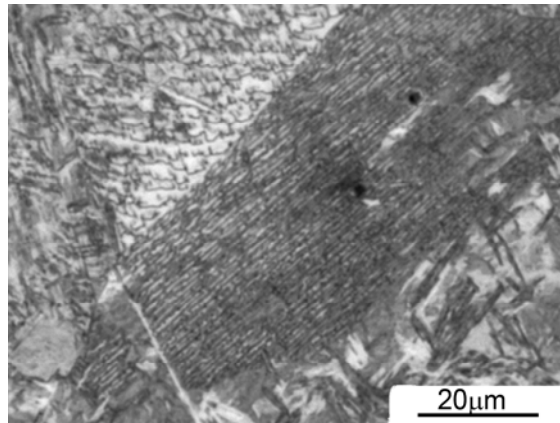
(h) 350 °C /45s/500X/ Ti-V-N steel
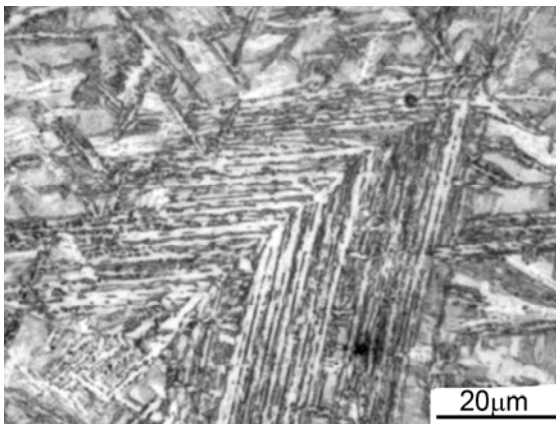
(k) 350°C /45s/500X/ V-N steel

(l) 350°C / 45s/500X/ Ti-V-N steel

(m) 350°C /10sec/500X/ V-N steel

(n) 350°C /20s/500X/ V-N steel

(x) 350°C /20s/1000X/ V-N steel (1446)

(y) 350°C /600s/500X/ V-N steel (1478).
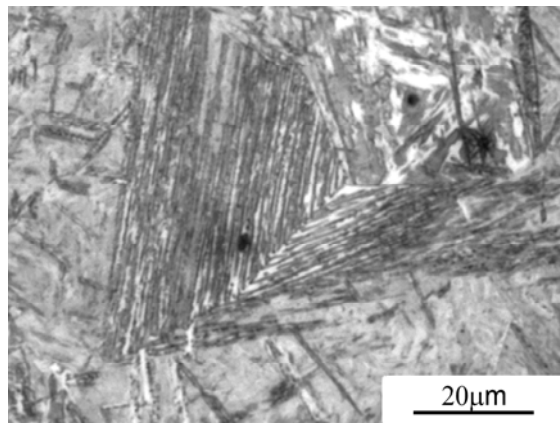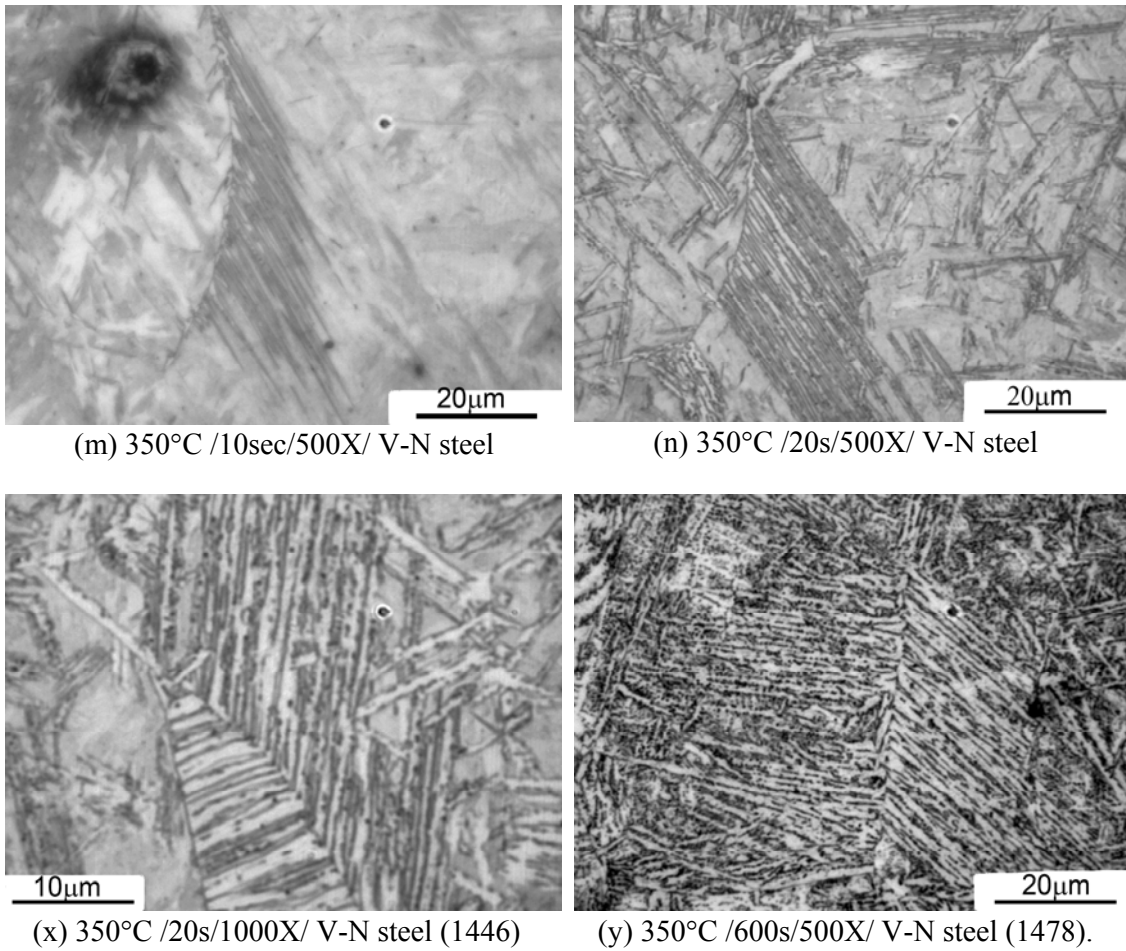
Fig. 4.17 (a-y) Optical micrograph showing the onset nucleation of Bainitic Sheaves (BS).

Bainitic sheaves are present in temperature range 350-400°C. Bainitic sheaves are identified as set of parallel plates originating from austenite boundary. Typical microstructures showing onset of bainitic sheaves are presented in figures 4.17(a-y), 4.23(f) and 4.24(f). The times for onset of bainitic sheaves are given in table 4.11.

Table 4.11 Bainitic sheaves start time formation for both steel investigated.

Temperatures °C.	Bainitic sheaves start time, s	
	V-N steel	V-N-Ti steel
350	10	10
400	10	20

4.4.6 INCOMPLETE REACTION PHENOMENON

The phenomenon of incomplete transformation is registered in both steels after isothermal treatment at 550 and 600 °C, and even at 500 °C, for V-N steel. The microstructure consists of polygonal intragranulary nucleated ferrite idiomorphs, combined with grain boundary ferrite and pearlite, together with some retained austenite were produced and followed by an incomplete transformation phenomenon, as can be seen in Figure.4.18.
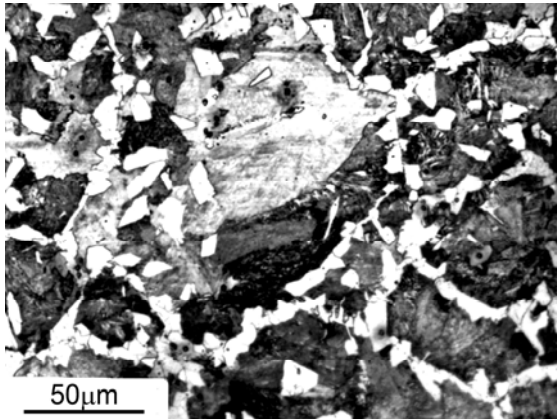
(a) 600 °C /600s/200X/ V-N steel.
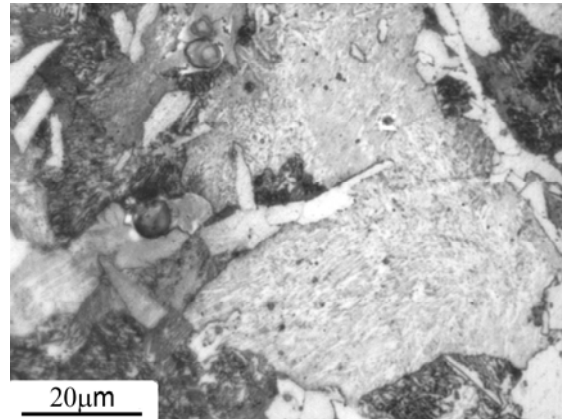
(b) 600 °C /1200s/500X/ V-N steel
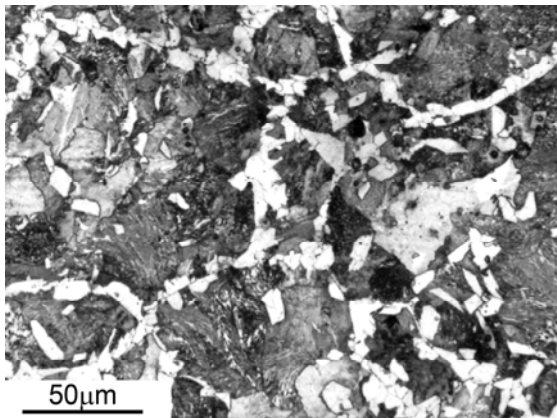
(c) 600°C /600s/200X/ V-N steel
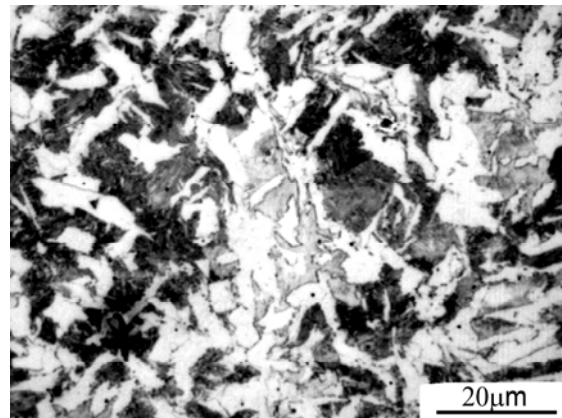
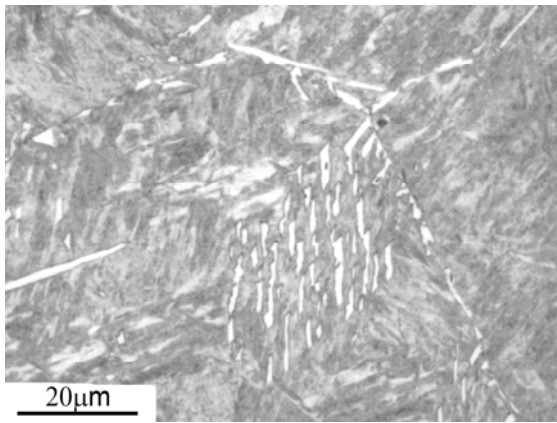(d) 550°C/ 600s/500X/ V-N steel
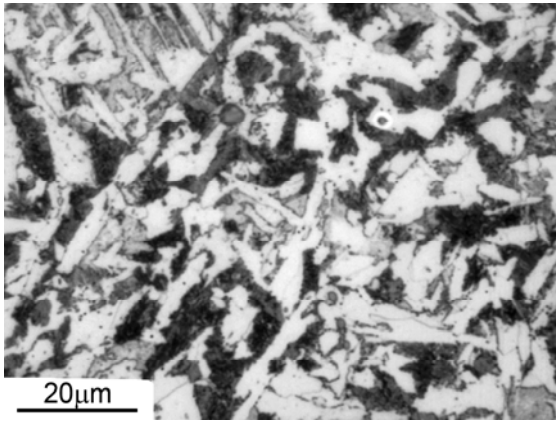
(e) 550°C /1200s/500X/ V-N steel
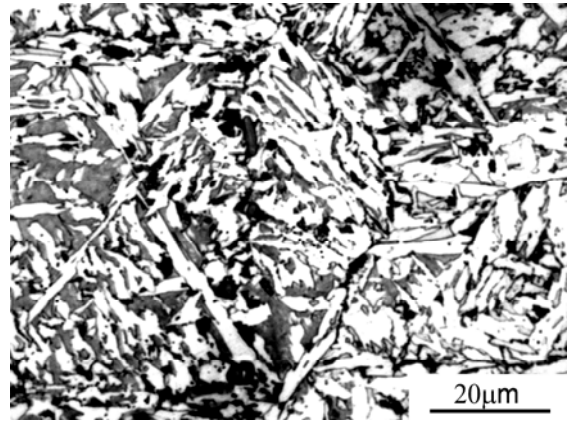
(f)500°C /420s/500X/ V-N steel
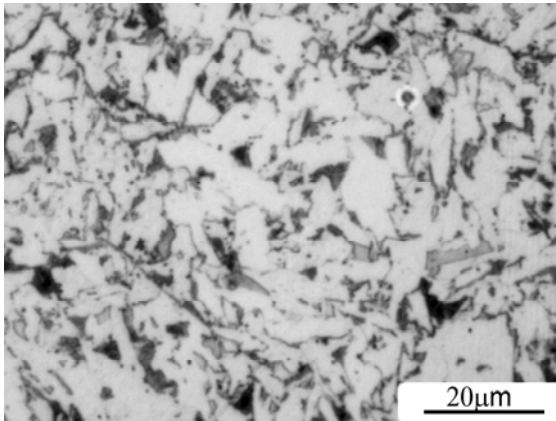
(g)500°C /1200s/500X/ V-N steel(825)
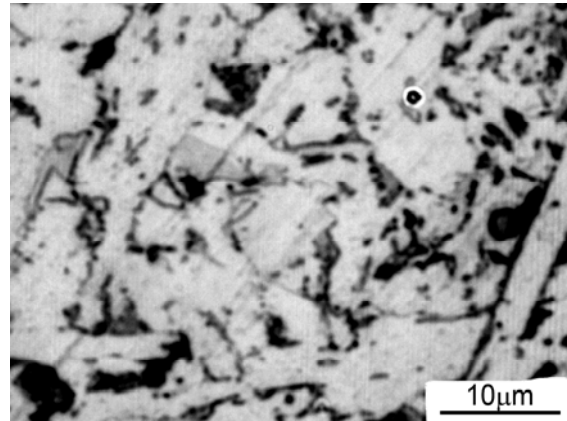
(h)500°C /1200s/1000X/ V-N steel(826)
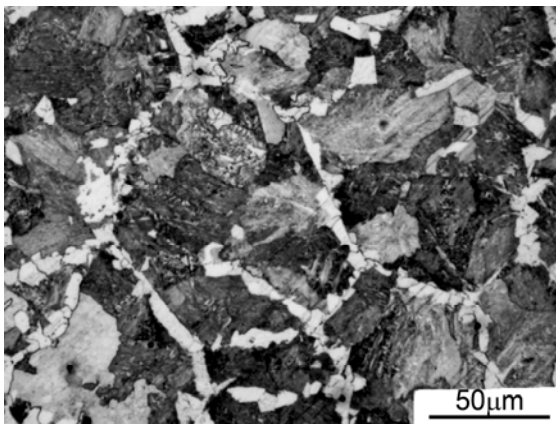
(k)600°C /600s/200X/ Ti-V-N steel (1339)
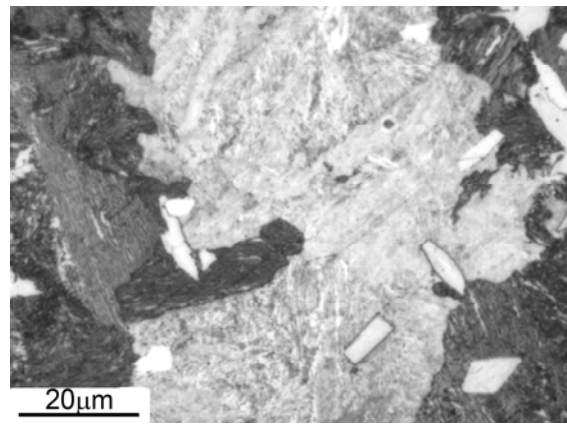
(l) 600°C /1200s/500X/ Ti-V-N steel(1344)
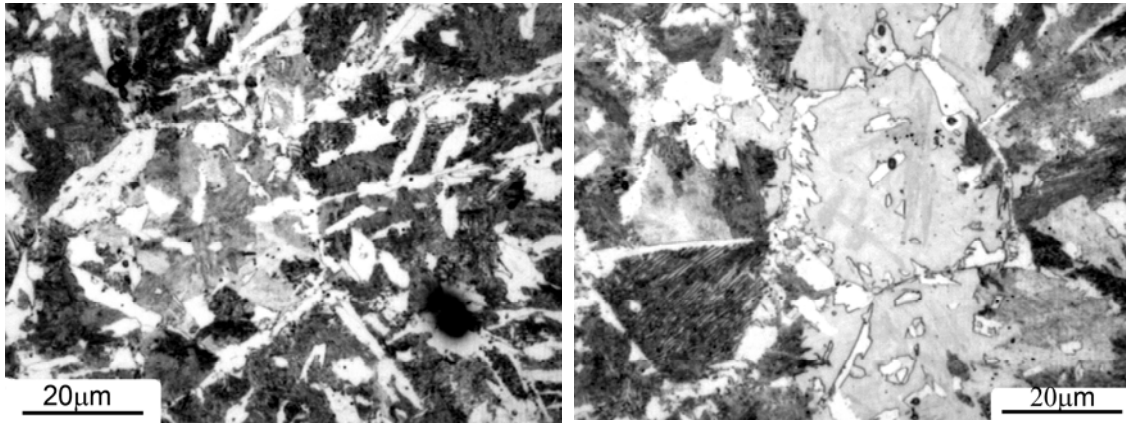
(m)550°C /1200s/500X/ Ti-V-N steel   (n)550°C /1200s/500X/ Ti-V-N steel

Fig. 4.18(a-n) Optical micrographs showing Incomplete Reaction Phenomenon of the microstructures obtained after 1200s of isothermal treatment at 600°C, 550°C, and 500°C for V-N steel and at 600°C, 550°C for Ti-V-N steel.

4.4.7 POPULATION DENSITY OF FERRITE

At 600 °C, the volume of the untransformed austenite and the population density of ferrite plates is lower than at 550 °C as can be observed in Fig. 4.19. This seems to indicate that at 600 °C, the carbon rejected from the few ferrite plates formed diffuses rapidly leading to a fast homogenising of its concentration in austenite. The carbon enrichment of the remaining austenite together with relatively small driving force for transformation at 600 °C is enough to inhibit the formation of new ferrite plates .The transformation of the austenite by displacive mechanism energetically impossible above 550 °C [234].At temperature ≥ 550 °C, the kinetics of the transformation is very slow for that reason the number density of acicular ferrite phase formed is small and part of austenite has been transformed into a mixture of allotriomorphic, idiomorphic ferrite grains and pearlite, however, the majority of the austenite remains stable, and only after the final water quenching it transforms to martensite as shown in figure 4.19.
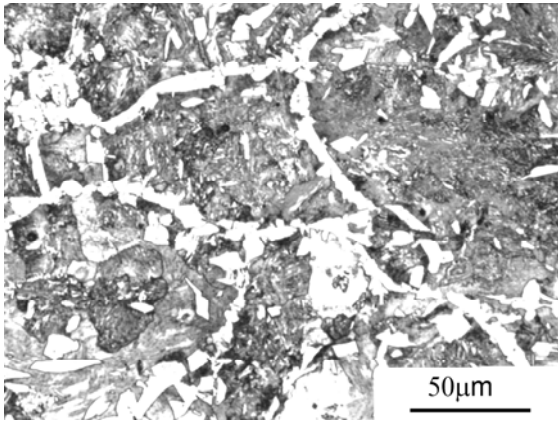
(a)OM/600°C /120s/200X/ V-N steel
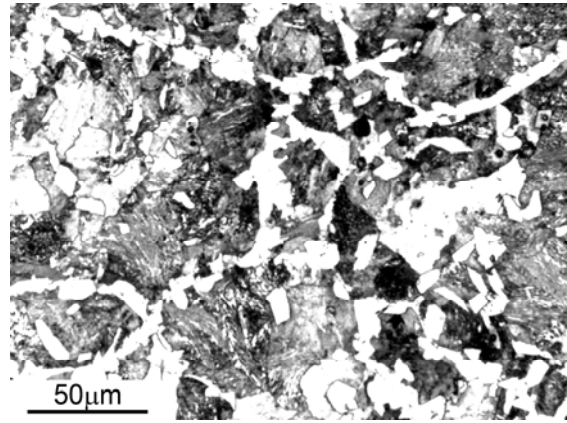
(b)OM/600°C /600s/200X/ V-N steel
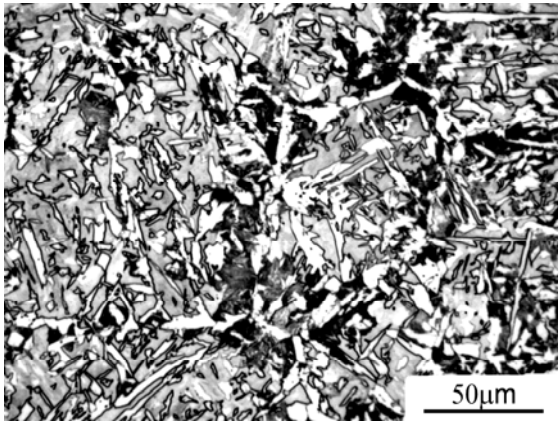
(c)OM/550°C /120s/200X/ V-N steel (671).
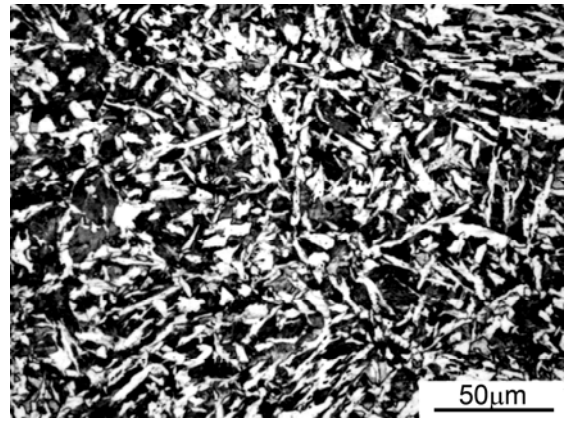
(d)OM/550°C /600s/200X/ V-N steel (1090)
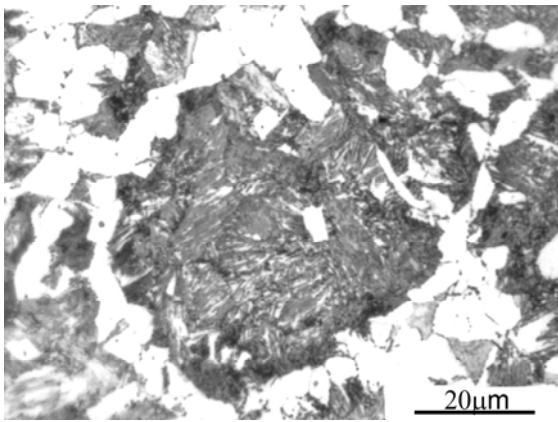
(e)OM/600 °C /1200s/500X/ V-N steel
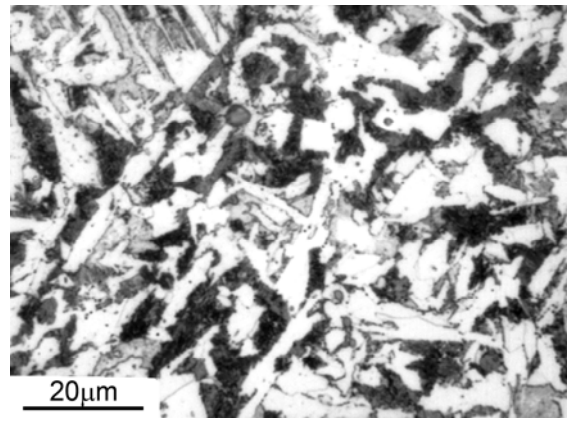
(f)OM/550°C /1200s/500X/ V-N steel
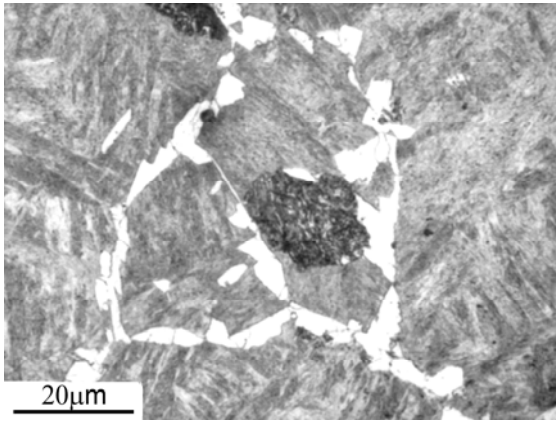
(g)OM/600°C /120s/500X/Ti-V-N steel
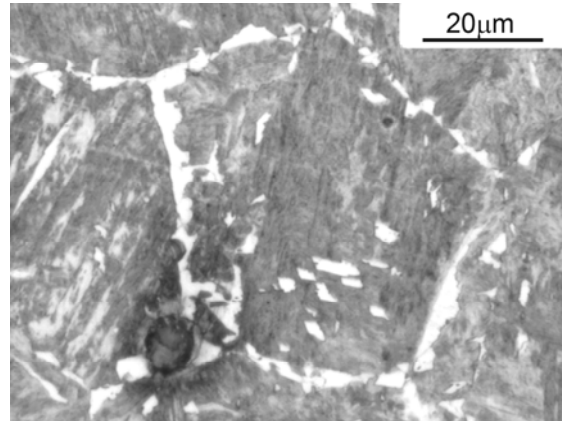
(h)OM/550°C /120s/500X/ Ti-V-N steel
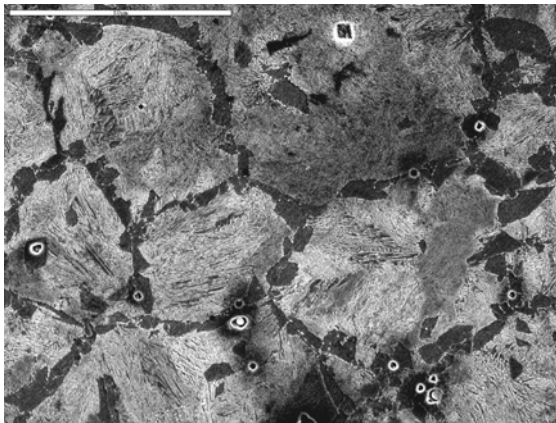
(k) SEM /600°C /1200s/1000X/ Ti-V-Nsteel
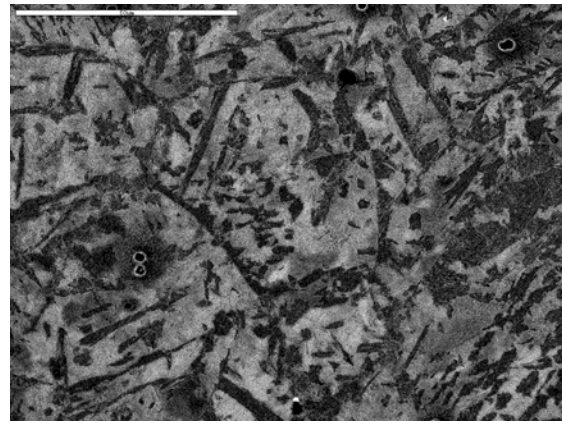
(l) SEM /550°C /1200s/1000X/ Ti-V-N steel
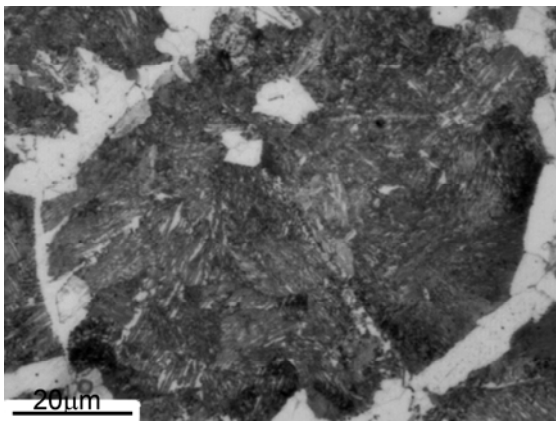
(m)OM/600°C 500s/500X/ Ti-V-N steel
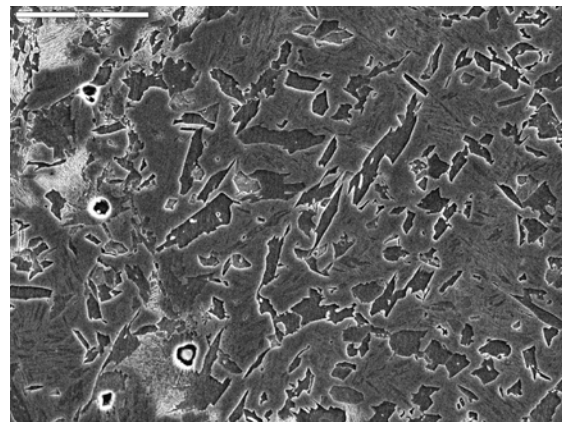
(n)SEM / 550°C /600s/500X/ Ti-V-N steel

Fig. 4.19 (a-n) SEM and OM (optical micrograph) showing the Population Density of Ferrite

4.4.8 PRECIPITATION FREE PLATES

In a previous work [15,235,236], it is expected for carbon to precipitate inside the ferrite (cementite particles) at transformation temperature lower than a bout 450 °C. The present results clearly show in general no carbides were observed to form within the ferrite plates at intermediate time and temperature (450-500 °C) as can be seen in Fig. 4.20. This is good a greement with published data [234]. As well as the earlier work on carbide-free bainitic steels demonstrated promising combinations of strength and toughness [33,34,38,203, 289]. At 450-500 °C, the majority of plates are free of precipitates due to the carbon diffusion is higher, favouring the decarburisation of the majority of ferrite plates, and the microstructure can be better identified as upper acicular ferrite. By contrast at 400 °C, the carbon diffusivity in austenite decreases and this element probably concentrates in the austenite close to the ferrite plate faces favouring the nucleation of the same variants from the tips of the primary plates. The lower redistribution of carbon in austenite, as a result of the decrease of its diffusivity, together with the formation of sheaves of parallel plates at 400 °C, produces as a consequence, high amounts of carbon remain trapped in thin layers of austenite between parallel plates favouring its stabilization. For large times, this carbon probably precipitates as cementite or carbides, it is appear at the ferrite plates interiors.This carbides are elongated and form angles comprised between 50° and 60° with the α/γ interfaces. The presented results clearly show no cementite precipitation was observed at intermeddiate time and temperature (450-500 °C), the reason is probably due to the presence of enough Si in the steel, which, delays cementite precipitation [36,124,134,187,203].
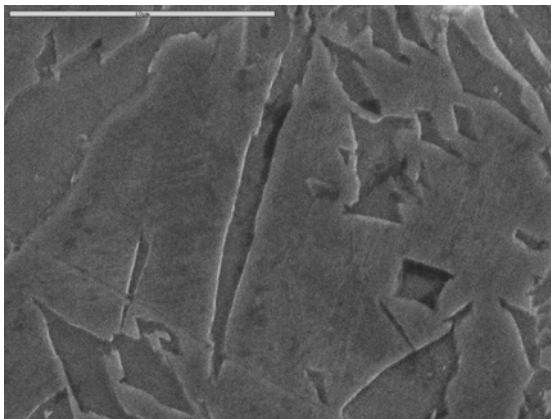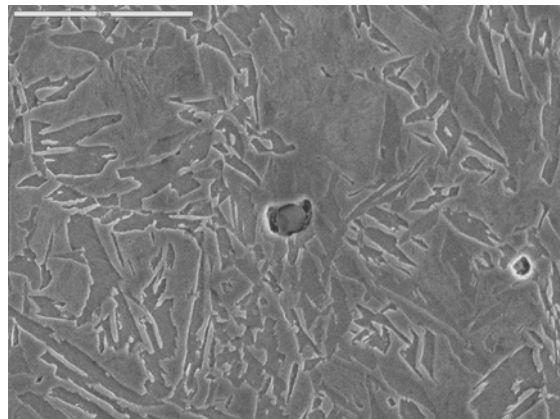
(a)SEM/500°C /30s/ V-N steel
(b)SEM /500°C /30s/ V-N steel
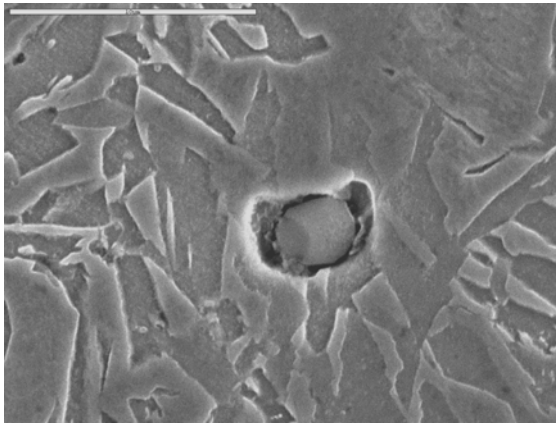
(c)SEM 500°C /30s/ V-N steel (1950301)
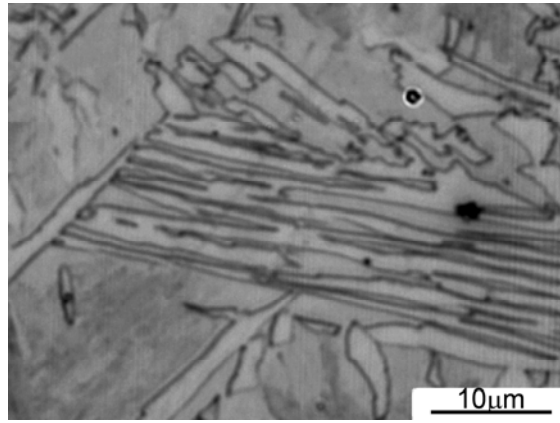
(d)OM/500°C /30s/1000X/V-N steel (754)
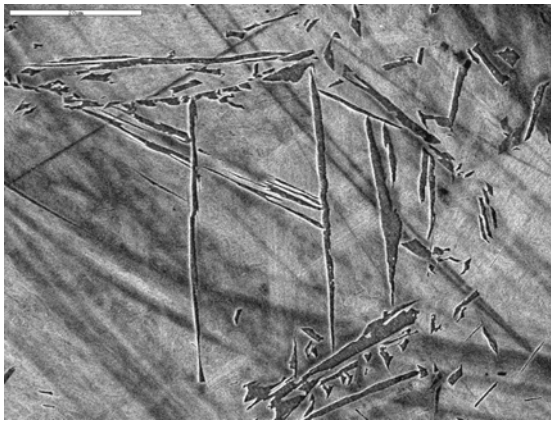
(e)SEM/500°C /30s/ Ti-V-N steel
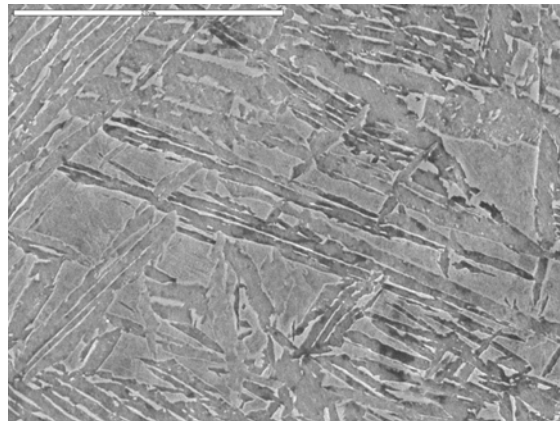
(f)SEM/ 450°C /20s/ Ti-V-N steel
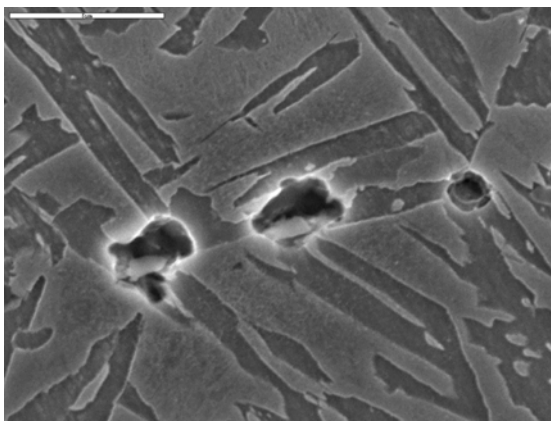
(g)SEM/500°C /80s/Ti-V-N steel
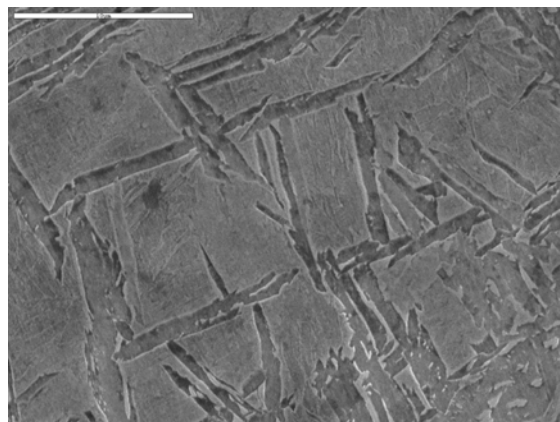
(k)SEM/ 450°C /20s/ Ti-V-N steel

Figure 4.20(a-k) SEM and OM images shows the ferrite plates seems to be free of precipitate.

4.4.9 BANDED MICROSTRUCTURE

By refering to Figure 4.21, the banded microstructure was clearly start observed at (t ≥ 600s), for Ti-V-N steel after isothermalty transformed at 550 °C. It is attributed due to chemical solute segregation. The microstructure bands follow the segegation pattern becouse it is the local chemical composition that determines the onset of transformation. The Mn segregation of substitutional solutes which is the real cause of banding [15].The substitutional-solute depleted regions cause a partitioning of carbon into the adjacent substitutionally-enriched regions as can be seen in Fig. 4.21. Khan and Bhadeshia [237], suggest that the segregated steel is able to transform in its solute-depleted region at temperature above B_S temperature (B_S ≡ 500 °C for Ti-V-N steel). This is in good a greement with present study. By contrast,most of the partitioned carbon remains in the substitutional solute depleted regions of the segregated sample and retards the development of transformation [15].Where as the presence of horizontal parallel lines was clearly observed on the surface of the sample during polishing processes.

(a)550°C /600s/100X/ Ti-V-N steel   (b)550°C /600s/200X/ Ti-V-N steel

(c)550°C /600s/500X/ Ti-V-N steel   d) 550°C /1200s/500X/ Ti-V-N steel
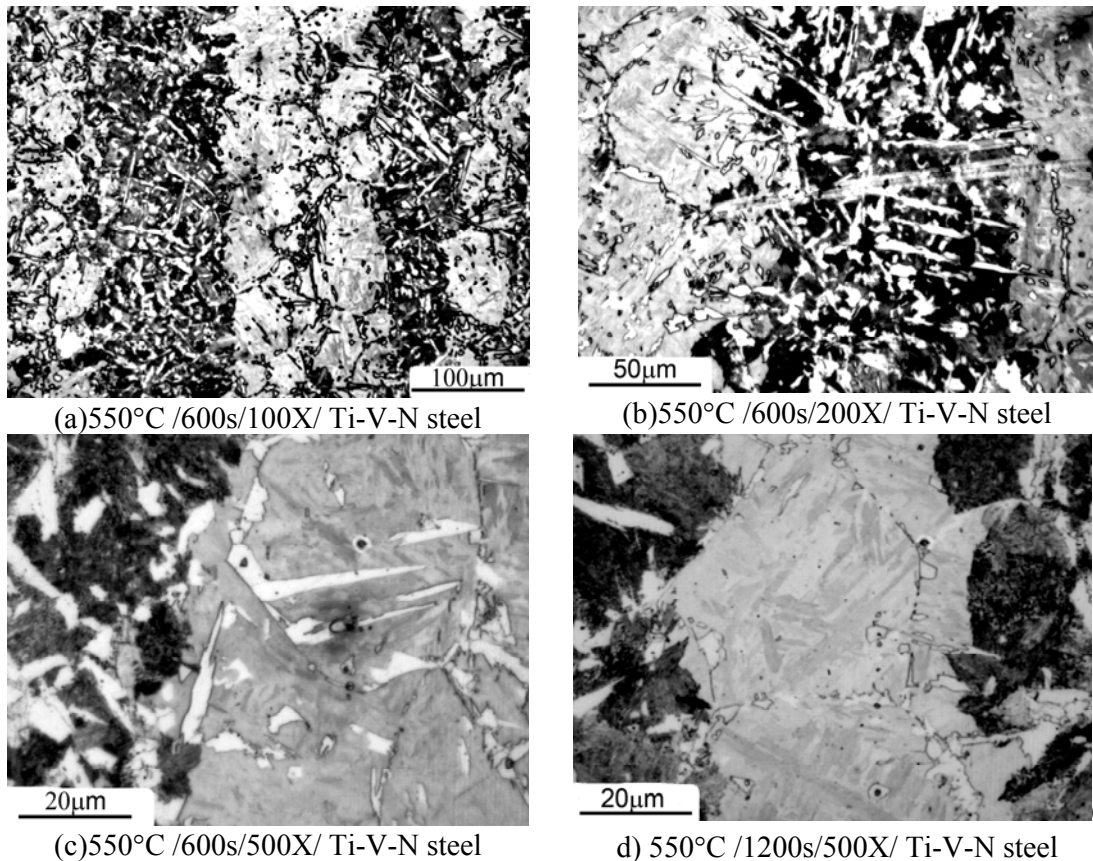
Fig.4.21(a-d) Optical micrographs illustrating the banded microstructure obtained in Ti-V-N steel, isothermally transformed at 550 °C for 600s and 1200s.

4.4.10 AUSTENITE TO PEARLITE TRANSFORMATION

Pearlite is present in temperature range 500-600°C. Pearlite is always nucleated on the surface between proeutectoid ferrite and austenite. Typical microstructures showing onset of pearlite are presented in figures 4.22a to 4.22L. The times for onset of austenite to pearlite transformation are given in table 4.12.and as represented in Fig. 4.30 by closed triangles-Pearlite (P) start curve. Incubation time for onset of pearlite decrease with decrease of temperature.

Table 4.12 Pearlite start time for both steels

Temperature, °C	Pearlite sheaves start time, s	
	V-N- steel	V-N-Ti steel
500	80	120
550	45	80
600	30	60
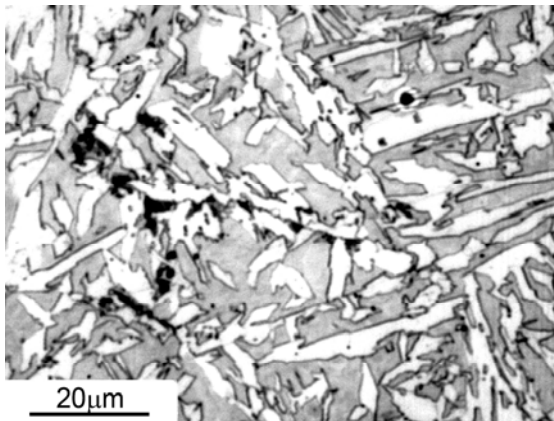
Fig. 4.22(a) 500°C /80s/500X/Ti F
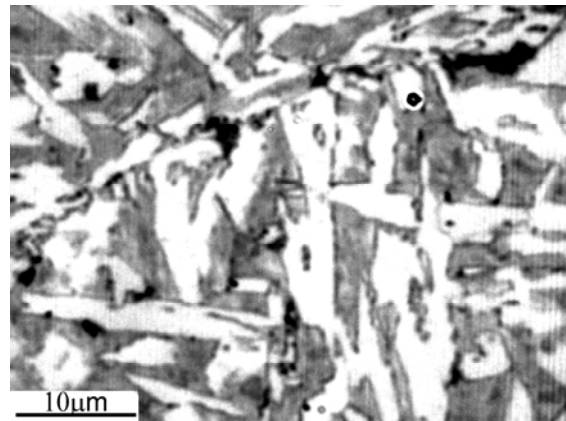
Fig.4.22 (b) 500°C /120s/1000X/TiS
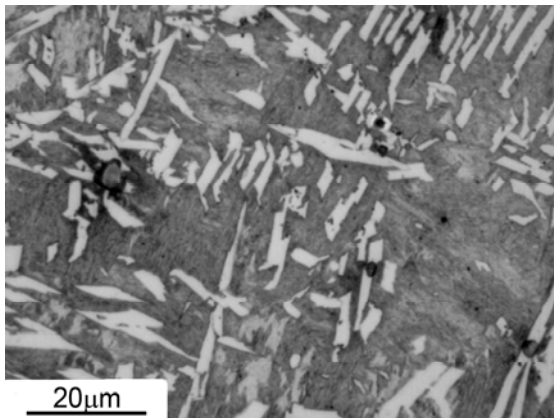
Fig.4.22(c) 550°C /45s/500X/Ti F
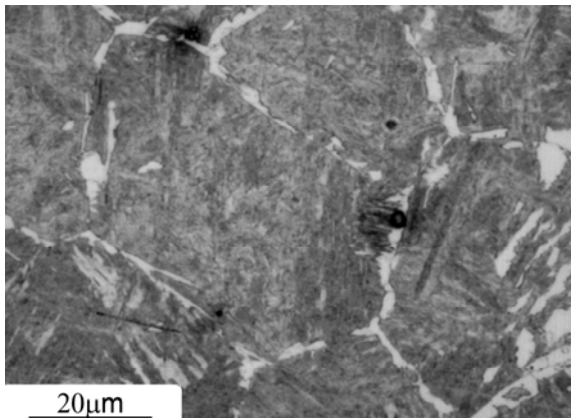
Fig.4.22 (d) 550°C /80s/500X/Ti.S
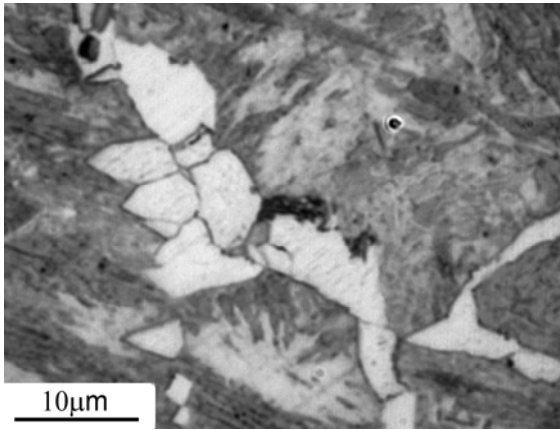
Fig.4.22(e) 600°C /30s/1000X/Ti-F(23)
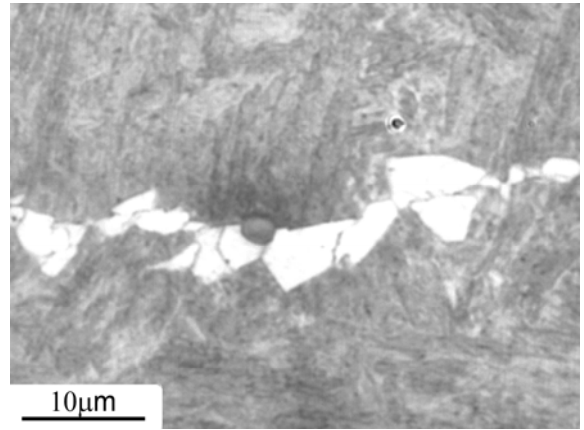
Fig.4.22(f) 600°C /60s/1000X/Ti S
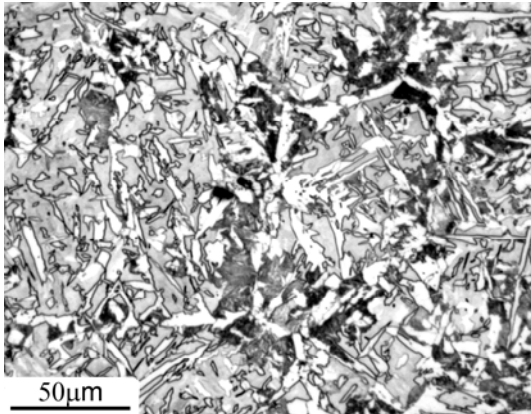
Fig.4.22(g) 550°C /120s/200X/Ti F(671)
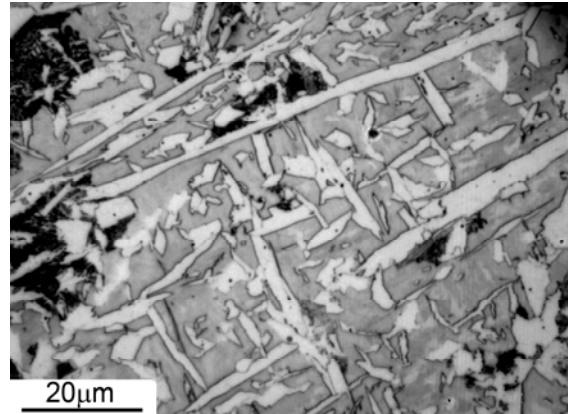
Fig.4.22(h)TiF/ 550°C /120s/500X/672
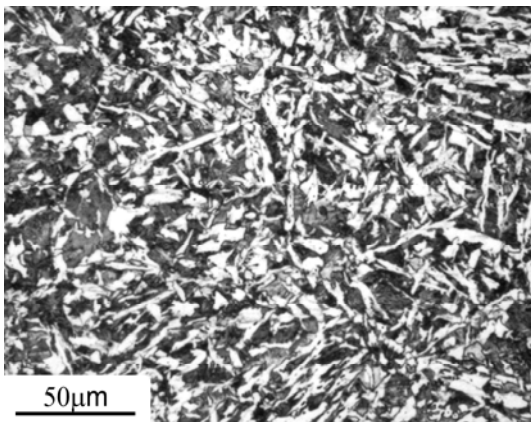
Fig.4.22(i) 550°C /600s/200X /(1090)/ Ti F
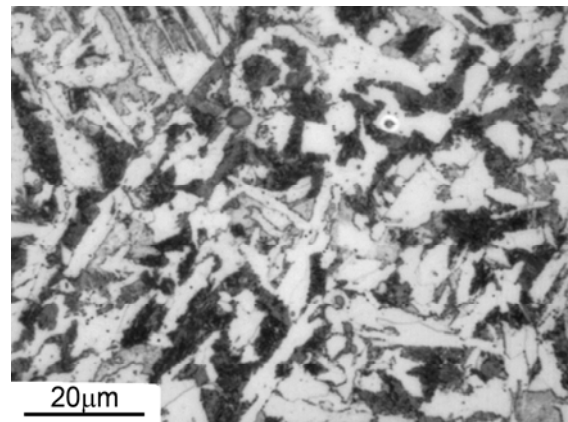
Fig.4.22(j) 550°C /1200s/500X / Ti F

Fig.4.22 Optical micrographs illustrating (a-f) the pearlite onset form at temperature $\geq 500^{\circ}C$; (g-j) the pearlite growth processes.

4.4.11. FINAL MICROSTRUCTURES (AFTER 1200S)

The microstructures obtained after 1200s of isothermal treatments at 350, 400, 450, 500, 550 and 600 °C are presented in figure 4.23 and figure 4.24 respectively, for both steels investigated. As can be seen in all cases three different morphologies have been observed depending upon the isothermal treatment temperature. Firstly, at high temperatures ($\geq$ 550 °C) intragranulary nucleated ferrite combined with grain boundary ferrite (GBF) and pearlite (P) are produced, Figures 4.23(a) and 4.24(a). The intragranular ferrite is characterized by polygonal idiomorphic (IGF) Ferrite. The idiomorphic ferrite nucleates intra-granularly at the inclusions distributed inside the austenite grains. The transformation after1200s of isothermal treatment at 550 and 600 °C reveals a fraction of untransformed austenite, Fig. 4.23(a,b) and 4.24(a,b).
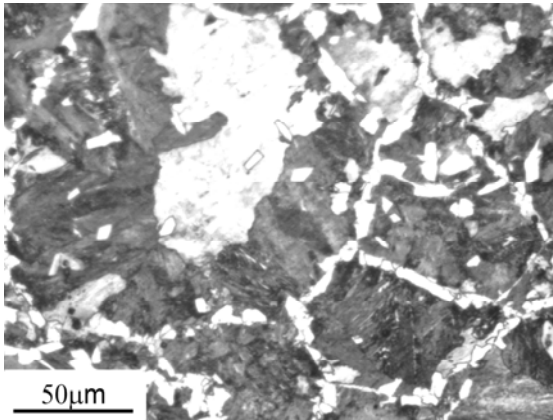
Fig .4.23(a) TiS / 600°C /1200s/200X(1345)
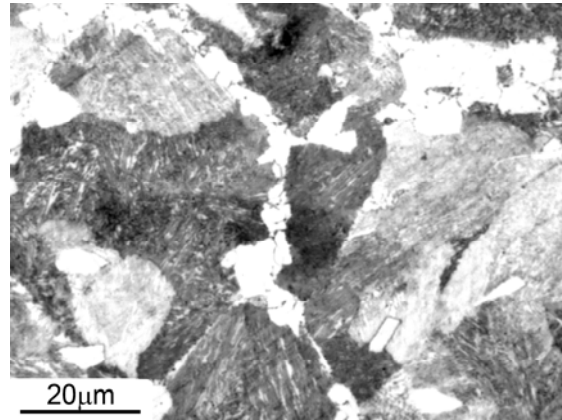
Fig.4.23(a) Ti S/ 600°C /1200s/500X(1343)
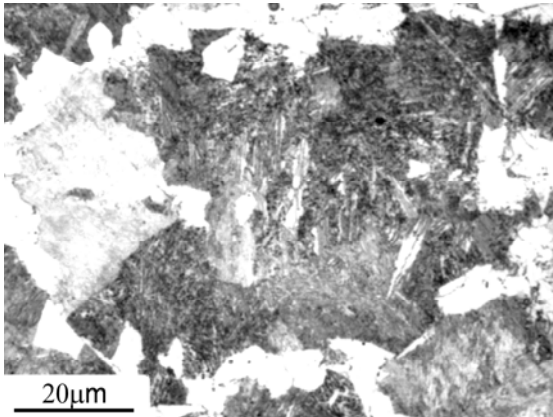
Fig. 4.23(a)600°C /1200s/500X (1061)/Ti S
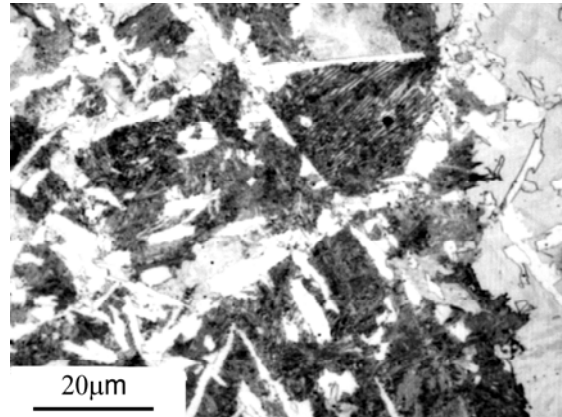
Fig 4.23.(b) 550°C /1200s/500X/Ti S(693)
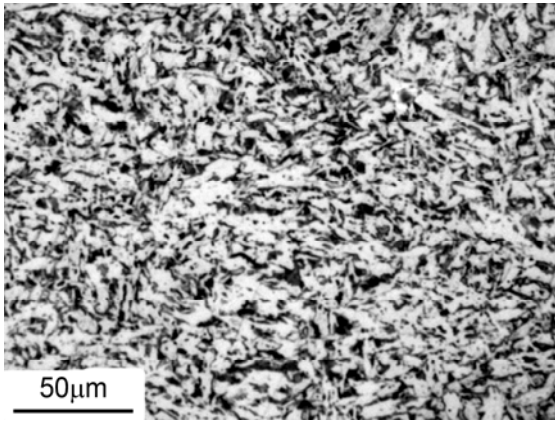
Fig. 4.23(c)500 °C(822/1200s/200X)/Ti S
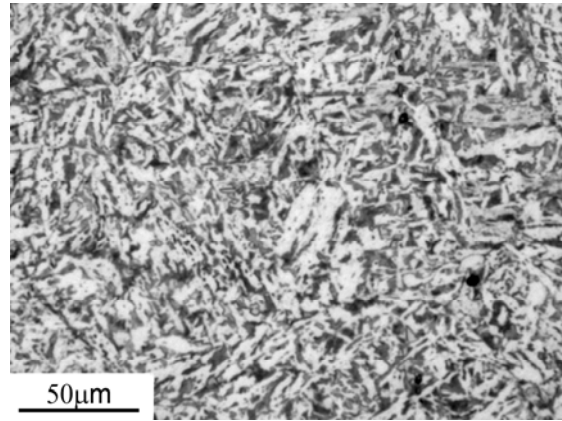
Fig.4.23(c)500°C(821/1200s/200X)/Ti S
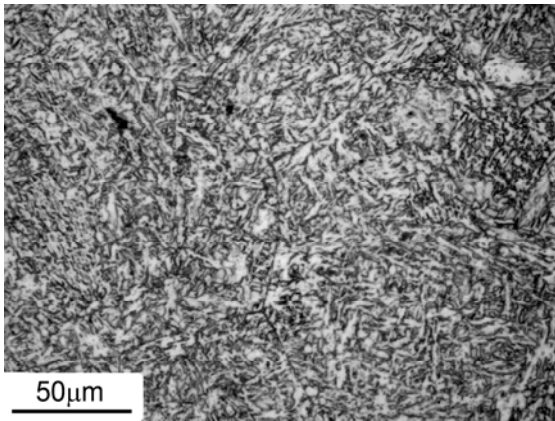
Fig. 4.23(d) 450°C(167/1200s/200X)/Ti S
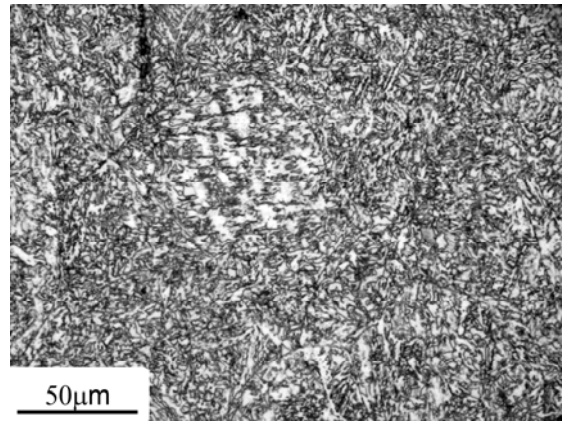
Fig. 4.23(d) 450°C(165/1200s/200X)/Ti S
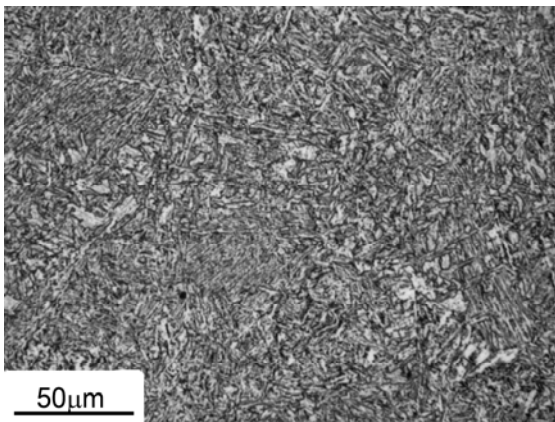
Fig.4.23(e) 400°C(1183/1200s/200X)/Ti S
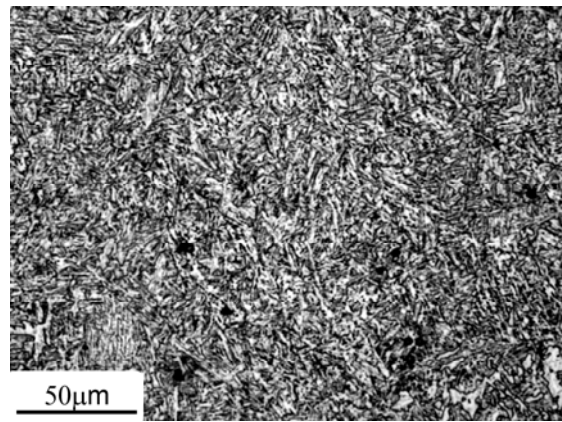
Fig.4.23(e) 400°C(1177/1200s/200X)/TS
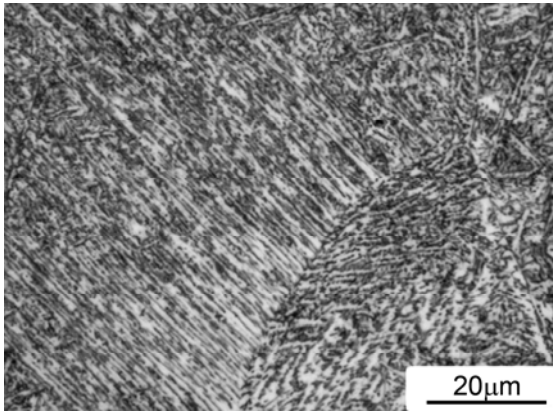
Fig. 4.23(f) 350 °C/1200s/500X/Ti S.
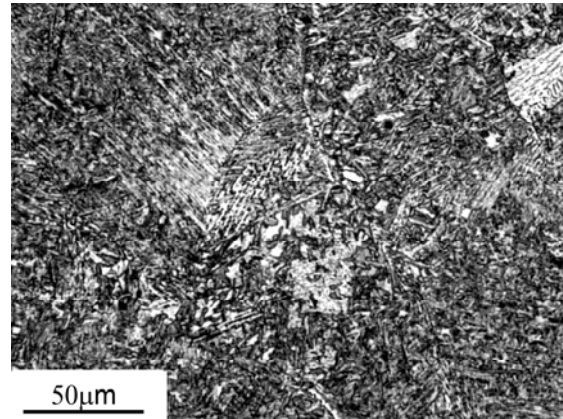
Fig. 4.23(f) 350°C/1200s/200X/Ti S

Fig.4.23 Microstructures of Ti-V-N steel obtained after 1200s of isothermal treatment: (a) 600 °C, (b) 550 °C. (c) 500 °C, (d) 450 °C, (e) 400 °C, and (f) 350 °C.
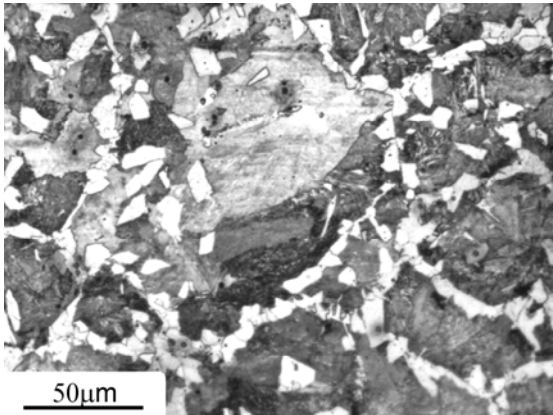
Fig 4.24 (a) 600°C /600s/200X (066)/Ti F
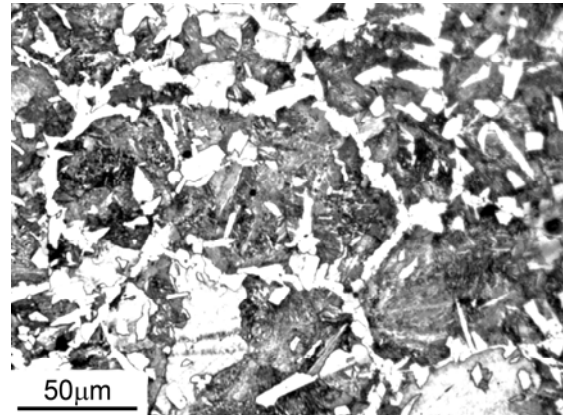
Fig 4.24(a) 600°C /1200s/200X (073) /Ti F
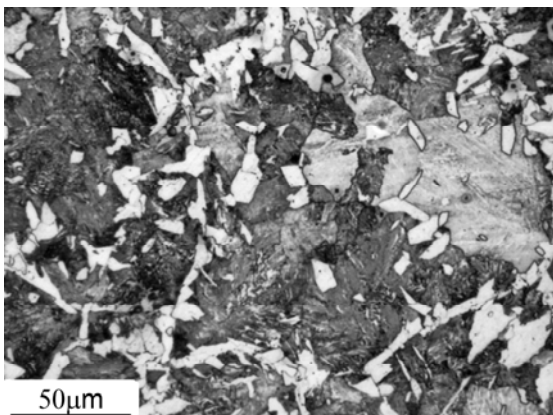
Fig 4.24(a) 600°C /1200s/200X (080)/Ti F
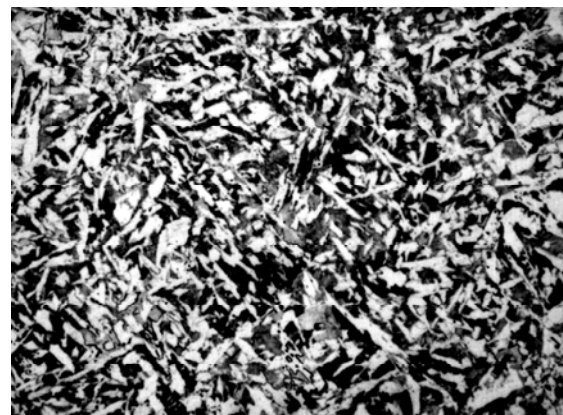
Fig 4.24(b) 550°C/ 1200s/200X/ Ti F
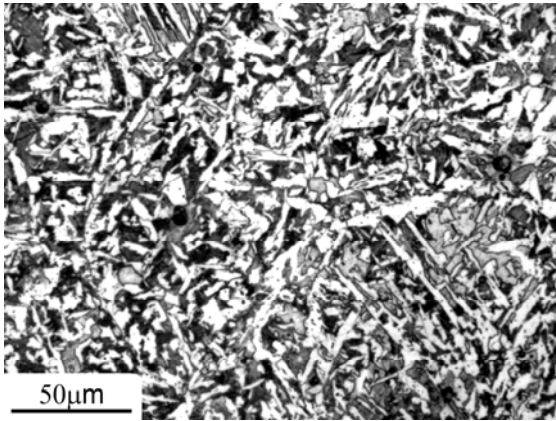
Fig 4.24(b) 550°C /1200s/200X Ti F/(1091)
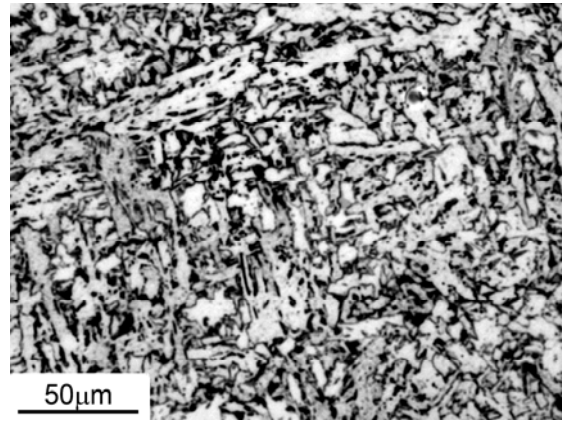
Fig. 4.24(c) 500°C /1200s/200X/ Ti F
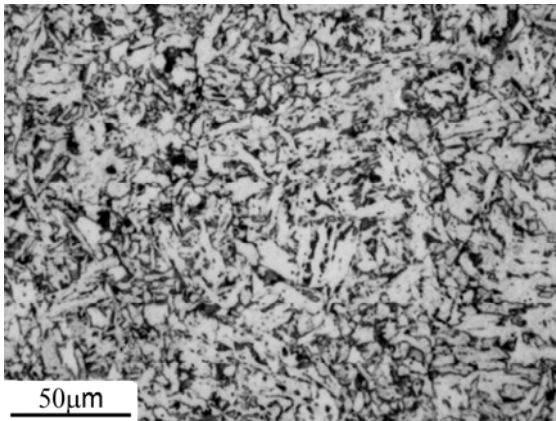
Fig. 4.24(c) 500°C /1200s /Ti F
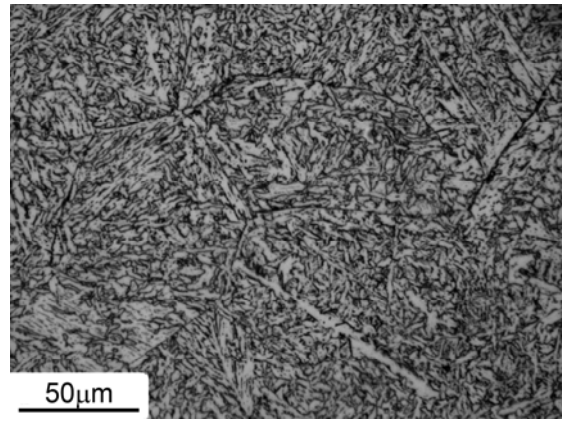
Fig. 4.24(d) 450°C /1200s/ Ti F/
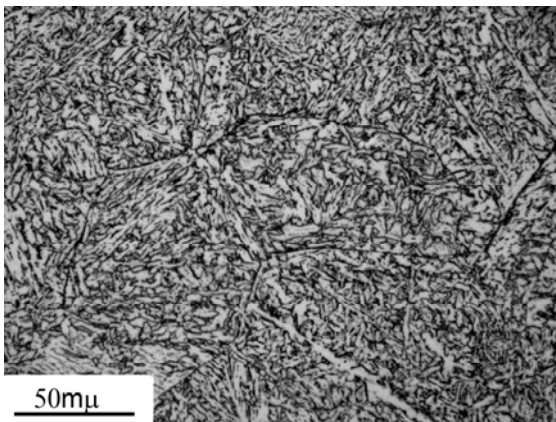
Fig. 4.24(d) 450°C /1200s/200X/TiF/(174).
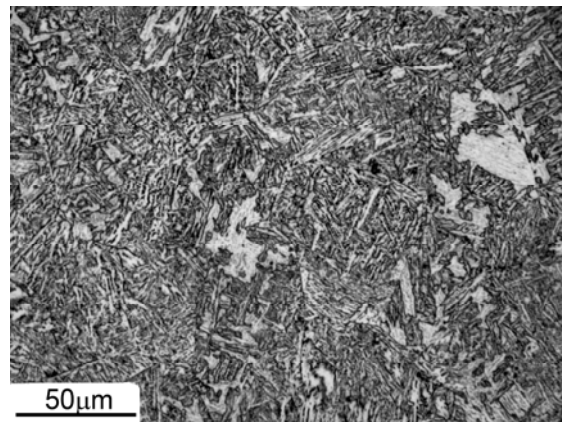
Fig. 4.24(e) 400°C /1200s/200X/372/Ti F
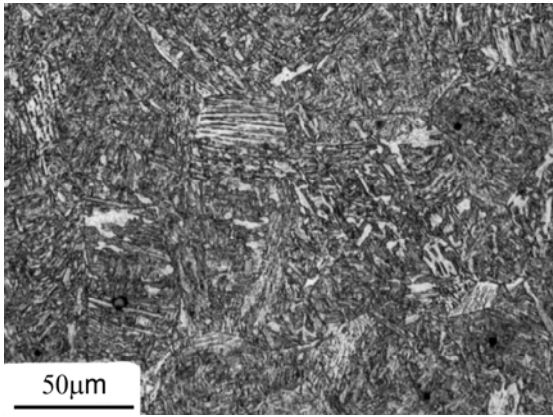
Fig.4.24(f) 350°C /1200s/200X./Ti F   Fig.4.24(f)SEM /350 °C/600s/TiF
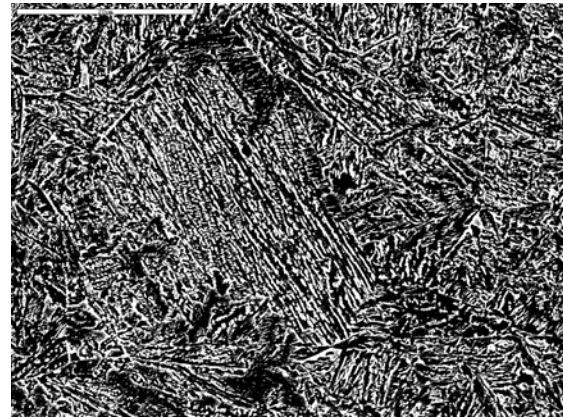
Fig.4.24 Microstructures of V-N steel obtained after 1200s of isothermal treatment: (a) 600 °C, (b) 550 °C. (c) 500 °C, (d) 450 °C, (e) 400 °C, and (f) 350 °C.

Second type of intragranular ferrite morphologies occurs at intermediate temperature (450 and 500 °C). An interlocked acicular ferrite (AF) microstructure is produced as can be seen in Fig. 4.10(k,l,m,n), Fig 2.23(d) and Fig 2.24(d).However the temperature at which the incubation time for ferrite nucleation is at minimum is approximately at 450 °C (Figure 4.30). The incubation time is the minimum time at which it is possible to find some ferrite nucleated at the austenite grain boundary.The maximum acicular ferrite content in the present steel is found for treatment carried out at 450 °C. This treatment is characterised by the fully acicular ferrite formation. On the other hand, it is possible to find, in certain localized places, bainite formed at the grain boundaries, as shown in Figure 4.25. The onset of pearlite at different a treatment temperature (≥ 500 °C) is illustrated in Figure 4.22 and P-line in Figure 4.30.
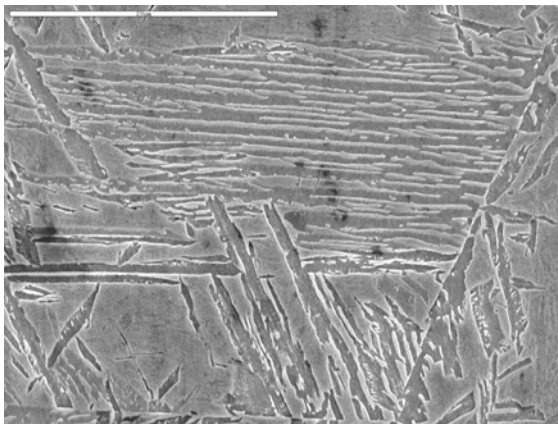
Fig.4.25 (a) 450°C /20s (7S04x3k) –TiS.   Fig.4.25 (b) 450°C /30s-SEM(1945303) –TiF
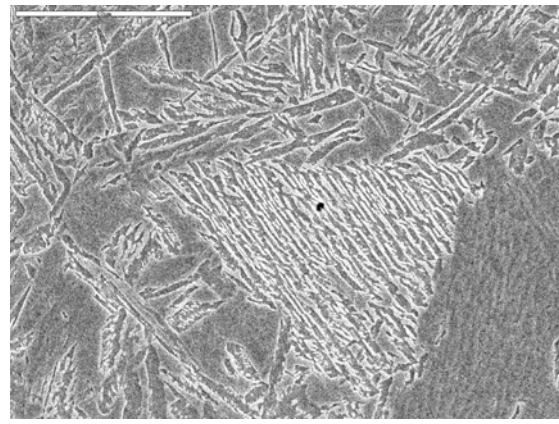
The third type of intragranular ferrite morphology exist at low temperatures (350, 400 °C). Two different morphologies are present at the beginning of the transformation, Bainite sheaves BS as can seen in Figure 4.17 and interlocked AF as can seen in 4.10(k,l,m,n), 2.23(d) and 2.24(d).The origin of Bainitic sheaves are exclusively the grain boundaries. The nucleation of (BS) is indicated in Fig. 4.30 by open triangles.When the isothermal treatment times is increased a new intragranular morphology known as the sheaf type acicular ferrite (STAF) [235] is observed as can be seen in Fig. 4.12.The microstructures in Figures 4.23 and 4.24, for both steels are obtained after 1200s of isothermal treatments at 350, 400, 450, 500, 550 and 600 °C. Refer to the competition of transformation (finish line in Fig.4.30). At temperature $\geq$ 550 °C, the austenite has been transformed into a mixture of allotriomorphic and idiomorphic ferrite and pearlite. However, some of the austenite remains stable, and only after the final water quenching it transforms to martensite as shown in Figure 4.23(a,b) and 4.24(a,b). At 500 °C, some small colonies of pearlite have been formed between the acicular ferrite plates as shown in Figure 4.26 and Figs.4.23(c) and 4.24(c).

(a) 500°C /240s/500X/TiF (893)

(b) 500°C /600s/200X/TiF (0817)

(c) 500°C /600s/500X /TiF (0818)

(d) 500°C /600s/1000X /TiS (814).
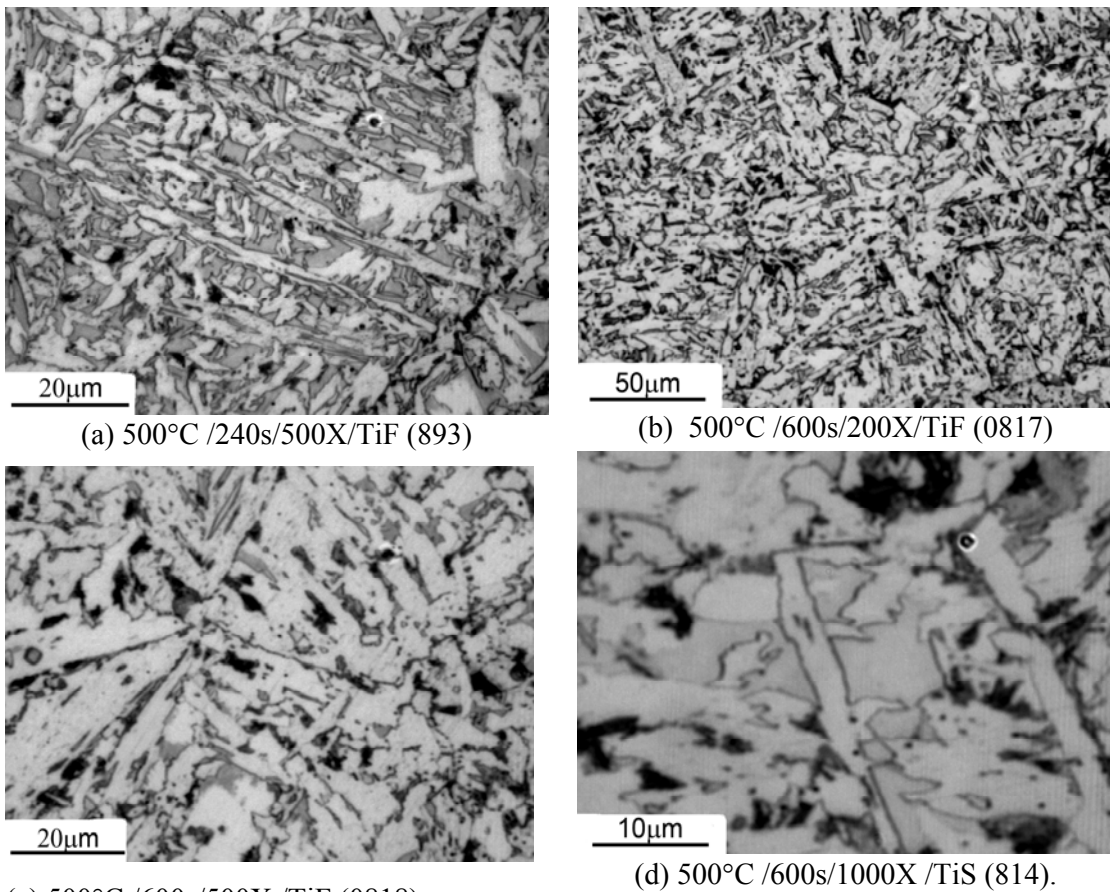
Figure 4.26 (a-d) OM images showing the colonies of pearlite between acicular ferrite plates

As the transformation temperature is reduced to 450 $^\circ$C, the refinement of the ferrite plate is achieved (agreat number of adjacent ferrite plates present) as shown by OM in Figures 4.23(d), 4.24(d) and 4.27 (a, b) for both steels and by SEM in Figure 4.10(k,l,m,n). In this case, the austenite has transformed to acicular ferrite, giving rise to the characteristic interlocked microstructure. As temperature is decreased to 400 and 350 $^\circ$C, mainly two morphologies are observed BS and sheaf type acicular ferrite, as demonstrated in Figs. 4.12 and 4.17. The acicular ferrite sheaf morphology are frequently observed when the isothermal transformation time is increased at 400 $^\circ$C as can seen in Fig. 4.23(e), 4.24(e) and Fig.4.12. However the bainitic sheaves are more observed when the isothermal transformation time is increased and temperature diminishes to 350 $^\circ$C as seen in Figure 4.23(f) , 4.24(f) and Fig. 4.17(k,l,y).
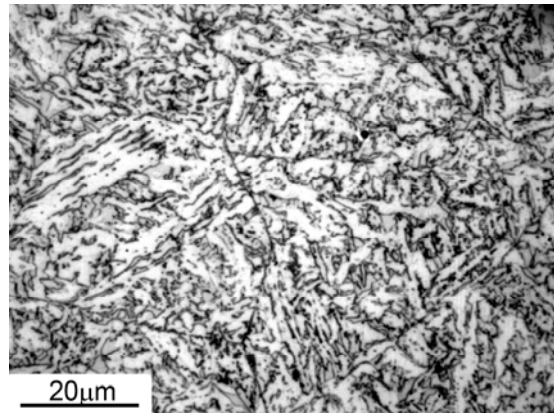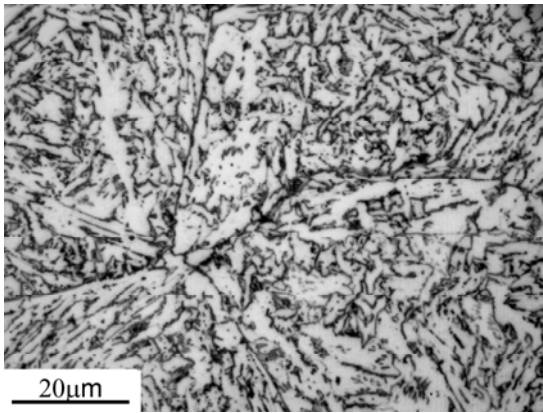
Fig.4.27(a) 450°C /1200s/500X –TiF(179).   Fig.4.27(b) 450°C /1200s/500X –TiS(169).

4.5. TIME–TEMPERATURE-TRANSFORMATION DIAGRAMS

The isothermal transformation approach follow several isothermal reactions at a series of temperatures, enabling plotting characteristic time–temperature–transformation or TTT diagram for each steel tested. In present study, these transformation curves are illustrated in Fig. 4.30 (a, b). As mentioned before the TTT curves are divided into the higher and the lower temperatures segments, where the nose of the curve represents the temperature at which the reaction proceeds most rapidly. The beginning and end of transformation over a wide temperature range tested is plotted to produce two curves making up the diagram, the ferrite

reaction will also take place and this is represented by another curve and which normally precedes the pearlite reaction curve (At T $\geq$ 500 $^{\circ}$C for both steels), however at the lower transformation temperatures other constituents can appear, e.g. bainite, as can be seen in Fig. 4.30 (a, b), also the martensite will exist if the transformation lowered below M_S temperature. Metallographic analysis was used to determine the nucleation curves of isothermally transformed allotriomorphic ferrite.The incubation time is defined as the minimum time at which it is possible to detect some ferrite nucleated on the austenite grain boundaries. Fig.4.28 shows the allotriomorphic ferrite nucleation curves for the two steels. In regard to the effect of microalloying elements on the kinetics of isothermal transformation it has been shown that presence of vanadium delays the nucleation of ferrite, whereas Ti speeds it up [98].Therefore, the temperature at which the incubation time for ferrite nucleation is at minimum (2 seconds) (nose of the nucleation curves) is approximately the same for both steels (approx. 450 $^{\circ}$C). A full description of this behaviour is given in Table 4.13 and illustrated in Fig 4.28. In this sense Ti addition do not exerts any influence on this temperature; neither the prior austenite grain size has any clear effect on the transformation as a whole.

Table 4.13. Nucleation onset time by sec. For both steel investigated.

Tempreture, °C.	Nucleation onset time, s	
	Ti-V-N steel	V-N steel
350	7	7
400	5	2
450	2	2
500	5	3
550	7	5
600	10	7
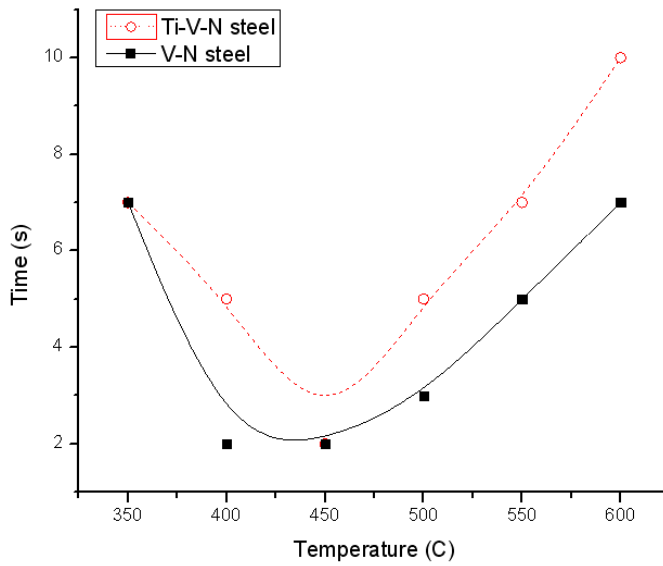
Fig 4.28. Nucleation onset curves for both steels..
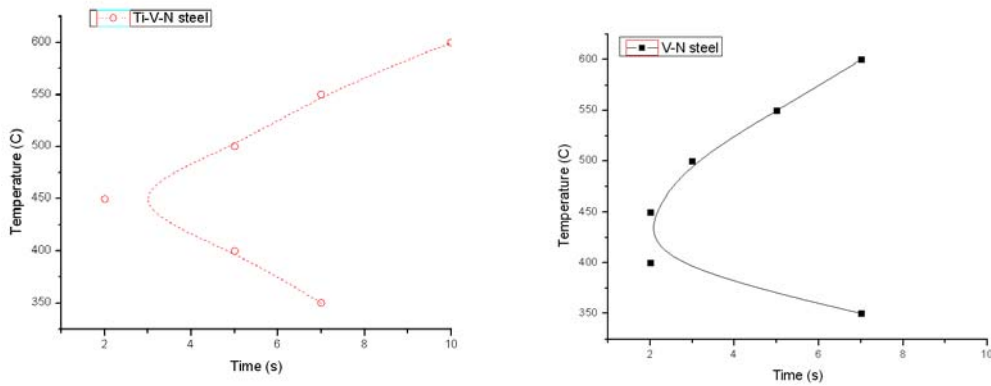
Fig 4.28. Nucleation onset curves for both steels investigated.

Apart from linear dependence, TTT diagrams are plotted in usual semi-log manner. Data given in tables (4.6-4.13) for both steels are summerized in table 4.14

Table 4.14. Nucleation onset time for different phases by sec.For both steel investigated.

Time for onset of new phase, seconds

Temperature	V-N steel					Ti-V-N steel				
°C	GBF	IGF	BS	P	R_f	GBF	IGF	BS	P	R_f
350	7	-----	10	-----	600	7	-----	10	-----	600

168

400	2	-----	20	-----	600	5	-----	10	-----	600
450	2	-----	-----	-----	1200	2	-----	-----	-----	600
500	3	10	-----	80	>1200	5	10	-----	120	1200
550	5	20	-----	45	>1200	7	30	-----	80	>1200
600	7	30	-----	30	>1200	10	60	-----	60	>1200

Grain Boundary Ferrite (GBF), Intra-Granular Ferrite (IGF), Bainite Sheaves (BS), Pearlite (P) and Reaction Finish (R_f).

On increasing the isothermal time further, the nucleation of pearlite (P), Fig. 4.29, is initiated what is represented by the P symbol in Fig.4.29 and Fig 4.30. In the low temperature region in certain localized places Bainitic Sheaves (BS) and/or Widmanstatten Ferrite (WSF) are formed on grain boundaries. The nucleation of these phases is indicated in Fig. 4.30 by open triangles.

Three curves are found to be relevant for initiation stage of transformation: first curve is related to grain boundary nucleated ferrite (GBF), second curve is related to intragranularly nucleated ferrite (IGF) and the third the pearlite (P) curve. GBF and IGF curves are divided into the high temperature and the low temperature segments as consequence of either displacive or diffusion nature of transformation. Additionally, bainitic sheaves occurrence is presented (close triangles) on both diagrams. Time corresponding to the finish of isothermat transformation is designated to lower temperatures, since due to incomplete transformation, it was not possible to determine is accurately for high temperatures. Also it is apparent, from the shape of TTT-diagram in Figure 4.30, that the bainitic transformation start temperature (B_S) occurs at 530 ± 10 °C, for V-N microalloyed steel. However for V-Ti steel its occur at 510 ± 10 °C.
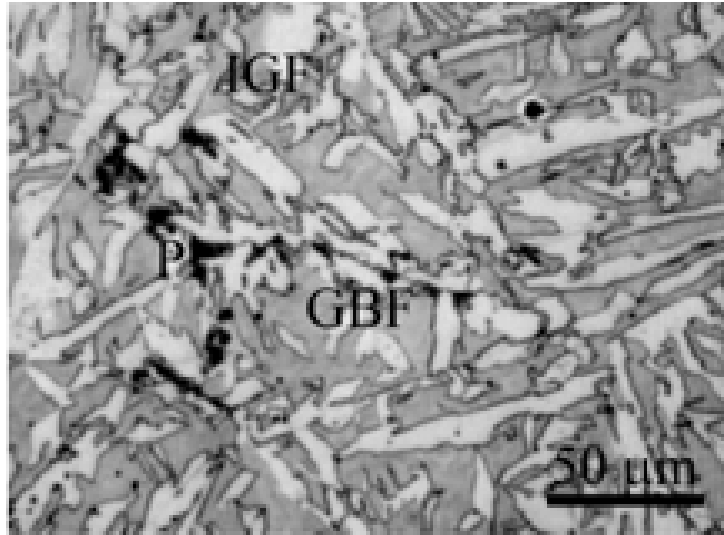
Fig. 4.29. Intragranular ferrite (IGF), at 500 °C /80s, V-N Steel, optical image of (GBF), polygonal ferrite (IGF) and pearlite (P).
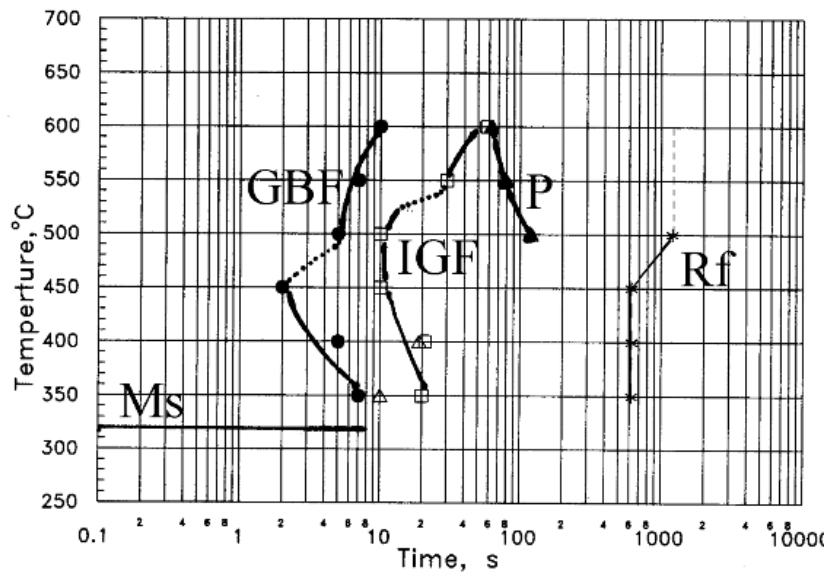
(a)
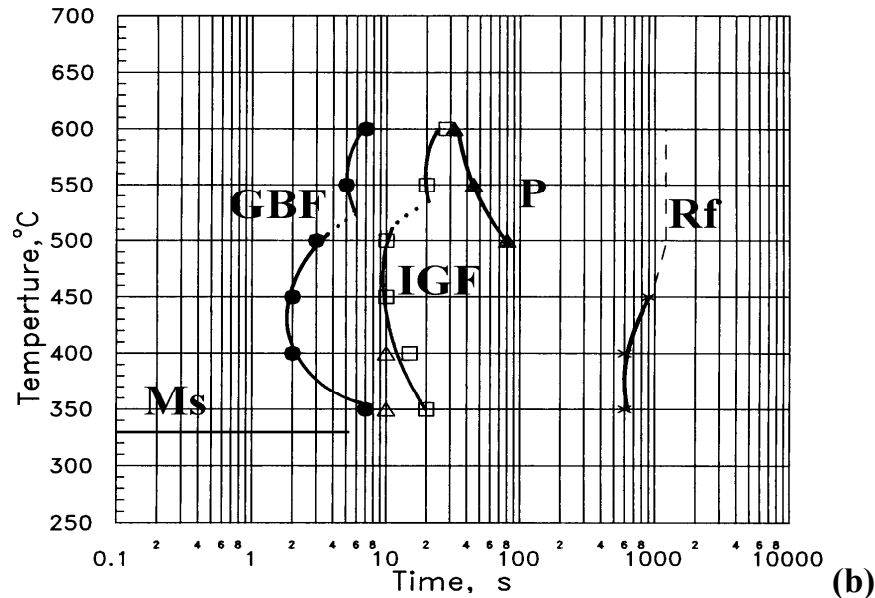
Figure 4.30 (a, b).Time-Temperature-Transformation (TTT) diagram of present steel showing the closed circles- Grain Boundary Ferrite (GBF) start curve, open squares-Intra-Granular Ferrite (IGF) start curve, Bainite Sheaves (BS) are indicated by open triangles, closed triangles-Pearlite (P) start curve, Martensite Start (M_S) temperature and Reaction Finish (R_f) Curve (where incomplete reaction is indicated by dashed line). Thus for (a) Ti-V-N steel. (b) V-N steel.

4.6 MECHANICAL PROPERTIES

The results of the compression testing and hardness testing are summarized as below

4.6.1 HARDNESS RESULTS

The average Vickers hardness value was taken as the representative hardness and its values are listed in table 4.14(a-f).The hardness for both steels and conditions investigated here are summarized in Fig.4.32 where results of isothermal treatments as function of holding time is plotted in Fig.4.31 (a-f). There is a striking similarity between all these figures where the hardness in plotted as a function of heat treatment holding time in a salt bath at (350 to 600 °C) after austenitisation, then followed by water quenching. There is in each case a fairly unifrom gradient in hardness values as holding time increased. The rapidly quenched steels have high hardness. As the holding time is increased the hardness values decreased as listed in table 4.15(a-f).

Table 4.15(a): Average Hardness measurements at 350 $^\circ$C

Holding time, s	Ti-V-N steel,(Hv_{30})	V-N steel,(Hv_{30})
10	652	610
20	626	462
30	543	439
60	420	404
120	451	415
600	351	366
1200	351	351

Table 4.15(b): Average Hardness measurements at 400 $^\circ$C

Holding time, s	Ti-V-N steel, (Hv_{30})	V-N steel,(Hv_{30})
2	586	586
5	565	579
10	493	496
20	550	353
30	459	344
60	368	368
120	349	349
600	315	287
1200	302	315
1800	302	302

Table 4.15(c): Average Hardness measurements at 450 $^\circ$C

Holding time, s	Ti-V-N steel, (Hv_{30})	V-N steel,(Hv_{30})
2	505	557
5	550	530
10	470	473
20	520	375
30	502	305
60	351	297
120	348	290
600	287	271
1200	287	287
1800	287	287

Table 4.15(d) : Average Hardness measurements at 500 °C

Holding time, s	Ti-V-N steel,(Hv_{30})	V-N steel,(Hv_{30})
5	661	602
10	543	543
20	635	427
30	530	432
45	517	406
60	586	370
80	470	400
120	418	362
600	318	294
1200	294	268

Table 4.15(e) : Average Hardness measurements at 550 °C

Holding time, s	Ti-V-N steel,(Hv_{30})	V-N steel,(Hv_{30})
5	720	622
`10	540	605
20	626	606
30	626	583
45	505	454
60	614	429
80	579	436
120	626	389
600	454	271
1200	404	256

Table 4.15(f): Average Hardness measurements at 600 °C

Holding time, s	Ti-V-N steel,(Hv_{30})	V-N steel,(Hv_{30})
5	606	618
10	606	614
20	583	511
30	652	505
60	517	502
80	583	481
100	657	441

120	522	362
600	358	264
1200	304	262

(a)

(b)

(c)

(d)
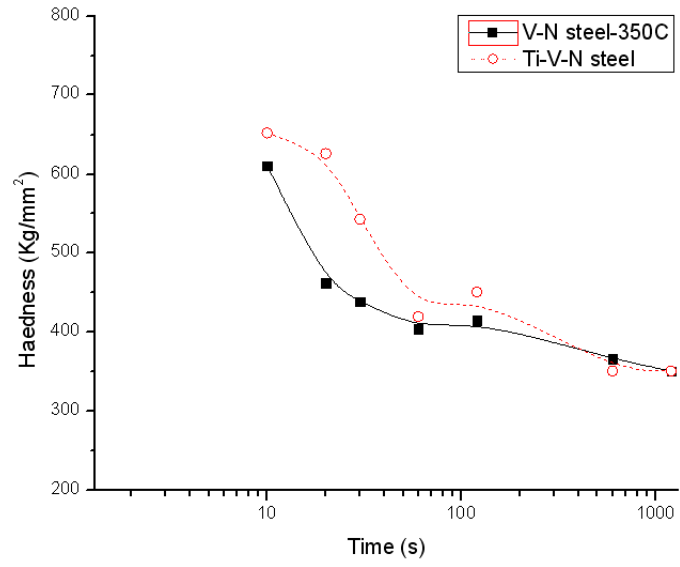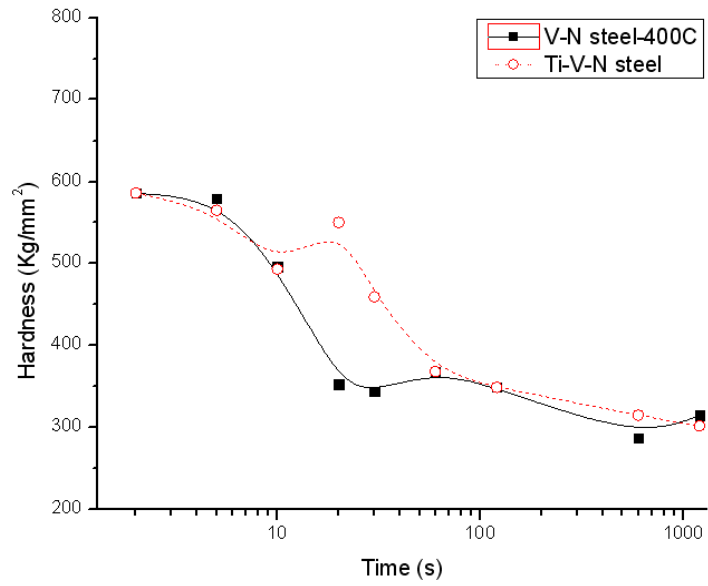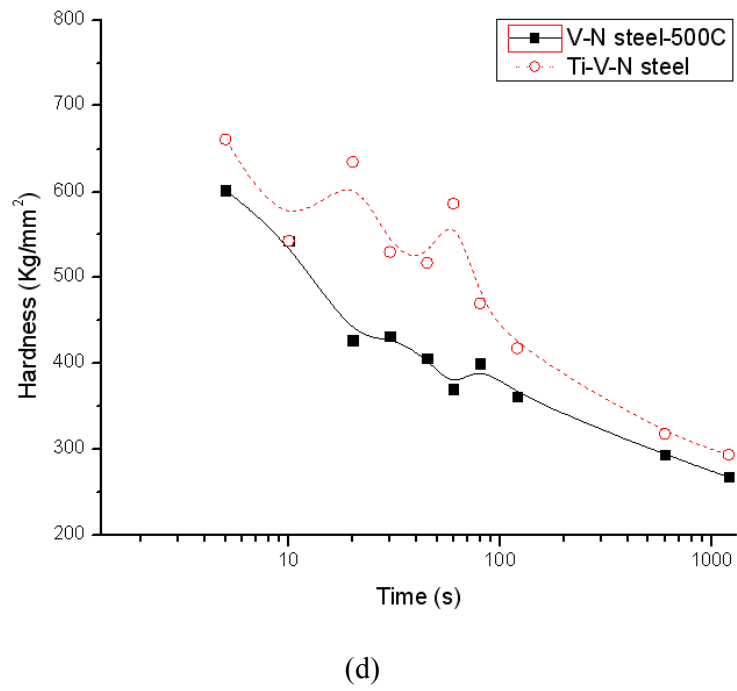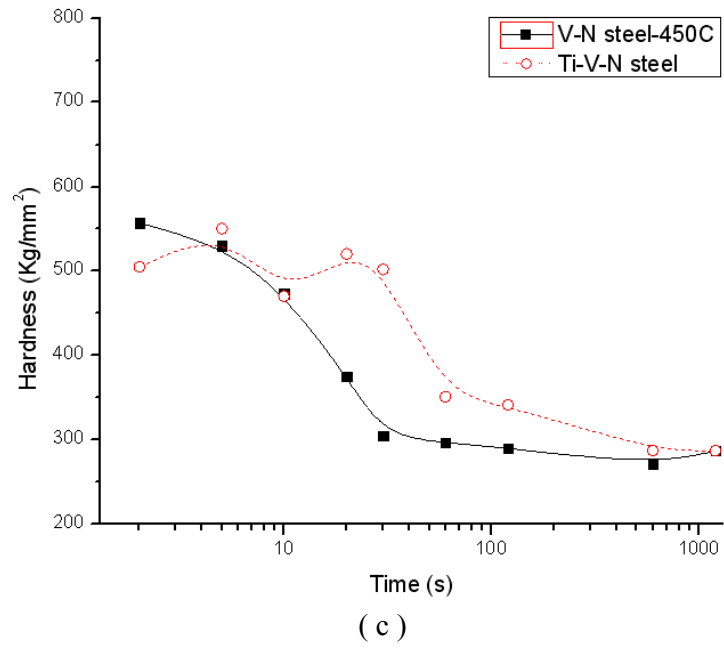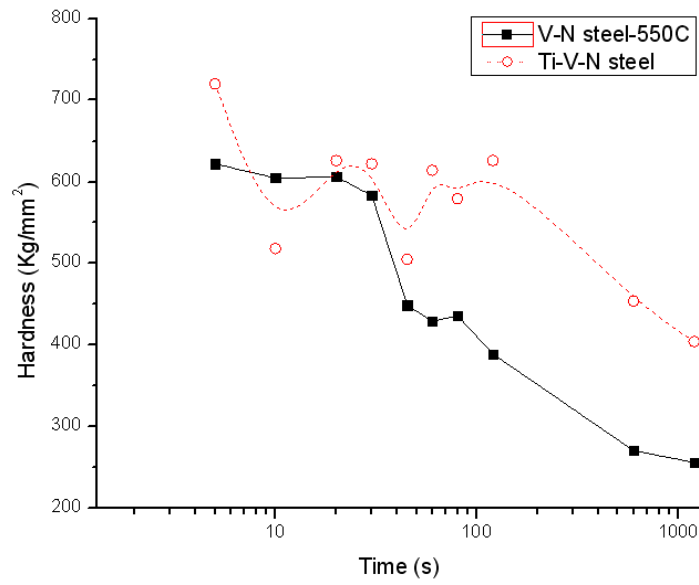
(e)
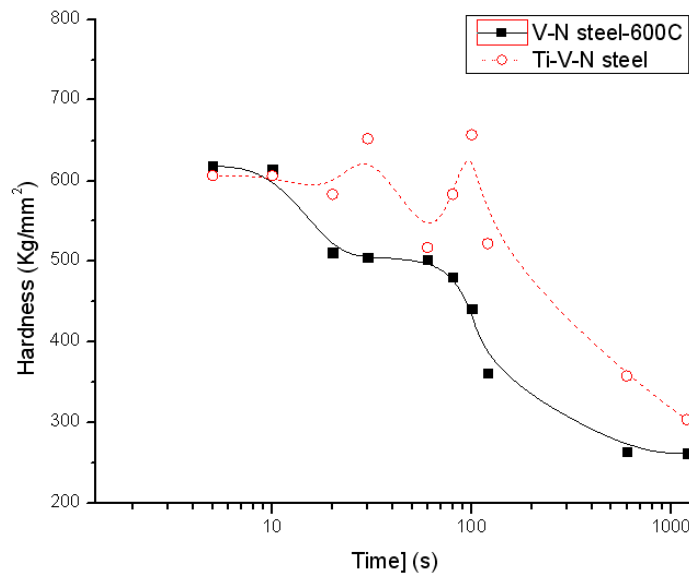
(f)

Fig. 4.31 Average hardness for both steels as function of holding time as demonstrated in Table 3.3. Thus for (a) 350°C, (b) 400°C, (c) 450°C, (d) 500°C, (e) 550°C and (f) 600°C.
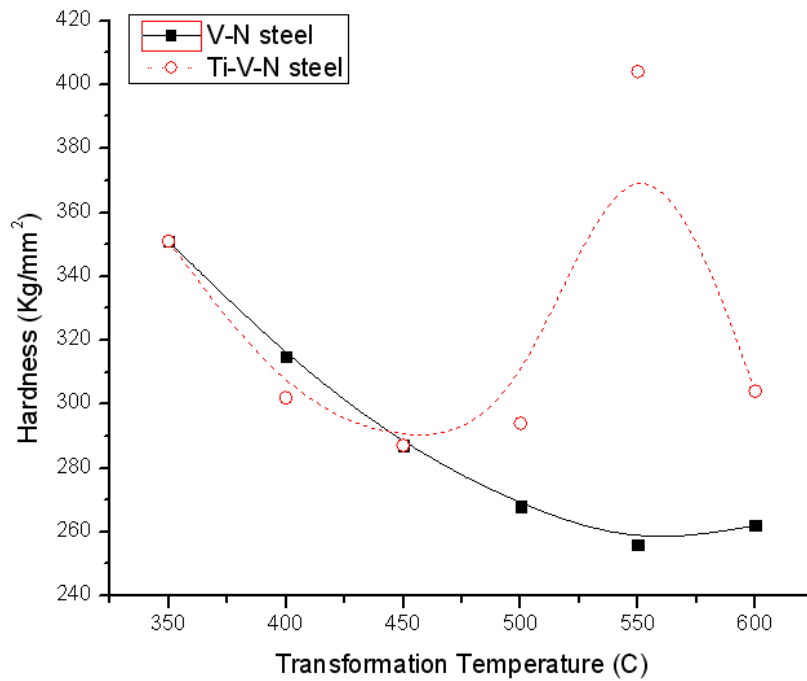
Fig. 4.32 Average Vicker Hardness meaurements (H_V 30) for both steels after 1200s holding time at 350 to 600°C as isothermal temperat

4.6.1.1. Quantitative Estimation of the Cementite Volume Fraction

The hardness changes during isothermal transformation processes can be used to derive a function which expresses the change in the volume fraction of cementite precipitation as a function of time and temperature.This is in good a greement with Avrami equation. A full description of isothermal phase transformation represented by Avrami equation is given in chapter 2.2.3. In present results, the hardness of the as-quenced condition (H_0) was experimentally investigated and the result reviewed that its equal 705 H_V and 635 H_V for for Ti-V-N and V-N microalloyed steel respectively. This is in good a greement with result deduced from the data reported by Speich [15], and find its equal 680 H_V for Ti-V-N steel and 612 H_V for V-N steel. However the hardness when all the carbon has precipitated but before any significant recovery, recrystallisation or coarsening has occurred (H_F) was caculated by use empiricall equation. A full description of this caculation is given in 2.5.2 Kinetics of Cementite Precipitation, and results are 341 H_V for Ti-V-N and 326 H_V for V-N steel. In respect to the volume fraction of cementite ξ{t}is related to hardness at any time H{t}, the hardness of the as-quenced condition H_0 and its hardness when all the carbon has precipitated

H_F. The corresponding results of $\xi\{t\}$ are given in Table 4.16(a) - 4.16(f) and illustrated in Fig. 4.33.

Table 4.16(a) The volume fraction of cementite as function of time and hardness for both steel at 350 °C

Time,s	$\xi\{t\}$ 350 °C /V-N steel	$\xi\{t\}$/350°C/ Ti-V-N steel
10	0.080	0.14
20	0.56	0.22
30	0.63	0.44
60	0.75	0.78
120	0.71	0.70
600	0.87	0.97
1200	0.92	0.97

Table 4.16 (b) The volume fraction of cementite as function of time and hardness for both steel at 400 °C

Time,s	$\xi\{t\}$/400 °C /V-N steel	$\xi\{t\}$/400 °C Ti-V-N steel
2	0.16	0.32
5	0.18	0.38
10	0.45	0.58
20	0.91	0.42
30	0.94	0.67
60	0.86	0.92
120	0.92	0.98

Table 4.16 (c) The volume fraction of cementite as function of time and hardness for both steel at 450 °C

Time,s	$\xi\{t\}/450$ °C /V-N steel	$\xi\{t\}/450$ °C Ti-V-N steel
2	0.25	0.55
5	0.34	0.42
10	0.52	0.64
20	0.84	0.51
30	1.0	0.56
60	----	0.97
120	----	1.0

Table 4.16 (d) The volume fraction of cementite as function of time and hardness for both steel at 500 °C

Time,s	$\xi\{t\}/500$ °C /V-N steel	$\xi\{t\}/500$ °C Ti-V-N steel
5	0.107	0.120
10	0.29	0.44
20	0.67	0.19
30	0.66	0.48
45	0.74	0.52
60	0.85	0.33
80	0.76	0.64
120	0.88	0.79
600	>1.00	1.0

Table 4.16 (e) The volume fraction of cementite as function of time and hardness for both steel at 550 $^{\circ}$C

Time,s	$\xi\{t\}$/550 $^{\circ}$C /V-N steel	$\xi\{t\}$/550 $^{\circ}$C Ti-V-N steel
5	0.042	0.00
10	0.098	0.45
20	0.094	0.22
30	0.17	0.22
45	0.56	0.55
60	0.67	0.25
80	0.64	0.35
120	0.79	0.22
600	>1.00	0.69
1200	------	0.83

Table 4.16 (f) The volume fraction of cementite as function of time and hardness for both steel at 600 $^{\circ}$C

Time,s	$\xi\{t\}$/600 $^{\circ}$C /V-N steel	$\xi\{t\}$/600 $^{\circ}$C Ti-V-N steel
5	0.055	0.27
10	0.067	0.27
20	0.40	0.33
30	0.42	0.15
60	0.43	0.52
80	0.49	0.33
100	0.63	0.13
120	0.88	0.50
600	>1.00	0.95

(a)

(b)

(c)

(d)

182
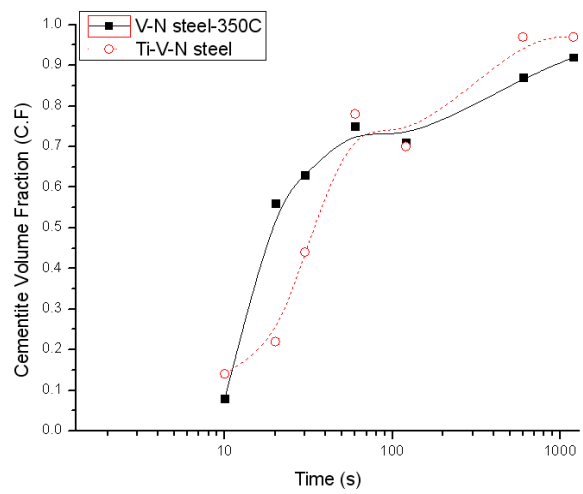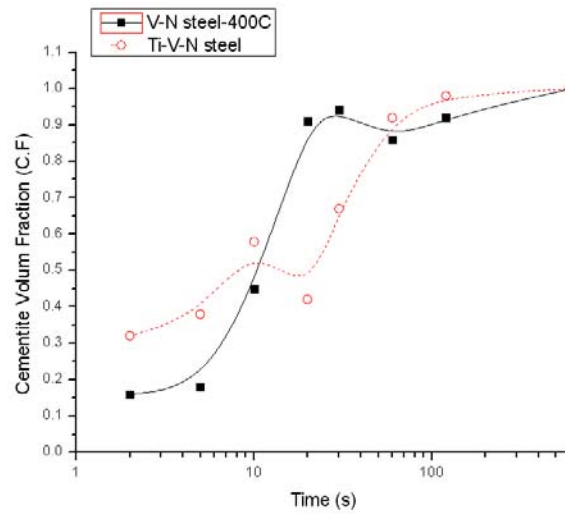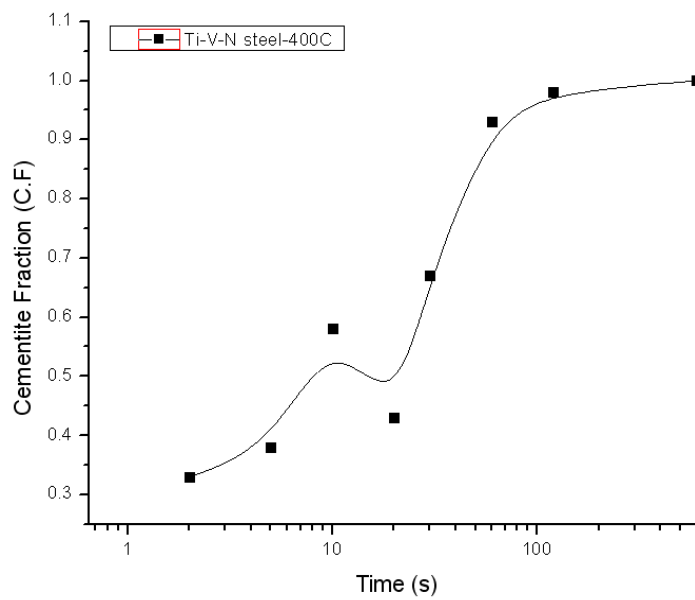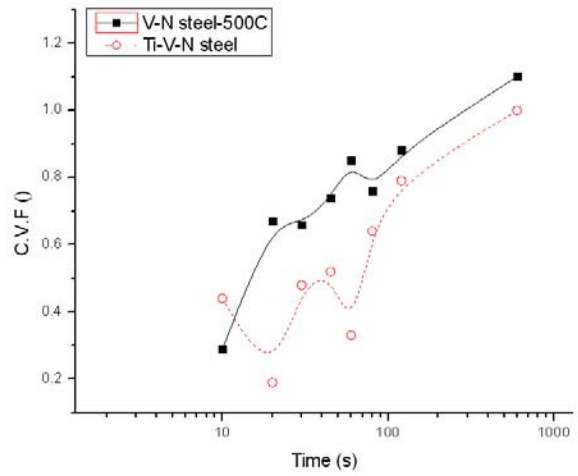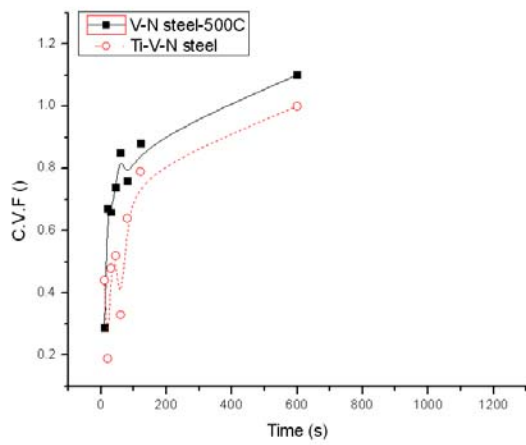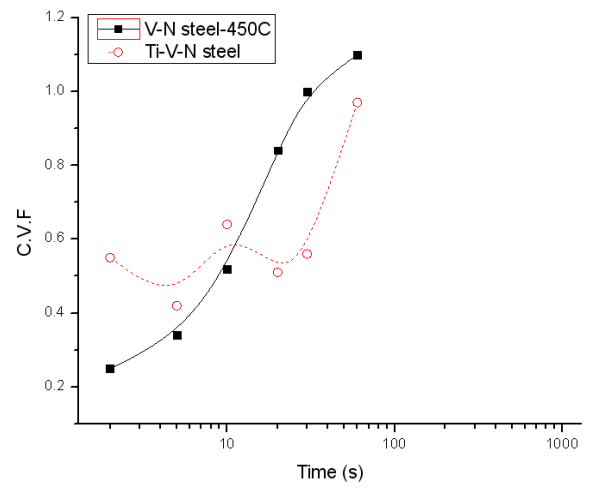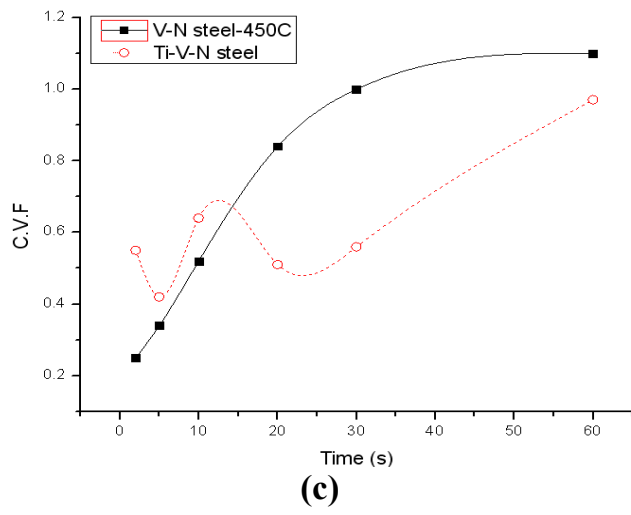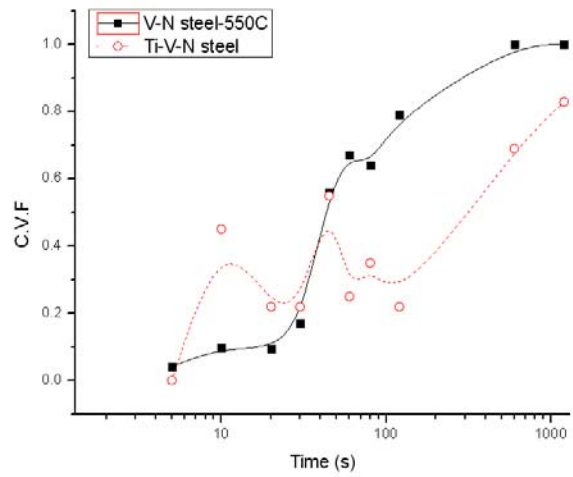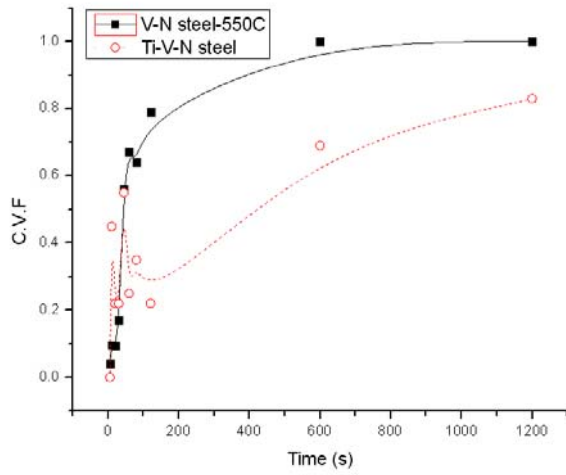
(e)
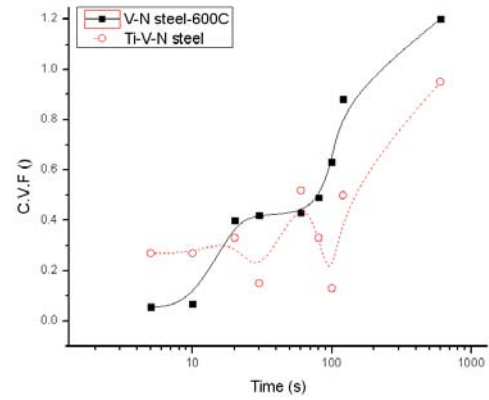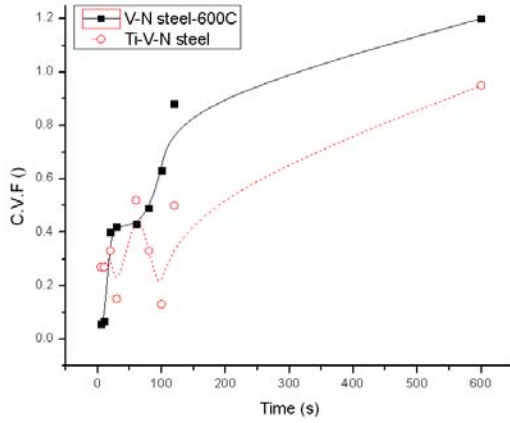
(f)

Fig. 4.33 (a-f). The volume fraction of cementite as function of time and hardness for both steels. Thus for (a)350 $^{\circ}$C(b) 400 $^{\circ}$C (c) 450 $^{\circ}$C (d) 500 $^{\circ}$C (e) 550 $^{\circ}$C (f) 600 $^{\circ}$C

4.6.3 YIELD STRESSES

The yield strength in this work is determined using offset method. Raw diagrams are given in figures 4.34 and 4.35. However the yield stress results for final microstructures of V-N and V-Ti-N microalloyed steels are summarized in Table 4.17 and Figure 4.36.

Table 4.17 Average Yield stresses ($\sigma_{y.s}$) by MPa for both steels investigated.

Temperature, °C	Ti-V-N Steel ($\sigma_{y.s}$)- MPa	V-N Steel ($\sigma_{y.s}$)- MPa
350	1000	900
400	880	800
450	700	680
500	705	680
550	800	700
600	800	700

(a)

(a)
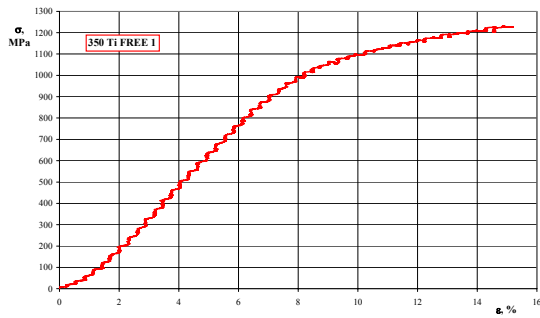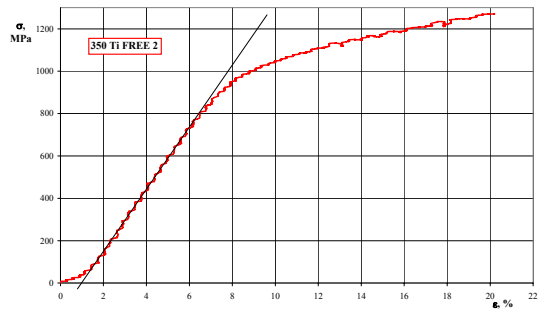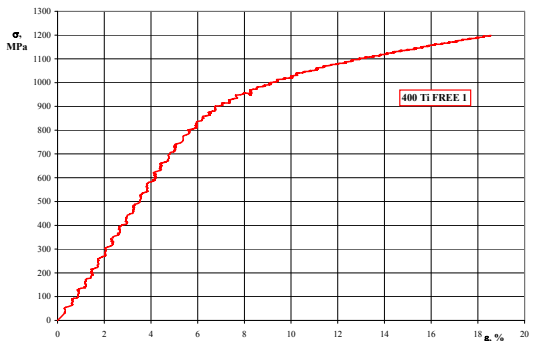
(b)
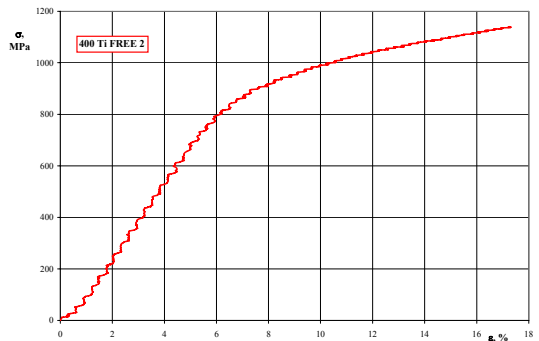
(b)
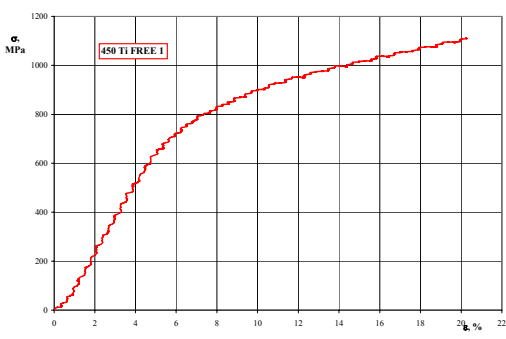
(c)
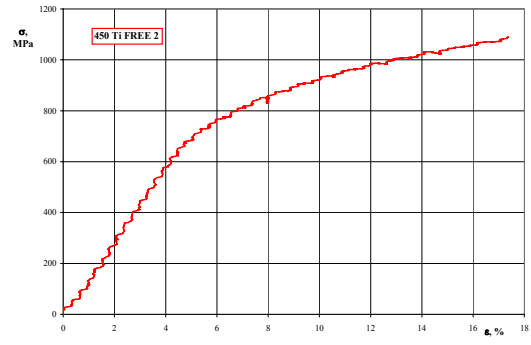
(c)
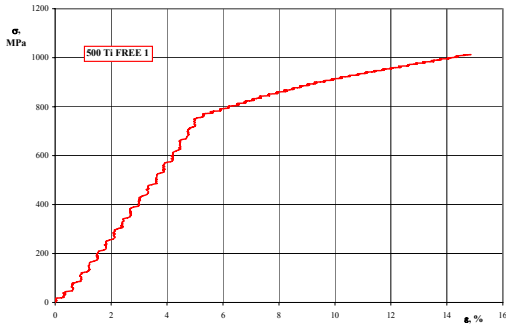
(d)
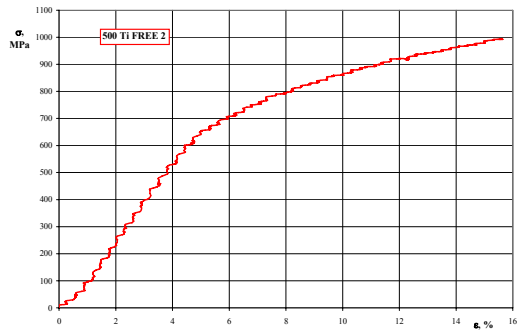
(d)
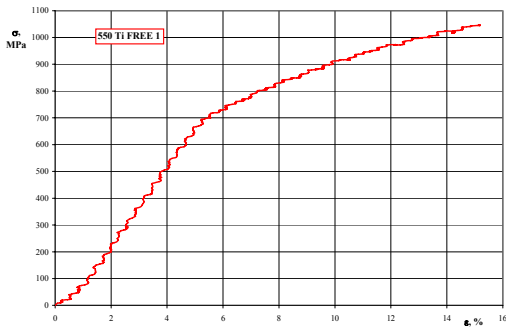
(e)
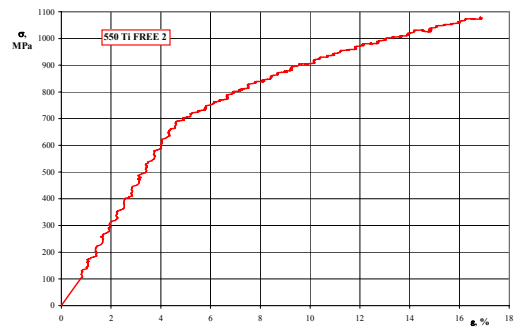
(e)
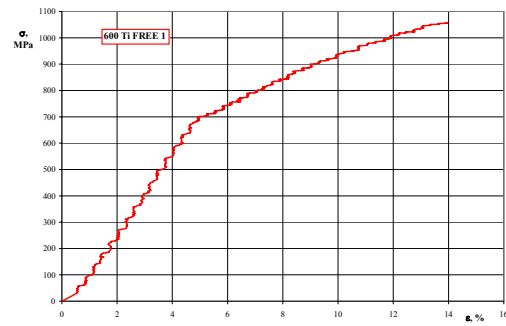
(f)
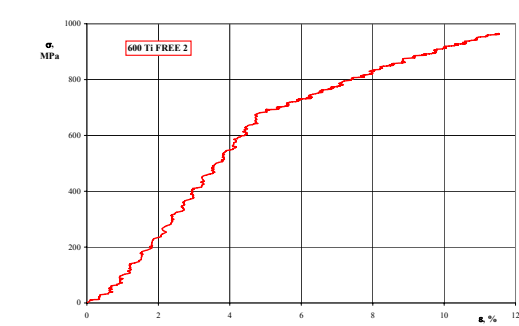
(f)

Fig. 4.34. Yield stresses ($\sigma_{y.s}$) by MPa as function of percent elongation (ε, %) for medium carbon V-N micro-alloyed steels at (a) 350°C, (b) 400°C, (c) 450°C, (d) 500°C, (e) 550°C and (f) 600°C.

185

(a)

(a)

(b)

(b)

(c)

(c)

(d)

(d)

(e)   (e)

(f)   (f)
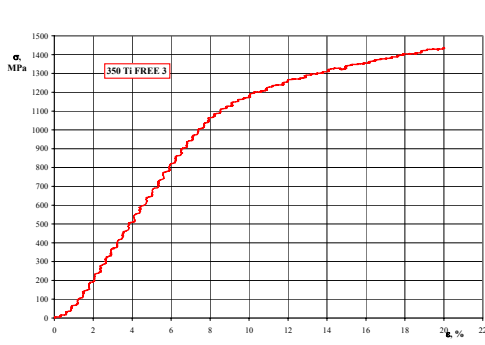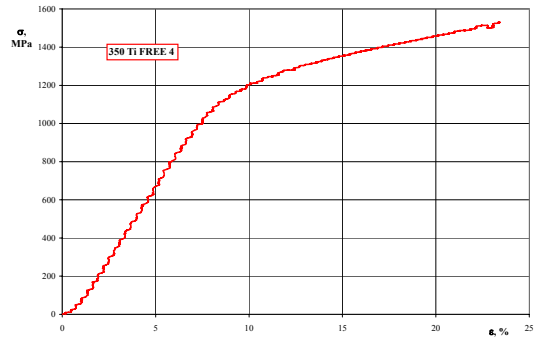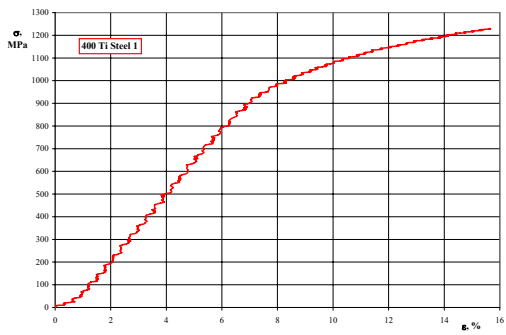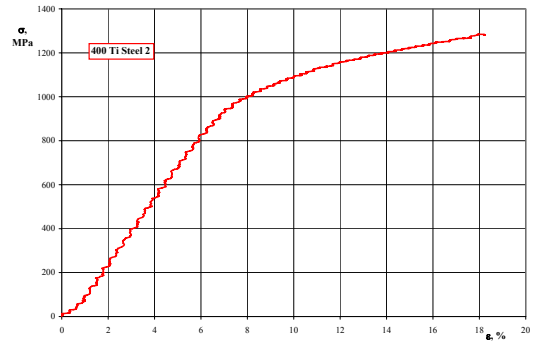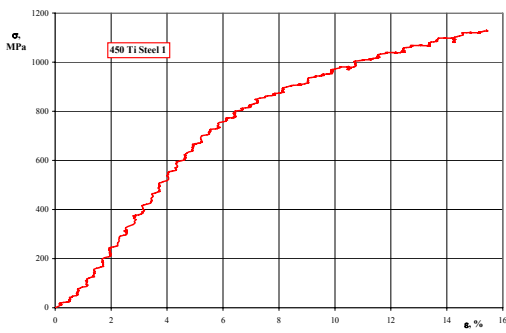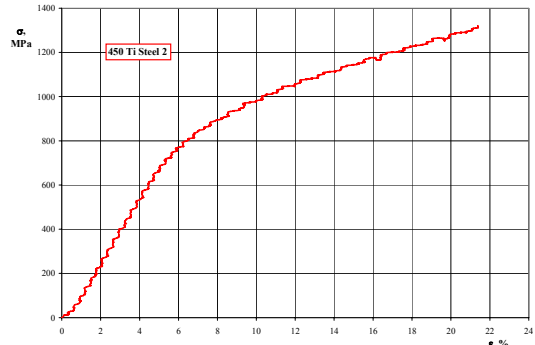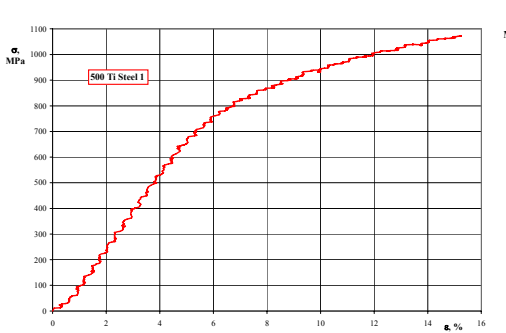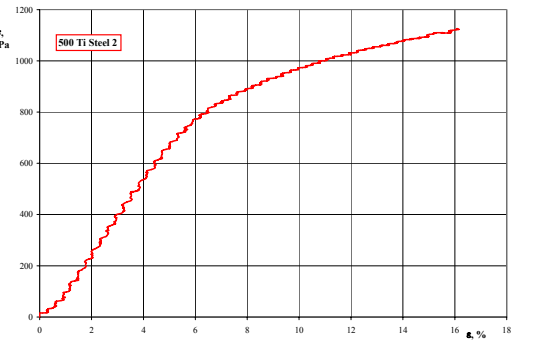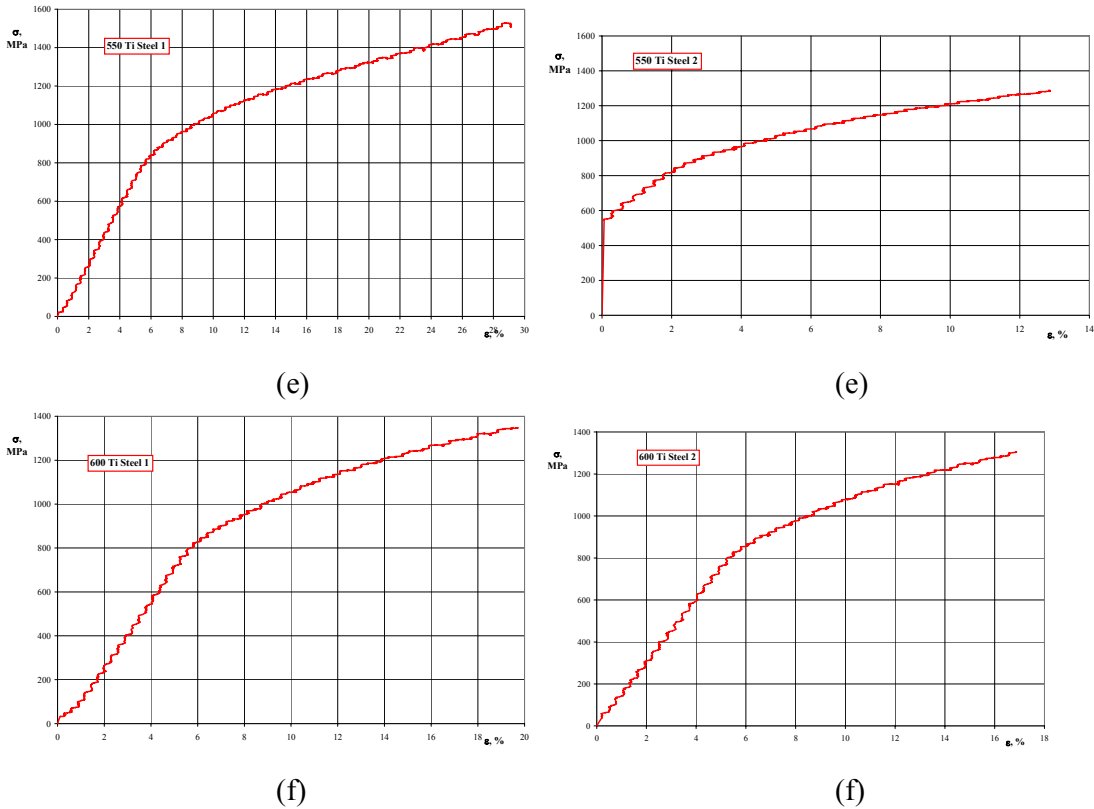
Fig. 4.35-continue. Yield stresses ($\delta_{y.s}$) by MPa as function of percent eloungation (ϵ, %) for medium carbon Ti-V-N micro-alloyed steels at (a) 350°C, (b) 400°C, (c) 450°C, (d) 500°C, (e) 550°C and (f) 600°C.
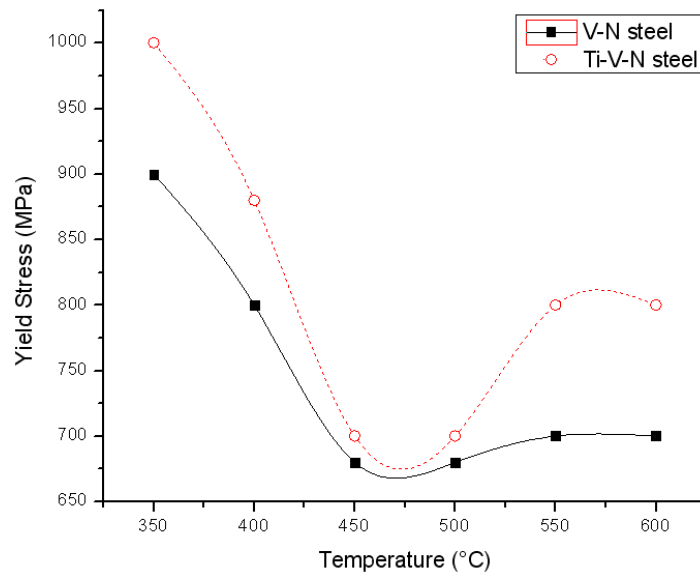
Fig 4.36. Yield stresses (σ_{02}) on different transformation temperatures for Ti-V-N (open symbols) and V-N (closed symbols) micro-alloyed steels (transformation time 1200s)

In both steels, maximal value of YS is for specimens transformed at 350 $^\circ$C. With increase of temperature, YS decreases and reaches minimal value at approx 450-500 $^\circ$C for both steels. Further increase of isothermal test temperature leads to increase in YS. This phenomenon is more pronounced in Ti-V-N steel. Also, over the whole temperature region, YS of Ti-V-N steel exhibits higher values of YS. The actual decrements in yield stress lie in the range of 80-100 MPa, for both low (400, 350 $^\circ$C) and high temperatures ($\geq$ 550 $^\circ$C), 20-25 MPa for intermediate temperatures (450, 500 $^\circ$C).

5   DISCUSSION

5.1   REHEATING TEMPERATURE

The austenite grain size control is important factor in development of the final mechanical properties of the product [129].Previous results showed that prior austenite grain size of approx 60μm provides optimal conditions for formation of acicular ferrite [142,143]. In that respect, samples were reheated at 950, 1050, 1100, 1150, and 1250 °C. The prior austenite grain size was estimated and values are listed in the table 4.1 and Fig. 4.1m. Two main mechanisms for grain size control are presence of alloying elements in solid solution (solution drag) and as precipitates on grain boundaries (pinning effect) [14,46,238,154,174,239]. For that reason, both steels grain coarsening is expected to occur when the particles pinning the austenite grain boundaries start to dissolve. This is produced at around 1100°C in both steels. However the presence of precipitates suppressing grain growth.The driving force for abnormal grain growth is usually the reduction in grain boundary energy as for normal grain growth. Abnormal grain growth can only occur when grain growth is inhibited. The main factors which lead to abnormal grain growth are second-phase particles, texture and surface effects [174,240,241]. This indicates that for a given volume fraction, growth of the particles to a size in excess of the critical particle radius, $r_{crit.}$, will result in grain-coarsening.

5.1.2 AUSTENITE GRAIN GROWTH BEHAVIOUR

The austenite grain coarsening behaviour as a function of temperature is shown in Fig. 4.1m. For both steels investigated, clearly show two-stage grain growth. Below a critical temperature range, defined as the grain coarsening temperatures (GCT), the change in grain size is very small, From the bottom graph in Fig. 4.1m , it can be seen that compared with the austenite grain size of both steels, the V-N steel has the smallest austenite grain size. The austenite grain growth of both steels retains a steady slow growth up to 1100°C i.e. it has the characteristics of normal grain growth. While above this critical temperature range the grain size increases with temperature very rapidly. Another obvious feature is that both steels which followed an abnormal grain growth behaviour at certain temperature. These temperature corresponds to the grain coarsening temperature for both steels (see Fig. 4.1m).However before

grain coarsening temperature ranges there is a duplex structure represented by the cross-hatching in Fig. 4.1m. This kind is clearly shown in Figure 4.1.(a,b).When the temperatures were higher than the grain coarsening temperatures, the dissolution of precipitates in the steels allows more grains to grow, which is considered to be a abnormal process (see Figure 4.1.**(k,l)**). As expected for the V-N steel, with high Al and N contents possesses the smallest grain size, if compare it by Ti-V-N steel, with low Al and N. Therefore Ti-V-N Steel with lowest volume fraction of AlN among these steels has the largest grain size at temperature less than 1100 $^{\circ}$C. As clearly shown from bottom graph in Fig. 4.1m, it can be seen that compared with the austenite grain size of the V-N steel, the Ti-V-N steel has the largest austenite grain size. The reason becouse, the AlN particles which are responsible for controlling austenite grain growth in the low austenising temperature. The predicted result in rather good a greement with the experimental data derived from similar steels [174].In the present work it was not possible to measure the particles that can restrain the growth of austenite grains from metallographically prepared specimens. Calculations based on the stoichiometry (Table 4.2) indicate that, the Ti-V-N steel has sufficient nitrogen to form TiN, AlN and almost no nitrogen left for VN. The TEM observations with EDAX analyses based on the results of similar steels given in Ref. [174] and is proved that there are many AlN and TiN particles.Therefore, AlN and TiN particles are considered to play a role in inhibition of austenite grain growth for this steel. By contrast, the only AlN particles for V-N steel. These attribute to increase grain growth for V-N steel at T > 1100 $^{\circ}$C.The latter temperature corresponds to the grain coarsening temperature for both steel (see Fig. 4.1m). This may indicate that the process of particle coalescence and dissolution is occurring simultaneously in these temperature ranges**.** Therefore, with temperature increasing from 950 to 1100°C, the number of particles decreased due to particle size increases slightly by particle coarsening.This indicates that for a given volume fraction, growth of the particles to a size in excess of the critical particle radius, $r_{crit.}$, will result in grain-coarsening. However, at temperature higher than 1100°C, the particle size decreases due to dissolution (see Table 4.2) and grain size start to increases suddenly with increase temperature. Based on the result in Ref.[174]. The volume fraction of AlN, f_{AlN} , and The volume fraction of TiN, f_{TiN} , decreases with increasing austenitising temperature for the two tested steels and obviously there is more AlN in V-N Steel with high Al and N contents than in the other steel.

5.2. AUSTENITE DECOMPOSITION

Since alloying elements have different tendencies to exist in the ferrite and carbide phases, it might be expected that the rate at which the decomposition of austenite occurs would be sensitive to the concentration of alloying elements in steel [19].There are pronounced morphological changes as the transformation temperature is lowered. Bainite describes the resultant microstructure in steels of the decomposition of austenite (γ) into ferrite (α) and cementite (Fe_3C) in the temperature range above the martensitic transformation and below that for pearlite [123]. Therefore the equilibrium is said to exist in a system with minimum free energy or lowest free energy state. A bainite microstructure is far from equilibrium. The free energy change accompanying the formation of bainite. Little is known about the nucleation of bainite except that the activation energy for nucleation is directly proportional to the driving force for transformation [19,52].However, unlike martensite, carbon must partition into the austenite during bainite nucleation, although the nucleus then develops into a sub-unit which grows without diffusion. The nucleation rate is dependent on the activation energy [19,195,134].All the phase transformations in steels can be discussed in the context of these two mechanisms as illustrated in Figure 2.9 [19]:

1) Displacive Tansformation (martensitic) is like shear process, because it is often associated with a change in crystal structure.

2) Diffusional Transformations. This is some times called a reconstructive transformation.

One of the reasons why there is a great variety of microstructures in steels is because the same allotropic transition can occur with a variety of ways in which the atoms can move to achieve the change in crystal structure. The transformation can occur either by breaking all the bonds and rearranging the atoms into an alternative pattern (reconstructive transformation), or by homogeneously deforming the original pattern into a new crystal structure (displacive or shear transformation).The pearlite is the good example of a reconstructive transformation. All experimentall data show that the pearlite grows with the diffusion of substitutional solute atoms [82,83].The substitutional solutes do not diffuse at all during displacive transformation. However the reduction of carbon content from 0.309 to 0.256% has a significant influence in raising the the transformation temperature as it would be expected from the phase digram. There is no measurable effect of the titanium addition on the Ar3 temperature. As reported by S. Zajac et al [222] there is some tendency for the Ar3 temperature to reduce at higher nitrogen levels especially for faster cooling rates. This may reflect some effect of V(C,N)

precipitation on the kinetics of ferrite growth. They reported, for example, that raising the nitrogen level from 0.001 to 0.02% accelerated all stages of the transformation, reducing the times by about 40%. In present study all features are present and from the metallographic examination of the specimens isothermally transformed in a salt bath after austenitization, then followed by water quenching as can be seen in Fig. 4.30.

5.2.1. THE MARTENSITE–START (MS) TEMPERATURE

The martensite–start (M_S) temperatures experimentally estimated in this work, together with values calculated using different empirical equations for both steel are given in table 4.4. As indicated in table 4.3. The (M_S) values show reasonable agreement, since different equatuions for Ms temperature are developed for different chemical compositions of steels.

During fast cooling (cooling rate larger than critical) austenite transforms to martensite below M_S temperature. The mechanism of martensite transformation is diffusionless, both during nucleation and during growth [19]. It was known already that martensite first phase forms at a large under-cooling, below the T_0 temperature, at which ferrite and austenite of identical composition have equal free energy [242]. The microstructure, (dislocation, vacancies, grain, twin, inter-phase boundaries, and precipitates), external stress and plastic deformation, may sometimes play an important role, but the chemical composition of a steel is a main factor in affecting its M_S [192,231].The basis for the calculation of the martensite–start (M_S) temperature was reviewed recently by Kaufman and Cohen [243]. However its experimentally estimated values of 320 °C for Ti-V-N microalloyed steel and 330 °C for V-N steel emphasize the small difference. It has been shown recently [231,244] that both Ms and Mf temperatures depend on carbon content and the austenite grain size. As reported by [245,246] the number of plates per unit volume needed in order to obtain a detectable fraction of martensite increases as the austenite grain volume ($V\gamma$) decreases. Since the prior austenite grain size is very simillar, the main reason for difference between two steels can be attributed to slightly higher content in carbon content in Ti-V-N steel.

5.2.2. GRAIN BOUNDARY ALLOTRIOMORPHS

The Grain Boundary Ferrite (GBF) the first phase to nucleate over the entire temperature range tested, is shown in Figures4.4(a-h), 5.1(a-e) and Figures 4.5(a-l), 5.2(a-c) for both steels investigated. Grain Boundary Ferrites are divided in two separate temperature regions,

describing the effects of dominantly diffusional and displacive transformations.The morphologies are initiated, what is represented by closed circles in Figure 4.30.The allotriomorphs nucleate having a reproducible orientation relationship such as the approximate Kurdjumov–Sachs orientation with one austenite grain (γ_1) [15,19].By contrast they also grow into the adjacent austenite grain (γ_2) with which they should normally have a random orientation relationship. The disordered boundary responsible for this growth should migrate more readily at high temperatures. Therefore, ferrite which grows by diffusional mechanisms, can be classified into two main forms: allotriomorphic ferrite and idiomorphic ferrite [94,95].Allotriomorphic ferrite nucleates at the prior austenite grain boundaries and tends to grow along the austenite boundaries at a rate faster than in the normal direction to the boundary plane (Figure 4.4 and 4.5). An allotriomorph has a shape which does not reflect its internal crystalline symmetry [19].This is because it tends to nucleate at the austenite grain surfaces, forming layers which follow the grain boundary contours (Fig.4.4 and 4.5). The allotriomorph is in contact with at least two of the austenite grains and will have a random orientation with one of them, but an orientation which is more coherent with the other. It may, therefore, be crystallographically facetted on one side but with a curved boundary on the other side.

5.2.2.1   Effect of allotriomorphic ferrite on acicular ferrite

A number of parameters favour the formation of acicular ferrite over ordinary bainite: the presence of non-metallic inclusions, large austenite grain size, and the decoration of austenite grain boundaries with uniform layers of allotriomorphic ferrite. The mean size of the prior austenite grain measured by line intercept method is 60 μm for Ti-V-N steel and 55 μm, for V-N steel, which is in rather good agreement with the critical size for the transformation of acicular ferrite reported in previous work [141-144].In general, allotriomorphic ferrite at the prior austenite grain boundaries is helpful to the formation of acicular ferrite because it renders the boundaries inert to the formation of bainite sheaves [15].

5.2.2.2   Widmanstaetten Ferrite

These plates grow along well-defined planes of the austenite and do not grow across the austenite grain boundaries. Primary widmanstätten ferrite grows directly from the austenite grain surfaces, whereas secondary widmanstätten ferrite develops from allotriomorphs of ferrite already present in the microstructure Figures 5.1(e,g) and 5.2(d).During widmanstatten

ferrite formation carbon must partition into the austenite (carbon must be allowed to partition during nucleation) during bainite and Widmanstatten ferrite nucleation [15,52,105,134] although the nucleus then develops into a sub-unit which grows without diffusion.
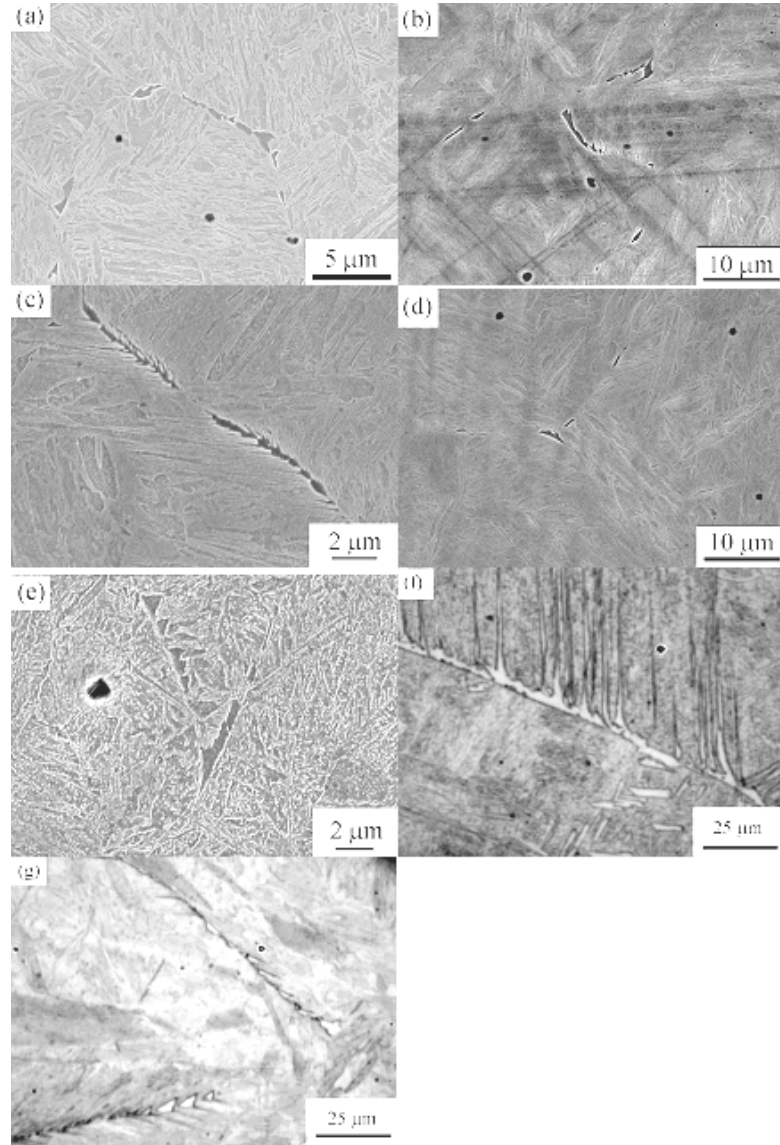
Figure.5.1 Selected microphotographs showing onset of Grain Boundary Ferrite (GBF)/ Widmanstatten formation at different isothermal treatment.in V-N steel: (a) 10s at 600°C (b) 5s at 550°C. (c) 03s at 500°C (d) 02s at 450°C (e) 02s at 400°C. (f) 10s at 400°C. (g) 02s at 450°C.
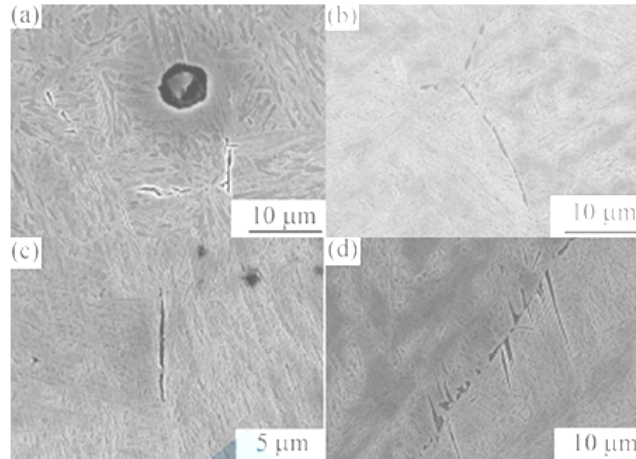
Figure 5.2. Selected microphotographs showing onset of Grain Boundary Ferrite (GBF) / Widmanstatten formation in Ti-V-N: (a)10s at350 °C; (b) 10s at 550 °C ; (c) 5s at 450 °C; and (d) 10s at 500 °C.

5.2.3.   FORMATION OF INTRAGRANULAR FERRITE (IGF)

5.2.3.1 Interlocked Acicular Ferrite

At the initial stages, the nucleation of the primary ferrite plates takes place intragranularly at second phase particles (nonmetallic inclusions and/or precipitates) present in the austenite, as can be seen in Fig. 4.8 and Fig. 4.9, which is in good a greement with [15,46,49,94,96,234]. By its nature, the microstructure of acicular ferrite is less organized, i.e. more chaotic. Several mechanisms have been proposed to explain why non-metallic inclusions favour the nucleation of ferrite: (i) the existence of local variations of the chemistry of the matrix [247](ii) generation of strain-stress field around the inclusions due to the different thermal expansion coefficient of austenite and inclusion [248,249] and (iii) improvement in the global energetic balance of the transformation by the reduction of the austenite-inclusion surface [250,251] and finally the creation of low-energy surfaces between ferrite and inclusion with the existence of a good lattice matching between them [15,36,252-258].For example, low degree of misfit between the ferrite matrix and the substrate crystal lattice is assumed [254-260] to increase the nucleation potential of inclusions. Therefore, TiN with a misfit ratio of 3.8 [256] should be much more effective than MnS with misfit ratio of 8.8 [254]. Additionally, the nucleation at particles can be more favorable energetically with the segregation of some alloying elements to grain boundaries, the reason because, the interfacial energy per unit area of the grain boundaries is lowered, as reported by Ricks et al [261].
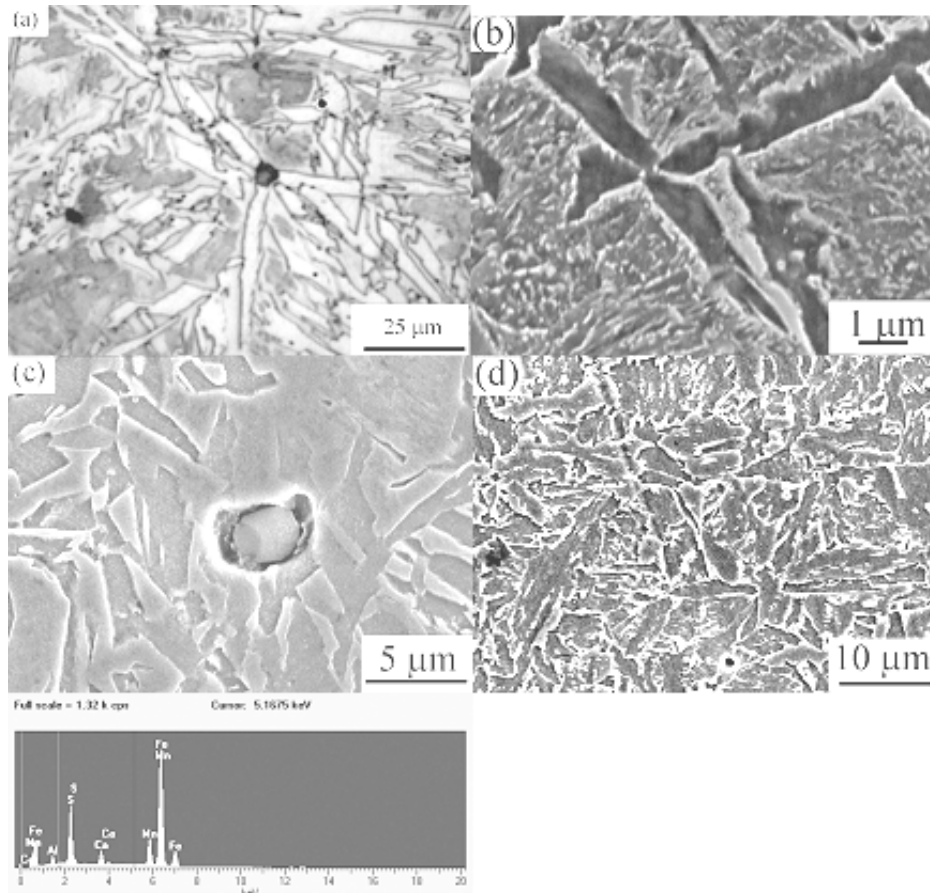
Figure 5.3 (a-d) Optical micrographs and SEM image of V-N steel showing of acicular ferrite on inclusion after (a) 30s at 500°C.(b) 20s at 450 °C.5(c) SEM image and EDX spectrum showing the type of the inclusion exist. 5(d) SEM image showing the acicular ferrite microstructure after 1200s at 450 °C.
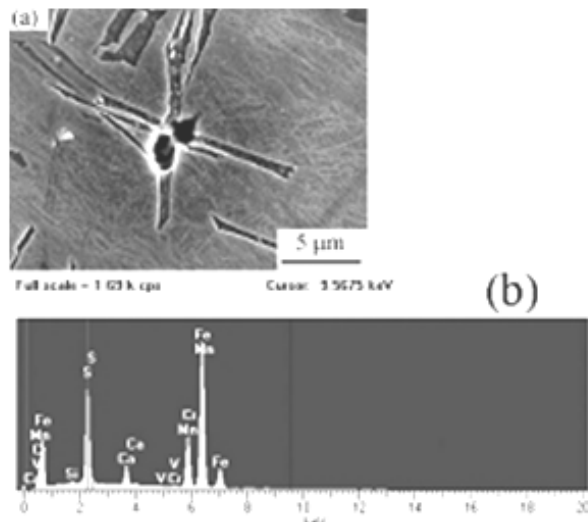
Figure 5.4(a) Acicular ferrite nucleation at inclusion after 30s at 500 °C - SEM image; (b) EDX spectrum of present inclusion: Thus for Ti-V-N steel.

In this work, MnS plays important role in acicular ferrite nucleation. The manganese sulfides have been reported previously to be active on nucleating acicular ferrite [36,39,94,96,208,235,262,291,292]. Moreover the inclusion size and shape is modified by Ca treatment. Presence of Ca significantly increases the elastic modulus of MnS and lowers its deformability. Another benefit is that together with Young's modulus, the surface tension is also increased, which in turn, provides globular shape of MnS inclusion and low concentration factor and improved toughness. MnS particles represented the largest contribution (60-70%) to the overall inclusion volume fraction [263],and they serve also as preferential places for VN precipitation. This is well documented on figures 4.8 and 4.9, where EDS have showed presence of Mn, S, Ca and V on the particle.

However the nucleation of AF plates is not restricted to inclusions, new ferrite plates can grow from pre-existing ones, as can be observed in Figure 5.3(c, d) and 5.4(b.c) , which supports the view, that nucleation occurs sympathetically. In Figure 5.3(c, d) and 5.4(b.c), the sympathetic nucleation of secondary acicular ferrite plates has been observed to occur at the austenite/primary acicular ferrite interface and continue to grow within the austenite matrix until impingement occurs with other plates. An example of impingement processes is illustrated in the SEM micrographs as clearly shown in Figure 5.3(d,f). The result of multiple sympathetic nucleation is an interlocking ferrite network, and after sufficient time, it results into a complex interlocking ferrite microstructure, characteristic of acicular ferrite, such as that shown in Fig. 4.10(k,l), Fig. 4.23(d), Fig. 4.24(d) and Fig. 4.27(a,b) respectively. The resulting microstructure with fully acicular ferrite structure in medium carbon microalloyed steel, with the exception of a few small bainitic zones is in good agreement with published data [36]

Effect of Vanadium on Acicular Ferrite Formation. The acicular ferrite microstructure was obtained in V -microalloyed steels containing high, medium or very low nitrogen levels [40]. This attributed to suggests that vanadium on its own can promote the formation of the acicular ferrite microstructure.For both types of steels investigated, it was shown that vanadium contributes to the onset formation of two types of intragranulary nucleated ferrite; polygonal (idiomorph) ferrite as illustrated in Fig. 4.7, and acicular (sideplate) ferrite as can be seen in Fig. 4.10, 4.23(d) and 4.24(d).This is in good a greement with published data[40]. Intragranular polygonal ferrite nucleates on VN particles that grow in austenite during isothermal holding or slow cooling throughout the austenite range.

Effect of allotriomorphic ferrite on acicular ferrite formation. A number of parameters favour the formation of acicular ferrite over ordinary bainite: the presence of non-metallic inclusions, large austenite grain size, and the decoration of austenite grain boundaries with uniform layers of allotriomorphic ferrite. The mean size of the prior austenite grain measured by line intercept method is 60 μm for Ti-V-N steel and 55 μm, for V-N steel its standard deviation is 5 μm, which is in rather good agreement with the critical size for the transformation of acicular ferrite reported in previous work[36,54,98,136,141,144].In general, allotriomorphic ferrite at the prior austenite grain boundaries is helpful to the formation of acicular ferrite because it renders the boundaries inert to the formation of bainite sheaves [15].

5.2.3.2. Sheaf Type Acicular Ferrite (STAF) Morphology

Two differences of microstructues were produced after 20 seconds of isothermal treatment at 450 °C and 400 °C: an interlocked microstructure and a microstructure composed by sheaves of parallel ferrite plates. This is in good agreement with published data [234,235], as can be seen in the Figure 4.12. At 450 °C, the austenite has transformed to acicular ferrite, giving rise to the characteristic interlocking microstructure. However, at 400 °C, the austenite has transformed to sheaf type acicular ferrite (STAF) or generation of plates developed in a parallel sheaf formation i.e there is more tendency to form sheaves composed by parallel plates, but the origin is not the grain boundaries and the final microstructure is composed of packets of plates following the same growth direction, as is shown in Figure 4.12 and it is called sheaf morphology or sheaf type acicular ferrite (STAF). In regards to the nucleation of the first acicular unites takes place intra-granularly at non-metallic inclusions present in the austenite and by comparing the micrographs corresponding to 10 seconds of isothermal at 450 °C and 400 °C, it can be seen that at initial stages, the transformation proceeds identically in both cases as demonstrated in Figure 4.6(f) and 4.8(h). The difference in the microstructure obtained at the two temperature become pronounced as the transformation progressed beyond 10 seconds, i.e., after the initiation of the first generation of plates from inclusion as can be seen in Figure 4.7(a-f). At 400 °C, the second generation of plates developed in a parallel sheaf formation as can be see in 4.12. By contrast the transformation at 450 °C progressed with non parallel plates. As illustrated in Figure 4.10(a-d), the plates nucleated on the face of a substrate plate must have a different habit plane and orientation, leading to a chaotic microstructure. By contrast, a plate nucleating at the tip of the substrate plate must be identical variant with the same habit plane and orientation, giving rise to a sheaf

microstructure. There is tendency to form sheaves composed of parallel plates but the nucleation does not take place at the grain boundaries.

Transition between an Interlocked and Sheaf Morphology. The transition between an interlocked morphology and sheaf type morphology was estimated to occur at 450/400 °C. This morphological transition can be related to the transition from upper to lower acicular ferrite and to differences in the carbon concentration profiles in the parent austenite in the front of the interface of the primary acicular plates depending on the treatment temperature. As it is suggested [234,235], that at the initial stages for the transformation at 400 °C, the carbon concentration profile in austenite close to the tips of primary plates must be lower than at the faces favouring the nucleation on the tips of same variants as the primary plates and that is the reason why sheaf type AF will form on the expense of interlocked type. Whereas at 450 °C, the stronger diffusion of carbon from the austenite/ferrite interfaces makes possible the plate nucleation on faces i.e the carbon is able to diffuse away from the austenite / ferrite interfaces in shorter times than at 400 °C. This is expected to allow the nucleation of new ferrite variants on the primary plate faces in agreement with interlocked plate microstructure obtained at 450 °C, as seen in Figures 4.23(d),4.24(d),4.27(a,b) and Fig 4.10(k,l),for both steels.The resulting microstructure with fully acicular ferrite structure in medium carbon microallyed steel, with the exception of a few small bainitic zones is in good agreement with published data [36]. Also as pointed out previously the presence of a uniform layer of allotriomorphic ferrite along the austenite grain boundaries induces the transformation of austenite in acicular ferrite instead of bainite. In spite of the absence of a ferrite layer at the grain boundaries, due to the severe cooling rate from the austenitizing to the isothermal treatment temperature. However the transition between an interlocked morphology and sheaf morphology was analyzed at two temperatures: 400 and 450 °C. This morphological transition can be related to the transition from lower to upper acicular ferrite and to differences in the carbon concentration profiles in the parent austenite in the front of the interface of the primary plates depending on the treatment temperature.

5.2.3.3. Intragranular Idiomorphs

Figure 4.7 show presence of the idiomorphic ferrite nucleated intra-granularly at the non-metallic inclusions present inside the austenite grains and can be identified in the microstructure by its equiaxed morphology (Figure 4.7),and the volume fraction of

idiomorphic ferrite is related to the volume fraction of inclusions in steel [94].It starts nucleation after grain boundary ferrites significantly decorates PAGS.

5.2.4. BAINITIS SHEAVES

Two different of intragranular ferrite morphologies are present at the beginning of the transformation at low temperatures (350, 400 °C), bainite sheaves BS, and sheaf type acicular ferrite (STAF) and at certain localized places widmanstatten ferrite (WSF), as can be observed in Fig. (4.16), (4.11) and (4.16) respectively.The origin of sheaves are the grain boundaries (grain boundary nucleation is always energetically more favorable than the nucleation on inclusions [15,98,134].

5.2.5 PEARLITE

Nucleation of pearlite directly depends on the chemical composition of austenite after interlocked acicular ferrite is formed. Due to faster growth of interlocked acicular ferrite, in the case of V-N steel, supersaturation of remaining austenite is earlier achieved, enabling start of pearlite transformation. It is worth noting that pearlite occurs in temperature region 500-600°C in both steels. Pearlite is a diffusional transformation so its growth requires the diffusion of all elements including iron. Pearlite has never been shown to grow by the para-equilibrium transformation of austenite [98]. As illustrated in Figure 4.22.The dark-etched pearlite is located at the ferrite grain boundaries. Because of the higher manganese content for both steel investigated. This is good a greement with published data [41].The presence of a hemispherical shape nodules of pearlite at austenite grain boundary is attributed to sideways nucleation and then by increase the treatment time it gradually growing into austenite grains by edge-ways growth. So by increase the treatment time it gradually growing into austenite grains, as can be clearly seen in Fig. 4.22 (b). Because the nucleation of pearlite will depend on the diffusion of carbon in austenite. By contrast as reported by Mehl and co-workers [19], the growth rate of pearlite will depend on both, diffusion coefficient of carbon in austenite and pearlite interlamellar spacing. Consequently, as the temperature is lowered the pearlite interlamellar spacing is reduced, its compensate decrease in diffusivity with decreasing temperature.

5.2.6.   INCOMPLETE TRANSFORMATION PHENOMENON

The transformation after1200s of isothermal treatment at 550 and 600 $^{\circ}$C reveals that a fraction of austenite remains untransformed, Fig. 4.18. This phenomenon has been described by Bhadeshia [19,104,208,234] and is known as incomplete reaction phenomenon. It is presented by dashed line on TTT diagram in Figure 4.30. At 600 $^{\circ}$C, there was higher grain boundary ferrite at the prior austenite grain boundary. In respect to the volume of the untransformed austenite and the population density of ferrite plates inside the prior austenite grains is lower than at 550 $^{\circ}$C as can be observed in figures 4.24(a,b). This seems to indicate that at 600 $^{\circ}$C, the carbon rejected from the ferrite plates diffuses rapidly leading to supersaturation in austenite. The carbon enrichment of the remaining austenite together with relatively small driving force for transformation at 600 $^{\circ}$C is enough to inhibit the formation of new ferrite plates [15,104,208,234]. This additionally confirmed by the sharp increase of yield strength in specimens transformed in range 500-600°C. The increase is attributed to presence of martensite due to presence of stabilized austenite.

5.2.7. OTHER PRODUCTS OF AUSTENITE DECOMPOSITION

5.2.7.1.   Precipitation Free Plates

The present results clearly show no carbides were observed to form within the ferrite plates at intermediate time and temperature (450-500 $^{\circ}$C), the reason is probably due to the presence of enough Si in the steel, which, delays cementite precipitation [36] as can be seen in Fig.4.19. This is good a greement with published data [19,234,235,264] At 450-500 $^{\circ}$C, the majority of plates are free of precipitates due to the carbon diffusion, favouring the decarburisation of the ferrite plates body and the microstructure can be better identified as upper acicular ferrite. By contrast at 400 $^{\circ}$C, the carbon diffusivity in austenite decreases and this element probably concentrates in the austenite close to the ferrite plate faces favouring the nucleation of the same variants from the tips of the primary plates. The lower redistribution of carbon in austenite, as a result of the decrease of its diffusivity, together with the formation of sheaves of parallel plates at 400 $^{\circ}$C, produces as a consequence, high amounts of carbon remain trapped in thin layers of austenite between parallel plates favouring its stabilization. For longer times, this carbon probably precipitates as cementite or alloyed carbide, it is appear at the ferrite plates interiors. These carbides are elongated and form angles comprised between 50° and 60° with the α/γ interfaces.

5.2.7.2. Intragranular Plates:

These plates are similar to those growing from the grain bundaries, but they nucleate entirely within the austenite grains (Fig. 4.15).

5.2.7.3. Banded Microstructure

The microstructure obtained after certain treatment time and temperature as mentioned in section 4.3.9 contains banded microstructure.It is attributed due to chemical solute segregation. The microstructure bands follow the segegation pattern becouse it is the local chemical composition that determines the onset of transformation. The Mn segregation of substitutional solutes which is the real cause of banding [15].The substitutional-solute depleted regions cause a partitioning of carbon into the adjacent substitutionally-enriched regions as can be seen in Fig. 4.20. Khan and Bhadeshia [237], suggest that the segregated steel is able to transform in its solute-depleted region at temperature above B_S temperature ($B_S \equiv 500$ $^\circ$C for Ti-V-N steel). This is in good a greement with present study. By contrast,most of the partitioned carbon remains in the substitutional solute depleted regions of the segregated sample and retards the development of transformation [15].Where as the presence of horizontal parallel lines was clearly observed on the surface of the sample during polishing processes.

5.3. EFFECT OF ALLOYING ELEMENTS ON MICROSTRUCTURE

5.3.1 THE EFFECT OF VANADIUM

For high reheating temperature (1250 °C) transformation behavior changes in both the V-N and V-Ti steel. It could be expected that, in addition to a larger austenite grain size, the VN particles are completely dissolved at these temperatures. The presence of grain boundary ferrite in both steel (Fig. 4.4 and Fig.4.5) imply that the effect of vanadium segregation to grain boundaries and consequently hardenability are somehow diminished. It can be assumed that at high reheating temperatures, due to the thermal dispersion, vanadium is more evenly distributed throughout the austenite grain interior[265],so it's concentration at grain boundaries is diluted and therefore an inhibiting effect on grain boundary ferrite nucleation is precluded. The increase of austenite grain size at high austenitization temperatures, (Fig. 4.1m.), acts in favor of the acicular ferrite formation, since intragranular nucleation is

promoted by a greater number density of inclusions than austenite grain surface nucleation sites [15].By contrast the V-containing steel shows higher retarding effect on transformation than the V-free steel. Due the role of VN particles in intragranular nucleation of acicular ferrite [140,169,259,260,266], it is assumed that acicular ferrite nucleation in the V-free steel is less probable. In this regard, TiN particles shouldn't be omitted, but it seems that they are less potent as nucleation sites, since crystal lattices misfit ratio with ferrite (3.8%) is higher than in the case of VN (1.3%) [256].This consideration and present results support earlier findings that VN particles are preferential sites for intragranular nucleation of acicular ferrite. In fact, VN precipitates on the manganese sulfide particles which then act as sites for the intragranular nucleation of acicular ferrite [140,259,260].On the other hand, He and Edmonds [162,173], offer an alternative mechanism for intragranular acicular ferrite nucleation. They suggest that vanadium segregates to austenite grain interiors and form vanadium rich regions or Fe–V clusters that could be energetically favorable sites for acicular ferrite nucleation.

5.3.2 EFFECT OF NITROGEN

In the present steels (High-N steels) great deal of vanadium is assumed to be in VN at 1100°C (temperature for complete dissolution of VN is 1100 °C, Table 4.2), implying that less vanadium is available to segregate to grain boundaries. Therefore, grain boundary ferrite formation is not suppressed and intragranular nucleation of acicular ferrite is promoted. It seems that higher nitrogen content suppresses the formation of bainite. Therefore the high nitrogen creates the more favorable condition for VN precipitation on MnS inclusions which then serve as the preferred site for acicular ferrite nucleation[259].In regard to the austenitization at (1100 °C), the microstructures of both steels are practically the same. They consist predominantly of acicular ferrite structure at (450 and 500°C) as isothermal treatment (which is favored on transformation from a large austenite grain size [15], as illustrated in Fig. 4.23(c,d) and Fig.4.24(c,d). The fact that the microstructures of both steels are similar indicates that 6 ppm of N in Ti free steel seems to be sufficient to promote the precipitation of VN on MnS particles,which then serve as the nucleation sites for the formation of acicular ferrite. Recent results of Garcia-Mateo et. al *,* show that VN particles formed in austenite are particularly effective as acicular ferrite nucleation sites [39,40,140,169,266].In that respect, it could be assumed that even at low nitrogen content VN particles precipitate in austenite when

cooled from high austenitizing temperatures since there would be enough vanadium available in the grains interior due to thermal dispersion.

5.3.3. EFFECT OF TITANIUM

Based on the results in Fig. 4.1m , it can be seen that compared with the austenite grain size of the V-N steel, the Ti-V-N steel has the smallest austenite grain size above 1100°C. These can attributed to, the addition of Ti can result in fine TiN precipitates, which can inhibit austenite grain growth at high temperatures because of their strong high-temperature Stability, the predicted results is rather good agreement with the data given in Refs. [267-269].However, the level of added Ti must be well controlled because, an improper addition can easily produce coarse TiN particles and coarse TiN inclusions are so harmful to the toughness of steels.

5.3.4. EFFECT OF CARBON

The reduction of carbon content from 0.309 to 0.256% has a significant influence in raising the the transformation temperature as it would be expected from the phase digram. There is no measurable effect of the titanium addition on the Ar_3 temperature. As reported by S. Zajac et al [222], there is some tendency for the Ar_3 temperature to reduce at higher nitrogen levels especially for faster cooling rates. This may reflect some effect of V(C,N) precipitation on the kinetics of ferrite growth. Raising the nitrogen level from 0.001 to 0.02% accelerated all stages of the transformation, reducing the times by about 40%. In present study and from the metallographic examination of the specimens isothermally transformed in a salt bath after austenitisation, then folliwed by water quenching as can be seen in Fig 4.30. These results showed the time for the on-set of pearlite transformation in the 0.309%C (Ti-V-N) steel was about 2 times greater than for the 0.256%C (V-N) steel.

5.4 TTT DIAGRAMS

5.4.1 Nucleation Stages

Data related to nucleation phase of isothermal decomposition seems to be lacking; most of the published results deal with later steps (10s or longer). Metallographic evaluation using optical and scanning electron microscopy (SEM) enabled determination of the nucleation curves of isothermally decomposed austenite. Three curves are found to be relevant to this initiation

stage of transformation: as can be seen in Figure 4.30. First curve is related to grain boundary nucleated ferrite (GBF) Figures 5.1 and 5.2, second curve is related to intragranularly nucleated ferrite (IGF) – Figures 5.3 and 5.4 and the third the pearlite (P) curve -Figures 5.5 and 5.6. GBF and IGF curves are divided into the high temperature and the low temperature segments as consequence of either displacive or diffusion nature of transformation. The experimentally determined TTT diagram for both steels is presented in Figure 4.30. The main difference in nucleation stages for two steels tested is that Ti-V-N steel exhibits longer incubation period. This behaviour is attributed to higher content of carbon. Higher presence of carbon atoms in lattice (supersaturation) generally delays diffusion governed processes due to required higher difference in chemical composition between austenite and nuclei of allotriomorphic ferrite. In the case of Widmanstatten ferrite, higher supersaturation is also responsible for delay. In the case of intragranularly nucleated ferrite, it seems that due to higher presence of V and N, acicular ferrite is easily nucleated in V-N steel. Nucleation of pearlite directly depends on the chemical composition of austenite after interlocked acicular ferrite is formed. Due to faster growth of interlocked acicular ferrite, in the case of V-N steel, supersaturation of remaining austenite is earlier achieved, enabling start of pearlite transformation. It is worth noting that pearlite occurs in temperature region 500-600°C in both steels.

5.4.2 Microstructure Evaluation

The Grain Boundary Ferrite (GBF) the first phase to nucleate over the entire temperature range tested, is shown in Figures 5.1(a-e) and Figures 5.2(a-c) for both steels investigated and is represented by a two C curves, describing the effects of diffusional (upper C curve) and displacive (lower C curve) transformations. Within the lower C-curve a clear indication of Widmanstatten nucleation is observed Figure 5.1(e-g) and Figure 5.2(d).At a later stage of transformation different intra-granular ferrite (IGF)morphologies are initiated, what is represented again by the two- C (IGF) nucleation curves in Figure 4.30. In the (IGF) region, three different morphologies have been observed depending upon the isothermal treatment temperature.

Firstly, at high temperatures ($\geq$ 550 $^{\circ}$C) intragranulary nucleated ferrite combined with grain boundary ferrite (GBF) and pearlite (P) are produced, as can be seen in Figure 5.5(a,b). The intragranular ferrite is characterized by polygonal idiomorphic (IGF) Ferrite. The idiomorphic

ferrite nucleates intra-granularly at the inclusions distributed inside the austenite grains, and the volume fraction of idiomorphic ferrite is related to the volume fraction of inclusions in steel [94]. Also the transformation after1200s of isothermal treatment at 550 and 600 $^\circ$C reveals that a fraction of austenite remains untransformed, (UA) Fig.5.5. This phenomenon has been described by Bhadeshia [15,208,209,234] and is known as incomplete reaction phenomenon. It is presented by dashed line on TTT diagram in Figure 4.30.
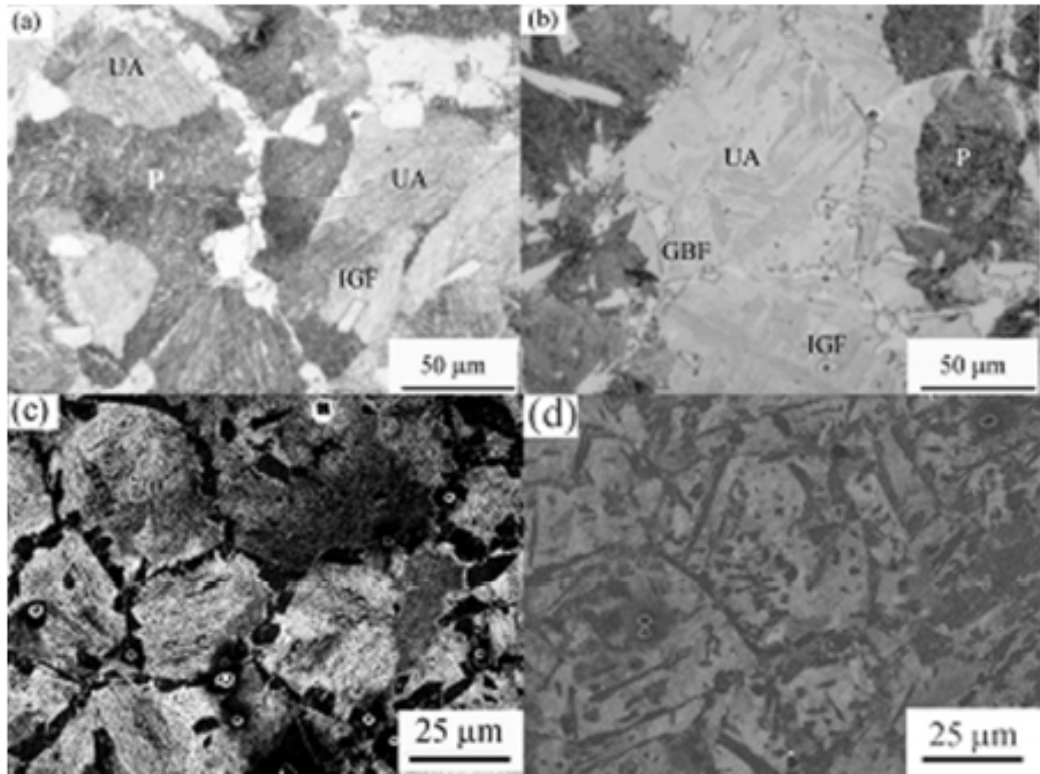
Figure 5.5 (a-d).Microstructures of Ti-V-N steel obtained after 1200s at high temperatures: (a) 600 $^\circ$C; (b) 550°C; (c) 600 $^\circ$C; (d) 550 $^\circ$C, (UA-Untransformed austenite).
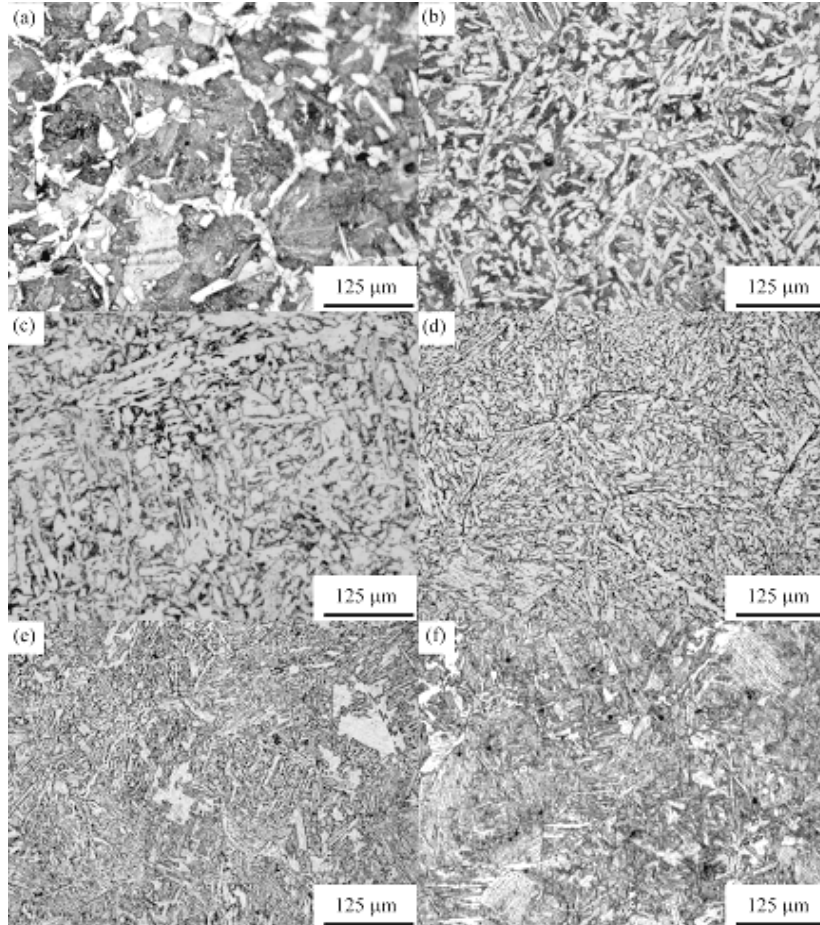
Figure 5.6 (a-f). Optical micrographs showing the microstructures obtained after 1200s at low (350, 400 °C), intermediate (450, 500 °C) and high (550, 600 °C) of isothermal transformation temperatures. : Thus forV-N steel.at (a) 600 °C (b) 550 °C (c) 500 °C (d) 450 °C (e) 400 °C (f) 350 °C.

At 600 °C, there was thicker grain boundary ferrite than at 550 °C, but in respect to the population density of ferrite plates inside the prior austenite grains it is lower as can be seen in Fig.5.9(a,b).This seems to indicate that at 600 °C, the carbon rejected from the ferrite plates diffuses rapidly leading to supersaturation in austenite. The carbon enrichment of the remaining austenite together with relatively small driving force for transformation at 600 °C is enough to inhibit the formation of new ferrite plates [234] Second type of intragranular ferrite morphologies occur at intermediate temperature (450 and 500°C). An interlocked acicular ferrite(AF)microstructure is produced for both of steel investigated. At the initial stages, the nucleation of the primary ferrite plates takes place intragranularly at second phase particles (nonmetallic inclusions) present in the austenite, as can be seen in Figure 5.3 and Figure 5.4, which is in good agreement with [15,46,49,94,96,234,284].The micrograph

present and an energy dispersive X-ray (EDX) spectrum analysis illustrate a typical active inclusion, with the corresponding chemical analysis at different points of the particle, it is identified as Ca-treated manganese sulfides inclusion (MnS) core covered or at least partially covered with VN or V(C, N) complex precipitate. This is in good agreement with results reported by Ochi et al and Ishikawa et al [208,260].

The resulting microstructure with fully acicular ferrite structure in medium carbon microallyed steel, with the exception of a few small bainitic zones is in good agreement with [36].However the temperature at which the incubation time for ferrite nucleation is at minimum is approximately at 450 ^{o}C (Figure 4.30). The incubation time is the minimum time at which it is possible to find some ferrite nucleated at the austenite grain boundary.The maximum acicular ferrite content in the present steel is found for treatment carried out at 450 ^{o}C as illustrated in Fig. 5.7(a,b) and Fig. 5.3(d). This treatment is characterised by the fully acicular ferrite formation. On the other hand, it is possible to find, in certain localized places, bainite formed at the grain boundaries, as shown in in Fig. 5.7e and 5.8d.
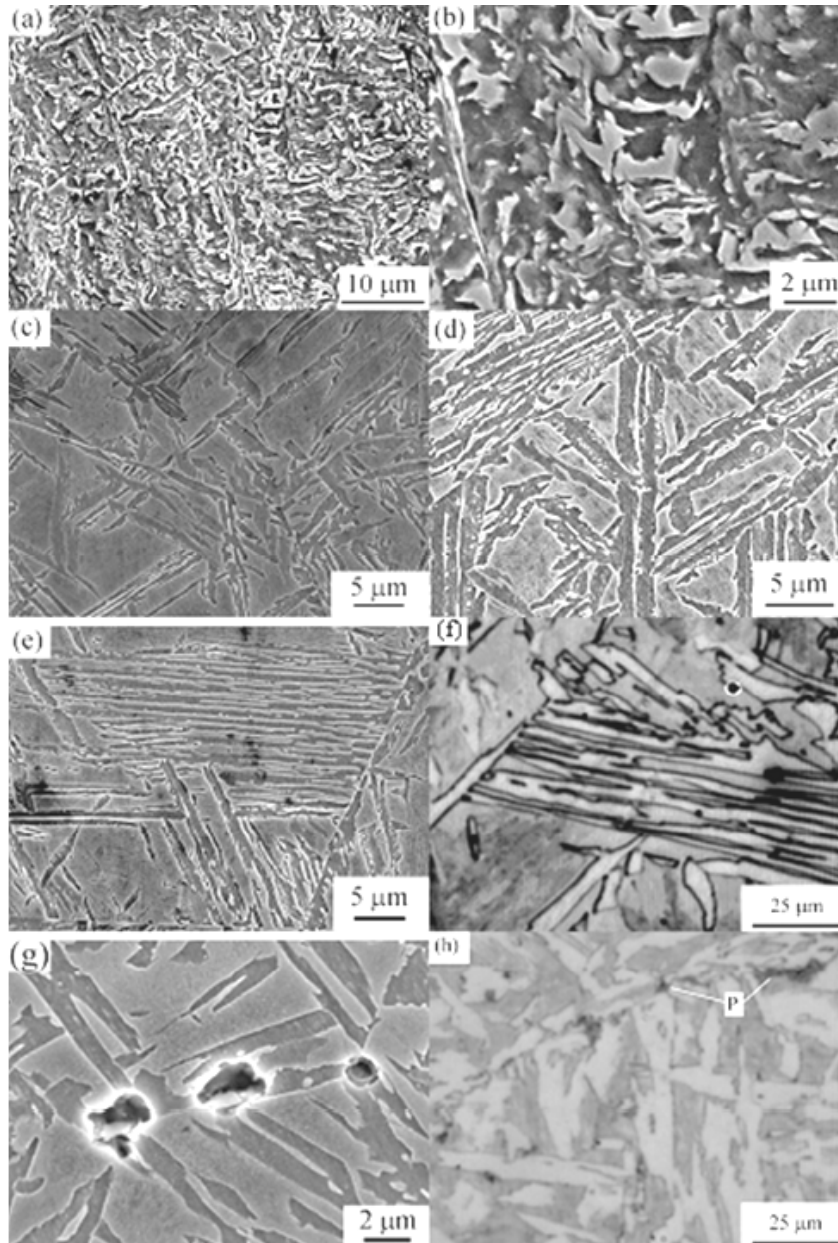
Figure 5.7. Details of microstructure of Ti-V-N steel produced at 450 and 500 $^\circ$C: (a,b) SEM image showing the acicular ferrite microstructure after 600s at 450 $^\circ$C. (c) Sympathetic nucleation of acicular ferrite after 20s at 450 $^\circ$C - SEM image (d) Impigment processes at 450 $^\circ$C /30s; (e) Bainite area formed after 20s at 450 $^\circ$C. (f) Optical and (g) SEM image showing dominance of precipitate free plates after 30 and 80s at 500°C respectively.(h) Pearlite (P) onset at 500 $^\circ$C / 120s.

At 450-500 $^\circ$C, the majority of plates are free of precipitates due to the carbon diffusion is high, favouring the decarburisation of the majority of ferrite plates, as can be seen in Fig.

5.8e. The microstructure can be identified as upper acicular ferrite. The onset of pearlite at different a treatment temperature (≥ 500 $^\circ$C) is illustrated in Fig. 5.6a and Fig.5.6b and P-line in Figure 4.30. Also it is apparent, from the shape of TTT-diagram in Figure 4.30, that the bainitic transformation start temperature (B_S) occurs at 510 ± 10 $^\circ$C for Ti-V-N steel. However the bainitic transformation start temperature (B_S) occurs at 530 ± 10 $^\circ$C for V-N steel. This result is in good agreement with B_S temperature calculated by Formula [15,19,224,232,270].
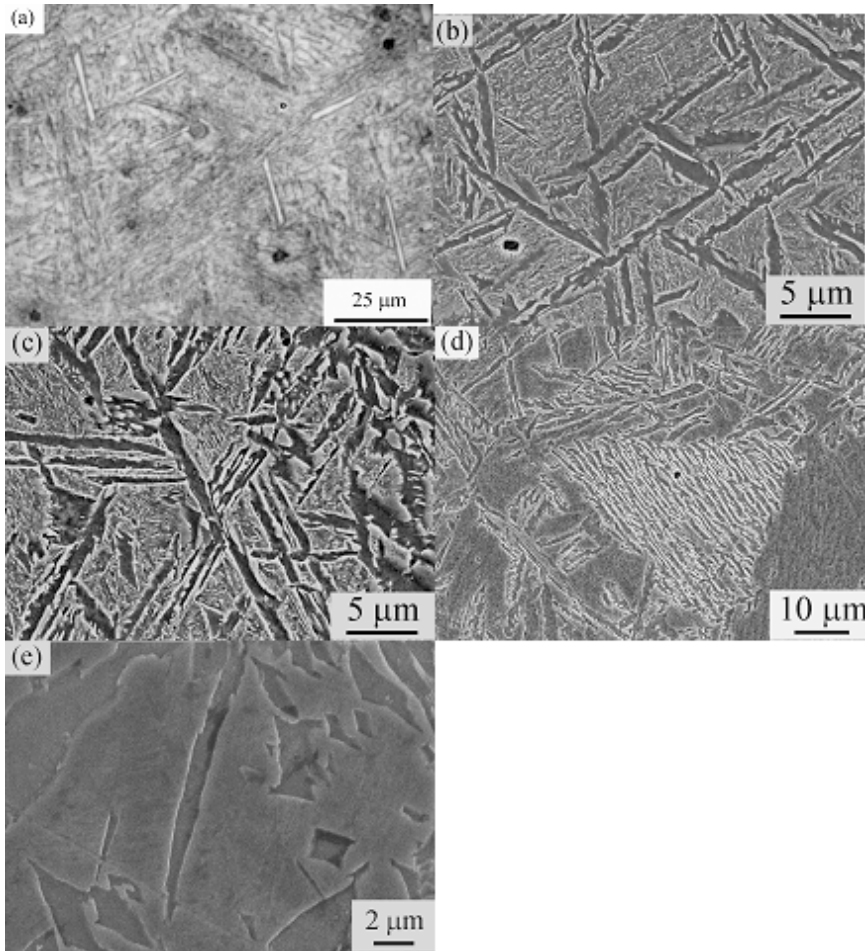
Figure 5.8 (a) Optical micrograph image of V-N steel after10s at 450°C. (b,c) SEM image after 20s at 450 $^\circ$C (d) SEM image showing an isolated bainite area formed in the steel sample treated for 30s at 450 $^\circ$C. 6 (e f) SEM image show the majority of plates are free of precipitates after 30s at 500 $^\circ$C.

The third type of intragranular ferrite morphology exist at low temperatures (350, 400 $^\circ$C). Two different morphologies are present at the beginning of the transformation, Bainite sheaves BS as can seen in Figure 5.3(a), 5.4(a) and interlocked AF as can seen in Figure 5.3

(b), 5.4(b). The origin of Bainitic sheaves are exclusively the grain boundaries. The nucleation of (BS)is indicated in Fig. 4.30. by open triangles.When the isothermal treatment times is increased a new intragranular morphology known as the sheaf type acicular ferrite (STAF) [235] is observed as can be seen in Figure 5.3(c), 5.4(c). There is tendency to form sheaves composed of parallel plates but the nucleation does not take place at the grain boundaries. The transition between an interlocked morphology and sheaf type morphology was estimated to occur at 450/400 °C. This morphological transition can be related to the transition from upper to lower acicular ferrite and to differences in the carbon concentration profiles in the parent austenite in the front of the interface of the primary acicular plates depending on the treatment temperature. As it is suggested [234,235], that at the initial stages for the transformation at 400 °C, the carbon concentration profile in austenite close to the tips of primary plates must be lower than at the faces favouring the nucleation on the tips of same variants as the primary plates and that is the reason why sheaf type AF will form on the expense of interlocked type. Whereas at 450 °C, the stronger diffusion of carbon from the austenite/ferrite interfaces makes possible the plate nucleation on faces i.e the carbon is able to diffuse away from the austenite / ferrite interfaces in shorter times than at 400 °C. This is expected to allow the nucleation of new ferrite variants on the primary plate faces in agreement with interlocked plate microstructure obtained at 450 °C.

However At 500 °C, some small colonies of pearlite have been formed between the acicular ferrite plates. As the transformation temperature is reduced to 450 °C, the refinement of the ferrite plate is achieved (agreat number of adjacent ferrite plates present). In this case, the austenite has transformed to fine or lower acicular ferrite, giving rise to the characteristic interlocked microstructure.

5.4.3 BAINITIC TRANSFORMATION START TEMPERATURE (B_S)

It is apparent, from the shape of TTT-diagram in Figure 4.30, the start temperature of the bainitic transformation (B_S) temperature seems to be occurs at 520 °C for Ti-V-N steel and at 550 °C for V-N steel. This result is in good agreement with B_S temperature calculated by use of different empirical formula [15,19,232,270] and by Kirkaldy, Suehiro, Zhao and Steven & Haynes in ref.[224] as shown in details in table (4.5). The calculation results have shown that, B_S temperature exist at 529 ± 5 °C for Ti –V-N steel and it is exist in good agreement for

V-N steel. Hence, in present results the transformation at temperature close to bainitic start temperature B_s led to the formation of upper bainite, followed by pearlite at some time later.

5.5. MECHANICAL PROPERTIES

5.5.1.   HARDNESS

The Vickers hardness in each test in isothermal conditions show fairly uniform decreasing gradient as holding time increases. The microstructure of specimen consists of product of decomposition and martensite formed after quenching. This is the reason why all diagrams show steady decrease with time. It is assumed that decrease is governed by the difference in hardness of martensite and newly formed phases (acicular ferrite, pearlite, etc). Also, in all cases, higher value of hardness in Ti-V-N steel is attributed to higher content of carbon, because carbon has the strongest influence on hardenability [38,40,222,214].The hardness for both steels and conditions investigated here is summarized in Fig.4.32. It show very similar behaviour as YS for these two steels, and the equal explanation can be used, i.e. due to incomplete reaction phenomenon after 1200 seconds, untransformed austenite transforms into martensite increasing hardness (see section 5.5.2).

5.5.1.1   Effect of Holding Time

It is clear from Fig. 4.31.At holding time shorter than10s, there was no significant change in hardness for all samples, the main change in hardness occurred for hold times between 10 and 600s. However, with increase holding time, the decrease in hardness was greater. This suggests that more extensive precipitation occur. Beyond 600 s, the hardness changed only slightly, which indicates that precipitation in the austenite has reached saturation.

5.5.2   YIELD STRENGTH

The yield strength is the most important value for structure design because it determines the stress at which the materials beginsto deform plastically after dslocations start the glide [271]. A usual practice when considering the strength of structural steels is to express the yield stress by a series of terms representing (i) the iron matrix, (ii) solid solution effects, (iii) grain size, (iv) precipitation hardening and in some cases also (v) pearlite content [222]. The V is usually

the preferred element when precipitation strengthening is required in forged products. A addition of 0.10%V can bring about a strength increase beyond 250 MPa, and in special cases even up to 300MPa [209]. Also nitrogen in small contents adds significantly to precipitation strengthening due to the larger driving force in the high-N steels than in the low-N steels [42] because it will cause a denser precipitation. The particle strengthening occurs by the Orowan mechanism – bowing of dislocations between particles – and in that case the decisive parameter is the interparticle spacing in the slip plane. In turn, that is determined by the density of the precipitates. This density is controlled by the nucleation frequency and the number of nuclei it creates until the supersaturation has diminished so that nucleation dies. The essential parameter governing the variation in nucleation is the chemical driving force for V(C,N) precipitation. Therefore, dissolution of all V containing particles plays very important role in industrial practice. The yield strength properties of the experimental steels are reported in Sec. 4.5.3. When the steels are separated into the two classes according to carbon and titanium content. More surprising are the marked decreases in yield stress for V-N steel occasioned by the reduction in carbon level from 0.309 to 0.256 % as well as by the the presence of so little as 0.011 % titanium.The actual decrements in yield stress lie in the range of 80-100 MPa, for both low (400, 350 $^\circ$C) and high temperatures ($\geq$ 550 $^\circ$C), 20-25 MPa for intermediate temperatures (450, 500 $^\circ$C).As can be seen in Table 4.17 and Fig. 4.36. The degree of precipitation strengthening of ferrite at a given vanadium content depends on the available quantities of carbon and nitrogen. It is concluded that nitrogen is a very reliable alloying element, increasing the yield strength of V-microalloyed steels by some 6 MPa for every 0.001% N [40]. Concurrently as the carbon content is increased the chemical driving force for precipitation is increased and particles becomes finer and more numerous (increase the hardenability of the matrix), thereby increasing the yield stress. This is in good a greement with published data [39,40,214], which have shown that the precipitation strengthening increases significantly with total C-content of the steel. The present results have shown that the precipitation strengthening of V-microalloyed steels increases significantly with the total C-content. It have been reported previously that increment is ~5.5MPa/0.01% C in the HSLA steel [222].Increasing C-content delays the pearlite formation and thereby maintains for a longer time the higher content of solute C in ferrite corresponding to the austenite/ferrite equilibrium as compared to that of ferrite/cementite, allowing more nucleation of V(C,N) particles and accordingly a more dense precipitation. The same phenomenon has been

recognized previously in lower carbon structural steels [272]. Although, recent studies and literature data [131,273-275], strongly suggest that vanadium can also by effectively used for ferrite grain refinement. By contrast presence of Ti forms nitrides (TiN) which reduce the N available for VN precipitation and hence, reduce the strengthening associated with this precipitation. Such an effect is to be expected as the amount of strengthening phase V(C, N) is necessarily decreased, as amount carbon decreased. When the yield stress data for the isothermally transformed steels are plotted against the transformation temperature as in Fig 4.36, there is seen to be the yield stress at the maximum in the vicinity of 350 $^\circ$C for both steels investigated. This may reflect to dislocation strengthening associated with the presence of hard phases such as bainite for (400, 350) $^\circ$C. As have been reported previously[19], the dislocation density of the ferrite increases with decreasing transformation temperature. This latter observation can be associated with a high strain-hardening rate imposed by bainite [276] However the lower in yield stress for Ti-free steel (V-N) compared with titanium –containig steels (Ti-V-N) is attributed to lower carbon content compared with titanium-containing steel. This is in good agreement with recent investigations [222,277,278], have demonstrated very clearly that the precipitation strengthening of V-steels increases significantly with the C-content of the steels.However the yield stress for both steels start to increase above 500 $^\circ$C its seems to be attributed to pearlite onset form as shown on Figure 4.22 and presence amount of martensite hard phase as can be seen in Fig. 4.18 , due to the transformation after1200s of isothermal treatment at 550 and 600 $^\circ$C reveals a fraction of austenite remains untransformed and only after the final water quenching it transforms to martensite as can be seen in Fig. 4.23(a,b) and Fig. 4.24(a,b). The decrease in yield stress for both steels investigated with increasing isothermal transformation temperature upto reach the minimum value at 450 and 500 $^\circ$C, as observed in Fig. 4.36, can be related to the lower content of pearlite and the presence of low strength ferrite i.e. increasing acicular ferrite (non-polygonal ferrite-NPF) in expense of polygonal ferrite-pearlite (PF-P), as can be seen in Fig. 4.23(c,d), Fig. 4.24(c,d) and Fig. 4.10(k,l). These microstrucrtural variations decreases the yield strength, due to suppression of precipitation within the NPF phase [279].In the acicular ferrite microstructure, refining the ferrite plate size, eliminating pearlite are critical for achievement of optimum strength and toughness properties [46].There was little visible difference between the the values in yield stress at intermediate isothermal temperatures of the titanium –containig steels and those microalloyed with vanadium alone. By contrast, the higher yield strength obtained

for specimens isothermally treated at ($\geq$ 550 $^\circ$C), can be attributed to the presence of a higher volume percent of pearlite and higher content of untransformed austenite. The pearlite constituent mainly determines the yield strength. It is well known [9], that the YS of polygonal Ferrite – Pearlite steels increases with increasing fraction of pearlite and there is additional strengthening is optained by precipitation of V(C,N) particles in ferrite. The transformation of retained austenite presents in microstructure to martensite during quenching processes have also the major role in determining the yield strength. The higher resistsnce of martensite and pearlite to deformation (weak resistance to necking) increases strain hardening. The most commonly used alloying elements for enhancing hardenability, manganese, chromium, and molybdenum, are all very effective in depressing the bainite transformation temperature and do so at approximately the same rate. For reasons of cost, the first two of those will be the most attractive choice [230]. For the present steels, yield stresses of between 1000 Mpa and 700MPa were achieved. The yield stresses for both steels and conditions investigated here are plotted in Fig. 4.36.The actual decrements in yield stress for both steels lie in the range of 705 to 680 MPa at 450 $^\circ$C as isothermal treatments. The yield stress data for the isothermally transformed steels are summarized against the transformation temperature as in Fig 4.36, there is seen to be a maximum in the vicinity of 350 and 600°C for both types of steels investigated. The loss of strength below 600°C must be attributed to incomplete precipitation as more of the vanadium is retained in solid solution due to its low diffusivity at these temperatures. However in the vicinity of 350 $^\circ$C, we find the higher yield stress and this is logical and expected result because at 350 $^\circ$C the bainite transformation is complete as demonstrated in Fig. 4.23 (f) and Fig. 4.24 (f)

5.5.2.1. Effect of Reheating Temperature on Yield Stresses

Figure 4.36, shows yield properties of the steel investigated samples as a function of soaking temperature. In general, there is decrease in yield strength with increasing reheating temperature up to 500°C, due to coarsening of the austenite grains, then start to increase due to pearlite start nucleate.

5.5.2.2. Effect of Carbon and Vanadium on Strengthening

Figure 4.36, shows the yield strength of both steel investigated. It is clear from figure 4.36 that the Ti-V-N steel has the largest yield strength at all soaking temperature. This behaviour is

attributed to larger volume fraction of VC in Ti-V-N steel, due to high C and V compare it with V-N steel, which contributes to the dispersion strengthening. These results in rather good agreement with similar steels given in Ref. [174]. Also as reported by [], the carbon is more effective to strengthen austenite

Carbon is very effective in suppressing the bainite start temperature with the aim of refining the microstructural scale [30].The addition of carbon shifts the TTT diagram to longer times as illustrated in table 4.14 and as shown in Fig. 4.30. However figure 4.36, shows the yield strength of both steel investigated. It is clear from figure 4.36 that the Ti-V-N steel has the largest yield strength at all soaking temperature. This behaviour is attributed to larger volume fraction of VC in Ti-V-N steel, due to high C and V compare it with V-N steel, which contributes to the dispersion strengthening. These results in rather good agreement with similar steels given in Ref. [174]. Also as reported by [290-293], the carbon is more effective to strengthen austenite due to the carbon is an austenite stabilizer, and facilitates the formation of non-equilibrium microstructures such as bainite and martensite. Increased carbon level lowers the Ae_3 temperature significantly and reduces the driving force for austenite decomposition at any temperatures.

5.5.2.3 Effect of Transformation Temperature

The effect of isothermal transformation temperature was investigated by lowering the temperature to $350^{\circ}C$ without changing other treatment conditions. Fig.4.32 shows the resulting hardness profiles for both steels and conditions investigated, where results of isothermal treatments as function of holding time is plotted in Fig.4.33 (a-f). The hardness values at the centre and at the end of all specimens are almost identical. In other words, the degree of mechanical stabilisation is reduced at large under-coolings (ΔT), the degree of under-cooling, $\Delta T = T_0 - M_S$ .This is expected since the driving force for transformation becomes larger. The volume fraction of cementite $\xi\{t\}$ results Fig. 4.33 (a-f) and the optical micrographs (Fig. 5.4.1) support these observations.

6. CONCLUSIONS

In order to evaluate austenite decomposition at isothermal conditions,and construct TTT diagram, series of isothermal tests were performed at 350, 400, 450, 500, 550 and 600°C. Isothermal holding times ranged from 2 to 1800 seconds. two vanadium mediumcarbon microalloyed steels, V-N (0.256%C, 0.0235%N, 0%Ti) and Ti-V-N (0.309%C, 0.221%N, 0.011%Ti), were tested with aim to establish the influence of difference in carbon and titanium on transformation behaviour. Isothermal decomposition of medium carbon vanadium microalloyed austenite was evaluated by optical and SEM metallography.

Established TTT diagrams for both steels show similar shape, i.e. the same features are present in both diagrams. The differences are in the incubation time and temperature regions, what is attributed to difference in nucleation stage. Three curves are found to be relevant to nucleation stage of transformation. First, GBF curves which extends over the entire temperature range studied (350-600oC), second, IGF curve which is divided into the high temperature polygonal and the low temperature acicular ferrite curve, and the third the pearlite (P) curve.

- Grain boundary ferrite is the first phase to be generated at all temepratures. In the lower temperature range the widmanstetten ferrite is formed, while on higher temperatures grain boundary allotriomorphs are produced. This difference is attributed to displacive nature of transformation at lower and diffusional transformation at higher temperatures.

- Second phase is related to nucleation of Intragranular ferrite (IGF). In the lower temperature range (350–400 ^{o}C) acicular ferrite plates are grouped in sheaves; at intermediate temperatures (450–500 ^{o}C), a more interlocked microstructure of acicular ferrite was clearly obsorved, while microstructure generated at high temperatures (550–600 ^{o}C) is characterized by polygonal idiomorphic ferrite.

- Third phase is related to onset of pearlite. It occurs at temperatures ≥ 500 $^{\circ}$C, followed by an incomplete reaction phenomenon.

- Acicular ferrite microstructure exhibiting different morphologies have been produced in both type of steels investigated by isothermal treatments. At low transformation temperatures acicular ferrite plates are grouped in sheaves, at intermediate temperatures a more interlocked microstructure is generated and at high temperatures, individual plates are formed following an incomplete reaction phenomenon.

- The transition between an acicular sheaf morphology and a more interlocked microstructure is related to the transition between lower and upper acicular ferrite and to different carbon diffusion rates in ferrite and austenite depending on the temperature. However the bainitic sheaves are frequently observed when the isothermal transformation time is increased and temperature diminished to 350 $^{\circ}$C.

- Fully acicular ferrite microstructures have been obtained in medium-carbon micro-alloyed steel through isothermal treatments at 450 °C.

- Acicular ferrite forms in both steels in two stages: nucleation at nonmetallic inclusions and sympathetically, from the already nucleated units.

- Acicular ferrite has been observed to nucleate on MnS inclusions, due to highly favorable conditions for the nucleation.

- The finish of transformation was clearly observed at temperatures below 500°C, for both steels. However at 550 and 600°C, incomplete reaction phenomenon occurs. This behaviour is attributed to carbon enrichment in austenite and decrease of driving force for austenite decomposition.

- Grain growth can be affected by the solute drag effect of any elements in solid solution and by the pinning forces associated to precipitates. So the grain coarsening temperatures (GCT) is expected to occur when the particles pinning the austenite grain boundaries start to dissolve. It is produced at around 1100°C. There fore the grain coarsening temperatures (GCT), it seems to be ≈ 1100 $^{\circ}$C for both steels investigated.

- Ti-V-N steel has smaller austenite grain size above 1100°C. This can attributed to the fact that addition of Ti can result in fine TiN precipitates, which can inhibit austenite grain growth at high temperatures (> GCT), because of their strong high-temperature

stability. By contrast, the V-N steel with high Al and N contents possesses smaller grain size, at temperature less than 1050 $^{\circ}$C. Therefore Ti-V-N steel with lowest volume fraction of AlN among these steels has the largest grain size at temperature less than 1100 $^{\circ}$C. These can attributed to, the AlN particles are responsible for controlling austenite grain growth only in the low austenising temperature (< GCT).

- The addition of Ti to V- microalloyed steel is balanced by increased content of C and Mn , leading to limited effect on nucleation stage of austenite decomposition.

- Sheaves of parallel ferrite plates, similar to bainitic sheaves, but intragranularly nucleated and its called Sheave Type Acicular Ferrite (STAF)was clearly observed at (≈ 400 $^{\circ}$C), for both steel investigated.

- The Ti-V-N steel has higher yield strength at all soaking temperature. This behaviour is attributed to larger volume fraction of VC, due to high C and V compared with V-N steel, which contributes to the dispersion strengthening.

- At holding time shorter than10s, there was no significant difference in hardness for both steels and treatment condition, the main change in hardness occurred for holding times between 10 and 600s. Beyond 600 s, the hardness changed only slightly.

- The lower yield stress for Ti-free steel (V-N) compared with titanium –containig steels (Ti-V-N) is attributed to lower carbon content compared with titanium-containing steel.

- Yield stress decreases from the maximum values for temperatures 350°C – 400°C for both steels investigated. It is assumed that it reflects dislocation strengthening associated with the presence of hard phases such as bainite, since the dislocation density of the ferrite increases with decreasing transformation temperature.

7. REFERENCES

[1] N.Radovic, D.Drobnjak, Development of steels for fabrication of welded construction with improved safety, Welding and Welded Structures 45 (2001) 81.

[2] T. D. Mottishaw,G. D. W. Smith,163 in ref. [285].

[3] I.Kozasu, Recent developments of microalloyed steel plate, in HSLA steels technology & application , Ed . M.Korchynsky, American Society for Metals, Pennsylvania (1984) 593.

[4] T. Gladman: The Physical Metallurgy of Microalloyed Steels, The Institute of Materials, London, England, (1997) 1-360.

[5] A.C.Kneissl, C.I.Garcia, A.J.DeArdo, Influence of processing on the nature of the precipitates in a microalloyed linepipe steel, International conference on processing, microstructure and properties of microalloyed and other modern high strength low alloy steel, Ed by A.J.DeArdo, The Iron and steel society, Pittsburgh (1991) 145.

[6] L.J.Cuddy, J.S.Lally, L.F.Porter, Improvement of toughness in the HSLA of high heat input welds in ship steels, HSLA steels technology & application, Ed. M.Korchynsky, American Society For Metals, Pennsylvania (1984) 697.

[7] S.S.Campos, E.V.Morales, H.J.Kestenbach, Met. and Mat. Trans. 32A (2001) 1245-1248.

[8] A.M.Sage, R.C.Cochrane, D.Howse, The Iron and Steel Society (1992) 443 in ref. [286].

[9] F.A. Khalid, D.A. Gilroy, D.V.Edmonds, 67 in ref. [286].

[10] A.M.Sage, R.C.Cochrane, The Development of a normalised Ti−treated vanadium steel with improved HAZ toughness, International conference on Processing, Microstructure And Properties Of Microalloyed And Other Modern High Strength Low Alloy Steel, Ed. A.J.DeArdo, The Iron and steel society , Pittsburgh (1991) 443.

[11] A M.Sage, An overview of the use of microalloys in HSLA steels with particular reference to vanadium and titanium, in HSLA steels, Processing, properties and applications, Ed by Geoffery Tither and Zhang Shouhua, The Minerals, Metals & Materials Society (1992) 51.

[12] Ji Yancheng, song han, Huo Bingshu, cao Yinzhi, Improving The Toughness of Steels By Microalloying With Ti, in HSLA Steels, Processing, Properties And Applications, Ed by Geoffrey Tither and Zhang Shouhua, The Minerals , Metals & Materials Society, (1992) 217.

[13] Dj.Drobnjak, A.Koprivica, Development of V-microalloyed steel for well sucker rod application, _____

[14] M.Cabibbo, A.Fabrizi, M.Merlin, G.L Garagnani: J. Mat. Sci.43 (2008) 6857-6865.

[15] H.K.D.H.Bhadeshia, Bainite in Steels, Second Edition, The Institute of Metals, London, UK (2001).

[16] G.Miyamoto, R.Hori, B.Poorganji, T.Furugara, ISIJ Int. 51 (2011) 1733–1739.

[17] C.Capdevila, C.Garcıa de Andres, F.G.Caballero, Scripta mater. 44 (2001)129–134.

[18] B. Yan, K. Xu, 44th Mechanical Working and Steel Processing Conference Proceedings, Iron and Steel Society, AIME, USA 40 (2002) 493.

[19]Steels Microstructure and Properties, H.K. D. H. Bhadeshia, R.W.K. Honeycombe, Elsevier Ltd, London, (2006).

[20] C. Pichard, Ortolland, 89 in ref. [286].

[21] C.I. Garcia, A.K. Lis, M. Maguda, A.J DeArdo, 395 in ref. [286].

[22] H. Hera, M. Kobayashi, The use of hot forged microalloyed steel in automobile components, Institute of Metals Vanadium, Award paper (1987).

[23] G. Krauss: Steels Heat Treatment and Processing Principles, ASM International, Materials Park, Ohio, (1990).

[24] G. Krauss, Vanadium Microalloyed Forging Steels, University Emeritus Professor, Colorado School of Mines, Metallurgical Consultant Evergreen, Colorado 80439, USA.

[25] AG. Thyssen Stahl, Hot rolled coil and strip, brochure 6751 AE 39, (1993).

[26] D.G. Younger, Metal Progress, 5(1975) 43-47.

[27] F . B. Pickering, Physical Metallurgy and the Design of Steels. Applied Science Publishers Ltd, London, UK (1978) 1.

[28] H. I. Aaronson, H. A. Domian, and G. M. Pound. Thermodynamics of the austenite-proeutectoid ferrite transformation: Fe-C alloys. TMS AIME,236(1966) 753-767.

[29] J. Mahieu. Contribution to The Physical Metallurgy of Crash-resistant Galvanized TRIP-assisted Steel for Automotive Structures. PhD thesis, Ghent University (2003).

[30] M. Y. Sherif. Strain-induced transformation of very strong metal. Master's thesis, University of Cambridge, August (2003).

[31] K. Hasegawa, K. Kawamura, T.Urabe, Y.Hosoya, ISIJ Int. 44 (2004) 603-609.

[32] N. R. Bandyopadhyay, S. Datta: ISIJ Int., 44 (2004) 927-943.

[33] F. G. Caballero, H.K.D.H. Bhadeshia, K. J. A. Mawella, D. G. Jones, P. Brown. Design of novel high strength bainitic steels: Part 1. Mater. Sci. Tech.-Lond 17(2001) 512-516.

[34] F. G. Caballero, H.K.D.H. Bhadeshia, K.J.A.Mawella, D.G. Jones, and P. Brown. Design of novel high strength bainitic steels: Part 2. Mater. Sci. Tech., Lond., 17 (2001)517-522.

[35] R. Hammond, Shock and Ballistic Properties of Bainitic Steels. PhD thesis, University of Cambridge, (2004).

[36] I. Madariaga, J. L. Romero, I. Gutierrez, Metall. and Mat. Tran:29A (1998)1003-1015.

[37] N.A. Chester, H.K.D.H. Bhadeshia, J. Phys. iv France 7, Colloque C5(1997) 41- 46.

[38] C.Garcia-Mateo, F.G.Caballero, H.K.D.H Bhadeshia ISIJ Int. 43(2003)1238-1243.

[39] S. Zajac, Materials Science Forum, 500-501 (2005) 75-80 (1995)195-200.

[40] S. Zajac, International Seminar on Application of Vanadium in flat-Rolled Steels (2005).

[41] C. Shiga, "Benefits of TMCP and its application to HSLA steels," Metallography`95,

[42] R.Lagneborg, T.Siwecki, S.Zajac, B.Hutchinson, The Role of Vanadium in Microalloyed Steels, Swedish institute for Metals Research, (1999).

[43] H.K.D.H. Bhadeshia, Thermodynamic analysis of isothermal transformation diagrams. Metal Science:16 (1982) 159.

[44] R.C.Sharma, G.R.Purdy, Metall. Trans. (1973) 4, 2303.

[45] H.K.D.H. Bhadeshia, The Bainite Reaction, POSCO Lectures: Graduate Institute of Ferrous Technology (GIFT), Pohang University of Science and Technology (POSTECH) Lectures, Pohang, South Korea.

[46] A. Khodabandeh, M. Jahazi, S. Yue, P. Bocher ISIJ int.45 (2005) 272-280.

[47] M. Dıaz-Fuentes, I. Gutiérrez,Mat. Sci and Eng A363 (2003) 316-324.

[48] I. Madariaga, I. Gutierrez : Scripta mater., 37 (8)(1997) 1185-1192.

[49] S.S. Babu, H.K. D. H. Bhadeshia. Mat. Trans, JIM, 32 (1991) 679-688.

[50] I. Madariaga, I. Gutierrez, C.Garcia De Andres, C.Capdevila, Scripta Mater.41(1999) 229-231.

[51] M. Takahashi, H.K.D.H. Bhadeshia. Mat. Sci. and Tech. 6 (1990) 592-603.

[52] Bhadeshia, H.K.D.H. rationalisation of shear transformations in steels. Acta Metall.29 (1981a) 1117–1130.

[53] D. Glisic, N. Radovic, A. Koprivica, A. Fadel and D. Drobnjak: ISIJ Int., 50 (4) (2010) 601–606.

[54] H.Adrian, Proc.of Int. Conf. Microalloying '95, ISS, Warrendale,PA, USA,(1995) 285.

[55] W.Roberts, A.Sandberg, Report IM-1489, Swedish Institute for Metals Research (1980).

[56] Dj. Drobnjak, A. Koprivica, Microalloyed Bar and Forging Steels, Edited by C.J.Van Tyne, G.Krauss, D.K.Matlock, The Minerals,Metals&Materials Society, (1996) 93-107.

[57] H.Nordberg, B. Aronsson, Solubility of Niobium Carbide in Austenite, Journal of the Iron and steel Institute, (1968) 1263.

[58] R. P. Smith, The Solubility of Niobium Carbide in Gamma Iron, Transations of the Metallurgical Society of AIME 236 (1966) 220.

[59] K.Narita, Physical Chemistry of the Groups IVa (Ti, Zr), Va (V, Nb, Ta) and the Rare Earth Elements in Steel, Transations of the Iron and Steel Institute of Japan 15 (1975) 145.

[60] T.H.Johansen, N.Christensen, B.Augland, The Solubility of Niobium Carbide in Gamma Iron, Transactions of the Metallurgical Society of AIME, 239 (1967) 1651.

[61] T.Mori et al., Thermodynamic Properties of Niobium Carbides and Nitrides in Steel, Tetsu −to−Hagane, 54 (1968) 786.

[62] H.L.Andrade, M.G.Akben, J.J.Jonas, Effect of Molybdenum, Niobium and Vanadium on static Recovery and Recrystallization and on solute Strengthening in Microalloyed Steels, Metallurgical Transactions 14A (1983)1967.

[63] R.C.Sharma, V.K.Lakshmanan, J.S.Kirkaldy, Solubility of Niobium Carbide and Niobium Carbonitride in Alloyed Austenite and Ferrite, Metallurgical Transactions 15A (1984) 545.

[64] V.K.Lakshmana, J.S.Kirkaldy, Solubility Product for Niobium Carbide in Austenite, Metallurgical Transactions 15A (1984) 541.

[65] Advances in Phase Transitions, Ontario , 22−23 (1987) , J.D.Embury and G.R.Purdy, Eds.,Thermodynamics of Fe−Ti−C and Fe−Nb−C Austenites and Nonstoichiometric Titanium and Niobium Carbides, by K.Balasubramanian and J.S.Kirkaldy, Oxford, UK , Pergamon Press (1988) 37.

[66] R. P. Smith, The Solubility of Niobium Nitride in Gamma Iron, Transactions of the Metallurgical Society of AIME 224 (1962) 190.

[67] Microalloying 75, Washington D . C . October 1−3 (1975), M . Korchynsky, Ed., Quantifying the Effects of Microalloying Elements on Structures During Processing, by T. M. Hoogendoorn M . J . Spanraft, (New York ,NY:Union Carbide Corporation, 1977) 75.

[68] M.L. Santella, Grain Growth and High−Temperature Hot Rolling Behavior of Low−Alloy Steel Austenite, PhD. Thesis, University of Pittsburg, (1981) 49.

[69] K.L.Irvine, F.B.Pickering, T. Gladman, Grain refined C−Mn Steels, Journal of the Iron and Steel Institute, (1967) 161.

[70] D.A.Porter, K.E.Easterling, Phase tranformation in metals and alloys, Van Nostrand Reinhold (UK) Co. Ltd, Molly Millars Lane, (1981).

[71] C M Sellars, The Physical Metallurgy of Hot Working, In Hot Working And Forming Processes, Ed. C.M. Sellars and G. J. Davies, The Metals Society, London, (1980) 3.

[72] A.Laasraoui, J.J.Jonas, Recrystallization of Austenite after Deformation at High Temperatures and Strain Rates, Analysis and Modeling, Metallurgical Transactions, 22A (1991) 151.

[73] P.Choquet et al., Mathematical Modelling of Hot Rolling of Steel, Ed. S.Yue, CIMM, Montreal, Canada (1990) 23–43.

[74] J.Williams, C.R.Killmore, G.R.Harris, Physical Metallurgy of Thermomechanical Processing of Steels and Other Metals, (THERMEC 88), Ed. I.Tamura, ISIJ, Tokyo (1988) 224 –231.

[75] P. D. Hodgson, Materials forum, 17 (1993) 403 –408.

[76] S. F. Medina, J . E .Mancilla, ISIJ Int.,36 (1996)1070 – 1076.

[77] P. D. Hodgson, R . K . Gibbs, ISIJ Int., 32 (1992) 1329 – 1338.

[78] W. Sun et al, Intl. Conference on Thermomechanical Processing of Steels and Other Materials (Thermec 97), Eds. T.Chandra et al., TMS, Warrendale, USA (1997) 685 – 691.

[79] S. F. Medina and J. E. Mancilla, ISIJ Int., 33 (1993)1257.

[80] S. F. Medina, Scripta Metallurgical and Materialia, 31 (1994) 315 –320.

[81] S.Devaraj, Y.Deke, T.Chandra, International Conference on Recrystallization in Metallic Materials, (Recrystallization 90), Ed. T.Chandra, TMS, Warrendale, USA (1990) 237 – 244.

[82] N. Ridley. Phase Transformation in Ferrous Alloys, TME-AIME, Warrendale, PA (1984) 210-236.

[83] S. A. Al-Salman, N. Ridley, Scripta Metall. 18 (1984) 789-791.

[84] H.K.D.H. Bhadeshia, Mater. Sci. and Tech. 15 (1999) 22-29.

[85] G.R.Speich, J.Cuddy, C.R.Gordon, AJ.DeArdo: "Formation of Ferrite from Controlled-rolled Austenite", in Phase Transformations in Ferrous Alloys, A.R.Marder and J.I Goldstein, Editors, The Metallurgical Society, Warrendale, Pennsylvania, (1984)341-389.

[86] M. Enomoto, W. F. Lang, H. I. Aaronson, Met, Trans. 17A (1986) 1399.

[87] W. F. Lang, M. Enomoto, H. I. Aaronson, Met, Trans. 19A (1988) 427.

[88] E. P. Simonen, H. I. Aaronson, Met, Trans. 4(1973) 1239.

[89] M. Militzer, R. Pandi, E. P. Hawolt, Met. and Mat. Trans. A, 27A (1996) 1547.

[90] H.I.Aaronson, C.Laird, K.R.Kinsman, Phase Transformation, ASM, Metals Park, OH,(1968) 313.

[91] M. Hillert, "Thermodynamics and Phase Transformation- The selected works of Mats, EDS Science, Les Ulis Cedex A, France, (2006).

[92] M. Hillert, Phase Equilibria, Phase Diagrams and Phase Transformation-their thermodynamics basis, Cambridge University Press, Second edition, Cambridge, UK (2008).

[93] H.K.D.H.Bhadeshia. Critical assessment:Diffusion-controlled growth of ferrite plates in plain carbon steels. Materials Science and Technology, 1(1985) 497-504.

[94] C. Capdevila, F.G. Caballero, C. Garcia De Andres, Metallurgical And Materials Transactions 32A (2001)1591.

[95] C.Capdevila, F.G.Caballero1, C.Garcıa de Andres: Scripta mater, 44 (2001) 593–600.

[96] T. Furuhara, T. Shinyoshi, G. Miyamoto, J. Yamaguchi, N. Sugita, N. Kimura, N. Takemura, T. Maki, ISIJ Int., 43 (2003) 2028–2037.

[97] M. Korchynsky, P.527 in ref. [286].

[98] C.Garcia De Andres, C.Capdevila, D.San Martin, F.G.Caballero, J. of Mat. Sci. 20 (2001) 1135 – 1137.

[99] K. R. Kinsman, H. I. Aaronson, Transformation and Hardenability in Steels, Climax Molybdenum Corporation, Ann Arbor, MI (1967) 39.

[100] T.Siwecki, B.Hutchinson, S.Zajac, Recrystallisation controlled rolling of HSLA steels, Int. Conf. "MICROALLOYING '95", Iron and Steel Society, June 11-14, Pittsburgh, USA (1995)197-212.

[101] R. Lagneborg, O. Sandberg, W. Roberts, Optimisation of Microalloyed Ferrite -Pearlite Forging Steels, in conference proceeding – Fundamentals of Microalloying Forging Steels, Golden, Colorado, (1986) 39-54.

[102] T. Siwecki, Modelling of Microstructure Evolution during Recrystallization Controlled Rolling, ISIJ Int., 32 (1992) 368-376.

[103] H.K.D.H. Bhadeshia, D.V.Edmonds, The mechanism of bainite formation in steels, Acta Metall, 28 (1980)1265–1273.

[104] H.K.D.H.Bhadeshia, D.V.Edmonds, The bainite transformation in a silicon steel, Metall. Trans. A10 (1979) 895–907.

[105] N. Ridley. Phase Transformation in Ferrous Alloys, TME-AIME, Warrendale, PA (1984) 210-236.

[106] A. B. Pippard, Chemical Thermodynamics, Cambridge University Press (1981).

[107] H.K.D.H.Bhadeshia, Mat. Sci. and Eng. A273-275, (1999) 58-66.

[108] H.K.D.H. Bhadeshia, Thermodynamic analysis of isothermal transformation diagrams. Metal Sci. 16 (1982) 159–165.

[109] A. Ali, H.K.D.H. Bhadeshia, Nucleation of Widmanstätten ferrite. Mater. Sci. Technol. 6 (1990) 781–784.

[110] H.K.D.H. Bhadeshia, J.W. Christian, Bainite in steels, Metall. Trans. A21 (1990) 767–797.

[111] H.K.D.H. Bhadeshia, Int. Conf. on Phase Transformation in Ferrous Alloys, Marder A.R. and Goldstein, J.I. eds. A.S.M.,Cleveland, Ohio, USA (1984) 335-340.

[112] S. Traint, A. Pichler, R. Tikal, P. Stiaszny, and E. A. Wemer. In 42nd Metal Working and Steel Processing Conf. Proceedings, Iron and Steel Society, USA, 38 (2000) 549-561.

[113] P. Jacques, X. Cornet, Ph. Harlet, J. Ladriere, F. Delannay, Metall. Mater. Trans. A, 29(1998) 2383-2393.

[114] P. J. Jacques, J. Phys. IV, 112 (2003) 297-300.

[115] S. Traint, A. Pichler, P. Stiaszny, K. Spiradek-Hahn, E. A.Werner, In 43rd MWSP conference proceedings, ISS, (2001) 449-467.

[116] H. Matsuda, F. Kitano, K. Hasegawa, T. Urabe, Y. Hosoya. Metallurgy of continuously annealed high strength TRIP steel sheet. In B. C. De Cooman, editor, International Conference on TRIP-aided High Strength Ferrous Alloys, Ghent 113-119 (2002).

[117] P. J. Jacques, E. Girault, T. Catlin, N. Geerlofs, T. Kop, S. van der Zwaag, F. Delannay. Mater. Sci. Eng. A, (1999) 273-275:475-479.

[118] E. Thelning, Steel and its Heat Treatment,Bofors Handbook, Butterworth, UK, (1975).

[119] R. Trivedi, Metall. Trans. 1 (1970) 921-927.

[120] M. Takahashi, H.K.D.H. Bhadeshia, Mat. Sci and Tech. 6 (1990) 592-603.

[121] W. T. Reynolds, H. I. Aaronson, G. Spanos, Materials Transactions, JIM 32(1991)737-746.

[122] G. Spanos, H. S. Fang, D. S. Sarma, H. I. Aaronson, Metall.Trans: 21A (1990) 1391.

[123] M. J. Perricone, Bainitic Structures, Metallography and Microstructures, ASM Handbook 9, ASM International (2004)179–185.

[124] H.K.D.H. Bhadeshia, J. Phys. iv France 7(1997) C5-367.

[125] H.K.D.H. Bhadeshia, Bainite: overall transformation kinetics. J. Phys. Paris C43 (1982), (Colloq. C4) 443–448.

[126] G. I. Rees, H.K.D.H. Bhadeshia, Bainite transformation kinetics, Part 1, Modified model,Mater. Sci. Technol. 8 (1992) 985–993.

[127] G. I. Rees, H.K.D.H. Bhadeshia, Bainite transformation kinetics, Part 2. Non-uniform distribution of carbon. Mater. Sci. Technol. 8 (1992) 994–996.

[128] C. L. Chang, H.K.D.H. Bhadeshia, Austenite films in bainitic microstructures. Mater. Sci. Technol. 11(1995) 874–881.

[129] R. W. K. Honeycombe, Met. Trans. Sect. A 7 (1976) 915.

[130] G. I. Rees, H.K.D.H. Bhadeshia, Mat. Sci. and Tech. 10 (1994) 353.

[131] F. Ishikawa, T. Takahashi ISIJ Int. 35(1995)1128-1133.

[132] A. J. DeArdo, New developments in the alloy design of microalloyed and other modern HSLA steels, in HSLA steels: Processing, Properties and Applications, Ed. Geoffrey Tither and Zhang Shouhua,The Minerals, Metals & Materials Society, (1992) 21.

[133] T. Nilsson, Formable hot rolled steel with increase strength, in HSLA steels technology & application, Ed. Michael Korchynsky, ASM, Pennsylvania (1984) 253 .

[134] C. G. Lee, S. J. Kim., C. S. OH, S. Lee, Effects of Heat Treatment and Si Addition on the Mechanical Properties of 0.1 wt% C TRIP-aided Cold-rolled Steels, ISIJ Int. 42 (2002) 1162-1168

[135] H.K.D.H. Bhadeshia, Mater. Sci. Tech. 1 (1985) 497.

[136] C. Capdevila, J. P. Ferrer, C. García-Mateo, F. G. Caballero, V. López, C. García de Andrés, ISIJ Int. 46 (2006)1093–1100.

[137] M. A. Linaza, J. L. Romero, I. San Martin, J. M. Rodriguez-Ibabe, J. J. Urcola, Scripta Met. 29 (1993) 1217.

[138]J. R. Yang, H.K.D.H. Bhadeshia: Advances in the Science and Technology of Welding, ed. By S. A. David. ASM International, Ohio, (1987)187.

[139] . Garcia de Andres, C. Capdevila, F. G. Caballero, D. San Martin, J of Mat. Sci 36 (2001) 565

[140] C. Garcia-Mateo, C. Capdevila, F. G. Caballero, C. Garcia de Andres. ISIJ Int. 48 (2008) 1270-1275.

[141] C.Garcia de Andres, F.G.Caballero, C.Capdevila, D.San Martin, Revealling austenite grain boundaries by thermal etching: advantages and disadvantages. Mater Charact 49 (2003) 121-127.

[142] C. Capdevila, F. G. Caballero. C. Gracia-Mateo and C. Garcia de Andres: Mater. Trans. 45 (2004) 2678.

[143] C. Capdevila, F. G. Caballero, and C. Garcia de Andres: Mater. Sci. Technol., 19 (2003) 195.

[144] C. Garcia de Andres, M. J. Bartolome, C. Capdevila, D. San Martin. Mater Charact 46 (2001) 389-398.

[145] S. S. Babu, H.K.D.H. Bhadeshia. Mat. Sci. and Tech, 6 (1990) 1005-1020.

[146] A. F. Gourgues, H.M.Flower, T.C. Lindley. Mat. Sci. and Tech. 16 (2000) 24-40.

[147] WU. Kaiming, LI. Zigang, A. M. GUO, HE XinLai, L. Zhang, A. Fang, L. Cheng: ISIJ Int. 46 (2006)161−165.

[148] M. Strangwood, PhD Thesis, University of Cambridge (1987).

[149] H.K.D.H. Bhadeshia, J.of Phys. Paris (1982 a) C4 437−441.

[150] H.K.D.H. Bhadeshia, Int. Conference on solid →solid phase transformations, eds. H.I. Aaronson et al. TMS-VIME, Warrendale, PA, U.S.A (1981b) 1041-1048.

[151] P. L. Harrison, R. A. Farrar, J. of Mat. Sci.16 (1981) 2218-2226.

[152] R. M .Kuziak, Yi −Wen Cheng, Microstructural Evolution In Microalloyed Medium Carbon Forging steels During Thermomechanical Processing, international conference on processing, microstructure and properties of microalloyed and other modern high strength low alloy steel, Ed by A .J .DeArdo, The iron and steel socity, pittsburgh (1991) 51.

[153] T. Gladman, Heat Treatment of Metals, 1(1994) 11.

[154] H. Adrian, F. B. Pickering, Mater. Sci. Technol., 7 (1991) 176.

[155] C. Zener, quoted by C. S. Smith, Trans. AIME., 175 (1948) 47.

[156] T. Gladman, Proc. Roy. Soc., 294A (1966) 298.

[157] P. Hellman, M. Hillert, Scan. J. Met., 4 (1975) 211.

[158] M. Hillert, Acta Metall., 36 (1988) 3177.

[159] P. R. Rios, Acta Metall., 35 (1987) 2805.

[160] R. Elst, J. Van. Humbeeck, L. Delaey, Acta Metall., 36 (1988) 1723.

[161] D. J. Senogles, Ph.D Thesis, University of Leeds, (1994).

[162] K.He, D.V Edmonds, Mat. Sci. and Tech, 18 (2002) 289.

[163] C. Garcia de Andres, C. Capdevila, I. Madariga, I. Gutierrez: Scripta Materialia 45 (2001) 709-716.

[164] D.J.Abson. Nonmetallic Inclusions in Ferritic Steel Weld Metals, International Institute for Welding, Document IX-1486-87(1987).

[165] M. Umemoto.,K. Horiuchi, I. Tamura, Acta.Metall. 34 (1986b) 2245-2245.

[166] S. Zajac, Materials Science Forum: 500-501(2005)75.

[167] G.F. Melloy, How changes in composition and processing affect HSLA steels, Metal Progr. 89 (1966) 129-133.

[168] S. Zajac, T. Siwecki, M. Korchynsky: "Importance of Nitrogen for Precipitation Phenomena in V-Microalloyed Steels", in Proc. Conf. Low Carbon Steels for the 90`s, (eds. R Asfahani and G. Tither), ASM/TSM, Pittsburgh, USA, (1993)139-150.

[169] S. Zajac, W. B. Hutchinson: Progress Report No 2 to Vanitec (2001).

[170] V. Ollilainen, H. Hurmola, H. Pontinen, Vanadium Structural Steels, Philadelphia, October 1983 (American Society for Metals, Metals Park, OH, 1985) 199.

[171] J. F. Held, "Fundamentals of Microalloying Forging Steels, edited by G. Kraus and S. K. Banerji (The Met. Soc. of AIME, Warrendale, PA, 1987) 175.

[172] HSLA steels: Processing, Properties and Applications, G. Tither and Z. Shouhua, eds., TMS, (1992).

[173] P. A. Manohar, D. P . Dunne, T. Chandra, R. Killmore, ISIJ Int. 36 (1996) 194.

[174] N. Gao, T. N. Baker, ISIJ Int. 38 (1998) 744.

[175] F . Penalba, C. Garcia De Andres, M. Carst, F . Zapirain, J. Mater. Sci. 31 (1996) 3847.

[176] F . Penalba, C. Garcia De Andres, M. Carst, F . Zapirain, F . Penalba, ISIJ Int. 32 (1992) 232.

[177] W. Roberts, A. Sandberg, T. Siwecki, T. Werlefors, Prediction of microstructure development during recrystallization hot rolling of Ti − V steels, HSLA Steels: Metallurgy and Applications, Ed . J . M . Gray et al, ASM, Metals Park, USA (1986).

[178] L. R. Link, M. G. Vassilaros, Stabilization of Coarse Grain HAZ of Ti Treated ULCB Steel, International Conference On Processing, Microstructure And Properties of Microalloyed and other Modern High Strength Low Alloy Steel, Ed by A .J .DeArdo, The Iron and Steel Society, Pittsburgh (1991) 421.

[179] Shi−Rong chen, Shyi−chin wang, Rong−Luan Hsieh, The Development of High Strength Low Alloy Steel Plates Suitable For High Heat Input Welding, International

Conference on Processing, Microstructure and Properties of Microalloyed and other Modern High Strength Low Alloy Steel, Ed by A .J .DeArdo, The Iron and Steel Society, Pittsburgh (1991) 435.

[180] G. M. Evans, Int. Inst. of welding, Document II-A-666-86 (1986).

[181] C. B. Dallum, D. L. Olson, American Welding Journal (1989) 198s-205s.

[182] M. Cohen, G. B. Olson, P. C. Clapp, Proc. Int. Conf. on Martensitic Transformations, ICOMAT,Massachusetts (1979) 1.

[183] K. Mukherjee, Trans. TMS-AIME, 1968, 242, 1495.

[184] J.W. Christian, "Physical Props. of Martensite and Bainite", ISI spec. rep. 93, London, 1965, p.1.

[185] Worked examples in the geometry of crystals, H.K.D.H. Bhadeshia, Second Edition, published (2001), up dated (2006) Published electronically with permission from the Institute of Materials 1 Carlton House Terrace London SW1Y 5DB

[186] J.W. Christian, Proc. Int. Conf. on Martensitic Transformations, icomat Massachusetts (1979) 220.

[187] Yi, Hongliang, Thesis for Doctor of Philosophy, Pohang University of Science and Technology, Korea (2010).

[188] A. R. Marder, Structure-Property Relationships in Ferrous Transformation Products, Phase Transformation of Ferrous Alloys, Proc. Int. Conf., TMS (1984)11–41.

[189] Martensitic Structures, Metallography and Microstructures, ASM Handbook 9, ASM International, (2004)165–178.

[190] G. B. Olson, W. S. Owen, Ed., Martensit*e:* A Tribute to Morris Cohen*,* ASM International, (1992).

[191] G. Krauss, Martensite in Steel: Strength and Structure, Mater. Sci. Eng. A 273–275, (1999) 40–57.

[192] J. Wang, P. van der Wolk, S. van der Zwaag. Mater. Trans, JIM,41(2000)761-768.

[193] Hong-Seok Yang, H.K.D.H. Bhadeshia, Scripta Materialia 60 (2009) 493–495.

[194] T. Maki, S. Shimooka, I. Tamura: Metallurgical Transactions 2 (1971) 2944–2955.

[195] W. F . Smith, Structure and Properties of Eng . Alloys, McGraw–Hill, New York, (1981).

[196] R.K.Amin, G.Butterworth, F.B.Pickering, Effects of rolling variables and stoichiometry on strain−induced precipitation of Nb(CN) in C−Mn−Nb steels, in Hot working and forming processes, Ed by C. M . Sellars and G. J. Davies, The Metals Society, London, (1980) 27.

[197] T. Tanaka, N. Tabata, T. Hatomura, C. Shiga, Three stages of the controlled rolling process, Mcroalloying 75, Ed. M.Korchynsky, Union Carbide (1977).

[198] T. N. Baker, Subgrain and dislocation strengthening in controlled−rolled microalloyed steels, in Hot working and forming processes, Ed. by C. M. Sellars and G. J. Davies, The Metals Society, London (1980) 32.

[199] R . E . Smallman, Modern Physical Metallurgy, Butterworths, London (1985).

[200] H.K.D.H. Bhadeshia, D.V.Edmonds. Bainite in silicon steels: a new composition property approach i. Metal Science, 17 (1983) 411−419.

[201] H.K.D.H. Bhadeshia, D. V. Edmonds. Bainite in silicon steels: a new composition property approach ii. Metal Science, 17 (1983) 420−425.

[202] Y. K. Lee, H. C. Shin, Y. C. Jang, S. H. Kim, C. S. Choi, Scripta Materialia 47(2002) 805−809.

[203] F. G. Caballero, H.K.D.H. Bhadeshia, K. J. A. Mawella, D. G. Jones,
P. Brown. Mate. Sci. and Tech 18 (2002) 279.

[204] Y.Sakuma, O. Matsumura, H. Takechi, A 22 (1991) 489-498.

[205] B. Mintz, The Influence of Al on the Mechanical Properties of Hot Rolled Steel Plates, Materials Science Forum 426-432 (2003) 1219-1224.

[206] E. Girault, A. Martens, P. Jacques, Y. Houbaert, B. Verlinden, J.Van Humbeeck, Scripta Materialia 44 (2001) 885-892.

[207] B. G. Kirkby, P. LaGreca, C. J. Van Tyne, D. K. Matlock, G. Krauss: "Effect of Sulfur on Microstructure and Properties of Medium-carbon Microalloyed Bar Steels", SAE Technical Paper 920532 (1992).

[208] T. Ochi, T. Takahashi, : "Improvement of the Toughness of Hot Forged Products "Through Intra-granular Ferrite Formation", in 30th Mechanical Working and Steel Processing Conference Proceedings, Vol. XXVI, ISS-AIME, Warrendale, Pennsylvania, (1988) 65-72.

[209] W. Roberts, A. Sandberg,T. Siwecki, Precipitation of V(C,N) in HSLA Steels Microalloyed with V, Proc. Conf. Vanadium Steels, Krakow, Vanitec (1980) D1-D12.

[210] M. Korchynsky, J. R. Paules, Microalloyed Forging Steels-State of the Art Review, Intern. Congress and Expo. Detroit, USA, SAE Paper 890801, (1989) 1-11.

[211] R.J. Baker, J. Nutting, Precipitation Processes in Steels, ISI Special Report No. 64, The Iron and Steel Institute, London, 1959.

[212] F.A. Khalid, D.A. Gilroy, D.V. Edmonds, Processing Microstructure and Mechanical Properties of Microalloyed and Other Modern HSLA Steels,TMS, Warrendale, PA (1992) 67.

[213] R. Lagneborg, S. Zajac: Metall. and Mat. Trans: 32A (2001) 39.

[214] R. Lagneborg, T.Siwecki, S. Zajac, B. Hutchinson, "The Role of Vanadium in Microalloyed Steels", Scandinavian Journal of Metallurgy 28 (1999)1-241.

[215] N. K. Balliger, R.W.K. Honeycombe: Metall. Trans., 11A (1980) 421.

[216] J. Daigne, M. Guttmann, J.P. Naylor. Mat. Sci. and Eng. 56 (1982) 1-10.

[217] S. j. Lechuk, M. A. Sc. Thesis, The university of British, Columbia, (2000).

[218] J. Reiter, C. Bernhard, H. Presslinger. Austenite grain size in the continuous casting process: Metallographic methods and evaluation. Mater Charact 59 (2008)737-746.

[219] G. V. Voort. Tech-Notes. Buehler Ltd. Vol.1, Issue 5.

[220] Annual Book of ASTM Standards, vol. 3.01, ASTM Standard Designation, E 112-88, Philadelphia Pa (1994) 227.

[221] Practical Application of Quantitative Metallography, V. Voort, American Society for Testing and Materials, (1984).

[222] S. Zajac, T. Siwecki, B. Hutchinson, R. Lagneborg: ISIJ Int.38 (1998) 1130-1139.

[223] T. Siwecki, J. Eliasson, R. Lagneborg, B. Hutchinson. ISIJ. 50 (2010) 760-767.

[224] Steel Forming and Heat Treating Handbook, Antonio Augusto Gorni São Vicente. (2011) 24.

[225] A.E. Nehrenberg: Transactions of the AIME, 167, 1946, 494.in ref. [224].

[226] K.W. Andrews, Empirical formulae for the calculation of some transformation temperatures, Journal of the Iron and Steel Institute 7(1965) 721-727.

[227] A.Grajcar, H.Krzton, J. of Achievements in Mat. and Manuf. Eng, 35/2 (2009) 169-176.

[228] B. Mintz, The influence of aluminium on the strength and impact properties of steel, Int. Con. on TRIP-aided H. S. Ferrous Alloys, Ghent (2002) 379-382.

[229] S. Chupatanakul, P. Nash, D. Chen, Met. and Mat. Int., 12 (2006)453~458.

[230] M. Arjomandi, H. Khorsand, S. H. Sadati, H. Addoos, Defect and Diffusion Forum 273-276 (2008) 329-334.

[231] G. F. Caballero, M. J. Santofimia, C. Garcı́a-Mateo, C. G. de Andre´s Mat. Trans, 45 (2004) 3272 – 3281.

[232] Y.-K. LEE, J. OF Mat. Sci. Letters 21(2002)1253 – 1255.

[233] J. R. Yang, H.K.D.H. Bhadeshia: Advances in the Science and Technology of Welding, ed. By S. A. David, ASM International, Ohio, (1987) 187.

[234] M. Diaz-Fuentes, I. Gutierrez, Mat. Sci. and Eng. A363 (2003) 316-324.

[235] Madariaga, I. Gutierrez, H.K.D.H. Bhadeshia, Metall. Trans. A 32A (2001) 2187-2197.

[236] A. A. B. Sudgen, H.K.D.H. Bhadeshia, Metall. Trans. A 20A (1989) 1811.

[237] S. A. Khan and H.K.D.H. Bhadeshia, Metall. Trans. A 21A (1990a) 859-875.

[238] G. Dini, M. M. Vaghefi, A. Shafyei: ISIJ Int. 46 (2006) 89–92.

[239] J.Moon,J.Lee,C.Lee: Mater.Sci.Eng.A459,(2007) 40-46.

[240] F. J. Humphreys and M. Hatherly, Recrystallization and Related Annealing Phenomena, Pergamon, Oxford, (1995).

[241] I Andersen, O. Grong and N. Ryum, Acta Metall. 43, (1995), 2689.

[242] Cohen, M., Machlin, E. S. and Paranjpe, V. G. Thermodynamics in Physical Metallurgy, ASM, Cleveland, Ohio, USA (1950).

[243] L. Kaufman, M. Cohen: Progress in Metal Physics 7 (1958) 165–246.

[244] H. S. Yang, H.K.D.H. Bhadeshia: Scripta Materialia 60 (2009) 493–495.

[245] H.S.Yang, J.H.Jang, H.K.D.H. Bhadeshia and D. W. Suh: CALPHAD 36 (2012) 16-22.

[246] J. Huang, Z. Xu: Materials Science & Engineering A A438–440 (2006) 254–257.

[247] Zhang, Z. and Farrar, R. A: Mater. Sci. Technol. 1996, 12,237.

[248] Ricks, R. A. , Howell, P. R. and Barritte, G. S: Jr. Mater. Sci. , 1982,17,732.

[249] Farrar, R. A. and Waston, M. N: Metall. Construct. , 1979, 11, 285.

[250] Barritte, G. S. and Edmonds, D. V., Advances in the Physical Metallurgy and Application of Steels. The Metals Society, London, (1982)126-135.

[251] Ralph, B: Mater. Sci. Technol., 1990, 6, 1139.

[252] I. Madariaga and I. Gutierrez : Scripta mater.,1997, 37(8), 1185.

[253] I. Madariaga and I. Gutierrez, in Proc. of Conf. on Microalloying ¨98. Trans. Tech. Publications Ltd, Switzerland, (1998).

[254] A.R. Mills, G. Thewlis and J.A.Whiteman, Ibid., 3 (1987),12,1051.

[255] G. Thewlis: Mater.Sci. Technol., 10 (1994),2,110.

[256] Y.Tomita et al., ISIJ International, 34,(1994),10,829.

[257] J.L.Lee, Acta Metallurgica and Materialia, 42,(1994),10,3291.

[258] J.L.Lee and Y.T.Pan, ISIJ Int.,35 (1995) 8, 1027.

[259] F. Ishikawa, T.Takahashi, T.Ochi:Proc. Int. Conf. on Solid Solid Phase Transformation, TMS-AIME, Warrendale, PA USA (1994) 171.

[260] F. Ishikawa, T. Takahashi, T. Ochi, Metallurgical and Materials Transactions A, 25A (1994) 5,929.

[261] R. A. Ricks, P. R. Howell, G. S. Barritte : J. Mater. Sci. 17 (1982) 732-40.

[262] I. Madariaga, I. Gutierrez: Acta mater., 47 (1999) 951-960.

[263] M. J. Balart, C. L. Davis, M. Strangwood: Mat. Sci. And Eng. A328 (2002) 48-57.

[264] A. A. B. Sudgen, H.K.D.H. Bhadeshia, Metall. Trans. A 20A (1989) 1811.

[265] F. B. Pickering: Proc. of Int. Conf. HSLA Steels Metallurgy and Application, ed. by J. M. Gray et al., ASM International, Metals Park, OH, (1986) 305.

[266] S. Zajac, 43rd Mechanical Working and Steel Processing Conference, Charlotte, NC, USA, 28-31 (2001) 497.

[267] M. Prikryl, A. Kroupa, G. C. Weatherly, S. V. Subramanian, Metall. Mater. Trans. A 27A (1996) 1147-65.

[268] Z. Chen, M .H. Loretto, R. C. Cochrane: Mater. Sci. Technol. 3 (1987) 836-44.

[269] P. L. Harrison, P. H. Bateson: Proc. Conf. on Titanium Technology in Micro-alloyed Steels. T.N. Baker, ed. Institute of Materials, London, U.K (1997)180-96.

[270] Z. Zhao, et al. Journal of Materials Science, 36 (2001) 5045-5056.

[271] R. O. Olivares. Requirements for the degree of Doctor of Philosophy in Materials Science and Engineering. University of Pittsburgh (2011).

[272] S. Zajac, T. Siwecki, B. Hutchinson, M. Attlegard: Metall. Trans. 22A (1991) 2681.

[273] S. Zajac, T.Siwecki, B.Hutchinson, L-E.Svensson, M.Attlegård, The Influence of Plate Production Processing Route, Heat Input and Nitrogen on the HAZ Toughness in Ti-V Microalloyed Steel", Swedish Institute for Metals Research, Report IM-2764, (1991).

[274] T. Kimura, A. Ohmori, F. Kawabata, K. Amano, Ferrite Grain Refinement through Intragranular Ferrite Transformation VN Precipitates in TMCP of HSLA Steel". Thermec 97, (1997) 645-651.

[275] T. Kimura, F. Kawabata, K. Amano, A. Ohmori, M. Okatsu, K. Uchida and T. Ishii, "Heavy Gauge H-Shapes with Excellent Seismic-Resistance for Building Structures Produced by the Third Generation TMCP", CAMP-ISIJ, (1999) 165-171.

[276] K. Irvine, F. B. Pickering, ISI Spec. Rep.93, London, (1965) 110.

[277] S. Zajac, T. Siwecki, W. B. Hutchinson, Precipitation phenomena in Vmicroalloyed 0.15-0.22%C structural steels, Swedish Institute for Metals Research, Internal Report IM-3453 (1996).

[278] S. Zajac, T. Siwecki, W. B. Hutchinson, R. Lagneborg, The role of carbon inenhancing precipitation strengthening of V-microalloyed steels. Contribution to the Int. Symp. "Microalloying in Steels: New Trends for the 21st Century, Sept. 7-9, San Sebastian, Spain (1998) 295-302.

[279] W. E. Heitmann, P. B. Babu. in Ref. [261] 55.

[280] A. Z. Hanzaki, P. D. Hodgson, S. Yue, ISIJ Int., 35 (1995)79-85.

[281] Y. Ito, M. Nakanishi, Y. Komizo: Metal. Constr. 14(1982) 472.

[282] J.R. Yang , H.K.D.H. Bhadeshia. Advances in welding science and Technology, ed.s A. David, ASM, Metals Park, Ohio, USA (1986) 187-191.

[283] H.K.D.H. Bhadeshia: Materials Science & Metallurgy, (2002)

[284] J. R. Yang, H.K.D.H. Bhadeshia, Mater. Sci. Technol. 5 (1989) 93-97.

[285] HSLA Steels Technology and Applications. Conf. organized by M. Korchynsky, ASM, Metals Park, OH,(1984).

[286] Processing, Microstructure and Properties of Microalloyed and other Modern High Strength Low Alloy Steels, A.J.De Ardo, ed., Iron and Steel Soc. Inc., (1992).

[287] Fundamentals of Microalloying Forging Steels, Eds. G. Krauss and S.K.Banerji, The Metallurgical Society, Warrendale, PA (1987) 55.

[288] G. Dini, M. M. Vaghefi, A. Shafyei: ISIJ Int. 46(2006) 89-92.

[289] F. G. Caballero, H.K.D.H. Bhadeshia, Solid State Mater. Sci. 8 (2004) 251-257.

[290] M. P. Pulus , J. S. Kirkadly, Metallurgical Transactions, 3A (1972) 2777.

[291] A.Fadel, D.Glišić, N.Radović, Dj.Drobnjak, , Journal of Materials Science & Technology 28 (2012) 1053-1058

[292] A.Fadel, N.Radovic, D.Glišić, Dj.Drobnjak, Intragranular Ferrite Morphologies In Medium Carbon Vanadium-Microalloyed Steel, Journal of Mining and Metallurgy, Section B: Metallurgy, ISSN: 1005-0302 DOI: 10.2298/JMMB120820001F

[293] D.Glišić, A.Fadel, N.Radović, Dj.Drobnjak, M.Zrilić, Deformation Behaviour Of Two Continuously Cooled Vanadium Microalloyed Steels At Liquid Nitrogen Temperature, Hemijska Industrija, DOI: 10.2298/HEMIND121214015G

Curriculum Vitae

Name: Abdunnaser Hamza.Ahmed Fadel
Date and Place of birth: 02.03.1964 Agelat, Libya

Education:

1989 B.Sc in Materials and Metallurgical Engineering	Tripoli university (before: Al-Fatah University) Faculty of Engineering /Department of Materials and Metallurgical Engineering
2003 M.Sc. in Materials and Metallurgical Engineering	Department of Metallurgical Engineering, Faculty of Technology and Metallurgy (TMF)-Belgrade Unversity

Trainings / Courses

- „PRINCIPLES AND PRACTICE IN METALLOGRAPHY" – 12/5/1997 to 27/6/1997 - Vinca institute of nuclear sciences -Belgrade-Yugoslavia
- „MATERIALS TESTING" - two weeks 12/2005 – Madrid, Spain
- „VIBRATION PROBLEM ANALYSIS" – 1999 - Faculty of Engineering - Tripoli university, Libya
- „X-RAY DIFFRACTION AND APPLICATION" – 1990 - Tajora industry Research Center-Tripoli, Libya
- „MATERIALS TESTING- Mechanical Testing, Metallography Inspection And Non-Destructive Testing (NDT)" – 1995 - Engineering Research Center-Tripoli -Libya

Employement:

1990 to 2006   Engineering Research Center, Tripoli, Libya
2006 to 2008   Zawia University-Faculty of Engineering.

Languages: Arabic and English

Family status: Married. Five children

IZJAVA O AUTORSTVU

Potpisani **Abdunnaser Hamza Fadel**

Izjavljujem

da je doktorska disertacija pod naslovom

AUSTENITE DECOMPOSITION IN MEDIUM CARBON MICROALLOYED STEELS: MECHANISM, STRUCTURE AND PROPERTIES (RAZLAGANjE AUSTENITA U SREDNjEUGLjENIČNIM MIKROLEGIRANIM ČELICIMA: MEHANIZAM, STRUKTURA I SVOJSTVA)

- rezultat sopstvenog istraživačkog rada,
- da predložena disertacija u celini ni u delovima nije bila predložena za dobijanje bilo koje diplome prema studijskim programima drugih visokoškolskih ustanova,
- da su rezultati korektno navedeni i
- da nisam kršio/la autorska prava i koristio intelektualnu svojinu drugih lica.

Potpis doktoranda

U Beogradu, 18.02.2013

Prilog 2.

IZJAVA O ISTOVETNOSTI ŠTAMPANE I ELEKTRONSKE VERZIJE DOKTORSKOG RADA
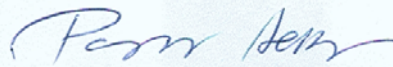
Ime i prezime autora **Abdunnaser Hamza Fadel**

Studijski program **Metalurgija**

Naslov rada **AUSTENITE DECOMPOSITION IN MEDIUM CARBON MICROALLOYED STEELS: MECHANISM, STRUCTURE AND PROPERTIES** (RAZLAGANjE AUSTENITA U SREDNjEUGLjENIČNIM MIKROLEGIRANIM ČELICIMA: MEHANIZAM, STRUKTURA I SVOJSTVA)

Mentor dr Nenad Radović, van.prof. Tehnološko metalurški fakultet

Potpisani/a _____

Izjavljujem da je štampana verzija mog doktorskog rada istovetna elektronskoj verziji koju sam predao/la za objavljivanje na portalu **Digitalnog repozitorijuma Univerziteta u Beogradu.**

Dozvoljavam da se objave moji lični podaci vezani za dobijanje akademskog zvanja doktora nauka, kao što su ime i prezime, godina i mesto rođenja i datum odbrane rada.

Ovi lični podaci mogu se objaviti na mrežnim stranicama digitalne biblioteke, u elektronskom katalogu i u publikacijama Univerziteta u Beogradu.

Potpis doktoranda

U Beogradu, 18.02.2013

Prilog 3.

IZJAVA O KORIŠĆENJU

Ovlašćujem Univerzitetsku biblioteku „Svetozar Marković" da u Digitalni repozitorijum Univerziteta u Beogradu unese moju doktorsku disertaciju pod naslovom:

AUSTENITE DECOMPOSITION IN MEDIUM CARBON MICROALLOYED STEELS: MECHANISM, STRUCTURE AND PROPERTIES (RAZLAGANjE AUSTENITA U SREDNjEUGLjENIČNIM MIKROLEGIRANIM ČELICIMA: MEHANIZAM, STRUKTURA I SVOJSTVA)

koja je moje autorsko delo.

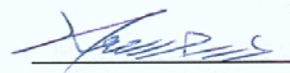Disertaciju sa svim prilozima predao/la sam u elektronskom formatu pogodnom za trajno arhiviranje.

Moju doktorsku disertaciju pohranjenu u Digitalni repozitorijum Univerziteta u Beogradu mogu da koriste svi koji poštuju odredbe sadržane u odabranom tipu licence Kreativne zajednice (Creative Commons) za koju sam se odlučio/la.

1. Autorstvo

2. Autorstvo - nekomercijalno

3. Autorstvo – nekomercijalno – bez prerade

4. Autorstvo – nekomercijalno – deliti pod istim uslovima

5. Autorstvo – bez prerade

6. Autorstvo – deliti pod istim uslovima

(Molimo da zaokružite samo jednu od šest ponuđenih licenci, kratak opis licenci dat je na poleđini lista).

Potpis doktoranda

U Beogradu, 18.02.2013

Abdunnaser Hamza Fadel